

A Thesis Submitted for the Degree of PhD at the University of Warwick

Permanent WRAP URL:

<http://wrap.warwick.ac.uk/173841>

Copyright and reuse:

This thesis is made available online and is protected by original copyright.

Please scroll down to view the document itself.

Please refer to the repository record for this item for information to help you to cite it.

Our policy information is available from the repository home page.

For more information, please contact the WRAP Team at: wrap@warwick.ac.uk

**Natural porphyrins and synthetic analogues as
photoredox catalysts in visible light catalysed
3D printing**

By

Jivan Singh Badhan

A thesis submitted for the degree of
Doctor of Philosophy in Chemistry



Photocentric

Supervisor: Professor Andrew Clark

Department of Chemistry,

University of Warwick, UK

February 2022

Table of contents

1	Introduction	1
1.1	Brief background of photochemistry	2
1.2	Photocatalyst mechanism	2
1.3	Use of photoredox catalysts in organic synthesis.....	3
1.4	Evolution of photopolymerisation.....	14
1.5	Metal-free photocatalysis	20
1.6	Porphyryns	22
1.7	Porphyryns used as photocatalysts	23
1.7.1	Organic synthesis	23
1.7.2	Porphyryns as photocatalysts in polymerisation.....	27
1.8	Chlorophyll a	29
1.9	Chlorophyll as a photoredox catalyst	30
1.10	Background of 3D printing	32
1.11	Visible light 3D printing methods	33
1.12	Development of light mediated 3D printing	34
1.13	Aims of this work	38
2	Zinc tetraphenylporphyrin and metal free tetraphenylporphyrin as photoredox catalysts in 3D printing	40
2.1	Introduction	41
2.2	Aims and objectives	43
2.3	Results and discussion.....	44
2.3.1	PET-RAFT polymerisation of methyl acrylate using ZnTPP 2.1 as a photocatalyst	44
2.3.2	UV-Visible spectrum of ZnTPP 2.1	45
2.3.3	Alternatives to BTPA/RAFT: Study of ATRP initiators	46

2.3.4	Polymerisation of MA 2.4 using ZnTPP 2.1 and 1-dodecanethiol	48
2.3.5	Optimisation of 1-dodecanethiol 2.10 mediated polymerisation	49
2.3.6	Polymerisations using multi-functional thiols	54
2.3.7	3D printing using ZnTPP 2.1 as a photocatalyst.....	56
2.3.8	Utilising TPP 2.3 as a photocatalyst	60
2.3.9	3D printing using TPP 2.3 as a photocatalyst	63
2.3.10	Potential mechanisms for polymerisation process	65
2.3.11	Summary	67
3	Assessment of tetraphenylporphyrin derivatives in 3D printing	69
3.1	Introduction	70
3.2	Aims and objectives	70
3.3	Results and discussion.....	71
3.3.1	Synthesis of tetraphenylporphyrin derivatives 3.1 – 3.4	71
3.3.2	3D prints with functionalised metal free porphyrins 3.1 -3.4	75
3.3.3	Incorporation of zinc into porphyrins 3.1 – 3.4	79
3.3.4	3D prints with zinc functionalised porphyrins 3.5 – 3.7	83
3.3.5	Position of the methoxy substituent on the aromatic ring: Preparing 2-MeO, 3-MeO derivatives of TPP 2.3	85
3.3.6	3D prints derived from 2-, 3- and 4-MeO-TPP derivatives	88
3.3.7	Studying the effect of increasing the amount of methoxy functional groups on photocatalytic ability	90
3.4	Summary	92
4	The absorption properties and photocatalytic activity of alkenyl-substituted porphyrins	94
4.1	Introduction	95
4.2	Aims and objectives	95
4.3	Results and discussion.....	96
4.3.1	Synthesis of 5,15-diphenyl-10,20-distyrylporphyrin 4.7	96

4.3.2	Polymerisation of MA using 5,15-distyryl-10,20-diphenyl-porphyrin	
4.7		102
4.3.3	Extending the conjugation in alkenyl-substituted porphyrins.....	103
4.3.4	Polymerisation of MA using mixtures 4.8/ 4.11 and 4.9/ 4.12	106
4.3.5	Study of methoxy variants of alkenyl-substituted porphyrins	107
4.3.6	Polymerisation of MA 2.4 using methoxy modified alkenyl-substituted porphyrins	111
4.4	Summary	113
5	Chlorophyll as a photocatalyst in visible light 3D printing	114
5.1	Introduction	115
5.2	Aims and objectives	116
5.3	Results and discussion.....	117
5.3.1	Isolation of chlorophyll a 5.1a from spinach	117
5.3.2	Absorption properties of chlorophyll a 5.1a	121
5.3.3	Polymerisation with chlorophyll a 5.1a from spinach.....	121
5.3.4	Polymerisation using crude spinach extract.....	125
5.3.5	3D printing using crude spinach extract	128
5.3.6	Alternate chlorophyll sources to spinach, <i>Chlorella pyrenoidosa</i>	129
5.3.7	Polymerisation of MA 2.4 using crude chlorella extracts.....	132
5.3.8	3D printing using crude chlorella as a photocatalyst	134
5.4	Summary	134
6	Concluding remarks	137
6.1	Conclusion.....	138
7	Experimental	141
7.1	General information	142
7.2	Chapter 2	143
7.2.1	Synthesis of tetraphenylporphyrin 2.3 . ¹³⁹	143
7.2.2	Synthesis of ZnTPP 2.1 ¹⁴⁰	143

7.2.3	RAFT polymerisation of MA 2.4 using BPTA 2.2 ⁸⁷	144
7.2.4	General procedure for polymerisation of MA 2.4 using ATRP initiators 145	
7.2.5	General procedure for the polymerisation of MA 2.4 , changing the concentration of thiol 2.10	145
7.2.6	General procedure for the polymerisation of MA 2.4 , changing the concentration of ZnTPP 2.1	147
7.2.7	General procedure for the polymerisation of MA 2.4 , studying the effect of changing the thiol	149
7.2.8	Polymerisation of MA 2.4 , using TPP 2.3 as a photocatalyst.....	150
7.2.9	General procedure for 3D printing.....	150
7.3	Chapter 3	151
7.3.1	Synthesis of 5,10,15,20-(4-methoxy)tetraphenylporphyrin 3.4 ¹³⁹	151
7.3.2	5,10,15,20-(4-Methyl)tetraphenylporphyrin 3.3 ¹³⁹	151
7.3.3	5,10,15,20-(4-Chloro)tetraphenylporphyrin 3.2 ¹³⁹	152
7.3.4	General procedure for metalation of porphyrins with zinc ¹⁷³	152
7.3.5	5,10,15,20-(4-Methoxy) zinc tetraphenylporphyrin 3.7	153
7.3.6	5,10,15,20-(4-Methyl) zinc tetraphenylporphyrin 3.6	153
7.3.7	5,10,15,20-(4-Chloro) zinc tetraphenylporphyrin 3.5	154
7.3.8	Synthesis of 5,10,15,20-tetrakis(3-methoxyphenyl)porphyrin 3.9 ¹⁷⁹	154
7.3.9	Synthesis of 5,10,15,20-tetrakis(2-methoxyphenyl)porphyrin 3.8 ¹⁸⁰	155
7.3.10	Synthesis of 5,10,15,20-tetrakis(3,5-dimethoxyphenyl)porphyrin 3.10 ¹⁸¹	155
7.3.11	Synthesis of 5,10,15,20-tetrakis(2,4,6-trimethoxyphenyl) porphyrin 3.11 ¹⁸²	156
7.3.12	Synthesis of 5,10,15,20-tetrakis(3,4,5-trimethoxyphenyl) porphyrin 3.12 ¹⁸³	157
7.3.13	General procedure for polymerisation of MA 2.4 using modified porphyrin variants	157

7.3.14	General procedure for 3D printing in chapter 3	161
7.4	Chapter 4	163
7.4.1	Synthesis of dipyrromethane 4.1 ¹⁸⁴	166
7.4.2	Synthesis of 5,15-diphenylporphyrin 4.2 ¹⁸⁵	166
7.4.3	5,15-Dibromo-10,20-diphenylporphyrin 4.3 ¹⁸⁶	167
7.4.4	General procedure for synthesis of alkenyl-substituted porphyrins...	167
7.4.5	5,15-Diphenyl-10,20-di((E)-styryl)porphyrin 4.7	167
7.4.6	5,15-Diphenyl-10,20-bis((1E,3E)-4-phenylbuta-1,3-dien-1-yl)porphyrin 4.8 and 5,15-Diphenyl-10-((1E,3E)-4-phenylbuta-1,3-dien-1-yl)porphyrin 4.11	168
7.4.7	5,15-Bis(4-methoxyphenyl)porphyrin 4.13 ¹⁷⁴	169
7.4.8	5,15-Dibromo-10,20-bis(4-methoxyphenyl)porphyrin 4.14 ¹⁸⁷	169
7.4.9	5,15-Bis((E)-4-methoxystyryl)-10,20-diphenylporphyrin 4.15	169
7.4.10	Synthesis of 5,15-bis(4-methoxyphenyl)-10,20-distyryl)porphyrin 4.16 170	
7.4.11	5,15-bis(4-methoxyphenyl)-10,20-bis((E)-4-methoxystyryl)porphyrin 4.17 171	
7.4.12	General procedure for the polymerisation of MA 2.4 using alkenyl substituted porphyrins	171
7.5	Chapter 5	174
7.5.1	Procedure to produce crude spinach extract.....	174
7.5.2	Extraction of chlorophyll a from spinach ¹⁵⁷	174
7.5.3	Procedure to extract crude chlorella extract from chlorella powder ..	176
7.5.4	Procedure to extract crude chlorella extract from chlorella tablet	176
7.5.5	Procedure for extracting chlorophyll a 5.1a from chlorella powder ..	177
7.5.6	General procedure for the polymerisation of MA 2.4 using spinach and chlorella extracts as photocatalysts	178
7.5.7	General procedure for 3D printing	182

8	References	183
---	------------------	-----

List of figures

Figure 1.1 - Structure of organic compounds investigated as photoredox catalysts in organic synthesis	13
Figure 1.2 - Examples of RAFT agents and monomers used by Boyer et al in polymerisations using fac-[Ir(ppy) ₃] 1.27 ⁵⁰	19
Figure 1.3 - Structures of modified 5,10-diphenyl-5,10-dihydrophenazine	20
Figure 1.4 - Structure of most basic porphyrin structure (theoretical)	22
Figure 1.5 - Structure of TPP-BSTP (TPP (tetraphenylporphyrin) and BTSP (3-....	29
Figure 1.6 - Structure of porphyrins used in near infra-red (NIR) polymerisation ⁹³	29
Figure 1.7 - Structure of chlorophyll a and chlorophyll b.....	30
Figure 1.8 - Structures of RAFT agents used in PET-RAFT polymerisation using chlorophyll a as a photoredox catalyst	32
Figure 1.9 - Examples of typical UV light photoinitiators in 3D printing	34
Figure 1.10 - Structures of components of copper catalysed visible light 3D printing	35
Figure 1.11 - Examples of visible light photoinitiators in 3D printing ¹¹⁸	37
Figure 2.1 – Reactants used in this study.	44
Figure 2.2 - UV-Vis spectrum of ZnTPP 2.1 in DMSO (0.1 mg / 1 mL).....	46
Figure 2.3 – Structures of different alkyl halide initiators studied	47
Figure 2.4 - Structure of 1-dodecanethiol 2.10	49
Figure 2.5 – Structures of 1-dodecanethiol 2.10 , trimethylolpropane tris(3-mercaptopropionate) 2.11 and pentaerythritol tetrakis(3-mercaptopropionate) 2.12	55
Figure 2.6 - Structures of triethylene glycol dimethacrylate (TEGDMA) 2.5 and urethane dimethacrylate (UDMA) 2.6	56
Figure 2.7 - 3D prints of 50:50 w: w TEGDMA 2.5 / UDMA 2.6 utilising thiols 2.11 and 2.12 as co-initiators in blue light, with an exposure time of 300,000 ms. Print B – using thiol 2.11 , Print C – using thiol 2.12 . (Print A – Photocentric standard).....	57
Figure 2.8 - TGA of 3D Print B (using thiol 2.11) and Print C (using thiol 2.12). ..	58
Figure 2.9 - 3D prints of 50:50 w: w TEGDMA 2.5 / UDMA 2.6 utilising thiol 2.12 in blue light, exposure time 300,000ms per layer (Print D) and 200,000ms per layer (Print E). (Monomer: thiol: ZnTPP = 200: 10: 0.25)	60
Figure 2.10 - UV-Vis spectrum of TPP 2.3 vs ZnTPP 2.1 in DMSO.....	62

Figure 2.11 - 3D prints – Photocentric standard (A). Using TPP 2.3 (F) and using ZnTPP 2.1 (D) used as a photocatalyst – Monomer: thiol 2.12: ZnTPP 2.1 or TPP 2.3 200: 10: 0.25.	64
Figure 2.12 - TGA of 3D prints, comparing ZnTPP 2.1 and TPP 2.3 as photocatalyst	64
Figure 2.13 – Comparison of the Q region of the UV-vis spectrum of ZnTPP 2.1 without thiol (top) and with 1-dodecanethiol (bottom).....	66
Figure 3.1 - UV-Vis of metal free porphyrins 2.3 and 3.2 – 3.4 in DMSO (0.1475 mM).....	72
Figure 3.2 – Row one: Photocentric test print A and 3D print using modified porphyrin. Print G = 4-Cl-TPP. Row two: 3D print using modified porphyrins: Print F = TPP 2.3, Print H = 4-Me-TPP 3.3, Print I = 4-OMe-TPP 3.4. Row three: Comparison of key areas in Print I = 4-OMe-TPP 3.4 and photocentric test print A. Row four: Resolution of the text in Print I and Print A.....	77
Figure 3.3 - TGA data of 3D prints using modified metal-free porphyrins 3.1 – 3.4 as photocatalysts.....	78
Figure 3.4 - UV-Vis of zinc para substituted porphyrins 2.1 and 3.5 – 3.7 in DMSO (0.1475 mM)	80
Figure 3.5 - 3D print using modified zinc porphyrin 3.1 and 3.5 – 3.7. Row one: Print J = 4-Cl-ZnTPP 3.5, print D = ZnTPP 2.1, print K = 4-Me-ZnTPP 3.6, print L = 4-OMe-ZnTPP 3.7. Row two (left): Resolution of cylinders and holes in prints D and L. Row two (right): Resolution of text in Print D and print L.....	83
Figure 3.6 - TGA data of ZnTPP 2.1 and para modified zinc porphyrins 3.5-3.7 3D prints.....	84
Figure 3.7 - UV-Vis spectrum of methoxy substituted porphyrins 3.4, 3.8 and 3.9 in DMSO (0.1475mM).....	86
Figure 3.8 - 3D prints using methoxy substituted porphyrins 2.1, 3.7 and 3.8 as photocatalysts. 2-OMe-TPP 3.8 (M), 3-OMeTPP 3.9 (N) and 4-OMeTPP (L)	88
Figure 3.9 - TGA of 3D prints photocatalyzed by methoxy modified porphyrin 3.4, 3.8, 3.9 (Figure 3.8).....	89
Figure 4.1 - Structures of 5,15-dibromo-10,20-diphenylporphyrin (4.3) and 5-bromo-10,20-diphenylporphyrin (4.4) porphyrin	97
Figure 4.2 - 400 MHz ¹ H NMR in CDCl ₃ of dibromo porphyrin 4.3.....	98
Figure 4.3 - Structure of distyryl porphyrin 4.7	99

Figure 4.4 - UV-Vis spectrum of 5,15-distyryl-10,20-diphenylporphyrin 4.7 in DMSO (0.1475 mM).....	101
Figure 5.1 - Structure of chlorophyll a 5.1a (left) and tetraphenylporphyrin 2.3 (right)	115
Figure 5.2 - Structures and nomenclature of Chlorophyll a and b 5.1a/b other components in spinach	117
Figure 5.3 – ¹ H NMR spectrum of chlorophyll a 5.1a and pheophytin a 5.2a mixture.	119

List of schemes

Scheme 1.1 – Mechanisms of photocatalysis	2
Scheme 1.2 - General reaction mechanism for photocatalysis by a ruthenium complex	3
Scheme 1.3 - Early example of visible light photocatalysis - Reduction of alkenes using Ru(bpy) ₃ Cl ₂ as a photocatalyst ¹⁷	4
Scheme 1.4 - Reaction scheme of reduction of alkenes using Ru(bpy) ₃ Cl ₂ as a photocatalyst ¹⁷	4
Scheme 1.5 - Photocatalytic Pschorr reaction	5
Scheme 1.6 - Oxidation of benzylic alcohol 1.7 to respective aldehyde 1.8 ¹⁶	6
Scheme 1.7 - Mechanism of the oxidation to aldehydes ¹⁶	6
Scheme 1.8 – Oxidation of sulfide to sulfoxides utilising [NPyc ^x -Ru(bpy)] as a photocatalyst	7
Scheme 1.9 - Reaction scheme of the direct asymmetric alkylation of aldehydes ²² ...	7
Scheme 1.10 - Photocatalytic and organocatalytic catalysis proposed mechanism	8
Scheme 1.11 - Reaction scheme of [2+2] dienone cycloaddition	8
Scheme 1.12 - Reaction mechanism of [2+2] dienone cycloadditions.....	9
Scheme 1.13 - Reaction scheme for photoredox-mediated reductive dehalogenation reaction.....	10
Scheme 1.14 - Proposed mechanism for radical reductive cleavage of alkyl, alkenyl and aryl iodides	11
Scheme 1.15 - Mechanism for atom transfer radical addition (ATRA) of haloalkanes ²⁵	11
Scheme 1.16 – Reaction scheme of copper catalysed ATRA	12
Scheme 1.17 - Mechanism of thiol-ene coupling of alkenes and thiols	13
Scheme 1.18 - Aerobic desulfurization of thioamides into amides	14
Scheme 1.19 - Formation of radicals from irradiating <i>S</i> -benzyl- <i>N,N</i> -diethyldithiocarbamate 1.23 with UV light to form radicals 1.24 and 1.25	15
Scheme 1.20 – General mechanism for photopolymerization using inferters ³⁵	15
Scheme 1.21 – General mechanism for copper mediated dithiocarbamate polymerisation under UV light.....	15
Scheme 1.22 – General mechanism of copper complex mediated polymerisation in UV light.....	16

Scheme 1.23 - Proposed mechanism for outer sphere electron transfer (OSET)-living radical polymerisation ⁴⁰	17
Scheme 1.24 - Mechanism for Ir(ppy) ₃ mediated visible light-controlled polymerisation.....	18
Scheme 1.25 - Fe-based ATRP reaction.....	18
Scheme 1.26 - The use of perylene 1.31 as an organic photocatalyst for the polymerization of methyl methacrylate (MMA) 1.29 with alkyl bromide 1.30 initiator. ⁵²	20
Scheme 1.27 - Reaction mechanism of the polymerisation of various monomers using 10-phenylphenothiazine as a photocatalyst. ⁵⁴	21
Scheme 1.28 - PET-RAFT polymerisation mechanism mediated by Eosin Y (EY) in the presence of triethylamine and oxygen.....	22
Scheme 1.29 – Formation of radicals using halogenated iron Fe(TPP)Cl ⁶⁶	24
Scheme 1.30 - Example of O=MnTPP ⁺ 1.34 oxidising a hydrocarbon to form an alcohol.....	24
Scheme 1.31 - Mechanism of oxidation of cyclohexene using Sb ^V (TPP) 1.35 , PPh ₃ 1.36 and methyl viologen	24
Scheme 1.32 – α -Alkylation of aldehydes using porphyrins as photocatalysts.....	25
Scheme 1.33 - Mechanism for light induced functionalization of aldehydes with EDA in the presence of tetraphenylporphyrin ⁷⁵	26
Scheme 1.34 – Reaction scheme of C-H arylation of heteroarenes with diazonium salts.....	26
Scheme 1.35 - Mechanism for arylation of heterocycles with diazonium salts using H ₂ TPP.....	27
Scheme 1.36 - Reaction scheme of visible light polymerisation, catalysed by cobalt porphyrins ⁸⁹	27
Scheme 1.37 - Mechanism of PET-RAFT polymerisation ⁸⁷	28
Scheme 1.38 - Mechanism for PET-RAFT polymerisation using chlorophyll a as a photocatalyst	31
Scheme 1.39 - Type 1 photocleavage of 2-hydroxy-2-methyl-1-phenyl-propan-1-one ¹⁰⁸	34
Scheme 1.40 – Radical generation from type II photoinitiators ¹¹¹	35
Scheme 1.41 - Mechanism of carbazole as a photoredox catalyst ¹¹³	36
Scheme 2.1 - Visible light polymerisation, catalysed by cobalt porphyrins	41

Scheme 2.2 - Mechanism of PET-RAFT polymerisation ⁸⁷	42
Scheme 2.3 - Synthesis route of BPTA 2.2 ¹¹⁹	45
Scheme 2.4 - Primary cyclisation mechanism of TEGDMA during polymerisation ¹³⁸	59
Scheme 2.5 - Reaction scheme of TPP 2.3 synthesis and metalation to ZnTPP 2.1 ¹³⁹	61
Scheme 3.1 – Synthetic route of TPP 2.3 ¹³⁹	70
Scheme 3.2 - Synthesis of para modified porphyrins 3.1 – 3.4 ¹³⁹	71
Scheme 3.3 – Synthetic route of zinc porphyrins 3.1 and 3.5 – 3.7 ¹⁴⁰	79
Scheme 3.4 – Synthetic route of ortho and meta methoxy modified porphyrins 3.8 and 3.9	86
Scheme 3.5 – Synthetic route of di- and tri-substituted methoxy porphyrins 3.10 - 3.12	91
Scheme 4.1 – Synthetic route of 5,15-dibromo-10,20-dihenylporphyrin 4.3	96
Scheme 4.2 - Synthesis route of 5,10,15-triphenylporphyrin-20-styrylporphyrin (4.6) ¹⁵⁰	98
Scheme 4.4 - Reaction mechanism of the Heck reaction of 4.3 to 4.7	100
Scheme 4.5 – Synthesis route of 5,15-diphenyl-10,20-bis(4-phenylbuta-1,3-dien-1- yl)porphyrin 4.8	104
Scheme 4.6 - Synthetic route of 5,15-bis(2-(naphthalen-1-yl)vinyl)-10,20- diphenylporphyrin 4.9	105
Scheme 4.7 – Synthesis route of 5,15-dibromo-10,20-bis(4- methoxyphenyl)porphyrin 4.14	108
Scheme 4.8 – Synthetic route of methoxy modified alkenyl-substituted porphyrins 4.15 – 4.17	109
Scheme 5.1 - Potential mechanism of action for polymerisation using chlorophyll a 5.1a as a photocatalyst.	135

List of tables

Table 2.1 – Polymerisation of methyl acrylate under different wavelengths using ZnTPP 2.1 as a photoredox catalyst.....	42
Table 2.2 – Polymerisation of MA using alkyl halide co-initiators, ratio of MA 2.4 : co-initiator: ZnTPP 2.1 was 200: 1: 1×10^{-5} , reaction time 2h.....	48
Table 2.3 - The effect of changing thiol 2.10 concentration on the polymerisation of MA 2.4 using ZnTPP 2.1 as a photocatalyst.....	49
Table 2.4 – GPC analysis of the kinetics of the polymerisation of MA 2.4 using ZnTPP 2.1 as a photocatalyst in blue light, altering the concentration of 1-dodecanethiol 2.10	51
Table 2.5 - Effect of changing concentration of ZnTPP 2.1 on the polymerisation of MA 2.4 using blue light.	52
Table 2.6 - The effect of changing concentration of ZnTPP 2.1 on polymerisation of MA 2.4 in blue light.....	53
Table 2.7 - Polymerisation of MA 2.4 with multifunctional thiols (2.11 and 2.12) vs 1-dodecanethiol 2.10 in blue and red light.....	55
Table 2.9 - Comparison of UV-Vis spectrum's of ZnTPP 2.3 and TPP 2.1 in DMSO (0.1475mM)	62
Table 2.10 - Comparing photocatalytic ability of ZnTPP 2.1 and TPP 2.3	63
Table 3.1 – Soret bands of para modified porphyrins 2.3 and 3.2 – 3.4 in DMSO (0.1475 mM)	73
Table 3.2 – Q region bands of para modified porphyrins 3.2 – 3.4 compared to TPP 2.3	73
Table 3.3 -Polymerisation of MA 2.4 using para modified porphyrin variants 3.1 – 3.4	74
Table 3.4 - Conversion study of polymerisation of MA 2.4 using TPP 2.3 and 4-MeO-TPP 3.4	75
Table 3.5 - $T_{50\%}$ and $T_{5\%}$ for TGA data of metal-free porphyrins 3.1 – 3.4 (Figure 3.3)	78
Table 3.6 - UV-vis data of zinc para substituted porphyrins 2.1 and 3.5 – 3.7 in DMSO (0.1475 mM).....	80

Table 3.7 – Polymerisations of MA 2.4 using modified zinc porphyrins 2.1 and 3.5 – 3.7 as photocatalysts.....	81
Table 3.8 – Conversion study of the polymerisation of MA 2.4 using ZnTPP 2.1 and 4-OMe-ZnTPP 3.7 as photocatalysts	82
Table 3.9 - T _{50%} and T _{5%} for TGA data for 3D prints using para modified zinc porphyrins 2.1 and 3.5 – 3.7	85
Table 3.10 – UV-Vis spectrum data of methoxy modified porphyrins 3.4 , 3.8 , and 3.9 in DMSO (0.1475 mM).....	87
Table 3.11 - Polymerisation data using methoxy modified porphyrins 3.4 and 3.8 – 3.9 as photocatalysts in the polymerisation of MA 2.4	88
Table 3.12 - TGA data of 3D prints photocatalyzed by methoxy modified porphyrin 3.4 , 3.8 , 3.9 (Figure 3.9).....	90
Table 3.13 - UV-Vis data of di-substituted 3.10 and tri-substituted porphyrins 3.11 - 3.12 compared to 4-OMe-TPP 3.5 in DMSO (0.1475 mM)	91
Table 3.14 – Polymerisation of MA 2.4 using -di and tri-substituted porphyrins 3.11 - 3.13 as photocatalysts, compared to TPP 2.3	92
Table 4.1 - UV-Vis bands of 5,15-distyryl-10,20-diphenylporphyrin 4.7 compared to TPP 2.3 in DMSO (0.1475mM).....	102
Table 4.2 - Polymerisation of MA using TPP 2.3 , 5,10,15,20-tetrakis(4-methoxyphenyl)porphyrin 3.4 and 5,15-distyryl-10,20-diphenylporphyrin 4.7 as photocatalysts.....	102
Table 4.3 - UV-Vis bands of porphyrin mixtures 4.8 / 4.11 and 4.9 / 4.12 compared to 4.7	106
Table 4.4 - Polymerisation of MA 2.4 using porphyrin mixtures 4.8 / 4.11 and 4.9 / 4.12	107
Table 4.5 - UV-Vis bands of methoxy modified alkenyl-substituted porphyrins 4.15 - 4.17 compared to 5,15-distyryl-10,20-diphenylporphyrin 4.7	110
Table 4.6 - Polymerisation of MA using porphyrins 4.7 and 4.15 – 4.17 as photocatalysts in blue and red light.....	112
Table 5.1 – PET-RAFT polymerisation of MA 2.4 using chlorophyll a 5.1a and crude spinach extracts a photocatalyst ⁹⁷	115
Table 5.2 – Data from the UV-Vis spectra of the 5.1a/5.3a in DMSO (0.1475mM)	121

Table 5.3- Polymerisation of MA 2.4 using chlorophyll a 5.1a as a photocatalyst in both blue and red light.....	123
Table 5.4 - Polymerisation of MA 2.4 using chlorophyll a 5.1a and crude spinach as photocatalysts in blue and red light.....	127
Table 5.5 – Conversion study of the polymerisation of MA 2.4 using chlorophyll a 5.1a and crude spinach extract as photocatalysts in blue light	128
Table 5.6 - Polymerisation of MA 2.4 using crude spinach and chlorella extracts as photocatalysts	132
Table 5.7 – Conversion study of polymerisation of MA 2.4 comparing chlorophyll a 5.1a and crude chlorella powder in blue light.....	133

List of graphs

Graph 2.1 – Conversion of monomer vs time for MA 2.4 using ZnTPP 2.1 as a photocatalyst in blue light, altering the concentration of 1-dodecanethiol 2.10	50
Graph 2.2 - Shows the effect of changing ZnTPP 2.1 concentration on the polymerisation of MA 2.4	52
Graph 2.3 - Comparison of kinetics of the polymerisation of MA 2.4 in blue light, changing ratio of MA 2.4 : 1-dodecanethiol 1.10 : ZnTPP 2.1	54
Graph 3.1 - Conversion vs time comparison of polymerisation of MA using TPP 2.3 , 4-OMe-TPP 3.4 , ZnTPP 2.1 and 4-OMe-TPP 3.7 as photocatalysts.....	82
Graph 4.1 – Conversion studies of the polymerisation of MA 2.4 using TPP 2.3 and 5,15-distyryl-10,20-diphenylporphyrin 4.7 in blue light	103
Graph 4.2 - UV-Vis of porphyrin mixture 4.8 / 4.11 and 4.9 / 4.12 compared to 4.7	106
Graph 4.3 - Conversion studies of polymerisation of MA 2.4 using methoxy-modified alkenyl-substituted porphyrin 4.15-4.17 compared to 5,15-distyryl-10,20-diphenylporphyrin 4.7	112
Graph 5.1 - Conversion study of polymerisation of MA 2.4 comparing chlorophyll a 5.1a and crude chlorella powder in blue light.....	133

Declaration

The work presented in this thesis was carried out by the author at the university of Warwick between October 2017 and November 2021, it has not been submitted for a degree at another institution. Where work has been compared to literature results it has been acknowledged and referenced, other previously reported results and ideas have also been acknowledged and referenced.

Jivan Singh Badhan

Abstract

The idea of this work is to utilise natural and synthetic porphyrins as photoredox catalysts in visible light 3D printing.

Chapter 1 provides a background of the use of light in organic synthesis, polymerisation and 3D printing.

Chapter 2 assessed the ability of both zinc tetraphenylporphyrin and tetraphenylporphyrin to photo catalyse the polymerisation of methyl acrylate in blue and red light, as well as the 3D print of a TEGDMA / UDMA solution in blue light.

Chapter 3 studied the effect of functionalising tetraphenylporphyrin with electron and donating groups and assessing the effect on photocatalytic ability in visible light 3D printing.

Chapter 4 looked at increasing the conjugation of the porphyrin core by utilising the heck reaction and studying the effect on absorption properties and photocatalytic activity for the polymerisation of methyl acrylate.

Chapter 5 analyses the use of chlorophyll a and pheophytin a from spinach and chlorella sources as a photocatalyst in the polymerisation of MA and 3D printing of a TEGDMA / UDMA solution. Also, the photocatalytic ability of crude extracts of chlorella and spinach was studied for the same purpose.

Chapter 6 is a summary of the work completed in this thesis.

Chapter 7 is the experimental procedures undertaken for this thesis.

Chapter 8 is a list of references used.

Table of abbreviations

Abbreviation	Expansion
3D	3-dimensional
ATRA	Atom transfer radical addition
ATRP	Atom transfer radical polymerisation
BNAH	1-benzyl-1,4-dihydronicotinamide
BTPA	2-(((butylthio)carbonothioyl)thio)propanoic acid
BSTP	3-(((benzylthio)carbonothioyl)thio)propanoic acid
CDB	2-phenylpropan-2-yl benzodithioate
CPADB	4-cyano-4-((phenylcarbonothioyl)thio)pentanoic acid
CPD	2-cyanopropan-2-yl benzodithioate
DC	Dithiocarbamate
DCM	Dichloromethane
DDQ	2,3-Dichloro-5,6-dicyano-1,4-benzoquinone
DMA	Dimethylacrylate
DMSO	Dimethylsulfoxide
EDB	Ethyl-4-(dimethylamino)-benzoate
GPC	Gel permeation chromatography
HOMO	Highest occupied molecular orbital
LCD	Liquid crystal display
LED	Light emitting diode
LMCT	Ligand-to-metal charge transfer
MA	Methyl acrylate
MMA	Methyl methacrylate
MeOH	Methanol
NIR	Near Infra-red
NMR	Nuclear magnetic resonance
PVC	Poly(vinyl) chloride
PET	Photoinduced electron transfer
RAFT	Reversible addition fragmentation
rt	Room temperature
SET	Single electron transfer
SLA	Stereolithography

TEGDMA	Triethylene glycol dimethacrylate
TFA	Trifluoro acetic acid
TGA	Thermal gravitational analysis
TPP	Tetraphenylpoprhyrin
UDMA	Urethane dimethacrylate
UV	Ultraviolet
ZnTPP	Zinc tetraphenylpoprhyrin

1 Introduction

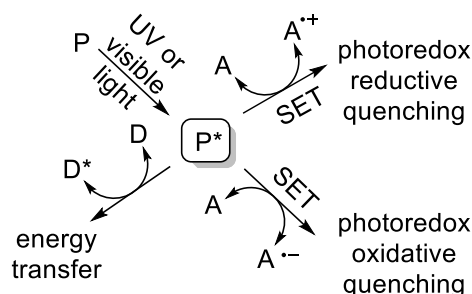
1.1 Brief background of photochemistry

The history of photochemistry is a long one.¹ It is arguable that the first recorded effect of photochemistry is the light induced fading of paint recorded by Vitruvius in 50 BC.¹ The first modern commercial processes utilising photochemistry are probably based around photography (from 1838). In 1872 Baumann reported the photopolymerisation of vinyl chloride to give PVC.² The realization that light is an abundant and renewable energy source for organic synthesis was first realized by Ciamician in 1912.³ The idea behind photochemistry is that a ground state molecule absorbs a photon of energy, which excites an electron from the HOMO to a higher orbital. This molecule is then in an excited state, after which it can participate in further chemical processes.⁴

Both visible and non-visible light sources can be utilised for this purpose, as long as the energy from the light is high enough to promote the electron from the HOMO to a higher lying orbital. The two main light sources used for photochemistry are UV light and lower energy visible light. Due to UV light being of a higher energy, these were the first photochemical reactions developed.⁴ However, the interest in using visible light in chemistry has increased in the past 20 years.⁵⁻⁸ This is due to visible light being cheaper, more accessible, and less hazardous than using UV light.

1.2 Photocatalyst mechanism

Photocatalysts are molecules which can be excited by UV or visible light and mediate the reaction of further chemical entities. Photocatalysts can initiate transformations either *via* electron transfer (SET, photoredox catalysis) or *via* energy transfer (EnT) (Scheme 1.1).



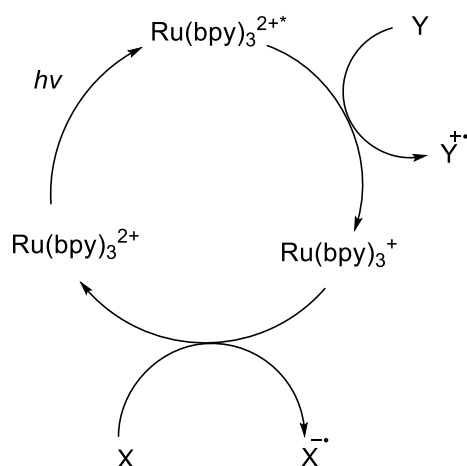
Scheme 1.1 – Mechanisms of photocatalysis

In the former, the excited photocatalyst P^* (normally a metal complex or an organic dye) can either donate an electron to another molecule A to give a radical anion $A^{\cdot-}$

(oxidative quenching) or gain an electron from molecule A giving a radical cation $A^{\cdot+}$ (reductive quenching).^{5,9} Alternatively, the excited photocatalyst P^* can act as a sensitizer and transmit energy to a suitable donor molecule D *via* energy transfer to give an excited D^* .¹⁰ Photocatalysts can often mediate reactions *via* both photoredox (SET) and energy transfer (EnT) mechanisms simultaneously. In recent years, a move away from UV mediated photocatalysis to visible light mediated approaches has been explored, with several reviews covering both electron transfer and energy transfer processes in organic transformations.^{4,5,9–14}

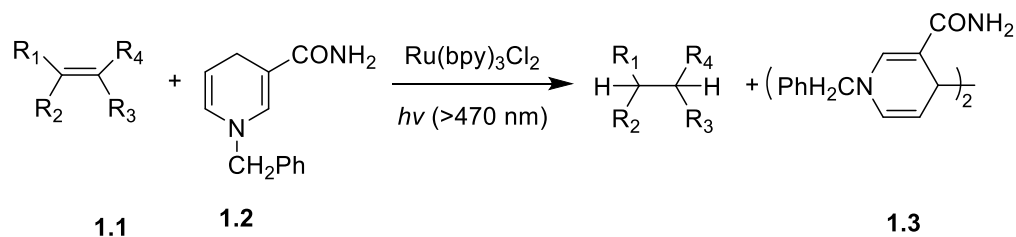
1.3 Use of photoredox catalysts in organic synthesis

The most well established photoredox catalysts that use visible light are based around metal complexes (most commonly bipyridyl complexes of ruthenium and iridium). These complexes are excellent SET oxidants and reductants in the excited state and can be used to mediate redox neutral reactions where both oxidation and reduction are required within the same processes. This behaviour is observed because on irradiation loss of the excited electron from the π^* orbital is facilitated but also a relatively low lying t_{2g} orbital can accept an electron readily. The general mechanism by which $\text{Ru}(\text{bpy})_3\text{Cl}_2$ can photocatalyse a reaction is shown in scheme 1.2.



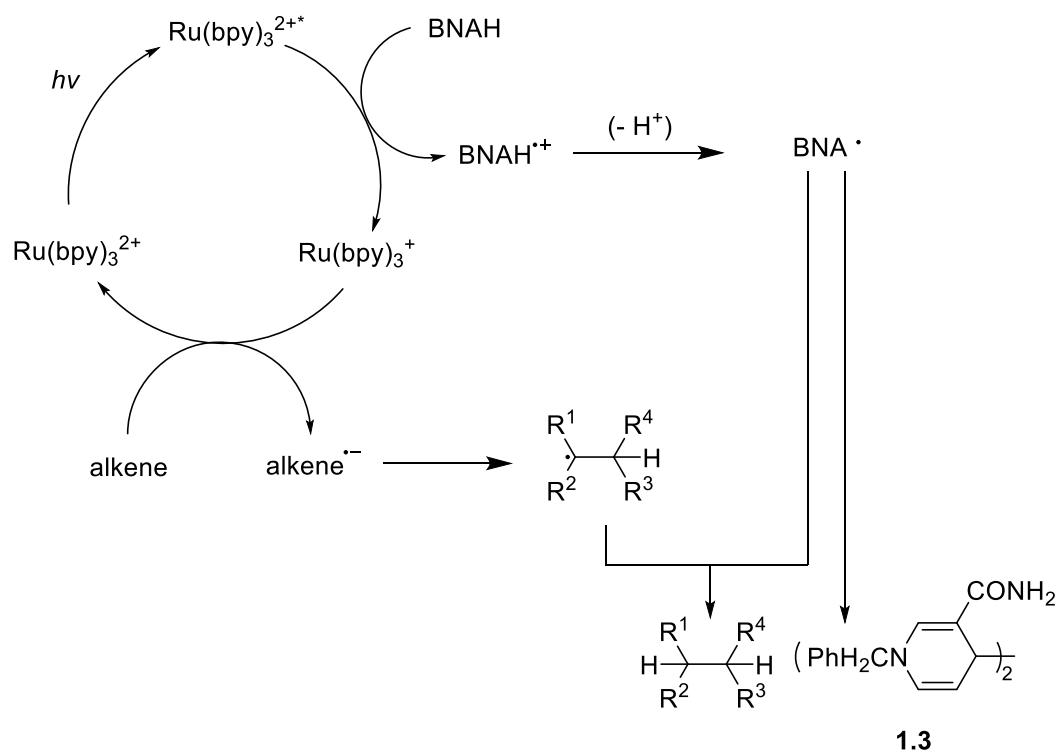
Scheme 1.2 - General reaction mechanism for photocatalysis by a ruthenium complex

As early as 1981 Ru complexes were used as photocatalysts for organic synthesis reactions.^{15–17} The Ru catalyst employed was normally $\text{Ru}(\text{bpy})_3\text{Cl}_2$, which is now one of the most widely used photocatalysts today.



Scheme 1.3 - Early example of visible light photocatalysis - Reduction of alkenes using $\text{Ru}(\text{bpy})_3\text{Cl}_2$ as a photocatalyst¹⁷

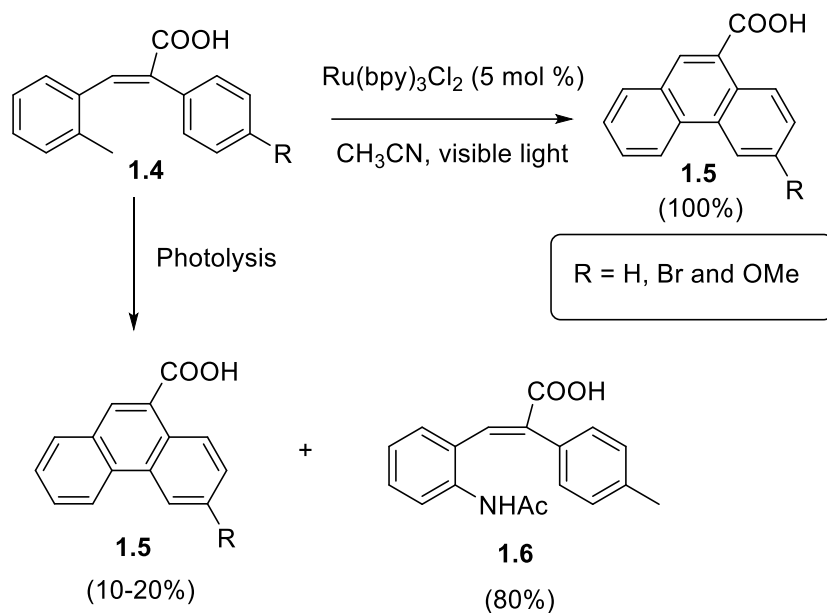
An early example of photocatalysis in organic synthesis was using $\text{Ru}(\text{bpy})_3\text{Cl}_2$ to reduce electron poor alkenes to alkanes (Scheme 1.3).¹⁷ The mechanism of this reaction involves exciting $\text{Ru}(\text{bpy})_3^{2+}$ to the $\text{Ru}(\text{bpy})_3^{2+*}$ complex, which then interacts with 1-benzyl-1,4-dihydronicotinamide (BNAH) **1.2**, forming BNAH^+ , which is then deprotonated with a base forming the BNA^\cdot radical (scheme 1.4). Two BNA^\cdot radicals then combine to form **1.3**. The new $\text{Ru}(\text{bpy})_3^+$ species that was formed by the interaction with BNAH is converted back into the ground state by the reaction with an alkene.



Scheme 1.4 - Reaction scheme of reduction of alkenes using $\text{Ru}(\text{bpy})_3\text{Cl}_2$ as a photocatalyst¹⁷

Another early use of $\text{Ru}(\text{bpy})_3\text{Cl}_2$ in organic synthesis was in 1984 by Cano-Yelo and Deronzier¹⁸ who were able to utilise $\text{Ru}(\text{bpy})_3\text{Cl}_2$ as a photocatalyst in the Pischorr reaction (Scheme 1.5). It was shown that visible light irradiation of the

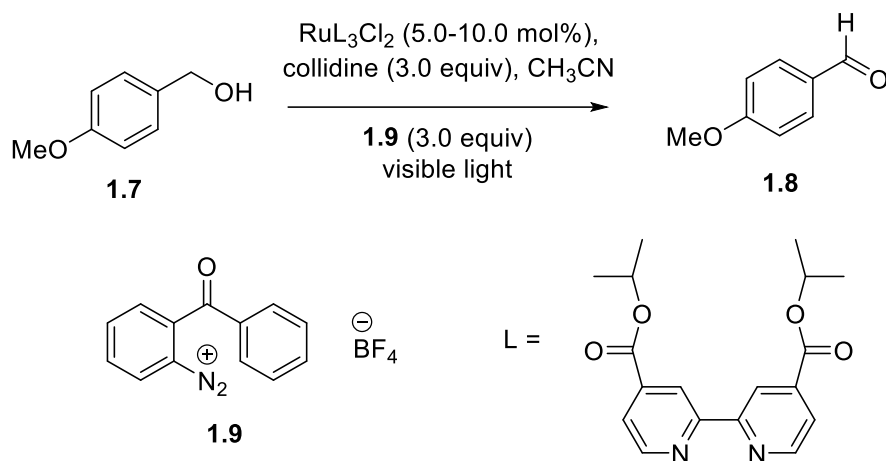
stillbenediazonium ion **1.4** without a photocatalyst resulted in the formation of the phenanthrene product **1.5** in low yields (10-20%) and produced the acetamide **1.6** as the major product due to an interaction with acetonitrile followed by hydrolysis.



Scheme 1.5 - Photocatalytic Pschorr reaction

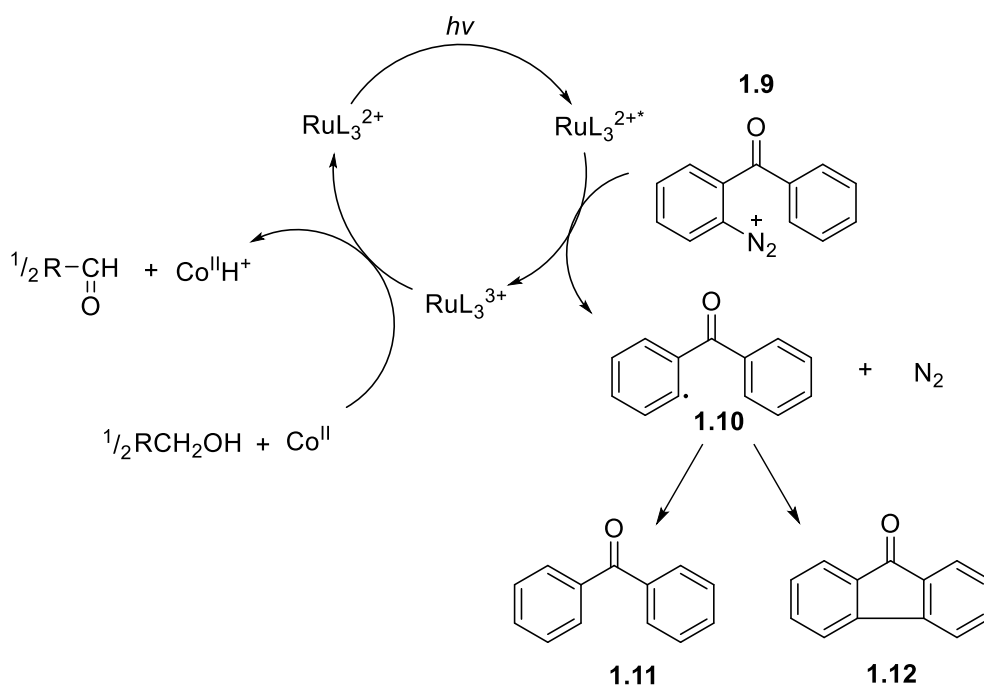
This result was not found when utilising $\text{Ru}(\text{bpy})_3\text{Cl}_2$, producing **1.5** as the only product. The mechanism for this reaction involved the excitation of $\text{Ru}(\text{bpy})_3\text{Cl}_2$ to form $\text{Ru}(\text{bpy})_3\text{Cl}_2^{2+*}$, which transferred an electron to **1.4** to produce a radical. This radical undergoes intramolecular radical arylation, which produces a species which is oxidised by the newly formed $\text{Ru}(\text{bpy})_3\text{Cl}_2^{3+}$, which is then deprotonated forming **1.5**.

Due to the success of this reaction, Cano-Yelo and Deronzier were able to use $\text{Ru}(\text{bpy})_3\text{Cl}_2$ to oxidize benzylic alcohols to their respective aldehydes (Scheme 1.6).¹⁶ It was found that the yield of this reaction decreased as the oxidation potential of the alcohol increased and the addition of excess collidine as a base increased the yield.



Scheme 1.6 - Oxidation of benzylic alcohol **1.7** to respective aldehyde **1.8** ¹⁶

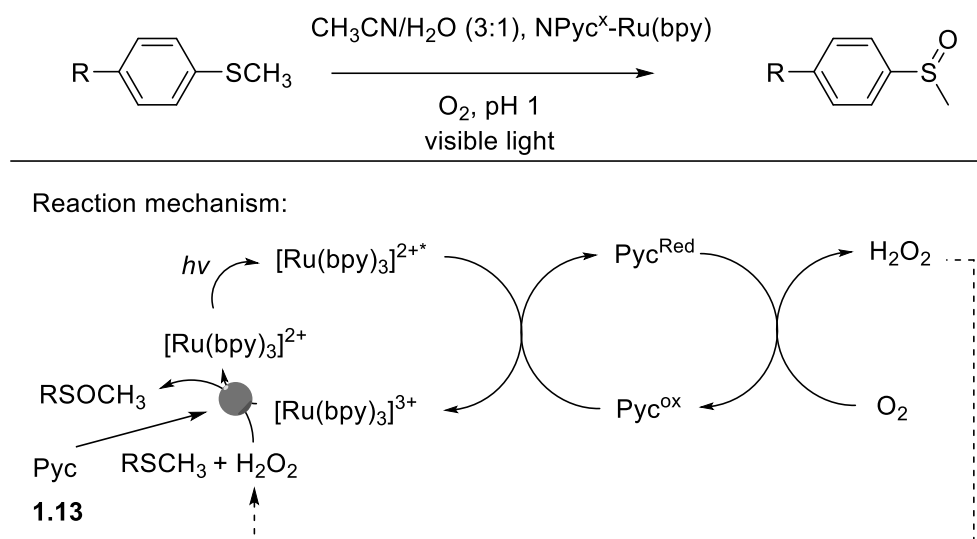
The first step in the reaction mechanism of this reaction is the excitation of RuL_3^{2+} to RuL_3^{2+*} by irradiation with visible light (Scheme 1.7). This species is quenched by the diazonium salt **1.9**, resulting in the formation of RuL_3^{3+} . The aryl radical **1.10** gives benzophenone **1.11** and fluorenone **1.12** in a 3:1 ratio, with **1.12** forming in a Pschorr reaction. The RuL_3^{3+} species can then oxidize the carbinol to produce an aldehyde, with this oxidation improved by the addition of collidine as a base.



Scheme 1.7 - Mechanism of the oxidation to aldehydes ¹⁶

Then in 2003, Zen and co-workers utilised $[\text{NPyc}^x\text{-Ru}(\text{bpy})]$ (a nafion membrane doped with a lead ruthenate pyrochlore (Pyc) catalyst and $\text{Ru}(\text{bpy})_3^{2+}$) for the

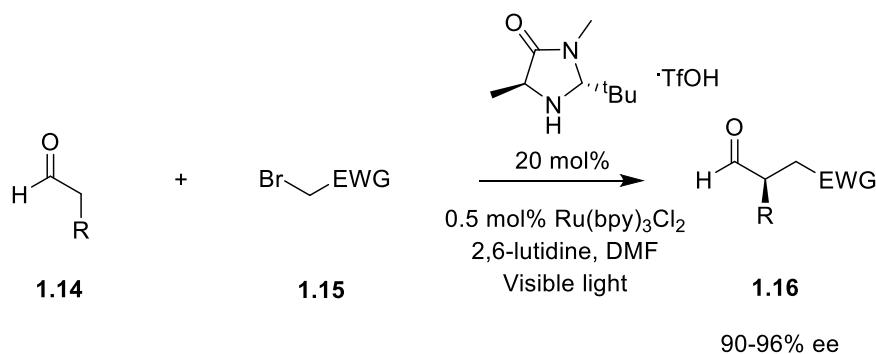
oxidation of sulfides to sulfoxides.¹⁹ The reaction mixture was irradiated with visible light and continuously purged with O₂ to afford sulfoxide in 97% yield.



Scheme 1.8 – Oxidation of sulfide to sulfoxides utilising [NPyc^x-Ru(bpy)] as a photocatalyst

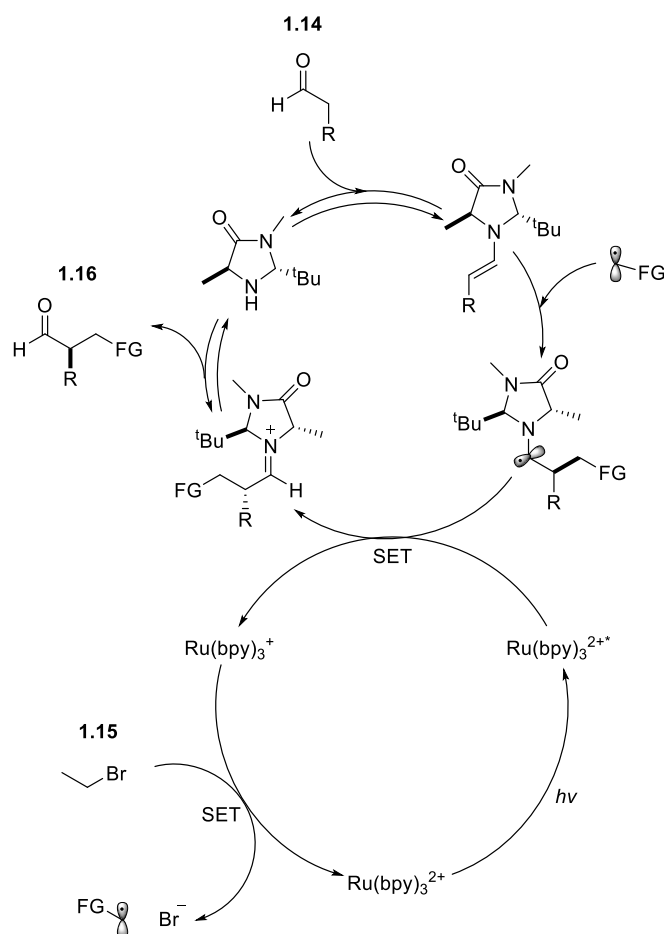
The proposed reaction mechanism utilises Pyc as a dual catalyst, acting as a reducing agent to produce H₂O₂ from O₂, while also accepting an electron from Ru(bpy)₃^{2+*} to form Ru(bpy)₃³⁺ (Scheme 1.8). The H₂O₂ produced is then able to oxidize the sulfide to a sulfoxide, while also regenerating the original ruthenium complex. This reaction was important as when this reaction is usually performed, the sulfoxide produced is oxidized further to produce a sulfone, however this did not occur in this reaction.

In 2008 three important papers on photoredox catalysis in organic synthesis were published.^{20–22} The first paper combined the emerging areas of Ru photoredox catalysis with organocatalysis for the direct asymmetric alkylation of aldehydes (Scheme 1.9).²² This required two separate catalysts, Ru(bpy)₃Cl₂ as the photocatalyst and an imidazolidinone as the organocatalyst.



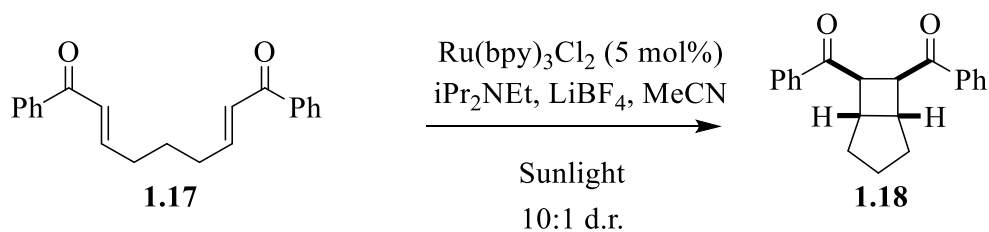
Scheme 1.9 - Reaction scheme of the direct asymmetric alkylation of aldehydes²²

Enamine formation followed by chiral auxiliary control of the approach of the electron deficient radical addition (generated from the photoredox catalyst) provides the α -alkylated product **1.16** in good yield and enantiomeric excess (Scheme 1.10).



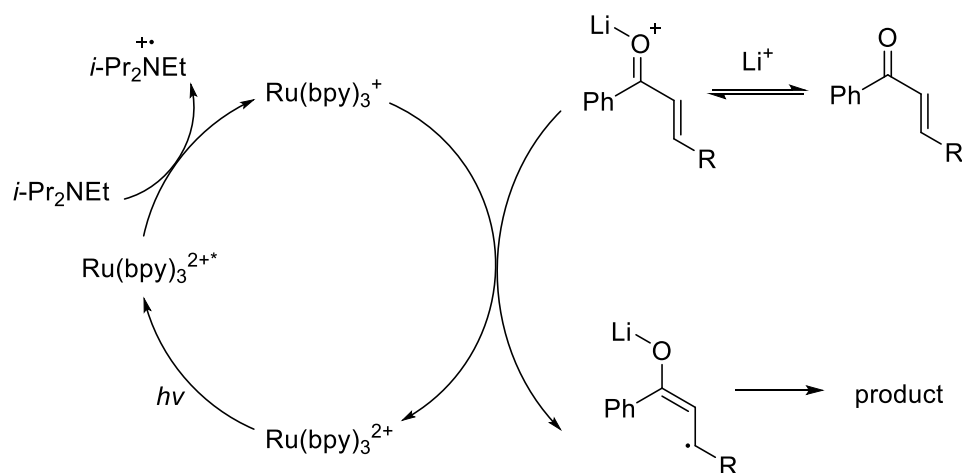
Scheme 1.10 - Photocatalytic and organocatalytic catalysis proposed mechanism

In the same year, Yoon *et al.* reported the photoredox-mediated [2+2] cycloaddition of dienones **1.17** (Scheme 1.11).²¹ Irradiation of dienone **1.17** with visible light, with $\text{Ru}(\text{bpy})_3$, $i\text{Pr}_2\text{NEt}$ and LiBF_4 in acetonitrile resulted in a [2+2] cycloaddition, forming **1.18**, with a $> 10 : 1$ diastereomeric ratio.



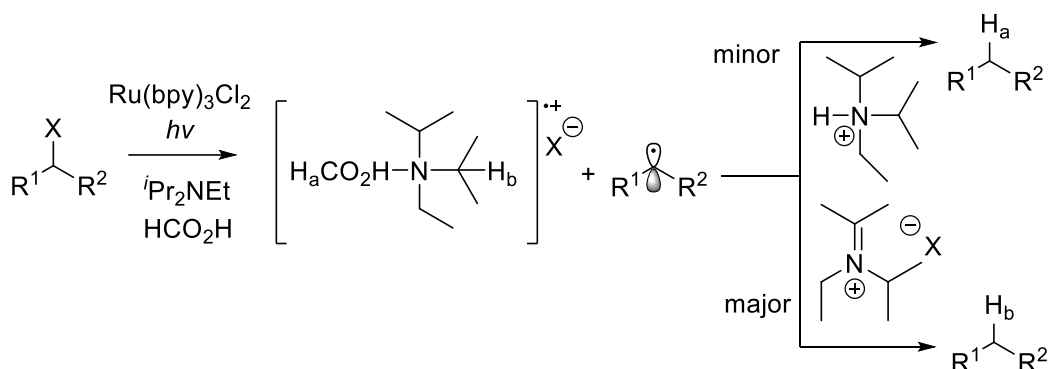
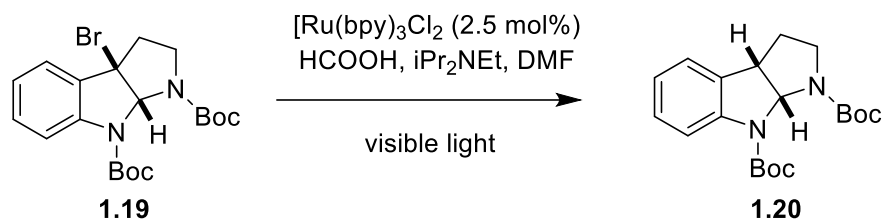
Scheme 1.11 - Reaction scheme of [2+2] dienone cycloaddition

In this case, the photoexcited $\text{Ru}(\text{bpy})_3^{2+*}$ undergoes reductive quenching by $i\text{-Pr}_2\text{NEt}$ to furnish the $i\text{-Pr}_2\text{NEt}^{\bullet+}$ radical cation and $\text{Ru}(\text{bpy})_3^{3+}$ which acts as a strong reducing agent, and transfers an electron to the lithium activated enone, initiating the [2+2] cycloaddition (Scheme 1.12).



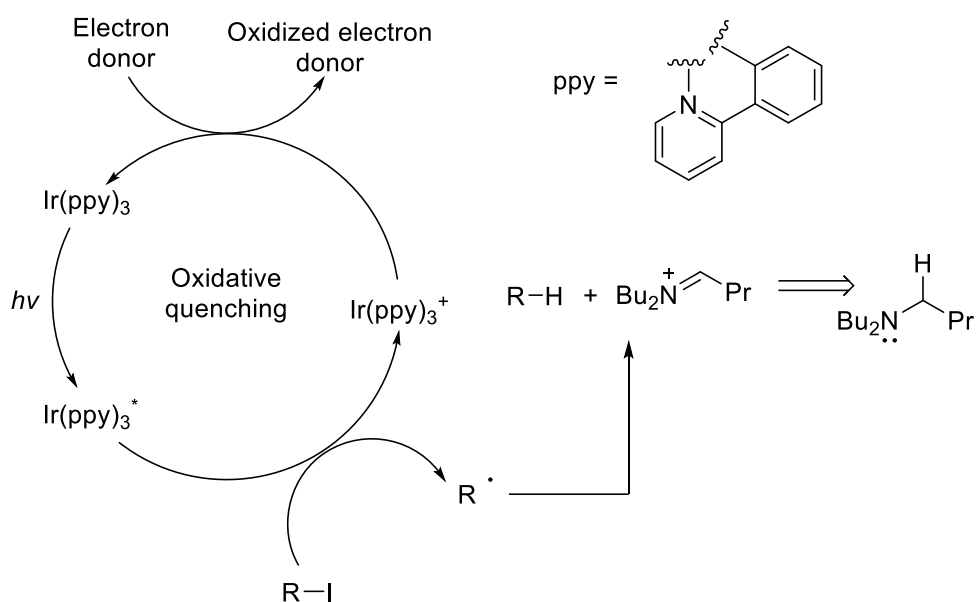
Scheme 1.12 - Reaction mechanism of [2+2] dienone cycloadditions

In 2009 Stephenson *et al.* (Scheme 1.13) was able to further develop photoredox-mediated reductive dehalogenation.²⁰ This paper once more utilised the $\text{Ru}(\text{bpy})_3\text{Cl}_2$ as a photoredox catalyst in both a reductive and oxidative manifold. The reaction proceeded with photoexcited $\text{Ru}(\text{bpy})_3^{2+*}$ reductively quenched by $i\text{-Pr}_2\text{NEtHCO}_2\text{H}$ to form $\text{Ru}(\text{bpy})_3^{3+}$, which initiated an electron transfer to cleave the C-X bond α - to the electron withdrawing group *via* the corresponding radical anion to generate an alkyl radical. This alkyl radical is then reduced to form the final dehalogenated product **1.20**.²⁰



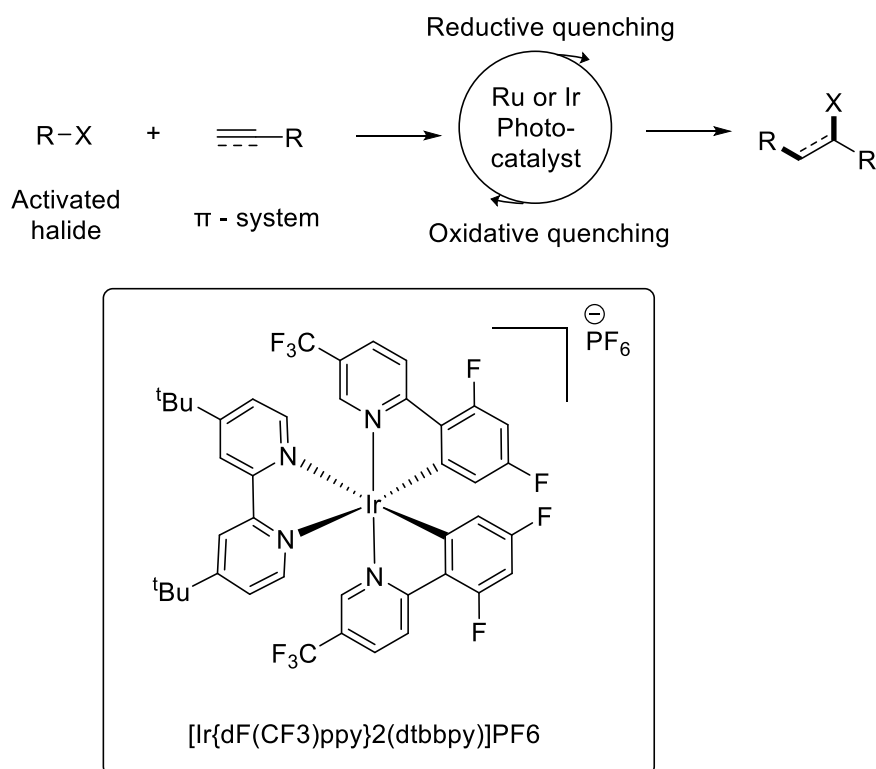
Scheme 1.13 - Reaction scheme for photoredox-mediated reductive dehalogenation reaction

Due to the similar properties of iridium and ruthenium poly-pyridyl complexes, there are a range of reactions that utilize iridium complexes in the same way as ruthenium complexes, sometimes resulting in improved catalytic activity, e.g., the reduction of alkyl, aryl, and alkenyl iodides by Stephenson *et. al.*²³ The general approach involves irradiation of Ir(ppy)₃ by visible light, which generates an excited iridium species which donates an electron to the carbon-iodide bond (Scheme 1.14). The radical anion formed cleaves to produce iodide (I⁻) and the desired carbon radical (R[•]). The resulting Ir(ppy)₃⁺ species is then reduced to its ground state by an electron donor (tributylamine or Hantzsch ester). The carbon radical produced undergoes hydrogen atom abstraction to give the desired reduced product. Ir(ppy)₃ was used in a similar method by Lee and Kim in the transformation of other organohalides.²⁴



Scheme 1.14 - Proposed mechanism for radical reductive cleavage of alkyl, alkenyl and aryl iodides

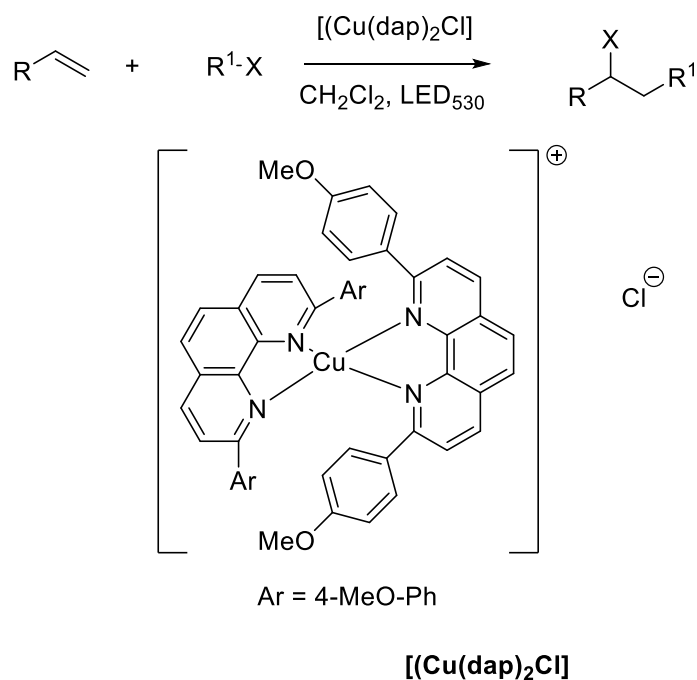
Stephenson and co reported the use of both $[Ir\{dF(CF_3)ppy\}_2(dtbbpy)]PF_6$ and $[Ru(bpy)_3]Cl_2$ for the atom transfer radical addition (ATRA) of haloalkanes onto alkenes and alkynes using a redox process (Scheme 1.15).²⁵



Scheme 1.15 - Mechanism for atom transfer radical addition (ATRA) of haloalkanes²⁵

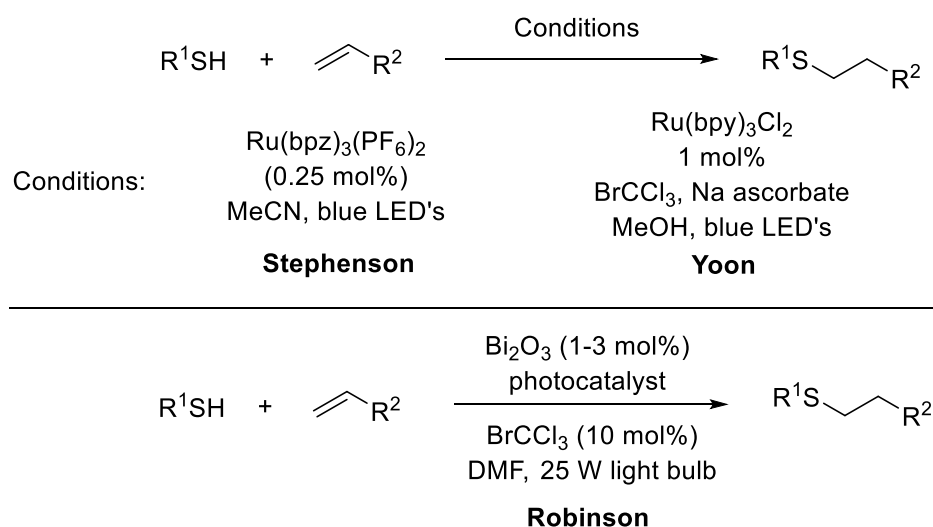
While many reactions have been reported to be catalysed by ruthenium and iridium complexes, their high cost and toxicity has inspired alternatives using lower costing

metal derivatives or non-metal compounds to be developed. One example of this is the use of $\text{Cu}(\text{dap})_2\text{Cl}$ to catalyse ATRA reactions in visible light (530 nm) or sunlight, in much the same way as the Ir and Ru complexes described earlier (Scheme 1.16).²⁶ A light source with a wavelength of 530 nm was chosen as $\text{Cu}(\text{dap})_2\text{Cl}$ absorbs light strongly between 400-600 nm.



Scheme 1.16 – Reaction scheme of copper catalysed ATRA

Alternatives to the ruthenium mediated thiol-ene coupling of alkenes with thiols reported by Yoon²⁷ and Stephenson²⁸ have been developed by Robinson *et al*, who were able to use a bismuth oxide based photocatalyst for the initiation of radical thiol-ene reaction (Scheme 1.17).²⁹ Unfortunately, catalyst loadings were higher and other additives (e.g. BrCCl_3) were required.



Scheme 1.17 - Mechanism of thiol-ene coupling of alkenes and thiols

The ability to use metal-free complexes as photocatalysts have two major benefits over metal complexes, reducing cost and the need to remove potentially toxic metals. A class of metal-free compounds of great historical and contemporary interest are organic dyes, as many absorb light across the visible spectrum, as well as being non-toxic. One of the most studied metal-free photocatalysts is Eosin Y, due to it being cheap, non-toxic, and having a relatively simple structure (Figure 1.1).

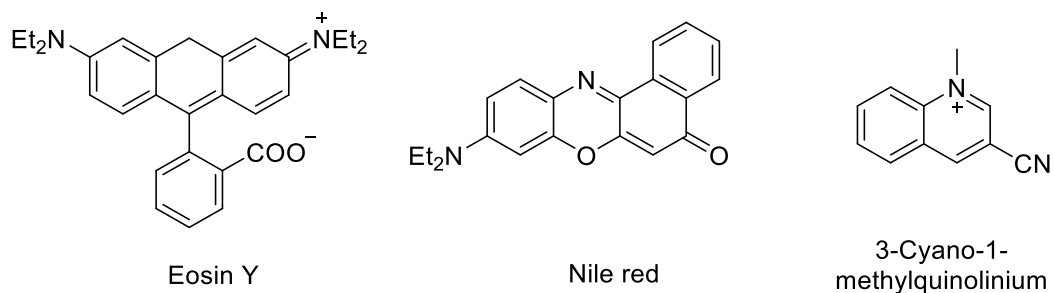
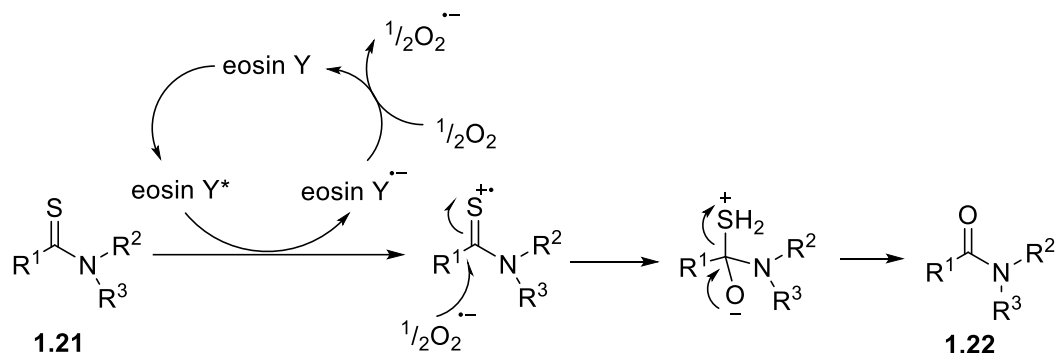
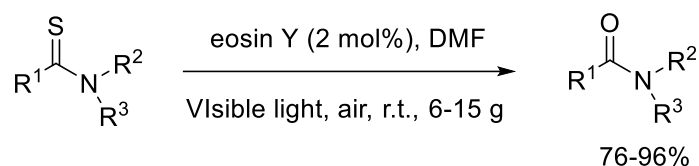


Figure 1.1 - Structure of organic compounds investigated as photoredox catalysts in organic synthesis. Eosin Y absorbs green light, with a characteristic peak in the UV-vis spectrum at 539 nm.³⁰ In the same way as the Ru and Ir catalysts described earlier, Eosin Y was used in a variety of organic synthesis reactions, some examples including bromination³⁰, desulfurization³¹ and arylation.^{32,33}



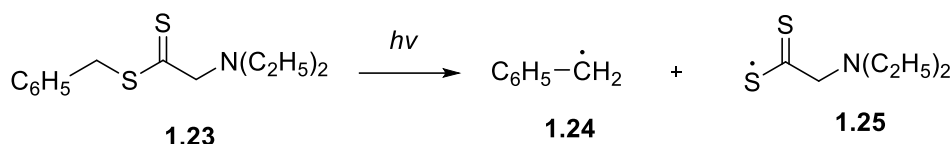
Scheme 1.18 - Aerobic desulfurization of thioamides into amides

The desulfurization of thioamides using Eosin Y is shown in Scheme 1.18 and shows photoexcited Eosin Y undergoing a single electron transfer with the thioamide species **1.21**, and the ground state reformed after quenching with oxygen. This is just one example of a move towards greener chemistry, using sustainable materials and less toxic photocatalysts.

1.4 Evolution of photopolymerisation

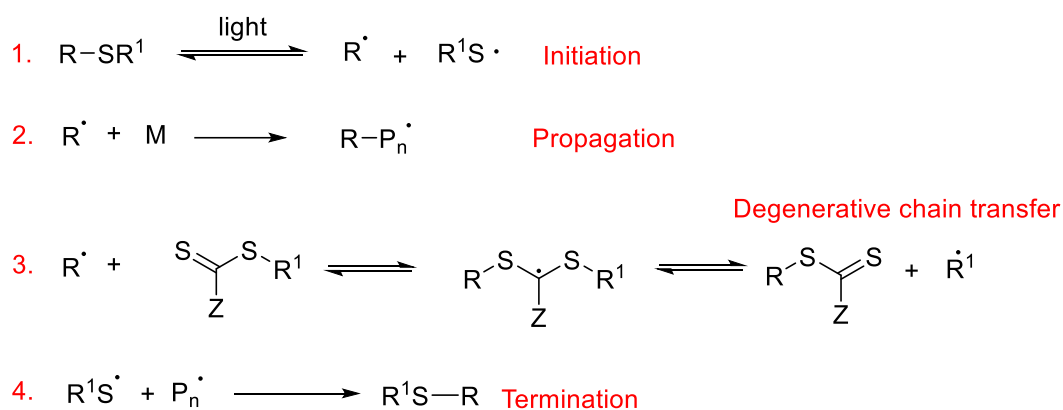
Photopolymerisation has been of great interest due to its cost effectiveness and lower environmental impact when compared to thermally initiated polymerisations. A photo excited species is able start a polymerisation *via* two main mechanisms. The first mechanism (type a) is an intramolecular homolytic bond cleavage. This results in the formation of two radicals, which can initiate a polymerisation. The second mechanism (type b) is a photoredox process, in which there is a single electron transfer between the photoexcited photoinitiator and a suitable donor or acceptor, resulting in the polymerisation of the newly formed radical species.

In 1981, Otsu *et al* polymerised methyl methacrylate (MMA) using *S*-benzyl-*N,N*-diethyldithiocarbamate **1.23** as a photoiniferter in an intramolecular process (type a). *S*-benzy *N,N*-diethyldithiocarbamate **1.23** was irradiated with UV light, which caused photodissociation of the C-S bond (Scheme 1.19), which resulted in the formation of radicals (**1.24** and **1.25**).³⁴ This reaction was one of many using thiocarbonylthio compounds as photoiniferters.



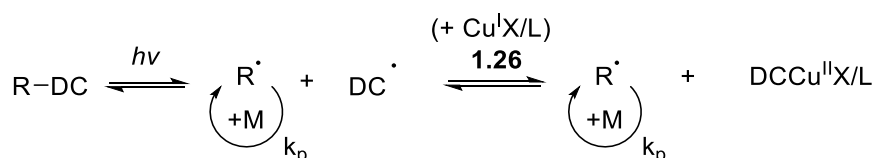
Scheme 1.19 - Formation of radicals from irradiating *S*-benzyl-*N,N*-diethyldithiocarbamate **1.23** with UV light to form radicals **1.24** and **1.25**

It was found that the benzyl radical ($\text{R}\cdot$) was more reactive towards the monomer MMA (M) than the thiyl radical ($\text{R}^1\text{S}\cdot$), therefore would primarily participate in the initiation of the polymerisation, while the thiyl radical would primarily perform the termination. Degenerative chain transfer to **1.23** was observed as expected (Scheme 1.20).



Scheme 1.20 – General mechanism for photopolymerization using inferfers³⁵

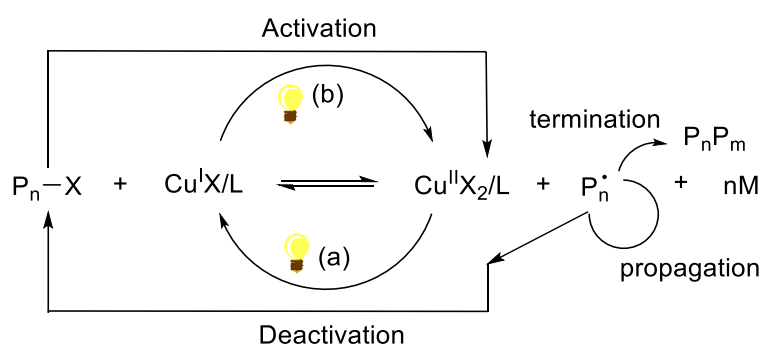
In 2010, Matyjaszewski *et al* introduced further control in this type of polymerisation by combining the inferfer polymerisation with ATRP, by introducing copper complexes (Scheme 1.21).³⁶ Much like the Otsu procedure, the dithiocarbamate (R-DC) is irradiated with UV light to produce two radicals ($\text{R}\cdot$ and $\text{DC}\cdot$). The inefficient chain transfer reactions that occurred from the thiyl radical ($\text{DC}\cdot$) were prevented due to the thiyl radical being deactivated by the copper (I) complex.



Scheme 1.21 – General mechanism for copper mediated dithiocarbamate polymerisation under UV light

This resulted in the more well-defined polymers and better control over the polymerisation.

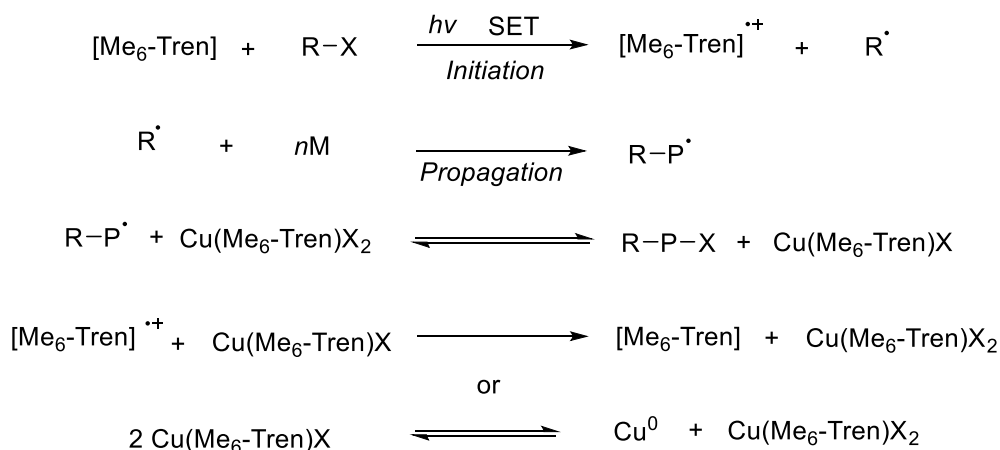
Then in 2011, Tasdelen *et al* directly activated the Cu^I complex itself with UV light.³⁷ The polymerisation was initiated by *in situ* photochemical generation of a Cu^I complex from a Cu^{II} species, resulting in a reaction with the alkyl halide (P_n-X). This forms the radical P_n[•], which can propagate by the addition of monomers, can terminate, and be deactivated by a reaction with Cu^{II}X₂/L (Scheme 1.22).



(a) Generation and regeneration of activators and (b) the acceleration of polymerisation

Scheme 1.22 – General mechanism of copper complex mediated polymerisation in UV light

A drawback of the method presented by Taselden is that equimolar amounts of copper catalyst and initiator is required. To combat this, a method for the photo catalysed ATRP of MMA was discovered, which involved using ppm amounts of CuBr₂ using UV light.³⁸ Matyjaszewski was able to expand the photochemically induced ATRP to use visible light, with Cu^{II}Br₂/L (L = tris(2-pyridylmethyl) amine, or N,N,N',N'',N''-pentamethyldiethylenetriamine, or tris((4-methoxy-3,5-dimethylpyridin-2-yl)methyl)amine) being the photocatalyst.³⁹ It was found the Cu^{II} complex could be reduced by visible light, with the reduction occurring due to ligand to metal charge transfer. This yielded a Cu^I complex and a bromine radical that initiated polymerisation. Polymerisation occurred when the reaction was irradiated with light sources of 392 and 450 nm, however no polymerisation occurred at 631 nm. It was shown that sunlight was also a viable light source of the polymerisation. The study of copper complexes was furthered by Haddleton *et al*, who used tris[2-(dimethylamino)-ethyl]amine (Me₆-TREN) as a ligand for photocatalysed ATRP.³⁹

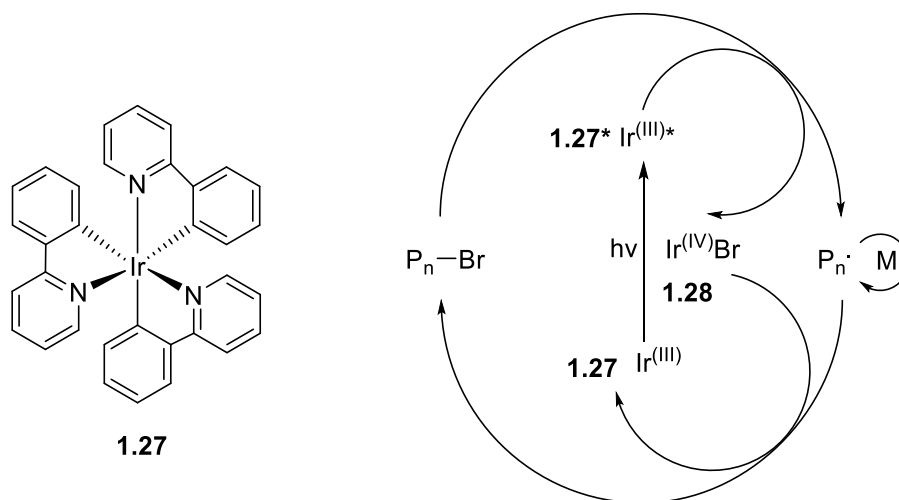


Scheme 1.23 - Proposed mechanism for outer sphere electron transfer (OSET)-living radical polymerisation⁴⁰

The mechanism for this reaction is shown in scheme 1.23. The growing radical chain R-P· can be capped by halogen atom transfer from the Cu(II)(Me₆-TREN)X₂ to provide the corresponding Cu(I)(Me₆-TREN)X complex which upon reaction with the oxidised (Me₆-TREN)^{•+} radical cation regenerates the (Me₆-TREN) initiator.

Copper complexes are not the only metal complexes studied for photo-controlled living type polymerisations. Due to the wide range of organic synthesis reactions using iridium and ruthenium complexes as photocatalysts, Hawker *et al* investigated how the Ir(ppy)₃ photoredox system can be utilized in order to polymerize methacrylate monomers (Scheme 1.24).⁴¹

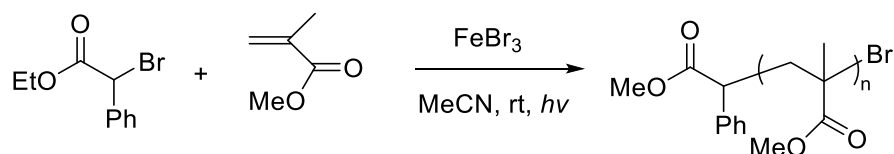
Fac-[Ir(ppy)₃] **1.27** was the catalyst studied and once irradiated with visible light formed the excited species *Fac*-[Ir(ppy)₃]^{*}. Electron transfer to the alkyl halide generates a radical (P_n·) and a Ir^{IV}(ppy)₃Br species **1.28**. The growing polymer chain (P_n·) can undergo halogen atom transfer to regenerate the ground state Ir(ppy)₃ **1.27**. The benefit of this reforming of the ground state is that the living ATRP process is photochemically controlled. This process was successful for methacrylate and acrylate monomers.



Scheme 1.24 - Mechanism for Ir(ppy)₃ mediated visible light-controlled polymerisation

Yang and co-workers further widened the scope of this approach by studying how different solvents effected polymerisation using Ir(ppy)₃ **1.27**, investigating anisole, DMF and acetonitrile.⁴² The polymerisation of MMA using ethyl α -bromisobutyrate (Ebib) as an initiator in anisole provided the best control over molecular weights. Ru(bpy)₃Cl₂ has also been used as a photoredox catalyst in visible light polymerisations in a similar approach.^{43,44}

Another metal that has been studied as a photoredox catalyst in polymerisations is iron.⁴⁵ Iron bromide complexes had been used previously in thermal polymerisations,³⁴ however due to the increased interest in using light as an initiator in polymer chemistry, Matyjaszewski *et. al* developed a method that used UV light to initiate an ATRP polymerisation (Scheme 1.25).

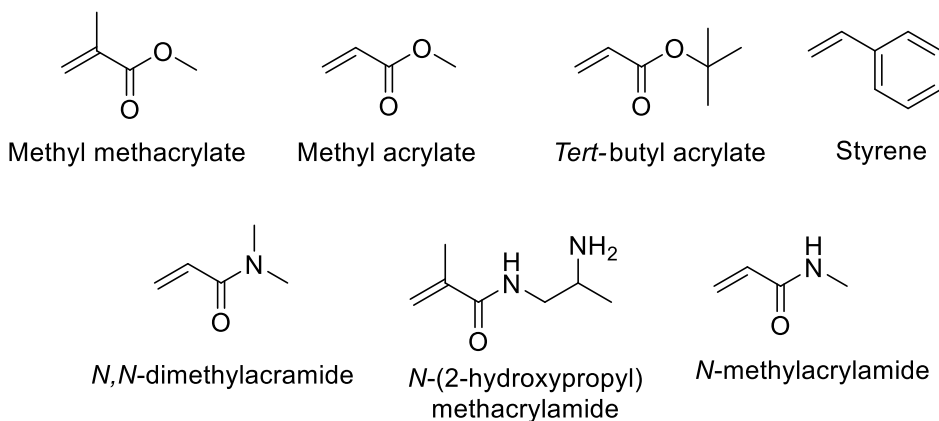


Scheme 1.25 - Fe-based ATRP reaction

The method presented by Matyjaszewski is notable in that it did not utilise additional ligands, reducing agents or radical initiators.⁴⁷ The proposed mechanism involved the photoreduction of Fe (III) to Fe (II) using the monomer, resulting in the alkyl halide initiator formed in situ, as well as direct photoactivation of the Fe(II) species. Other metal complexes that have been utilised as photocatalysts for light controlled polymerisation include niobium⁴⁸ and zinc based metal organic frameworks.⁴⁹

Most of the methods described so far have used alkyl halide to generate radicals to initiate polymerisations (normally *via* radical anions), however another large class of compounds used in photoredox polymerisations are thiocarbonylthio compounds such as CPADB, (Figure 1.2), or trithiocarbonate compounds such as BSTP and BTPA, (Figure 1.2).

Example monomers:



Example RAFT agents:

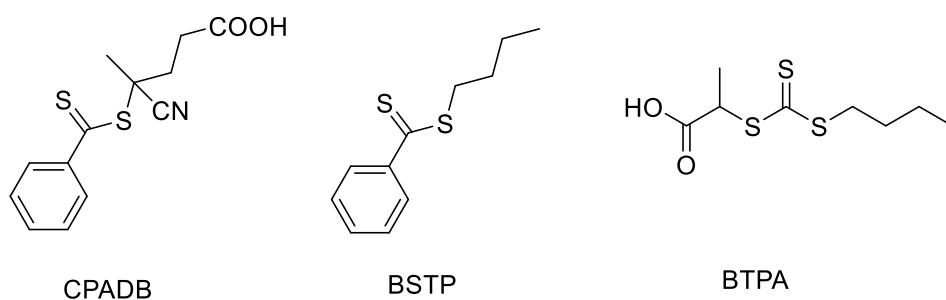


Figure 1.2 - Examples of RAFT agents and monomers used by Boyer *et al* in polymerisations using *fac*-[Ir(ppy)₃] **1.27**.⁵⁰

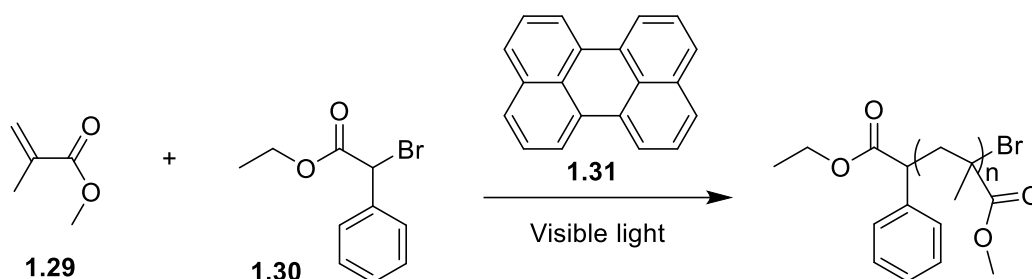
One of the first catalysts used for these polymerisations was *fac*-[Ir(ppy)₃] **1.27**. In 2014, Boyer *et al* managed to use *fac*-[Ir(ppy)₃] **1.27** to photocatalyse a wide range of monomers using visible light and thiocarbonylthio compounds.⁵⁰ The mechanism employed was similar to that used by Hawker, who instead of using thiocarbonylthio compounds used alkyl halides.⁴¹ They were able to control molecular weights of the polymers, producing polymers with narrow molecular weight distributions. One of the key attributes of this polymerisation was the ability to polymerise monomer in the presence of oxygen, as the iridium photocatalyst has the ability to act as an oxygen scavenger. Boyer *et al* further expanded their work by utilising Ru(bpy)₃Cl₂ in the

same reaction, with them being able to polymerise methyl acrylates, methacrylate's and acrylamides.⁵¹

1.5 Metal-free photocatalysis

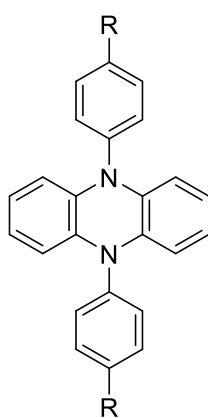
Just as in organic synthesis the current trend is to identify and apply metal free organic photoredox catalysts in order to reduce the expense, toxicity and unsustainable nature of the metal-based materials.

The first report of a metal free ATRP polymerisation was by Theriot and Miyake (Scheme 1.26),⁵² who used perylene **1.31** and alkyl bromides **1.30** to polymerise acrylates **1.29** and styrene. Once perylene is exposed to UV light it becomes a strong reductant, transferring an electron to the alkyl bromide.



Scheme 1.26 - The use of perylene **1.31** as an organic photocatalyst for the polymerization of methyl methacrylate (MMA) **1.29** with alkyl bromide **1.30** initiator.⁵²

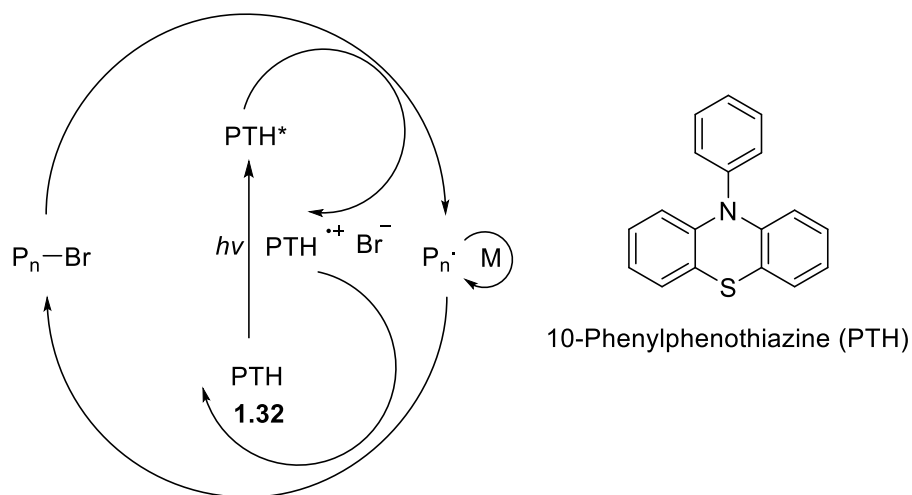
This work was further improved by using a class of photocatalysts with 5,10-diphenyl-5,10-dihydrophenazine at its core.⁵³ These catalysts were then modified with various substituents, including electron-donating, electron-withdrawing and neutral groups (Figure 1.3).



R = H, OMe, CF₃, CN

Figure 1.3 - Structures of modified 5,10-diphenyl-5,10-dihydrophenazine

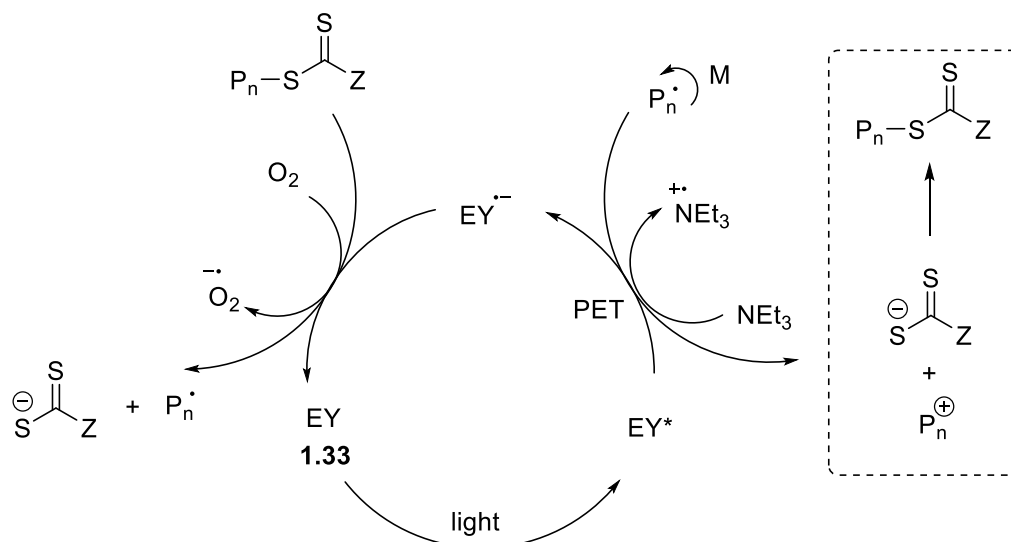
Photocatalysts were designed that were able to provide good control over polymerisations ($M_w/M_n = 1.10 - 1.15$). Hawker and co-workers were then able to progress these studies by helping develop a metal-free ATRP system using 10-phenylphenothiazine **1.32** as a catalyst, using a similar reaction mechanism as the photopolymerisation using fac-Ir(ppy)_3 (Scheme 1.27).⁵⁴



Scheme 1.27 - Reaction mechanism of the polymerisation of various monomers using 10-phenylphenothiazine as a photocatalyst.⁵⁴

Another metal free compound that was able to be utilised in visible light photoredox polymerisation was Eosin Y.⁵⁵ Boyer *et al* studied a wide range of photocatalysts to perform a visible light mediated radical polymerisation of methacrylates and found eosin Y to be the most effective.

It has been found that the photoexcited version of Eosin Y **1.33** undergoes intersystem crossing from a singlet excited state to a triplet excited state. The triplet excited state has strong oxidizing and reduction potential, making it suitable for photoredox polymerisation. Eosin Y was able to perform visible light mediated polymerisation utilising a photoinduced transfer-reversible addition-fragmentation mechanism, displaying good control over molecular weight and polydispersities.



Scheme 1.28 - PET-RAFT polymerisation mechanism mediated by Eosin Y (EY) in the presence of triethylamine and oxygen.

It was also found that the addition of a tertiary amine allowed the polymerisations to proceed in oxygen, participating in a reductive quenching cycle (Scheme 1.28).

1.6 Porphyrins

Porphyrins are heterocyclic molecules, that are composed of four pyrrole units connected by methine bridges (Figure 1.4). Porphyrins are aromatic due to 18 π -electrons forming a planar cycle.

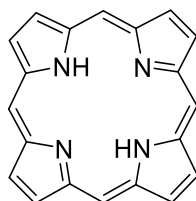


Figure 1.4 - Structure of most basic porphyrin structure (theoretical)

Due to the aromaticity of the porphyrin ring, porphyrins absorb light strongly across the electromagnetic spectrum.⁵⁶ The four nitrogen's at the centre of the porphyrin ring allows for metal complexes to be formed. When no metal is present at the centre of the porphyrin, they are called free base porphyrins. Porphyrins are widely found throughout nature, with the most noticeable example of this being part of the structure of heme, which is a precursor to haemoglobin. Porphyrin is a coordination complex in heme, with an iron atom coordinating to the porphyrin ring. Also, porphyrins play an important role in photosynthesis of plants, with the structure of chlorophyll a containing a porphyrin.

The characteristics of the absorption spectrum of metal-free porphyrins consist of two distinct regions: near the UV region and in the visible region.⁵⁶ The electron absorption near the UV region is called the Soret band, and usually absorbs light between 380-500 nm. This absorption is caused by the transition of the ground state to the second excited state. The wavelength range of the absorption depends on structural modifications to the porphyrin. The second region usually contains four bands (Q bands) with lower absorption and is called the Q region. This is due to the weak transition from the ground state to the first excited state, with the absorption range of 500-750 nm. The relative intensity of the Q region bands depends on the substituents on the porphyrin macrocycle.

When a metal is inserted into the centre of the porphyrin core, the absorption properties are affected. Due to the increased symmetry of the molecule, the Q region is simplified to only contain 2 Q bands (α and β). The intensities of these bands depend on the stability of the metal complex formed.

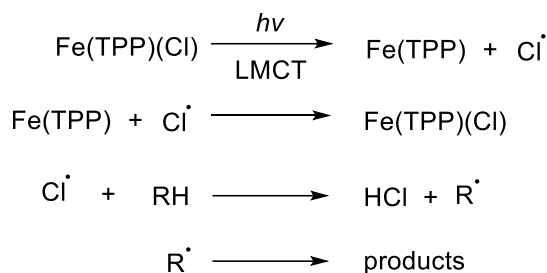
Due to these absorption characteristics, porphyrins have been the subject of great interest. They have been used in organic reactions⁵⁷⁻⁵⁹, photovoltaic chemistry⁶⁰⁻⁶², and medicine (photodynamic therapy)⁶³⁻⁶⁵.

1.7 Porphyrins used as photocatalysts

A useful property of photoexcited porphyrins is that they exhibit an affinity for both oxidation and reduction, however most of the research undertaken when studying porphyrins as photocatalysts in organic synthesis study the oxidation of compounds by the photoexcited porphyrin.

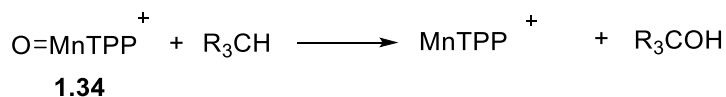
1.7.1 Organic synthesis

It has been shown that halogenated iron porphyrins are able to form radicals when photoexcited.⁶⁶ The radicals are formed by ligand-to-metal charge transfer (LMCT), and the resulting halide radical is able to interact with other organic compounds (cumene, ethylbenzene, toluene, and cyclohexane) (Scheme 1.29).



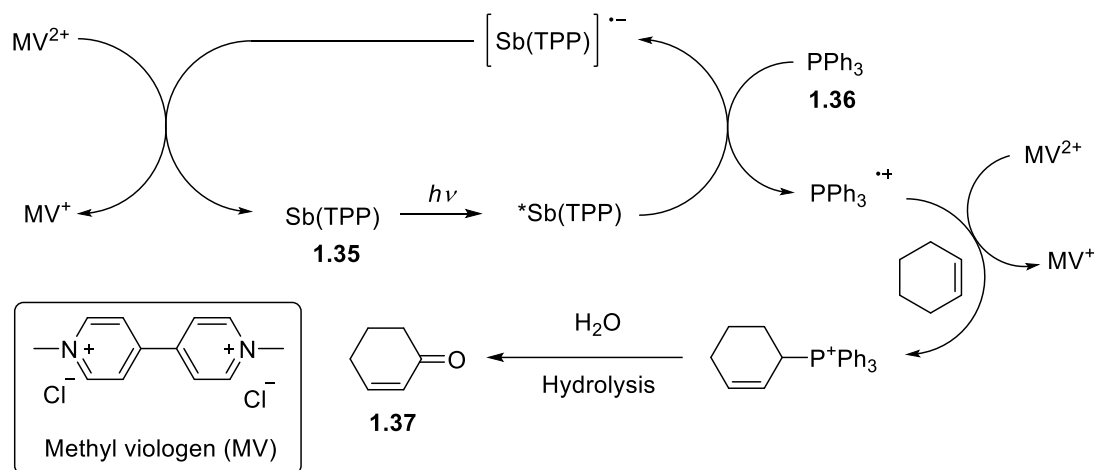
Scheme 1.29 – Formation of radicals using halogenated iron Fe(TPP)Cl⁶⁶

Other metal TPP complexes have been used to oxidise organic molecules. A variety of cyclic hydrocarbons were oxidized using either Mn^{III}(TPP) perchlorates and periodates (Scheme 1.30).⁶⁷ The ClO₄ or IO₄ act as oxygen sources by binding to the Mn^{III}(TPP). These complexes were irradiated with light, resulting in the formation of O=Mn(TPP)⁺ **1.34**, which can participate in oxidation of hydrocarbons.



Scheme 1.30 - Example of O=MnTPP⁺ **1.34** oxidising a hydrocarbon to form an alcohol

Inoue *et al* have utilised a large range of metallic porphyrins in organic synthesis often in conjunction with other organic redox active molecules such as viologens.^{68–74} One particular example used Sb^V(TPP) **1.35** for the photochemical oxygenation of cyclohexene to give cyclohexanone in water (Scheme 1.31).⁷⁰

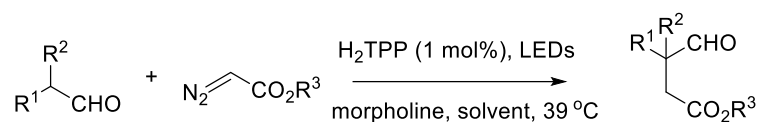


Scheme 1.31 - Mechanism of oxidation of cyclohexene using Sb^V(TPP) **1.35**, PPh₃ **1.36** and methyl viologen

The reaction mechanism of this oxidation involves the photoexcited Sb^V(TPP)* species being reductively quenched by PPh₃ **1.36** to give the PPh₃ radical cation and

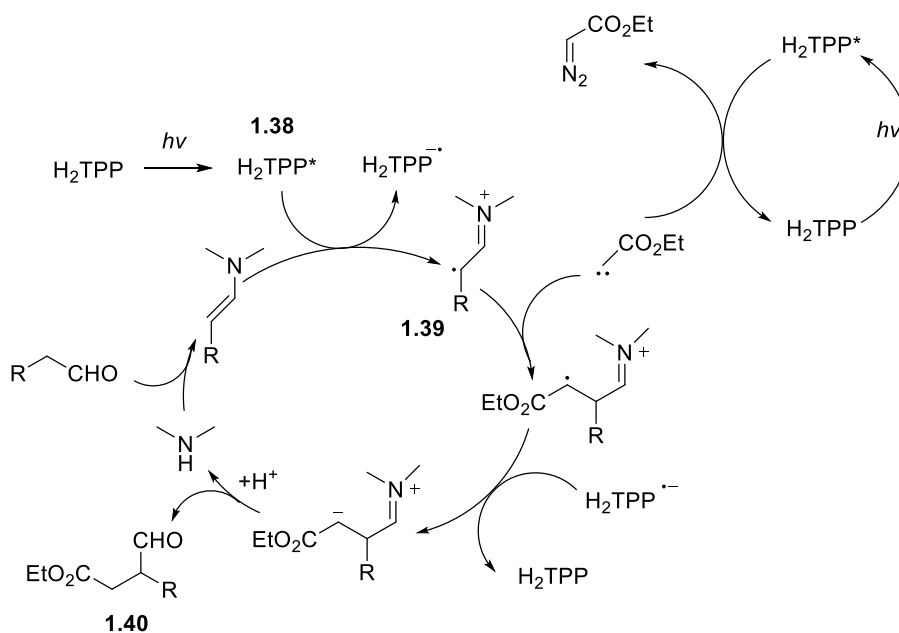
the Sb(TPP) radical anion respectively (Sb^{IV}). The reduced porphyrin then transfers an electron to methyl viologen (MV), reforming the ground state (Sb^{V}) and generating the MV^+ , (noting transfer of an electron from PPh_3 radical cation to MV^{2+} can also occur.) The PPh_3 cation that was formed binds to cyclohexene forming a C-P bond which upon hydrolysis forms cyclohexanone **1.37** (i.e. a C=O has been formed in the transformation).

More recently, porphyrins have been used in photoredox mechanisms for the formation of C-C bonds. In 2016, Gryko *et al* showed that photoexcited porphyrins can participate in energy and electron transfer simultaneously.⁷⁵ The porphyrins used were tetraphenylporphyrin (H_2TPP) and zinc tetraphenylporphyrin (ZnTPP), and they were able to use them for the photoredox α -alkylation of aldehydes with diazo compounds (Scheme 1.32).



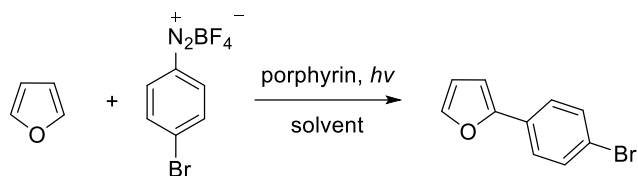
Scheme 1.32 – α -Alkylation of aldehydes using porphyrins as photocatalysts

The proposed mechanism of α -functionalisation is illustrated in scheme 1.33 and shows the essential interaction between the photoexcited porphyrin and ethyl diazoacetate, forming a carbene in the triplet state. Simultaneously, an aldehyde reacts with a secondary amine, producing an intermediary enamine. A photoexcited H_2TPP **1.38** then oxidized the enamine to form a H_2TPP radical anion and an iminium cation radical **1.39**. This iminium cation radical interacts with the carbene species, forming a new radical species, after which an electron is transferred from H_2TPP radical anion (regenerating H_2TPP) and protonation of the resulting enolate forms the final product **1.40**.



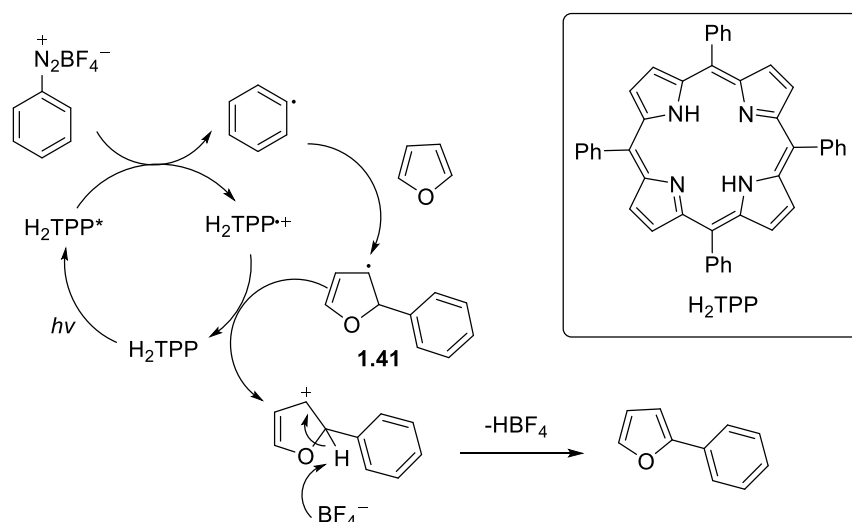
Scheme 1.33 - Mechanism for light induced functionalization of aldehydes with EDA in the presence of tetraphenylporphyrin⁷⁵

Following this study, Gryko *et al* showed that porphyrins are suitable photoredox catalyst for the direct C-H arylation of heteroarenes with diazonium salts, although in this case the excited H₂TPP forms a radical cation (Scheme 1.34).⁷⁶



Scheme 1.34 – Reaction scheme of C-H arylation of heteroarenes with diazonium salts

The mechanism proposed is shown in scheme 1.35 and involves the photoexcited H₂TPP* species reducing the diazonium salt, giving an aryl radical and the H₂TPP radical cation. The aryl radical adds to the furan to form the allylic radical **1.41**, which is upon oxidation by the H₂TPP radical cation, followed by proton elimination, furnishes the arylated furan product and regenerates the ground state catalyst. The reaction scope was widened by using diazonium salts with different functional groups, as well as arylating thiophene and coumarin.



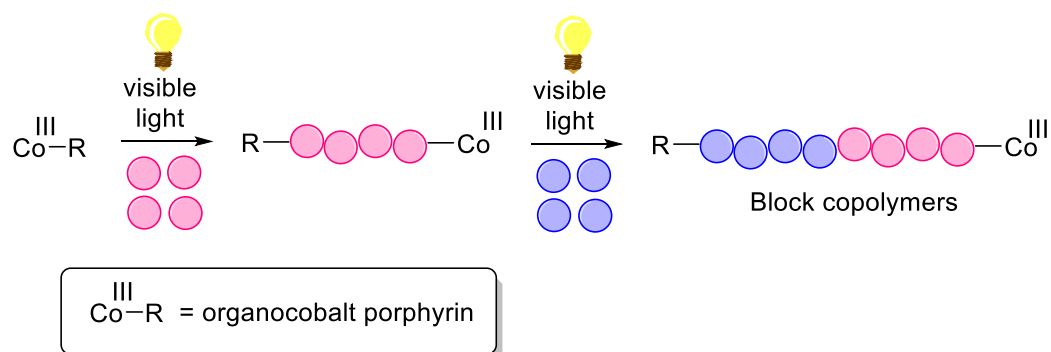
Scheme 1.35 - Mechanism for arylation of heterocycles with diazonium salts using H₂TPP

Other metals porphyrin complexes that have been used in organic synthesis include rhodium^{77,78}, cobalt⁶⁷, and nickel⁷⁹.

1.7.2 Porphyrins as photocatalysts in polymerisation

In the 1990s porphyrins were utilized as photocatalysts in polymerisations,^{80–82} in this instance aluminium porphyrins were used in ionic polymerisations.⁸³ More recently, Matyjaszewski *et al* used naturally occurring hemin and synthetic derivatives to perform ATRP.⁸⁴

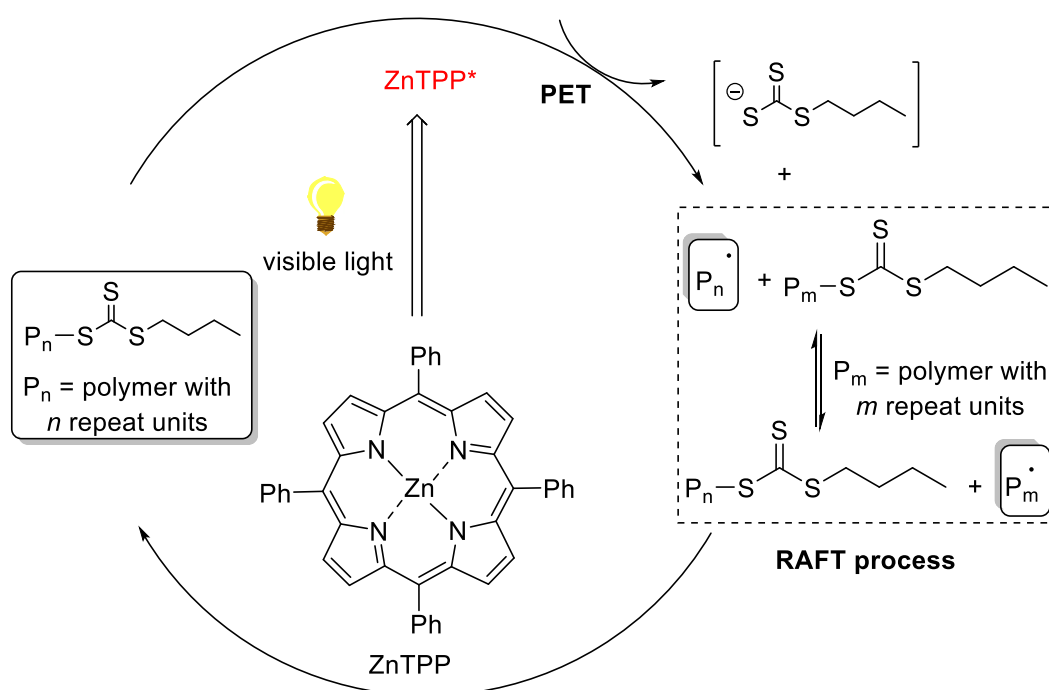
It has been reported that metalloporphyrin's can be used as photoredox catalysts to catalyse free-radical polymerizations, but very little work has involved metal free porphyrins or natural porphyrins (e.g. chlorophyll).^{85–88} Most catalysts are initiated by UV light with few reports initiated by lower energy visible light, one exception is an organocobalt porphyrin reported by Yaguang Zhao *et al* (Scheme 1.36).



Scheme 1.36- Reaction scheme of visible light polymerisation, catalysed by cobalt porphyrins⁸⁹

In this process, the visible light energy initiates a homolytic cleavage of the relatively weak $\text{Co}^{\text{III}}\text{-R}$ bond, which generates a Co^{II} species and a carbon radical ($\text{R}\cdot$), which in turn initiates a polymerisation. The growing polymer chain can be capped by the Co^{II} species allowing formation of block copolymers.⁸⁶ Most metalloporphyrins use high energy UV light to initiate polymerisation. Visible light being less energy intensive is an attractive alternative for industrial applications (such as 3D printing) and significant work has focused on visible light polymerizations.^{11,90,91}

In 2015, Boyer *et al* used $\text{Zn}(\text{TPP})$ as a photocatalyst for a PET-RAFT polymerisation in visible light (Scheme 1.37).



Scheme 1.37 - Mechanism of PET-RAFT polymerisation⁸⁷

To perform the PET-RAFT polymerisation ZnTPP is excited by visible light, producing an excited species ZnTPP^* . This excited species performs an electron transfer to a RAFT agent, which then leads to the formation of a radical and a living polymerisation. The properties of ZnTPP are such that it can maintain its excited state for a relatively long period of time, increasing the chance of this electron transfer taking place. A range of different porphyrins were tested as photocatalysts for the polymerisation of MA, including metal free H_2TPP , as well as different metalated complexes.

This work was furthered by synthesising a novel porphyrin compound that attached the initiating trithiocarbonylthio species directly to porphyrin (TPP-BSTP, Figure 1.5).⁹² The proposed mechanism would involve the porphyrin absorbing the visible light, and upon being photoexcited donate an electron to the thiocarbonylthio group attached to it. It was found that the donation of this electron in an intramolecular fashion was much more efficient than when the thiocarbonylthio species was not connected to the porphyrin. The efficiency of the polymerisation was increased greatly (after 6 h, 3% conversion vs 56% conversion) under identical conditions.

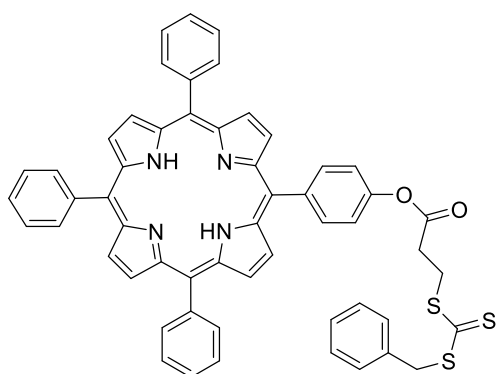


Figure 1.5 - Structure of TPP-BSTP (TPP (tetraphenylporphyrin) and BTSP (3-benzylsulfanyl thiocarbonylthiosulfanyl propionic acid))

More recently, metalated porphyrins were used in polymerisation using near infra-red light (NIR).⁹³ The structures of the porphyrin used is shown in Figure 1.6. It was shown that while the molar extinction coefficients were low at 785 nm (NIR), they still proved to be suitable photocatalysts for polymerisation of methacrylates, giving conversions of between 40 and 55%.

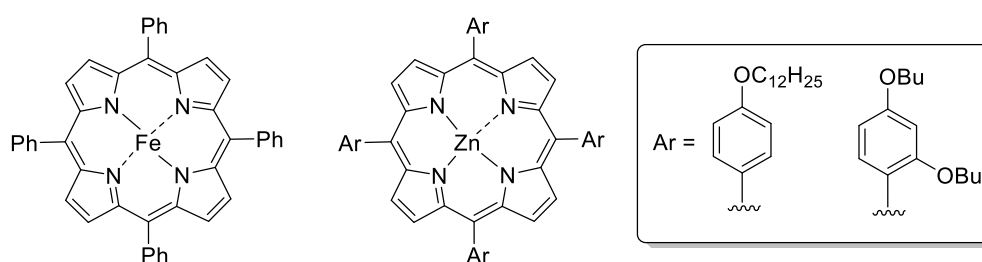


Figure 1.6 - Structure of porphyrins used in near infra-red (NIR) polymerisation⁹³

1.8 Chlorophyll a

Chlorophyll a absorbs light across the visible spectrum, mainly reflecting green light, giving it a green colour (Figure 1.7). Plants contain both chlorophyll a and b, which absorb light at slightly different wavelengths. This maximises the range at which the

plant can absorb light, allowing for a larger range of wavelengths to be used for photosynthesis. The structure, nomenclature, and photochemical behaviour of chlorophyll a will be expanded in chapter 5.

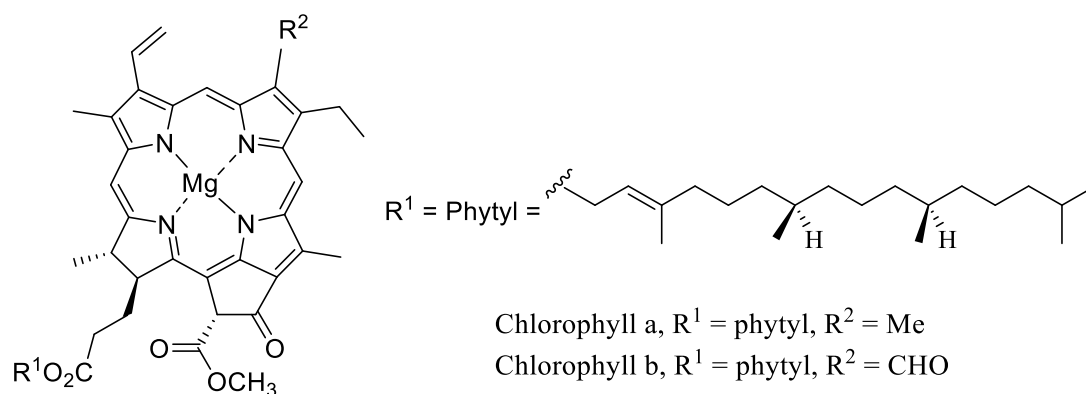
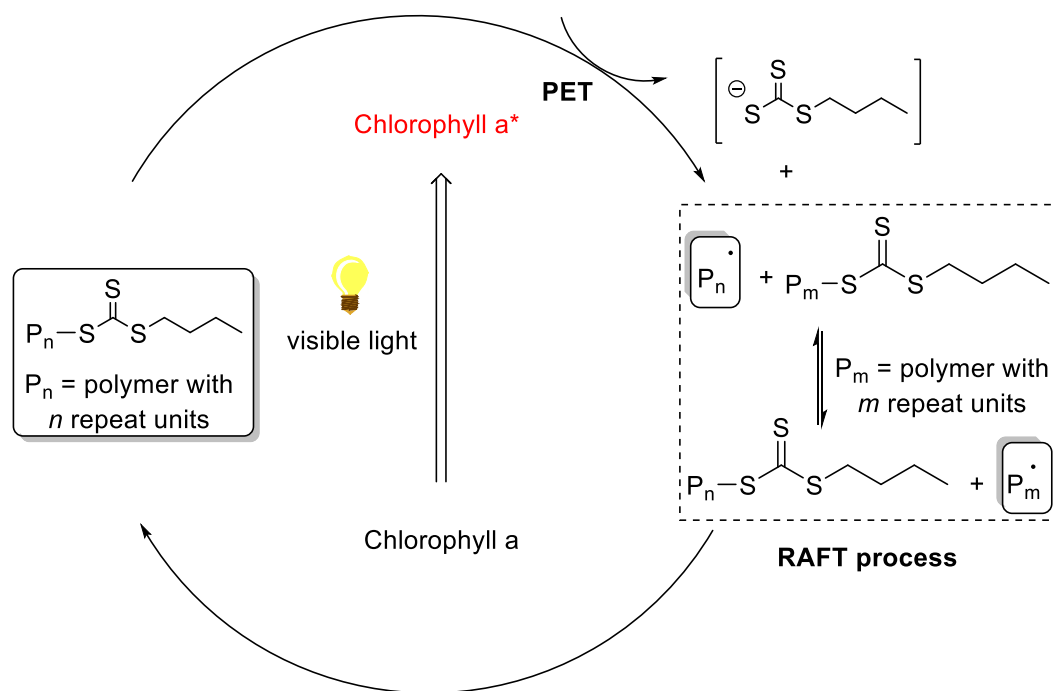


Figure 1.7 - Structure of chlorophyll a and chlorophyll b

1.9 Chlorophyll as a photoredox catalyst

It is beyond the scope of this introduction to focus on how chlorophyll mediates photosynthesis in plants. The reader is directed to a number of reviews in this area.^{94–96} It is known that during photosynthesis, chlorophyll absorbs a photon from sunlight, resulting in the excitation of chlorophyll from its ground state to an excited state.⁹⁷ This initiates a complicated electron transfer cascade where excited chlorophyll transfers an electron to an electron acceptor (in photosynthesis this a molecule of chlorophyll that does not contain the magnesium atom called pheophytin). Further electron transfer between a range of molecules finally leads to reduction of NADP to NADPH. The initial electron transfer process results in a positive charge forming on chlorophyll (radical cation) and a negative charge on the acceptor (radical anion) *via* photoinduced charge separation.

It was theorized by Boyer *et al* that electron transfer from excited chlorophyll could be used to reduce a RAFT agent, resulting in the formation of a propagating radical and polymerisation after fragmentation of the initial radical anion, Scheme 1.38.⁹⁷



Scheme 1.38 - Mechanism for PET-RAFT polymerisation using chlorophyll a as a photocatalyst

The mechanism postulated was very similar to the mechanism of the PET-RAFT polymerisation using porphyrins as the photocatalyst. Chlorophyll a is excited by visible light, and then reduces the RAFT agent by photo electron transfer. The reduced RAFT agent generates a radical which initiates the reaction as well as acting as a chain transfer agent, resulting in polymerisation. The polymerisation is deactivated by the addition of the propagating radical to the π -cation radical chlorophyll-RAFT complex. This one electron reduction from chlorophyll a to form a π -radical cation has been shown previously to occur in other systems.⁹⁸ The electron from the excited chlorophyll a is shown to not come from the magnesium atom but from the π -system of the porphyrin.

Boyer *et al* showed that chlorophyll a could act as a photoredox catalyst in the PET-RAFT polymerisation of a variety of monomers using a variety of RAFT agents (Figure 1.8).⁹⁷ Polymerisations were repeated in darkness, and in the absence of chlorophyll a, both resulting in no polymerisation, showing that chlorophyll a was essential for polymerisation.

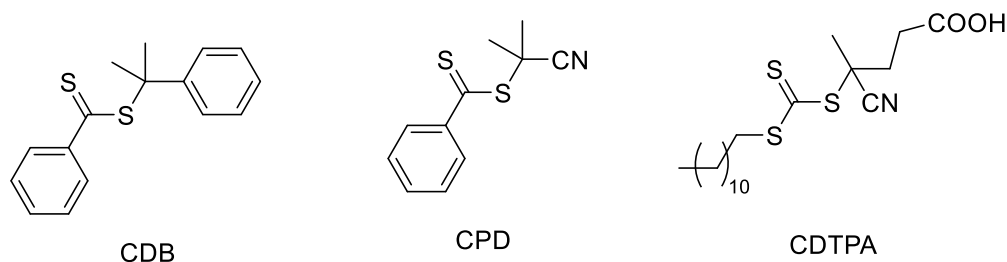


Figure 1.8 - Structures of RAFT agents used in PET-RAFT polymerisation using chlorophyll a as a photoredox catalyst

It was also reported that the crude acetone extract from spinach leaves can be used in the same way as pure chlorophyll a, in a PET-RAFT polymerisation.⁹⁹ The benefits of using the crude spinach extract were that less reagents and purification steps are required than needed to isolate purified chlorophyll a, saving on cost and time. Conversion was around 80% for both pure and crude chlorophyll a, however a one-hour inhibition period was observed when using the crude extract that was not present when using purified chlorophyll a. This was found to be due to the presence of β -carotene and other carotenoids in the crude spinach extract which act as radical quenchers. Polymerisation in air with the spinach extract was slower, but there was good oxygen tolerance (presumably due to the presence of carotenoids). In air the same conversion was achieved with just one extra hour. This was down to the fast production of singlet oxygen, which was then deactivated in the presence of DMSO, which yielded dimethyl sulfone. Also, when left under the light source, the chlorophyll a degraded from a green colour to brown, eventually becoming clear. This indicated that there might be no need to remove the photocatalyst from the final polymer products as it would not affect the colour of the polymer.

1.10 Background of 3D printing

The term 3D printing (also known as additive manufacturing) is the process by which a wide range of structures can be fabricated from three-dimensional model data. The process usually consists of printing (for example, polymerisation of monomers) of multiple layers on top of each other building up the desired object. The major benefit of this process is the reduction of waste, the ability to make complicated structures and the fast production of prototypes.^{100,101}

1.11 Visible light 3D printing methods

There are three main techniques used for 3D printing *via* photopolymerisation. The first of these is stereolithography (SLA). The first example of this was in 1986.¹⁰² The way this polymerisation works is by filling a transparent vat with resin. This vat sits directly on a movable photon source, which selectively illuminates specific areas of the resin. This results in the desired polymer layer forming. The solidified polymer is then lifted by a platform, while the photon source continues to build the object by successively printing layers. The first resin mixture used in this process contained urethane dimethacrylate (UDMA), acrylic acid, benzophenone as a photoinitiator and methyl ethyl hydroquinone to act as an inhibitor for premature polymerisation.¹⁰² A major advantage of this technique is the layers can be as thin as 10 μM , resulting in very fine resolution.

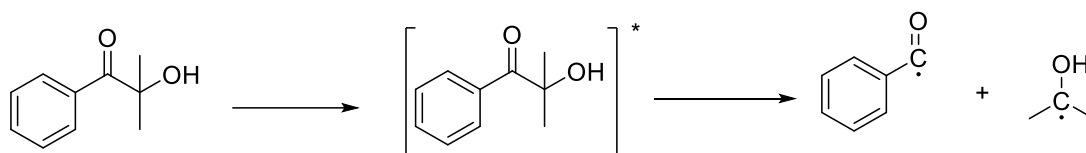
The next technique to be developed was digital light processing, which instead of using a movable light source, uses a light source that illuminates the entire layer at once. A resin vat will sit directly on the light source, and this will illuminate the resin with the shape of the first layer of the print. This results in the hardening of the entire first layer. A platform is placed into the vat, onto which the first layer is attached. The platform is then raised by a height of one layer, then the next layer is illuminated onto the resin, and this process is repeated until the final product is formed.^{103–105} Due to this, an advantage of this technique is that a small amount of resin is required to print objects. Also, due to the platform always being one layer thickness above the bottom of the vat, there is minimal contact of resin with air, resulting in more favourable polymerisation conditions.

The final technique is continuous liquid interface production and was introduced in 2015. The vat used for this technique has an oxygen-permeable window, which creates an oxygen-containing layer that inhibits polymerisation. This results in a layer of uncured resin forming between the platform and the window of the vat. This allows for continuous printing and does not print the object layer by layer, leading to a much faster printing time, as the object is continuously raised out of the resin by the platform.^{106,107}

The sponsor of this project (Photocentric Ltd) uses a 3D printing process with a liquid precision printer and the digital light processing technique.

1.12 Development of light mediated 3D printing

One of the commonest processes for initiating polymerisation in 3D printing applications using light is a radical system. Radical systems involve initiation, propagation, and termination steps, with the initiation step occurring from light irradiation in photo 3D printing. Radical photoinitiators can be generally separated into two systems: type I or type II.¹⁰⁸ Type I initiators are cleaved by light to form radicals, which then initiate the polymerisation. An example of the photocleavage mechanism of 2-hydroxy-2-methyl-1-phenyl-propan-1-one is given in scheme 1.37.¹⁰⁸ These photoinitiators usually require low energy UV light, and therefore have low energy $n \rightarrow \pi^*$ transitions, Scheme 1.39, Figure 1.9.



Scheme 1.39 - Type I photocleavage of 2-hydroxy-2-methyl-1-phenyl-propan-1-one¹⁰⁸

These photoinitiators usually require low energy UV light, and therefore have low energy $n \rightarrow \pi^*$ transitions. Some common photoinitiators are shown in Figure 1.9.

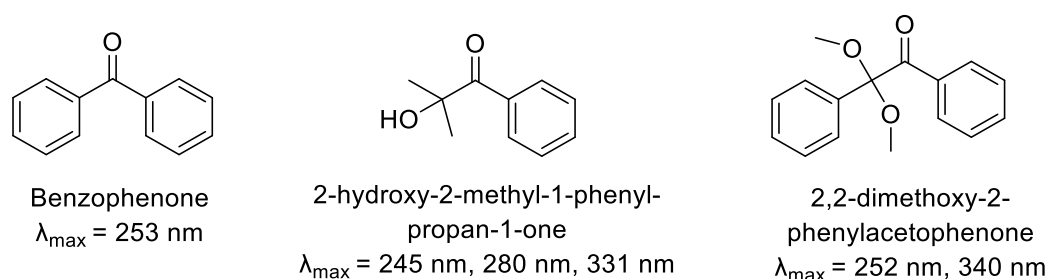
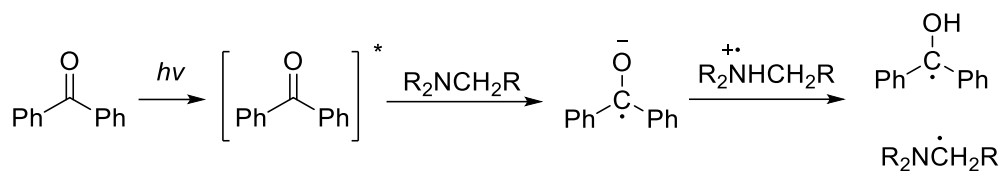


Figure 1.9 - Examples of typical UV light photoinitiators in 3D printing

Type II photoinitiation systems usually involve two species, containing a molecule that absorbs light (sensitizer), and a co-initiator that interacts with the light absorbing molecule. Once the sensitizer is excited, an electron is transferred to the co-initiator and produces a radical species. This radical then initiates the polymerisation.^{109,110}



Scheme 1.40 – Radical generation from type II photoinitiators¹¹¹

One of the first photoinitiators used in UV light 3D printing was benzophenone, which can be initiated by a 350 W mercury short arc lamp in stereolithography, with benzophenone absorbing light at 253 nm. This utilized a type II photoinitiation, with the mechanism of radical generation shown in scheme 1.40.¹¹¹

Due to the recent advancements in photoredox chemistry, there have been some 3D printing examples using photoredox catalysts in visible light. In 2017, Lalevee *et al* used copper complexes with pyridine-pyrazole ligands as photoredox catalysts in visible light (405 nm) 3D printing.¹¹² The other compounds involved in the polymerisation was iodonium salts and a novel additive CARET (Figure 1.10), that improved the performance of the photocatalyst. Mechanistically, irradiation of the Cu(I) complex followed by PET to the iodonium salt furnished a Cu(II) complex and a phenyl radical (after homolytic cleavage of the C-I bond). Generated phenyl radical could then be used to initiate a polymerisation.

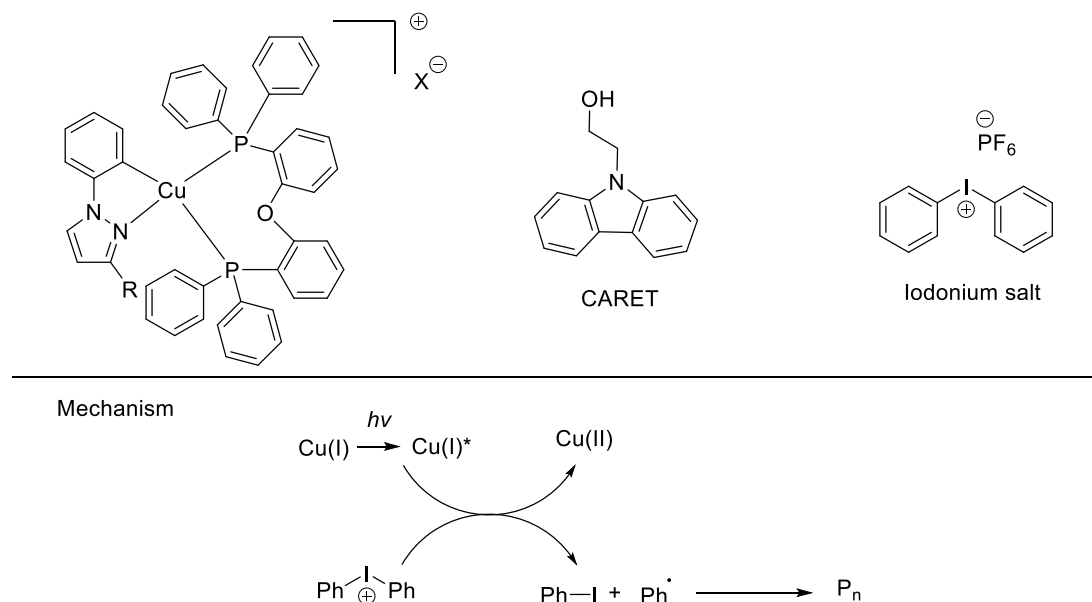
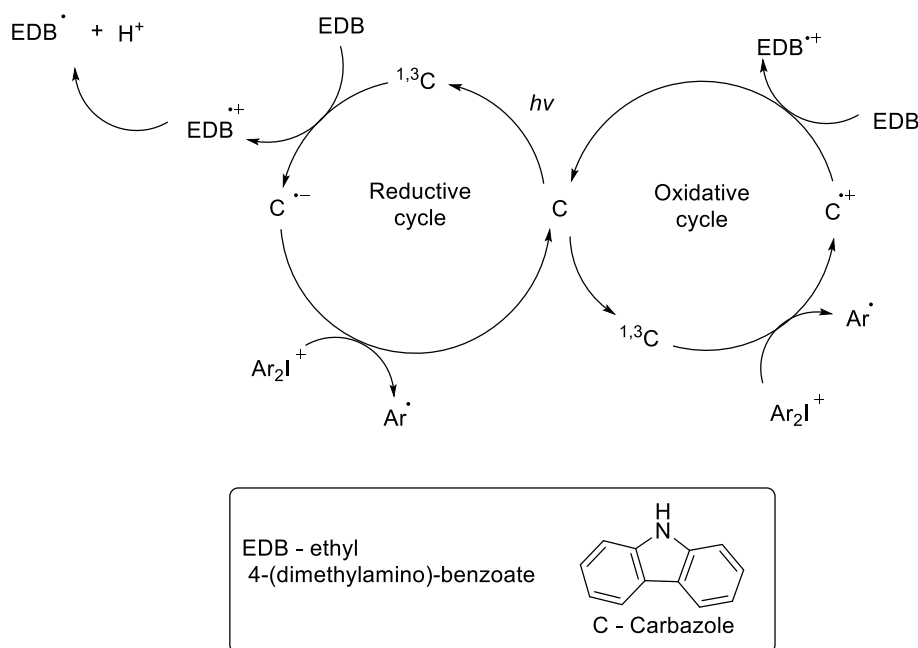


Figure 1.10 - Structures of components of copper catalysed visible light 3D printing

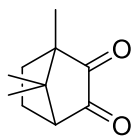
Due to the success of this study, Lalevee *et al* attempted to use a carbazole scaffold based photoinitiator for both free radical polymerisation of methacrylates and cationic

polymerisation of epoxides (scheme 1.41).¹¹³ It was also shown that the cationic polymerisation was able to be used for LED projector 3D printing using a 405 nm projector. The Ar radical species that is produced initiates the radical polymerisation, whereas the carbazole radical cation initiates the cationic polymerisation. Also, the EDB radical that is formed can initiate the free radical polymerisation.

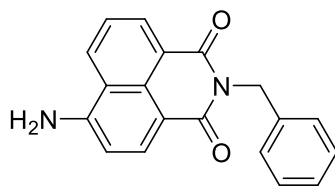


Scheme 1.41 - Mechanism of carbazole as a photoredox catalyst¹¹³

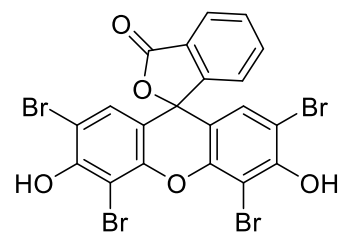
Figure 1.11 shows some other examples of reported metal-free visible light photocatalysts in 3D printing.^{114–117} The wavelength at which many photocatalysts absorb light is <550 nm. It is desirable to design systems that absorb light at higher wavelengths not only because of the lower energy requirements, making the system cheaper and safer, but also increasing the penetration depth of the light. This will lead to faster polymerisation, making the 3D print more efficient. So, although there are photocatalyst that absorb light towards the red end of the spectrum, there is still room for more photocatalysts to be employed at a higher wavelength.



Camphorquinone
468 nm



5-amino-2-benzyl-1H-
benzo[de]isoquinoline-
1,3(2H)-dione
 $\lambda_{\max} = 417 \text{ nm}$

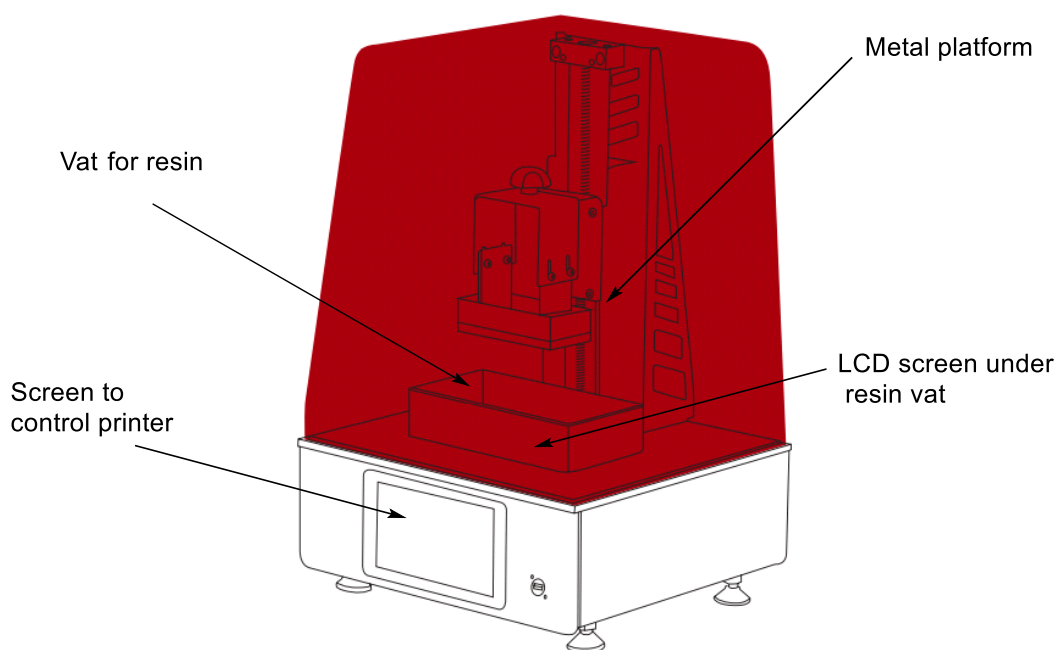


Eosin Y
 $\lambda_{\max} = 524 \text{ nm}$

Figure 1.11 - Examples of visible light photoinitiators in 3D printing¹¹⁸

1.13 Aims of this work

The main aim of this thesis is to explore the development of cheaper, less toxic and more environmentally friendly photocatalysts in 3D printing. More specifically we will initially study both zinc coordinated and metal-free porphyrins as photocatalysts in visible light 3D printing. A range of derivatives will be prepared, and structure activity relationships will be determined. While most printing involves UV or blue light, we will also explore using the less energetic red region of the spectrum. Finally, we will explore whether renewable porphyrin based photocatalysts like chlorophyll or non-metalated chlorophyll (pheophytin) can be used as photocatalysts in commercial 3D printing systems.



The printing system that will be used is known as daylight polymer printing, developed by Photocentric. This 3D printing process uses an LCD screen as the light source. A vat of resin is placed directly onto the LCD screen, with a metal platform positioned one layer above the bottom of the vat. The LCD screen then irradiates the resin with the shape of the first layer of the 3D print, which forms the solid first layer on the platform. The platform is then raised by a thickness of one layer, and the process is repeated until the print is complete.

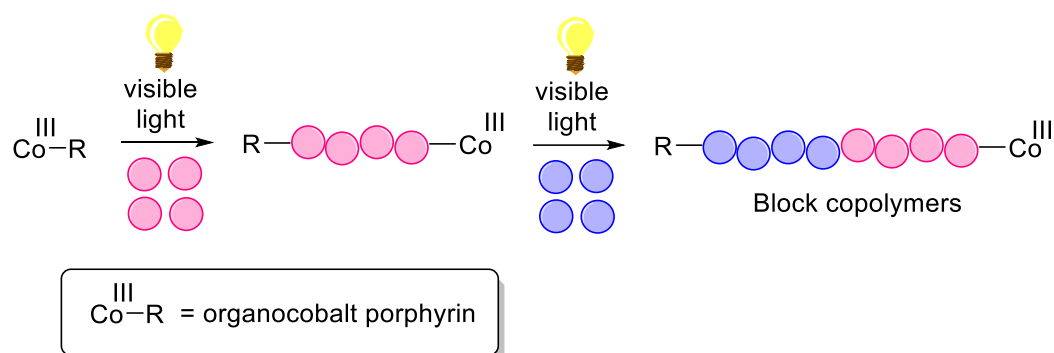
To meet the aims of this thesis, the following research outcomes will be described:

- In chapter 2, the ability of ZnTPP to polymerise methyl acrylate using a range of co-initiators will be assessed, determining which is most effective in both blue and red light. The results from this study will be used to determine the optimal ratio of reactants for 3D printing. Once 3D printing experimental conditions have been optimised, the study will be repeated for the metal free porphyrin TPP and the 3D prints assessed and compared. It has been previously shown that TPP was not able to mediate a PET-RAFT polymerisation and consequently the ability to use it in an air mediated 3D print would be significant⁹⁷ Primarily this study will determine if metalated or non-metalated porphyrins are candidates on which to build potential photocatalysts for Photocentric systems.
- In chapter 3, the effect of functionalising the phenyl groups present on TPP with electron and withdrawing groups on the photocatalytic ability of MA polymerisation and in 3D printing will be reported. Both metalated and non-metalated derivatives will be prepared and compared. It has been shown that changing the peripheral aryl substituents of porphyrins influences the absorption and electronic properties. These properties will be crucial for tailoring reactivity and red shifting reagents to be more efficient in 3D printing under red light.
- In chapter 4, the increasing the conjugation of the porphyrin core in order to red shift the photocatalysts further than described in chapter 3 will be reported. Conjugation of the porphyrin core has been previously reported to not only lead to the red shifting of absorption properties but also broadening of the absorption bands.
- In chapter 5, the aim was to utilise chlorophyll a as a renewable photocatalyst in the polymerisation of both MA and in 3D printing in the same way as the synthetic porphyrins in the previous chapters. A range of sources of chlorophyll will be studied. In addition, the ability of using a crude chlorophyll extract verses a more purified chlorophyll product will be assessed to determine if lower levels of purification and isolation (and hence lower cost) is possible.

2 Zinc tetraphenylporphyrin and metal free tetraphenylporphyrin as photoredox catalysts in 3D printing

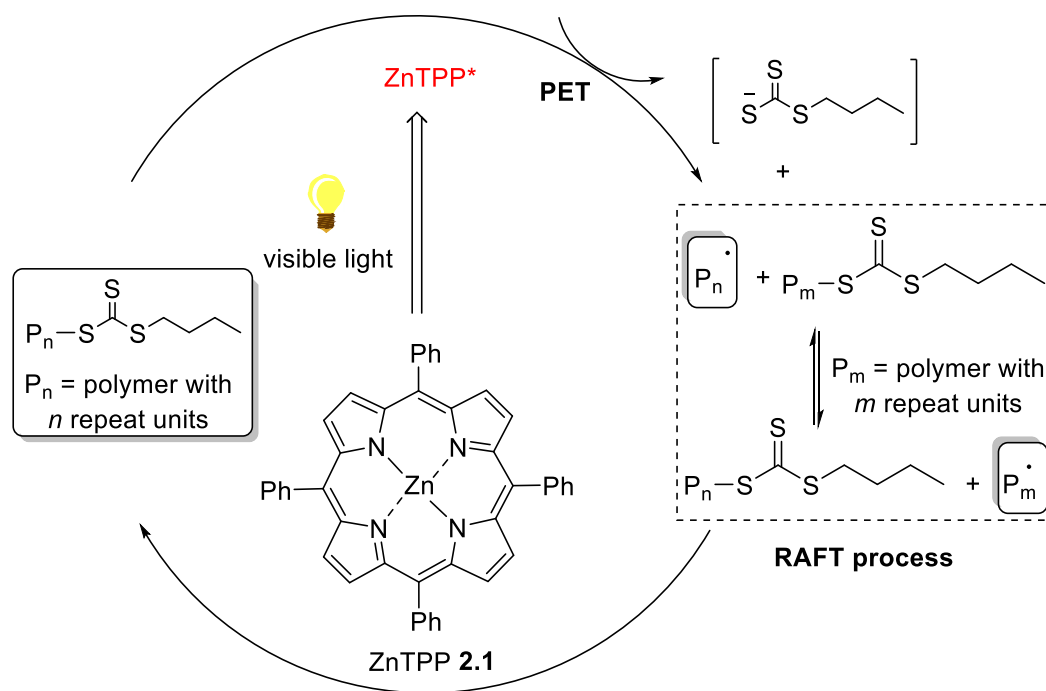
2.1 Introduction

Metalloporphyrins can be used as photoredox catalysts to catalyse free-radical polymerisations. Most reported porphyrin catalysts are activated by UV light, although organocobalt porphyrins are able to mediate polymerisation using lower energy visible light, (Scheme 2.1).⁸⁶ In this process, the visible light energy initiates a homolytic cleavage of the $\text{Co}^{\text{III}}\text{-R}$ bond, which generates a Co^{II} species and a carbon radical ($\text{R}\cdot$), which in turn initiates a polymerisation. The growing polymer chain can be capped by the Co^{II} species allowing formation of block copolymers.



Scheme 2.1- Visible light polymerisation, catalysed by cobalt porphyrins

In 2014 Boyer *et al.* - used zinc tetraphenylporphyrin (ZnTPP) **2.1** to polymerise a range of acrylates *via* a photoinduced electron transfer-reversible addition-fragmentation chain transfer (PET-RAFT) mechanism (Scheme 2.2), using visible light.⁸⁷ This polymerisation differs from the organocobalt porphyrin **2.1** mediated process, with the visible light exciting an electron from the π -system of the porphyrin, the excited state transfers an electron to a xanthate to give a radical anion, which then fragments to create a radical, as opposed to direct homolytic bond cleavage. *The fact that the electron comes from the π -system will theoretically allow us to alter the structure of the porphyrin, and hence its electronics, with the aim of optimising the formation of the radical and efficiency of the process.*



Scheme 2.2 - Mechanism of PET-RAFT polymerisation⁸⁷

ZnTPP **2.1** absorbs light over a wide range of wavelengths, most strongly in the blue light region (420 – 480 nm), with weaker absorption towards the red end of the spectrum (580 – 640 nm). Due to this absorption, ZnTPP **2.1** was able to polymerise methyl acrylate (MA) in blue, green, yellow, orange, and red light with a conversion >70% (Table 2.1).⁸⁷

Light source	Wavelength (nm)	Conversion (%) ^{1,2}
Blue	435-480	70
Green	480-560	80
Yellow	560-590	82
Orange	590-610	84
Red	610-655	75

¹ Ratio of concentration of reagents methyl acrylate: 2-(*n*-Butyltrithiocarbonate)-propionic acid: ZnTPP. [MA]: [BPTA]: [ZnTPP]¹ 200:1:1x10⁻³. ²Determined by 400 MHz ¹H NMR by integrating ratio of peaks at 3.6-4.0 ppm and 5.8-6.5 ppm.

Table 2.1 – Polymerisation of methyl acrylate under different wavelengths using ZnTPP **2.1** as a photoredox catalyst.

As stated previously, many 3D printing applications use UV light to mediate the printing. The ability to initiate a radical polymerisation using visible light in home 3D printing applications could be invaluable due to lower costs, higher safety, and higher accessibility.

2.2 Aims and objectives

Boyer *et al* were able to polymerise a wide range of acrylates using ZnTPP **2.1** as a photocatalyst, using different wavelengths of light to initiate the reaction *via* a PET-RAFT mechanism.⁸⁷ The ultimate aim of my work was to use the photocatalytic behaviour of porphyrins to 3D print multi-functional monomers using visible light, specifically blue and red light. Both light sources were of interest to Photocentric Ltd., as they had been used in their commercial 3D printers. In Boyer's work, the RAFT agent used was BTPA **2.2**, which is synthesised using small chain thiols, making them too expensive and consequently undesirable as an initiator for industrial 3D printing applications by the sponsor. Consequently, the initial aims were to first determine the scope and limitations of ZnTPP **2.1** and the cheaper metal free version TPP **2.3** as catalysts in visible light 3D printing, (Figure 2.1). The specific work packages consisted of:

- Repeating Boyer's work to confirm photocatalytic activity of ZnTPP **2.1**.
- Determining if the metal free porphyrin TPP **2.3** could be used to polymerise acrylates.
- Screening a range of potential initiators in the polymerisation of MA **2.4**, using both metal free TPP **2.3** and ZnTPP **2.1** as photocatalysts by determining percentage conversion and molecular weight conversion with time.
- Using the optimum MA **2.4** polymerisation data in solution as a guide, attempting to 3D print a commercial TEGDMA **2.5** / UDMA **2.6** solution, using both TPP **2.3** and ZnTPP **2.1**.

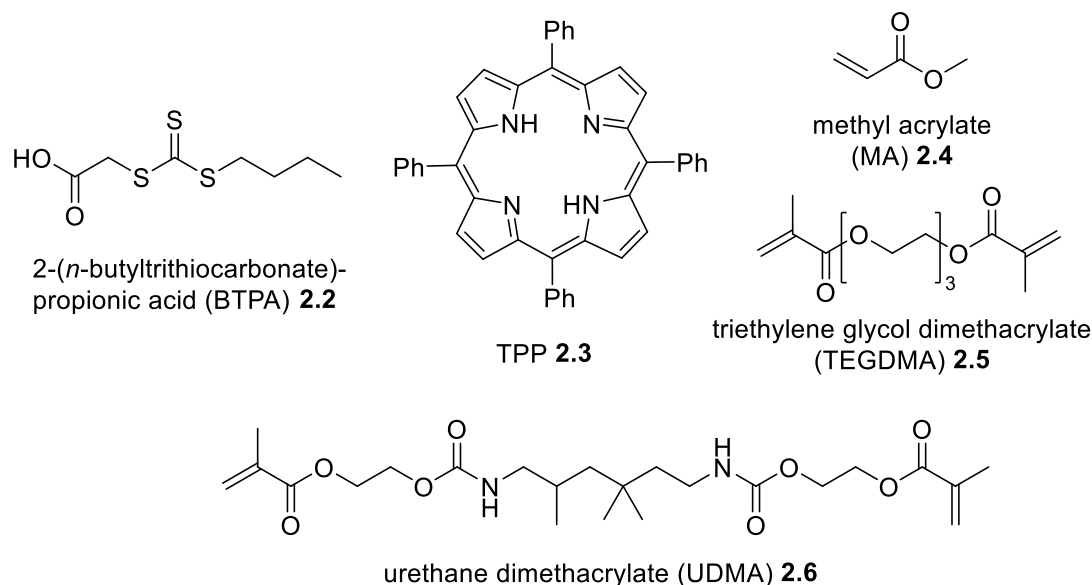


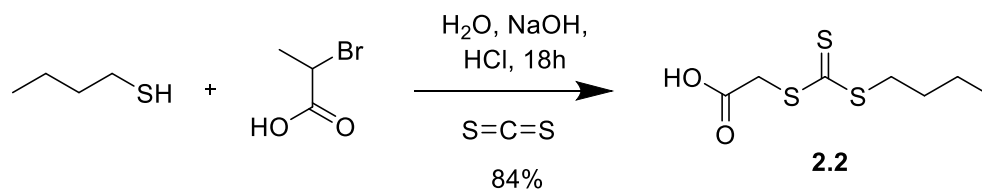
Figure 2.1 – Reactants used in this study.

2.3 Results and discussion

2.3.1 PET-RAFT polymerisation of methyl acrylate using ZnTPP **2.1** as a photocatalyst

Boyer polymerised a wide range of acrylates with a variety of RAFT initiators, while using different porphyrins as photocatalysts for these polymerisations.⁸⁷ One result from this study found that ZnTPP **2.1** was the most effective photoinitiator, with BTPA **2.2** being the co-initiator. However, this combination was unique as it was hypothesised that there was a specific interaction between ZnTPP **2.1** and BTPA **2.2**, allowing for controlled polymerisation of acrylates, even though the reduction potential of ZnTPP **2.1** and BTPA **2.2** suggested that other co-initiators would be more suited to this application.

The first reaction undertaken was therefore a repeat of the polymerisation done in Boyer's paper,⁸⁷ where ZnTPP **2.1** was used in the PET-RAFT polymerisation using BPTA **2.2** as a RAFT agent. The RAFT agent **2.2** was prepared in 84% yield from toxic CS₂, butane thiol and 2-bromopropionic acid (Scheme 2.3).¹¹⁹



Scheme 2.3 - Synthesis route of BPTA **2.2**¹¹⁹

The polymerisation was carried out using methyl acrylate (MA) **2.4** (0.38 mL), ZnTPP **2.1** (0.14 mL of a (1.475mM solution in DMSO)), BPTA **2.2** (5 mg) and DMSO (0.28 mL). This mixture was degassed and irradiated with blue light (5W LED) for 2 hours, with a distance of 4 cm between the light and the reaction mixture. The conversion was 76% (significantly lower than 92% previously reported) and was determined by ¹H 400 MHz NMR.

The discrepancy in these conversions is likely due to the distance between the light source and the reaction mixture. Boyer used a distance of 2 cm; however, the distance chosen was 4 cm, as this is the distance of the light in the Photocentric commercial 3D printer platform. This would explain the slightly lower conversion as light intensity would lessen with a greater distance between light source and reaction mixture for the same 5W powered light (intensity is proportional to 1/[distance]²).

2.3.2 UV-Visible spectrum of ZnTPP **2.1**

Porphyrin structure can be probed using UV-Visible (UV-Vis) spectroscopy. For metal free porphyrins there are two distinct regions of absorption. The Soret (or B Band) is the major absorption (between 380-500 nm) and is dependent upon substitution at the pyrrole and *meso* position, while up to 4 weaker Q band absorptions between 500-700 nm are also observed.⁵⁶ Complexation with metals normally changes the Q band region to give two absorptions, known as α - and β - bands. If the higher energy α -band (with absorptions normally around 500-600 nm) has the higher intensity the metalloporphyrin forms a relatively stable square-planar complex, although Zn porphyrins can also form pentacoordinated complexes of square-pyramidal shape with additional monodentate ligands.⁵⁶ The UV-Vis spectrum of ZnTPP **2.1** in the solvent used in the polymerisations, DMSO (0.1475mM concentration 0.1 mg / 1 mL), is shown in Figure 2.2 with the higher intensity Soret absorption peak at 427 nm ($\epsilon = 13700 \text{ M}^{-1}\text{cm}^{-1}$), and lower intensity peaks at 560 nm (α -band, $\epsilon = 820 \text{ M}^{-1}\text{cm}^{-1}$) and 599 nm (β -band, $\epsilon = 340 \text{ M}^{-1}\text{cm}^{-1}$). Considering both

the UV-Vis spectrum and the previous polymerisation results under various light sources when using BPTA **2.2** as a co-catalyst, the photocatalytic behaviour of ZnTPP **2.1** was chosen to be studied in both blue (435-480 nm) and red (610-655 nm) light as a baseline for comparison. Both commercial blue and red LED initiated polymerisations are of interest to Photocentric, with the current visible light 3D printers using the higher energy blue light only. One of the longer-term goals of Photocentric was to develop and introduce red LED 3D printers into the home and commercial markets. While the higher energy range of the wavelengths of the commercial blue LED light used would fall within the lower energy of the Soret Band absorption of ZnTPP **2.1**, the lower energy commercial red LED would only fall within β -band absorption. While the absorption regions were not perfectly matched to those of ZnTPP **2.1** they would serve as a baseline for determining the efficiency of this photocatalyst in polymerisation, 3D printing and a comparison to other porphyrins in due course.

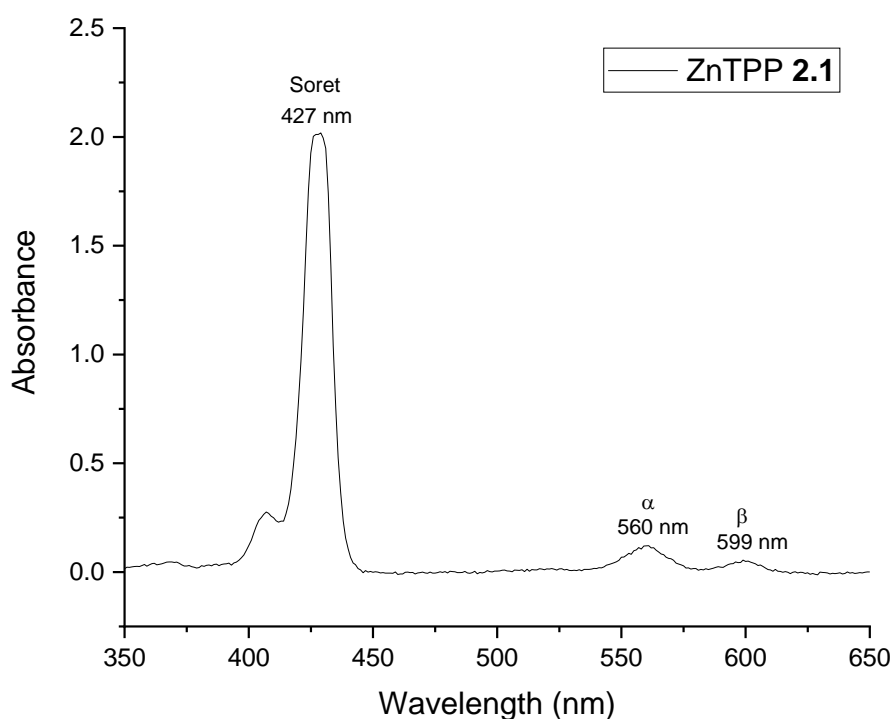


Figure 2.2 - UV-Vis spectrum of ZnTPP **2.1** in DMSO (0.1 mg / 1 mL)

2.3.3 Alternatives to BTPA/RAFT: Study of ATRP initiators

The RAFT process previously employed was assessed as too expensive for commercial use and there were additional concerns around the use of toxic reagents to prepare the initiator BTPA **2.3**.

When deciding whether the chemicals used are too expensive, it is important to analyse this using cost-benefit analysis. It is necessary to take into context not only how much the chemical costs, but also how much is required, and the time it takes to make the chemical. These factors then need to be compared to the benefits of using the specific chemical, and it can then be decided whether the chemical is too expensive or not.

Alkyl bromides are widely used as initiators for polymerisations in ATRP^{120–124} (and as one of the starting materials in RAFT agent synthesis) and have been used in light controlled ATRP photoredox catalysis.³⁵ A range of commercial alkyl and aryl bromides were screened as potential initiators for a ZnTPP **2.1** mediated photoredox initiated polymerisation. The three alkyl halide initiators chosen to test were benzyl bromide **2.7**, ethyl 2-bromopropionate **2.8** and ethyl α -bromoisobutyrate **2.9** (with ethyl α -bromoisobutyrate **2.9** being widely used in a variety of polymerisations), (Figure 2.3).^{125–129}

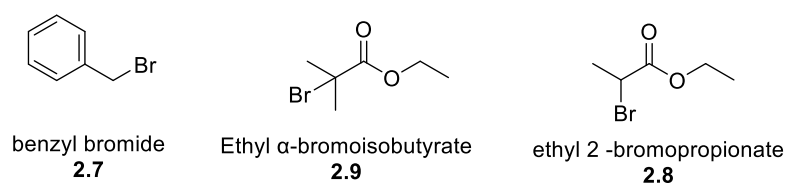


Figure 2.3 – Structures of different alkyl halide initiators studied

In order to compare to previous results MA **2.4** was used as the monomer in the polymerisation reactions.^{13–18} The polymerisation was repeated, with BPTA **2.2** being replaced by each alkyl halide **2.7–2.9** as co-initiators with the ratio of MA: **2.7–2.9**: ZnTPP **2.1** being 200: 1: 1×10^{-5} , with reaction time of 2 h and a solvent of DMSO (Table 2.2).

Co-initiator	Light source ¹	Conversion (%) ²
2.6	Blue	10
2.6	Red	5
2.7	Blue	4
2.7	Red	4
2.8	Blue	9
2.8	Red	10

¹ Blue light (420-460 nm) and red light (580-640 nm) at 4 cm. ² Determined by 400 MHz ¹H NMR by integrating ratio of peaks at 3.6-4.0 ppm and 5.8-6.5 ppm.

Table 2.2 – Polymerisation of MA using alkyl halide co-initiators, ratio of MA **2.4**: co-initiator: ZnTPP **2.1** was 200: 1: 1×10^{-5} , reaction time 2h.

From these experiments it was clear that all 3 alkyl halide initiators would not be suitable for further study, as conversion in both blue and red light was negligible, with no polymer being found *via* GPC analysis.

2.3.4 Polymerisation of MA **2.4** using ZnTPP **2.1** and 1-dodecanethiol

Due to the disappointing results using the bromo initiators (**2.7**, **2.8** and **2.9**) attention was turned to thiol initiators, such as 1-dodecanethiol **2.10**, used by the industrial sponsors in their current UV mediated 3D printing formulations (Figure 2.4). 1-Dodecanethiol **2.10** is an attractive initiator as it is cheap, as well as relatively nontoxic. Thiol mediated radical polymerisation of acrylates can be initiated (a) thermally, (b) with a photo-mediated radical initiator, or (c) with UV light (the S-H bond strength for 1-dodecanethiol = 88.7 kcal mol⁻¹).¹³⁴ The generated thiyl radicals can add to the acrylates and the new carbon radical generated can either add to another monomer (propagation) or abstract a hydrogen atom from another thiol group (chain transfer step) terminating the polymerisation and regenerating another thiyl radical. If the rate of polymerisation (propagation, k_p) occurs more rapidly than the chain transfer step (k_{CT}) then polymers will be produced. For acrylates the molecular weight will be determined by the thiol concentration. Thiol initiated radical polymerisations are not retarded by oxygen (as any peroxy radicals formed can abstract a hydrogen atom from the thiol and continue propagation), making this an attractive protocol for 3D printing in air.

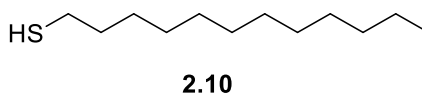


Figure 2.4 - Structure of 1-dodecanethiol **2.10**

Initially, the concentration of **2.10** used was the same as the concentration of BPTA **2.2** used in Boyer's studies,⁸⁷ (MA **2.4**: **2.1**: **2.10** ratio = 200: 1: 1×10^{-2} under both blue and red light) and 1-dodecaethiol **2.10** as a co-initiator over two hours (blue light, 420-460 nm = 90% conversion, red light 580-640 nm = 80% conversion). Both processes were able to polymerise MA **2.4** with conversions greater than the control reaction (75% conversion). As expected, conversion was higher using blue light because ZnTPP **2.1** absorbs much stronger in the blue region of the spectrum, so it will undergo photoexcitation more efficiently producing radical species for initiation of polymerisation.

2.3.5 Optimisation of 1-dodecanethiol **2.10** mediated polymerisation

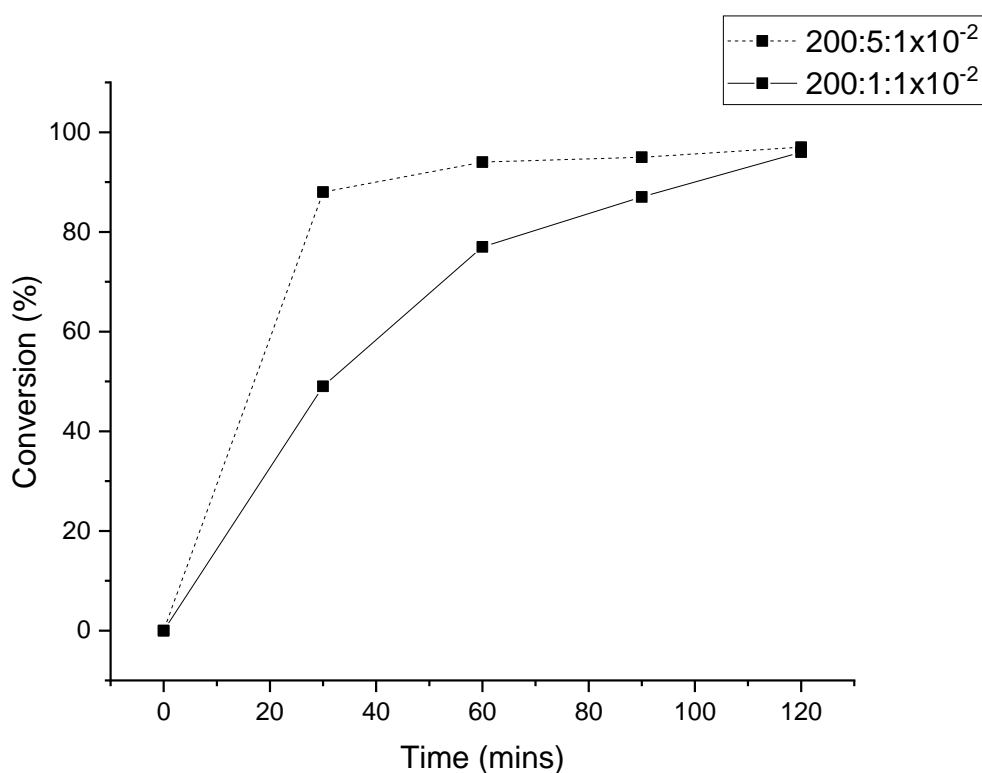
During the 3D printing process, the rate of polymerisation is essential to produce the desired print. If the polymerisation rate is too slow, little polymer is formed in each layer. However, if the polymerisation rate is too fast, an overcured print is produced. In addition, 3D printing at ambient temperature is a necessity for environmentally friendly low energy commercial applications, and attention turned to finding the optimum concentrations of thiol **2.10** and photocatalyst **2.1** with respect to conversion while keeping the reaction at room temperature.

Run	2.4: 2.10: 2.1 ¹	Conversion (%) ²	<i>M_n</i> ³	<i>M_w</i> ³	Đ ³
1	200: 0: 1×10^{-2}	5	16k	21k	1.35
2	200: 1: 1×10^{-2}	90	53k	96k	1.79
3	200: 2: 1×10^{-2}	91	43k	61k	1.43
4	200: 5: 1×10^{-2}	90	6.3k	13k	1.95
5	200: 10: 1×10^{-2}	94	2.6k	3.8k	1.44

¹ Experimental procedure: Run 3 – 0.38 mL MA **2.4**, 0.28 mL DMSO, 0.14 mL ZnTPP **2.1** (1.475mM in DMSO), 5μL 1-dodecanethiol **2.10** degassed in vial for 10 minutes. Irradiated with blue light for 2h at rt. ² Determined by 400 MHz ¹H NMR by integrating ratio of peaks at 3.6-4 ppm and 5.8-6.5 ppm. ³ Molecular weight and polydispersity index were determined by GPC analysis (CHCl₃ as eluent) calibrated to poly (methyl methacrylate).

Table 2.3- The effect of changing thiol **2.10** concentration on the polymerisation of MA **2.4** using ZnTPP **2.1** as a photocatalyst

The previously described process (run 3) was utilised as a benchmark value (Table 2.3). The first polymerisation that was attempted (run 1) was without any thiol present, which gave very low conversion (<5%). This is an important observation as it shows the necessity of the thiol **2.10** initiator. The low conversion suggests that either the photoexcited porphyrin can interact directly with MA **2.4** to initiate polymerisation, (albeit a very inefficient process) or this conversion represented a background self-polymerisation process at this wavelength, (as the inhibitor was removed from MA **2.4**). There is some evidence that MA **2.4** can undergo a radical induced homopolymerisation in the presence of oxygen in DMSO at 450 nm.¹³⁵ These reactions were degassed, therefore this is unlikely to occur, however this may become relevant during 3D printing which is performed in air. Increasing the concentration of thiol (runs 3-5) from that utilised in the control (run 3) did not increase the conversion significantly after 120 mins but did increase the rate of conversion of MA **2.4** to polymer as expected (Graph 2.1).



Graph 2.1 – Conversion of monomer vs time for MA **2.4** using ZnTPP **2.1** as a photocatalyst in blue light, altering the concentration of 1-dodecanethiol **2.10**

Run	Time (mins)	2.4: 2.10: 2.1	Conversion (%) ¹	M_n ²	M_w	\bar{D}
1	30	200: 5: 1×10^{-2}	88	5.9k	11k	1.95
2	30	200: 1: 1×10^{-2}	49	35k	60k	1.70
3	60	200: 5: 1×10^{-2}	94	6.3k	12k	2.12
4	60	200: 1: 1×10^{-2}	77	35k	59k	1.64
5	90	200: 5: 1×10^{-2}	95	6.7k	13k	2.08
6	90	200: 1: 1×10^{-2}	87	35k	61k	1.70
7	120	200: 5: 1×10^{-2}	97	6.3k	13k	1.95
8	120	200: 1: 1×10^{-2}	96	36k	60k	1.67

¹ Determined by 400 MHz ¹H NMR by integrating ratio of peaks at 3.6-4 ppm and 5.8-6.5 ppm.² Molecular weight and polydispersity index were determined by GPC analysis (CHCl₃ as eluent) calibrated to poly (methyl methacrylate)

Table 2.4 – GPC analysis of the kinetics of the polymerisation of MA **2.4** using ZnTPP **2.1** as a photocatalyst in blue light, altering the concentration of 1-dodecanethiol **2.10**

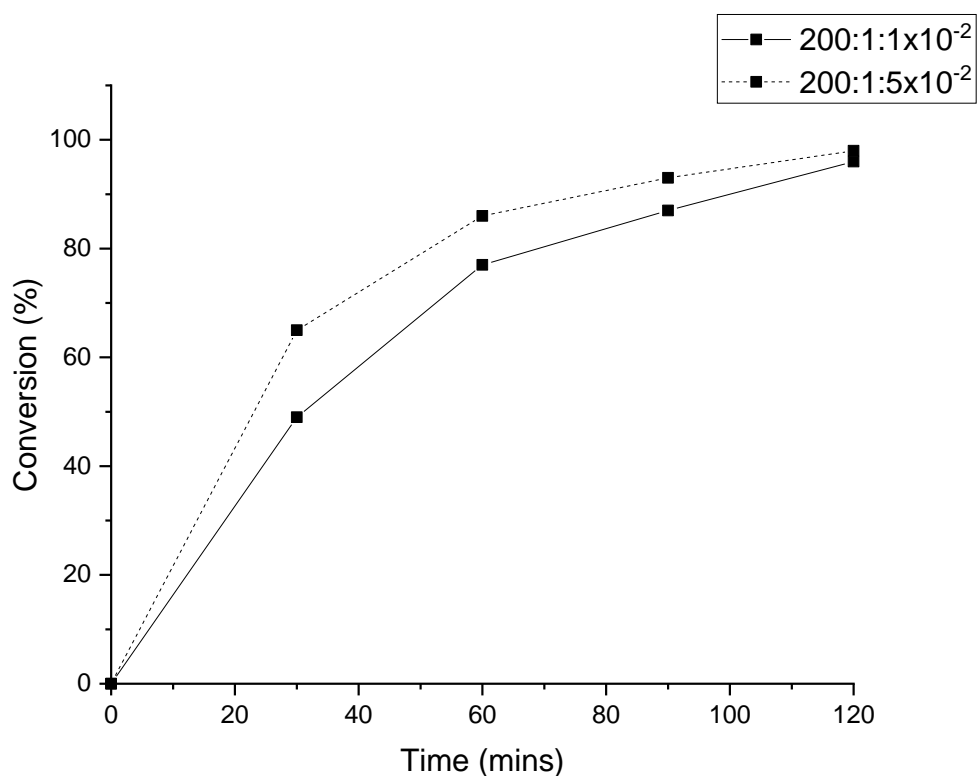
Increasing the concentration of 1-dodecanethiol **2.10** speeds up the polymerisation significantly, with the conversion after 30 minutes increasing from 30% to 88% (run 1 vs run 2). As expected, the increase in thiol **2.10** concentration results in a significantly lower molecular weight of the polymer produced, M_n (run 1 vs run 2 = 235k to 5.9k) and M_w (run 1 vs run 2 = 60k to 11k) (Table 2.4). The increase in rate is due to the higher concentration of initiator thiol radicals leading to more active chain ends, but the higher concentrations of chain transfer agent **2.10** leads to lower average molecular weights of the polymers. While an increase in thiol concentration leads to a decrease in molecular weight, when applied to 3D printing applications with multifunctional monomers the degree of polymerisation is still likely to be acceptable.

As expected, increasing the concentration of the ZnTPP **2.1** also led to higher conversion of MA **2.4** under blue light (Table 2.5). The amount of ZnTPP **2.1** used in any 3D printing must be kept as low as possible to minimise cost and any colour imparted by the porphyrin catalyst in the product, and consequently a ratio of MA **2.4**: thiol **2.10**: ZnTPP **2.1** of 200: 1: 5×10^{-2} was chosen as a compromise value (Graph 2.2). Increasing the amount of porphyrin had less effect on molecular weight (Table 2.6).

Run	2.4: 2.10: 2.1 ¹	Conversion (%) ²
1	200: 1: 0	0
2	200: 1: 1×10^{-4}	25
3	200: 1: 1×10^{-3}	37
4	200: 1: 1×10^{-2}	90
5	200: 1: 2×10^{-2}	95
6	200: 1: 5×10^{-2}	96
7	200: 1: 0.1	95

¹Irradiated with blue light for 2 hours. ² Determined by 400 MHz ¹H NMR by integrating ratio of peaks at 3.6-4.0 ppm and 5.8-6.5 ppm

Table 2.5- Effect of changing concentration of ZnTPP **2.1** on the polymerisation of MA **2.4** using blue light.



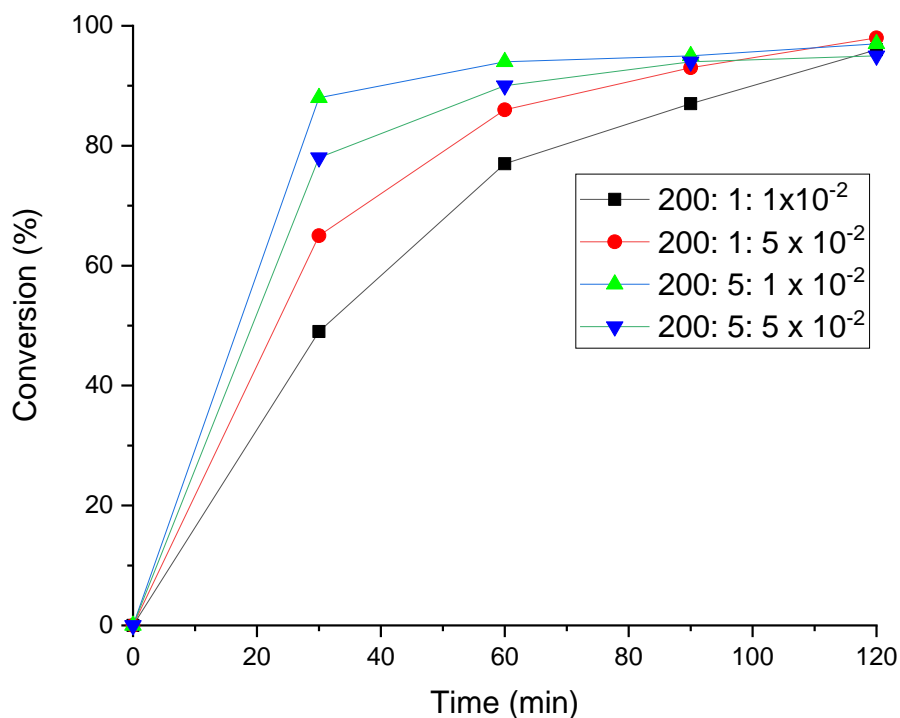
Graph 2.2 - Shows the effect of changing ZnTPP **2.1** concentration on the polymerisation of MA **2.4**

Run	Time (mins)	MA 2.4: thiol 2.10: ZnTPP 2.1	Conversion (%) ¹	M_n^2	M_w	\bar{D}
1	30	200:1:5x10 ⁻²	65	33k	48k	1.65
2	30	200:1:1x10 ⁻²	49	35k	60k	1.70
3	60	200:1:5x10 ⁻²	86	33k	48k	1.62
4	60	200:1:1x10 ⁻²	77	35k	59k	1.64
5	90	200:1:5x10 ⁻²	93	34k	48k	1.67
6	90	200:1:1x10 ⁻²	87	35k	61k	1.70
7	120	200:1:5x10 ⁻²	98	34k	49k	1.67
8	120	200:1:1x10 ⁻²	90	36k	60k	1.67

¹ Determined by 400 MHz ¹H NMR by integrating ratio of peaks at 3.6-4 ppm and 5.8-6.5 ppm.² molecular weight and polydispersity index were determined by GPC analysis (CHCl₃ as eluent) calibrated to poly (methyl methacrylate)

Table 2.6 - The effect of changing concentration of ZnTPP 2.1 on polymerisation of MA 2.4 in blue light

Increasing both ZnTPP 2.1 and 1-dodecanethiol 2.10 concentrations leads to faster polymerisation as expected, with a fivefold increase in 1-dodecanethiol 2.10 having a greater effect than a fivefold increase in ZnTPP 2.1 (Graph 2.3).



Graph 2.3 - Comparison of kinetics of the polymerisation of MA **2.4** in blue light, changing ratio of MA **2.4**: 1-dodecanethiol **1.10**: ZnTPP **2.1**

2.3.6 Polymerisations using multi-functional thiols

Typical monomers used in 3D printing protocols on the Photocentric platform are difunctional methacrylate's TEGDMA **2.5** and UDMA **2.6**. These are cured commercially under blue light irradiation with tri and tetra-functionalised thiols as further crosslinking agents and initiators. Before attempting to 3D print with ZnTPP **2.1** in visible light, it would be beneficial to study the typical multifunctional thiol initiators used compared to 1-dodecanethiol **2.10**. The two thiols studied were of trimethylolpropane tris(3-mercaptopropionate) **2.11** and pentaerythritol tetrakis(3-mercaptopropionate) **2.12** (Figure 2.5).

These thiols were used as co-initiators in the polymerisation of MA **2.4**, using the polymerisation conditions determined in section 2.3.5, under both red and blue light.

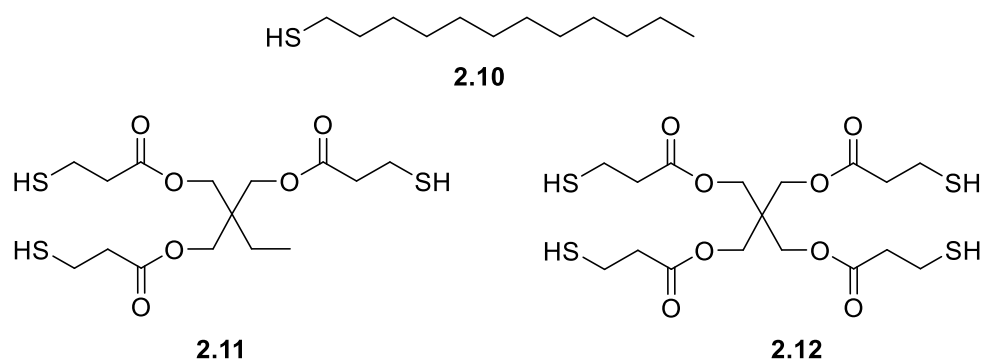


Figure 2.5 – Structures of 1-dodecanethiol **2.10**, trimethylolpropane tris(3-mercaptopropionate) **2.11** and pentaerythritol tetrakis(3-mercaptopropionate) **2.12**

Conversion was similar for all thiols under blue light with conversion above 90% (Table 2.7) after 2 h. In red light, conversion is lower as expected, but increasing the number of functional groups on the thiol has little effect on conversion after 2 h. The effect on molecular weight is more pronounced, with a direct correlation between the number of thiol functional groups (relative concentration of chain transfer agent) and molecular weight of the polymer produced as expected (runs 3 → run 5 → run 7: $M_n = 33\text{k} \rightarrow 24\text{k} \rightarrow 11\text{k}$).

Run	Light source ¹	Thiol	Time (h)	Conversion (%) ²	M_n^3	M_w^3	\bar{D}^3
1	Blue	-	16	0	-	-	-
2	Red	-	16	0	-	-	-
3	Blue	2.10	2	94	33k	45k	1.36
4	Red	2.10	2	80	33k	47k	1.41
5	Blue	2.11	2	96	24k	37k	1.52
6	Red	2.11	2	74	20k	33k	1.63
7	Blue	2.12	2	90	11k	17k	1.46
8	Red	2.12	2	86	12k	17k	1.46

Reaction conditions – MA **2.4**: thiol: ZnTPP **2.1** 200: 1: 1×10^{-2} , irradiated with light for 2 hours in DMSO ¹ Blue light (420-460 nm) and red light (580-640 nm) at 4 cm. ² Determined by 400 MHz ¹H NMR by integrating ratio of peaks at 3.6-4 ppm and 5.8-6.5 ppm. ³ Molecular weight and polydispersity index were determined by GPC analysis (CHCl₃ as eluent) calibrated to poly (methyl methacrylate)

Table 2.7 - Polymerisation of MA **2.4** with multifunctional thiols (**2.11** and **2.12**) vs 1-dodecanethiol **2.10** in blue and red light

2.3.7 3D printing using ZnTPP **2.1** as a photocatalyst

In the previous sections it has been shown that ZnTPP **2.1** is able to be an effective photoinitiator for the visible light polymerisation of methyl acrylate, using a variety of thiols as co-initiators. However, it was not clear how useful this procedure would be for 3D printing at ambient temperature in air using the less reactive methacrylate's **2.5** and **2.6**.

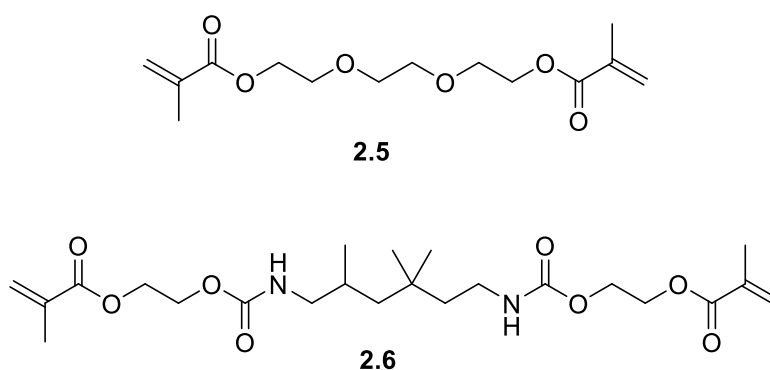


Figure 2.6 - Structures of triethylene glycol dimethacrylate (TEGDMA) **2.5** and urethane dimethacrylate (UDMA) **2.6**

Consequently, a blue light photocentric liquid crystal precision printer was used for the 3D prints. The light exposure time per layer was 300,000ms, with a distance from the light of 4 cm and the printing was carried out at room temperature. The monomers used for the 3D print were a 50/50 ratio of TEGDMA **2.5** / UDMA **2.6** (Figure 2.6), which were provided by Photocentric. Both monomers are multifunctional, which allows for cross-linking. Crosslinking is further enhanced using multifunctional thiols, which also create multiple chain ends.¹³⁶

All three thiols (**2.10**, **2.11** and **2.12**) were tested. The optimised conditions for the 3D print used the ratios of monomer: thiol: porphyrin (200: 5: 5×10^{-2}). A mixture of 15g of the 50:50 *w: w* UDMA **2.5**/ TEGDMA **2.6** mixture was used, with all three thiols tested for a 3D print, with an exposure per layer of 300,000 ms. The image printed was a standard Photocentric test print that allows for easy comparison between prints, and the control print (Print **A**) used a commercial resin provided by Photocentric. Print **A** was produced using blue light, with the exposure per layer being 50 ms.

As expected, there was no solid image produced when thiol **2.10** was used indicating that the multifunctional nature of the thiol initiators (**2.11** and **2.12**) was necessary for

an appropriate suitable cross-linked material to be produced under the reaction conditions.



Figure 2.7 - 3D prints of 50:50 w: w TEGDMA **2.5** / UDMA **2.6** utilising thiols **2.11** and **2.12** as co-initiators in blue light, with an exposure time of 300,000 ms. Print **B** – using thiol **2.11**, Print **C** – using thiol **2.12**. (Print **A** – Photocentric standard)

Assessing the quality of a print is subjective but involves assessing the resolution of the wording of the different font sizes (top left of the print), determining the clarity of definition of the edging and depth of the circular depression and raised circular patterns on the right as well as the other shapes. In addition to the subjective assessment and in order to provide a degree of quantification between results the thermal properties of the crosslinked polymers were compared.

When using thiols **2.11** (Print **B**) and **2.12** (Print **C**), a very rigid, purple, partly translucent material was formed, however while there was some resolution in some of the print, the image was very under cured (Figure 2.7). When using thiol **2.11**, the text is not at all visible, as well as the cylinders at the top right of the image being barely visible. However, the image is better using the 4-arm thiol **2.12** as the text is starting to be visible, as well as the cylinders starting to form.

The thermal stability of both Prints **B** and **C** were measured using Thermal Gravimetric Analysis (TGA). Hence, Print **B** and Print **C** were heated at 10 °C per minute over the temperature range 0-600 °C in air, using a Mettler-Toledo TGA instrument (Figure 2.8). The thermal stabilities were similar (Print **B**: $T_{5\%} = 322^{\circ}\text{C}$, $T_{50\%} = 395^{\circ}\text{C}$, high temperature residue at 600 °C = 0.72%; Print **C**: $T_{5\%} = 308^{\circ}\text{C}$, $T_{50\%} = 387^{\circ}\text{C}$, high temperature residue at 600 °C = -0.33%) indicating the extra thiol functional group has a small lowering effect on the thermal stability properties of the print.

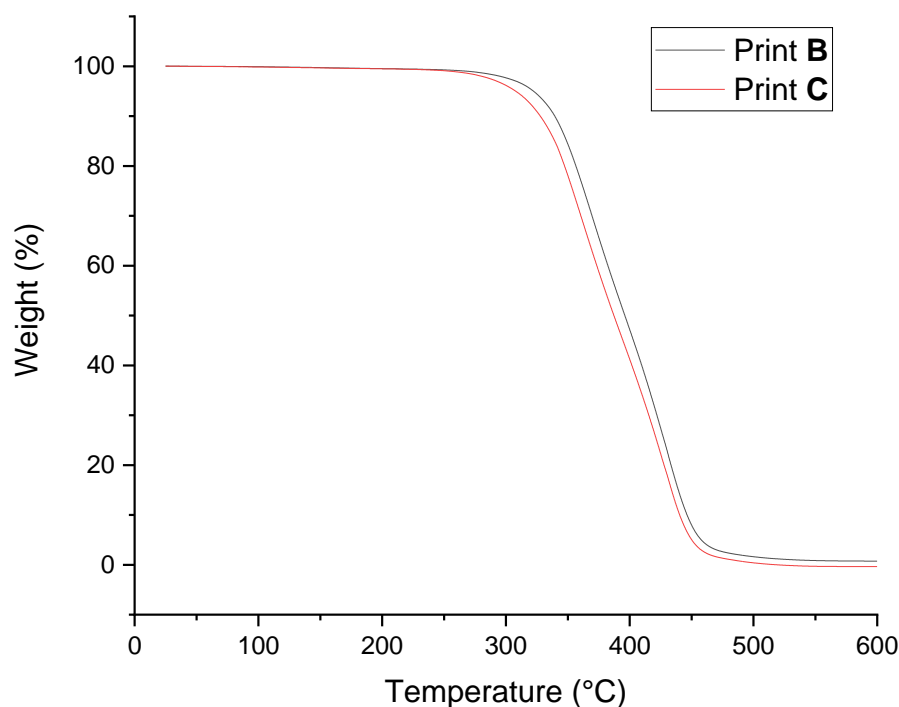
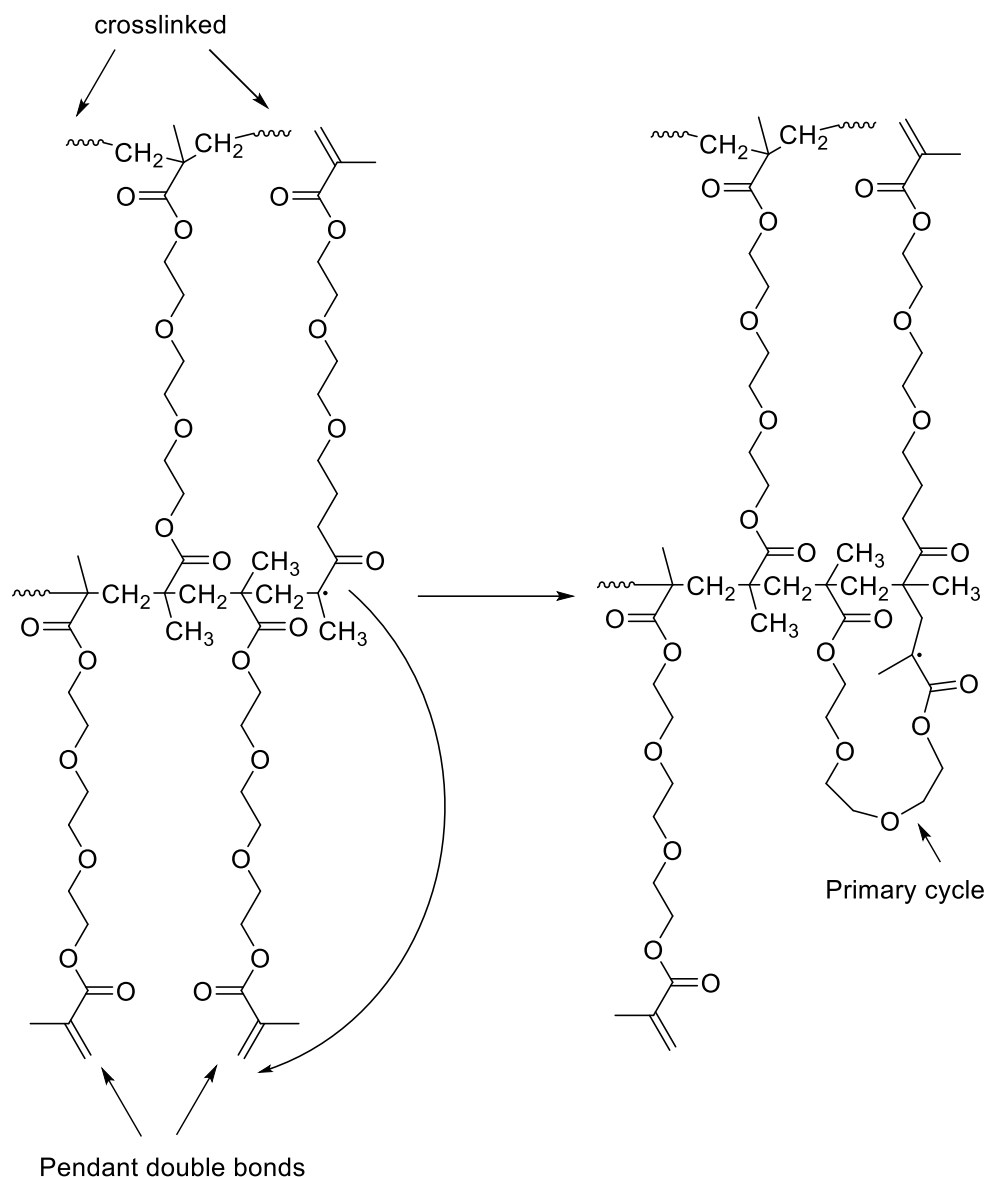


Figure 2.8 - TGA of 3D Print **B** (using thiol **2.11**) and Print **C** (using thiol **2.12**).

The thermal characteristics of the two homopolymers P_{UDMA} and P_{TEGDMA} prepared by photoinitiated radical reactions are known and show two degradation steps due to inhomogeneity in their network structures with low residual char <2% at 600 °C.¹³⁷ Inhomogeneities arise for two reasons, firstly under photochemical reaction multiple initiation sites can lead to microgel regions which are more crosslinked than elsewhere leading to pooling of unreacted monomer, and secondly during the polymerisation a competing cyclization step can lead to localised lower crosslinking density (Scheme 2.4).¹³⁸

P_{UDMA} has a greater thermal stability $T_{50\%} = 409$ °C than P_{TEGDMA} $T_{50\%} = 320$ °C due to additional hydrogen bonding which leads to a greater energy requirement to break the network bonds as well as less competing cyclization reactions due to more flexible monomer size (molecular mass of UDMA **2.6** = 470, TEGDMA **2.5** = 286). Interestingly the degradation rate maxima for P_{TEGDMA} (first degradation 277-320 °C, second degradation 371-416 °C) and P_{UDMA} (first degradation 321-372 °C, second degradation 417-454 °C) are almost perfectly complementary and it comes as no surprise that the thermal characteristics of the 3D prints in both Prints **B** and **C** utilising a 50:50 mix of UDMA **2.6** / TEGDMA **2.5** show an apparent single decomposition step.



Scheme 2.4 - Primary cyclisation mechanism of TEGDMA during polymerisation¹³⁸

On close examination (Figure 2.8) there may be a slight step indicative of a second decomposition pathway around 40-60% mass loss for both 3D prints and this is in line with the homopolymers (P_{UDMA} the second decomposition occurs around 40—50% mass loss compared to 60-70% mass loss in P_{TEGDMA}). The slightly lower thermal stability for Print **C** (using the tetra functionalised thiol **2.12**) is likely a consequence of the greater number of photochemical initiation sites rather than any increased crosslinking.

As highlighted above, utilising thiol **2.12** gave the more defined 3D print image, Print **C**, consequently, it was decided to repeat the printing with 5x the concentration of ZnTPP **2.1** and 2 x the concentration of **2.12** in the reaction mixture (monomer: thiol:

ZnTPP **2.1** = 200: 10: 0.25) to give print **D**. Increasing both the amount of thiol **2.12** and ZnTPP **2.1** gave a much clearer image, Print **D**, that looked very similar, and in places superior to the standard Photocentric test print **A**, albeit in a translucent purple colour, (Figure 2.9). There was acceptable resolution of the text and the horizontal bars on the right of the print as well as the depressed and raised circles. The disadvantage of the procedure was the long reaction times per layer and so the print was repeated with the exposure time per layer decreased to 200,000 ms to give Print **E**), however the image produced while better than the initial Prints **B** and **C**, was significantly degraded compared to Print **D**. The optimised procedure utilised 2.2 mg/g ZnTPP **2.1** and 68.0 mg/g thiol **2.12** in the monomer mixture using blue light (420-460 nm) for 300,000ms per layer curing time.



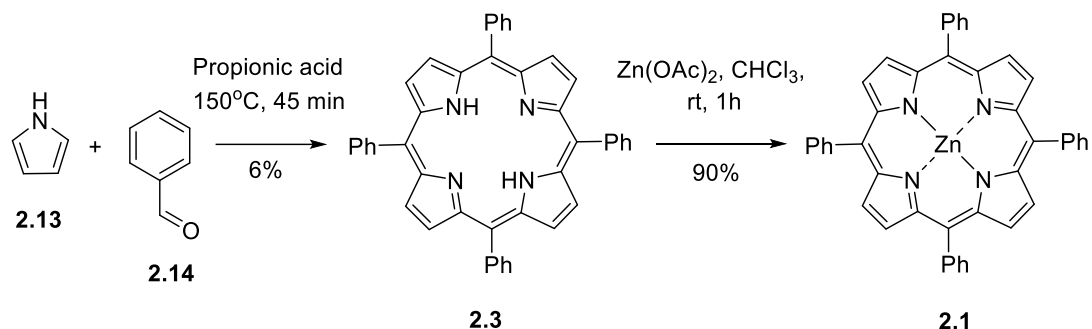
Figure 2.9 - 3D prints of 50:50 w: w TEGDMA **2.5** / UDMA **2.6** utilising thiol **2.12** in blue light, exposure time 300,000ms per layer (Print **D**) and 200,000ms per layer (Print **E**). (Monomer: thiol: ZnTPP = 200: 10: 0.25)

Due to the high cost of the photoinitiator **2.1**, using a smaller concentration of ZnTPP **2.1** would be favourable, so an attempt was made to increase the concentration of thiol **2.12** further (in order to subsequently be able to lower the amount of ZnTPP **2.1**). The final print was tested with 10x the concentration of thiol **2.12** (monomer: thiol: ZnTPP **2.1** = 200: 50: 2.5×10^{-1}), however this led to an overcuring of the monomer and premature gelling of the monomer mixture during storage in the monomer reservoir vat, meaning it was not suitable for 3D printing.

2.3.8 Utilising TPP **2.3** as a photocatalyst

While it was pleasing that it was possible to 3D print to an acceptable standard with ZnTPP **2.1** and thiol **2.12**, the large quantities of both compounds and the long reaction times were unpractical for a commercial application.

The ability to determine whether it was possible to mediate the process using a metal free porphyrin was advantageous for several reasons. Firstly, it would allow a simpler synthesis (lowering the cost) but concentrating on an all organic mediated photoredox catalyst (without a metal) would allow for analogues to be prepared and tested more rapidly and simply.



Scheme 2.5 - Reaction scheme of TPP **2.3** synthesis and metalation to ZnTPP **2.1**¹³⁹

The porphyrin TPP **2.3** was synthesised by refluxing pyrrole **2.13** and benzaldehyde **2.14** in propionic acid for 45 minutes at 150 °C, a method developed by Adler (Scheme 2.5).¹³⁹ The reaction was then filtered and the solid washed with cold methanol and hot water. This gave TPP **2.3** with a low 6% yield after purification. While ZnTPP **2.1** is commercially available (and the commercial material was used in the previous study) it would also be useful to add a metal (e.g., Zn) to any novel porphyrins prepared in the future. Addition of Zn was accomplished by dissolving TPP **2.3** in CHCl₃ and adding Zn(OAc)₂ in MeOH.¹⁴⁰ This was stirred for 1 h and washed with water and brine. This gave ZnTPP **2.1** with a 90% yield.

Comparing the UV-Vis spectra of ZnTPP **2.1** with TPP **2.3** shows the addition of the metal atom shifts the spectrum more towards the red end of the spectrum. In metal free porphyrins there are normally five absorbances (Figure 2.10, Table 2.9).⁵⁶ The Soret peak (normally between 380-500 nm) and 4 Q bands (due to the first excited state S₀ → S₁) in the range 500-750 nm. They are numbered from the red end of the spectrum as I, II, III, and IV, Q bands respectively. Porphyrin TPP **2.3** is an etioporphyrin and in this class the intensity of the Q bands is defined as being IV > III > II > I. If the *meso* positions of a porphyrin (phyllo porphyrins) are substituted, then the intensity order shifts and the II band becomes more intense than the III band (this leads to an increased intensity in the red end of the spectrum). Substitution of a vinyl group or a

carbonyl group at the β -positions (as in chlorophyll) normally leads to the III band being the most intense. Due to the wavelengths of the blue light (420 – 480 nm) and the red light LEDs (580 – 640 nm) used in this study it was expected that TPP **2.3** itself would be a poorer photoredox catalyst compared to ZnTPP **2.1** due to a worse matching of the Soret band with the LED wavelength (blue light) and a significantly lower intensity of absorbance for the Q III band ($\epsilon = 200 \text{ M}^{-1}\text{cm}^{-1}$) and Q II band ($\epsilon = 140 \text{ M}^{-1}\text{cm}^{-1}$) in TPP **2.3** vs the β -band ($\epsilon = 13700 \text{ M}^{-1}\text{cm}^{-1}$) in ZnTPP **2.1**.

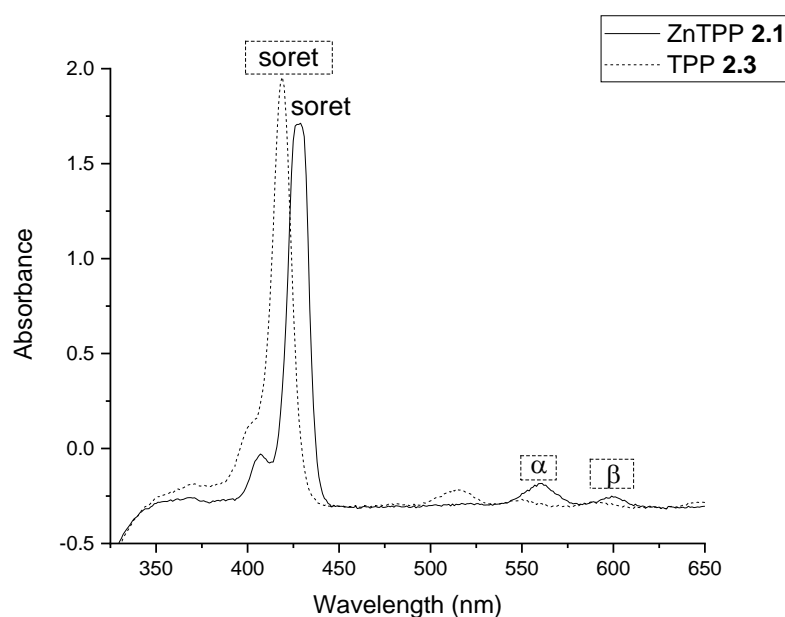


Figure 2.10 - UV-Vis spectrum of TPP **2.3** vs ZnTPP **2.1** in DMSO

Porphyrin	Soret peak (nm)	ϵ ($\text{M}^{-1}\text{cm}^{-1}$)	Other notable peaks (nm)	ϵ ($\text{M}^{-1}\text{cm}^{-1}$)
TPP 2.3	419	15300	515, 551, 589	610, 200, 140
ZnTPP 2.1	427	13700	560, 599	820, 340

Table 2.8 - Comparison of UV-Vis spectrum's of ZnTPP **2.3** and TPP **2.1** in DMSO (0.1475mM)

In the Boyer *et al* paper, it was shown that ZnTPP **2.1** was an effective photoinitiator due to its specific interaction with BPTA **2.2** in the PET-RAFT polymerisation.⁸⁷ This could be due to a possible co-ordination of the carboxylic acid group in BPTA **2.2** as a fifth ligand to the zinc atom. A similar interaction between the zinc atom and the sulfur atom of 1-dodecanethiol **2.10** is theoretically possible and if an important interaction would also suggest that the metal free TPP **2.3** would be unlikely to be as

an efficient photoinitiator. On the other hand, if this interaction is not important it could indicate that TPP **2.3** may also be successful in initiating the polymerisation of MA **2.4**. As in the previous section the thiol used was 1-dodecanethiol **2.10** which acted as both an initiator and a chain transfer agent. Reaction of TPP **2.3** with MA **2.4** in DMSO at room temperature for 120 minutes produced polymers with conversions of monomer of 56% (Run 1) and 43% (Run 3) for blue and red light respectively (Table 2.10). Conversion was higher using blue light (Run 1 vs Run 3), due to the greater absorption at the shorter wavelengths.

Run	Photocatalyst	Light source ¹	Conversion (%) ¹
1	TPP 2.3	Blue	56
2	ZnTPP 2.1	Blue	96
3	TPP 2.3	Red	43
4	ZnTPP 2.1	Red	81

Reaction conditions – MA **2.5**: thiol **2.10**: ZnTPP **2.1** or TPP **2.3** = 200: 1: 5×10^{-2} , irradiated with light for 2 hours in DMSO at 4 cm. ¹ Blue light (420-460 nm) and red light (580-640 nm) ²Determined by 400 MHz ¹H NMR by integrating ratio of peaks at 3.6-4.0 ppm and 5.8-6.5 ppm.

Table 2.9 - Comparing photocatalytic ability of ZnTPP **2.1** and TPP **2.3**

Conversion was poorer compared to ZnTPP **2.1** in both blue (Run 2 vs Run 1) and red light for ZnTPP **2.1** (Run 4 vs Run 3), which again is explained by the slight shift to more suitable matched wavelengths of absorption for ZnTPP **2.1** when compared to TPP **2.3**. *The ability to tailor the porphyrin ligand so that its UV-Vis absorption characteristics are best matched to either blue LED light at (420-460 nm) and red LED light (580-640 nm) will be explored further in the next chapter, where the parent porphyrin TPP **2.3** structure is modified, with the aim of affecting the absorption properties of the porphyrin.*

2.3.9 3D printing using TPP **2.3** as a photocatalyst

Although conversion was found to be lower with TPP **2.3** as a photocatalyst in the polymerisation of MA **2.4**, it was possible to use it to mediate 3D printing using the Photocentric liquid crystal precision printer. Using the optimised conditions reported in section 2.3.7 (monomer 50:50 **w:w 2.5:2.6**: TPP **2.3**: thiol **2.12** = 200: 10: 0.25, 30000 ms, rt), an attempt was made to print the test image. The image printed relatively successfully, Print **F**, (albeit showing some poor resolution of the text in the top left) and was of a similar quality to the print using ZnTPP **2.1**, showing that both

TPP 2.3 and ZnTPP 2.1 are photocatalysts for visible light 3D printing and *indicating that the parent porphyrin structure 2.3 could act as a scaffold in which to design, synthesise and assess any structure activity relationships of novel photocatalysts in the 3D printing arena (Figure 2.11).*

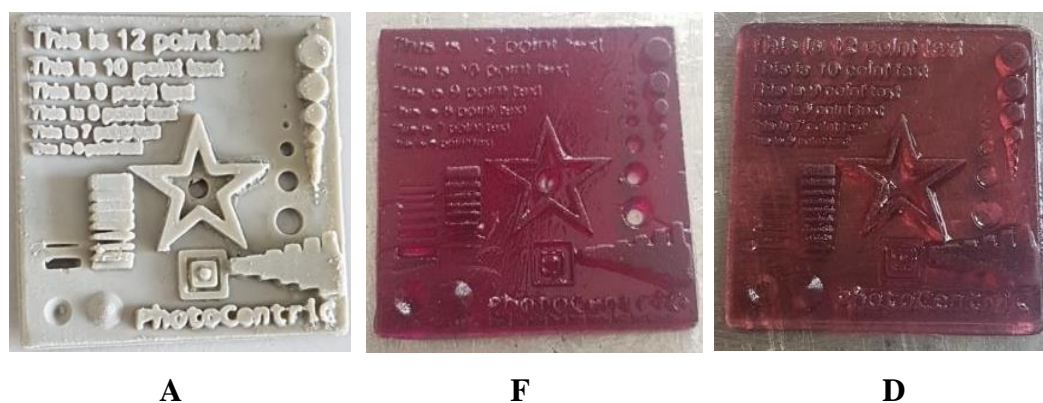


Figure 2.11 - 3D prints – Photocentric standard (A). Using TPP 2.3 (F) and using ZnTPP 2.1 (D) used as a photocatalyst – Monomer: thiol 2.12: ZnTPP 2.1 or TPP 2.3 200: 10: 0.25.

The thermal properties were similar for both Print F and Print D (Figure 2.12, Print F: $T_{5\%} = 403\text{ }^{\circ}\text{C}$, $T_{50\%} = 461\text{ }^{\circ}\text{C}$, high temperature residue at $500\text{ }^{\circ}\text{C} = 2.92\%$; Print D: $T_{5\%} = 397\text{ }^{\circ}\text{C}$, $T_{50\%} = 452\text{ }^{\circ}\text{C}$, high temperature residue at $600\text{ }^{\circ}\text{C} = -1.02\%$).

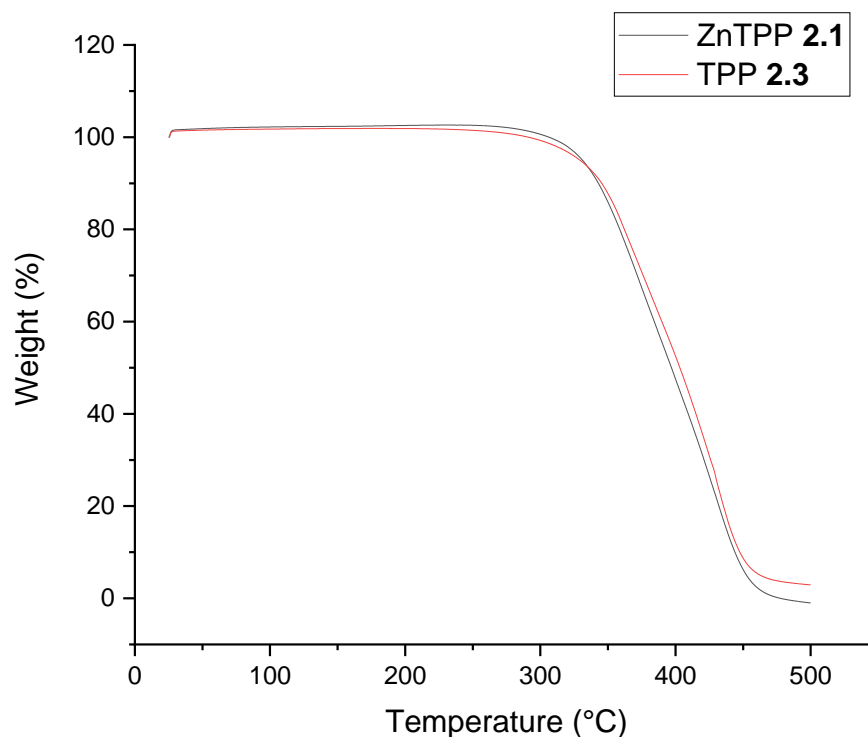


Figure 2.12 - TGA of 3D prints, comparing ZnTPP 2.1 and TPP 2.3 as photocatalyst

2.3.10 Potential mechanisms for polymerisation process

There are a range of potential initiation mechanisms for the generation of radicals using ZnTPP **2.1** or TPP **2.3** and a thiol (such as **2.10**) to prepare polymers. It is assumed that the generation of a thiyl radical is important in initiating the polymerisations, although polar base catalysed Michael thiol-ene processes can also theoretically take place and may be important in the reaction with multivalent thiol **2.12** and TEGDMA **2.5** and UDMA **2.6**. Thiols can form charge transfer complexes between themselves and alkenes which can generate radicals. This process could increase in rate under photocatalysis initiating polymerisation.¹⁴¹ Thiol mediated 3D printing takes place in air and traces of peroxides can also generate thiyl radicals which can initiate chains.

It is known that blue light irradiation of MA **2.4** in DMSO in air can initiate a polymerisation with a RAFT agent without the need for a photocatalyst in blue light.¹⁴² Although no polymerisation was observed in blue light when thiol and photocatalyst were absent, a low conversion (10%) of MA **2.4** was observed in blue light with ZnTPP **2.1** only (no thiol). This indicates there is an interaction between the excited ZnTPP* **2.1** species and MA **2.4** which can initiate the polymerisation, presumably *via* a SET to give a monomer radical anion. However, conversion increases to 90% when 1-dodecanethiol **2.10** is introduced. This could be due to a range of potential reasons. One being that because while the interaction between MA **2.4** and the excited ZnTPP* **2.1** species is inefficient, the competing reaction (chain transfer) between 1-dodecanethiol **2.10** and the propagating radical species is more favourable which increases the rate on initiation of polymerisation *via* chain transfer. This results in 1-dodecanethiol **2.10** controlling both the rate of polymerisation and the molecular weight by behaving as a chain transfer agent and propagating the polymerisation.

Another potential method for generating initiating thiyl radicals from the thiol additive may be *via* the homolysis of the S-H bond mediated by electron transfer or by the cleavage of a pentacoordinated thiol ZnTPP complex. Boyer *et. al.* hypothesises an interaction between the zinc atom of ZnTPP **2.1** and the carboxylic acid of BTPA **2.2** in the RAFT mediated polymerisation of MA **2.4**. To determine if an interaction occurs between thiol **2.10** and ZnTPP **2.1**, a UV-vis spectrum of ZnTPP **2.1** with 1-dodecanethiol **2.10** was recorded and compared to the visible spectrum of ZnTPP **2.1** (Figure 2.13). The resulting spectrum did not show any major difference, suggesting

this interaction did not take place and the large α -band confirming the square planar geometry.

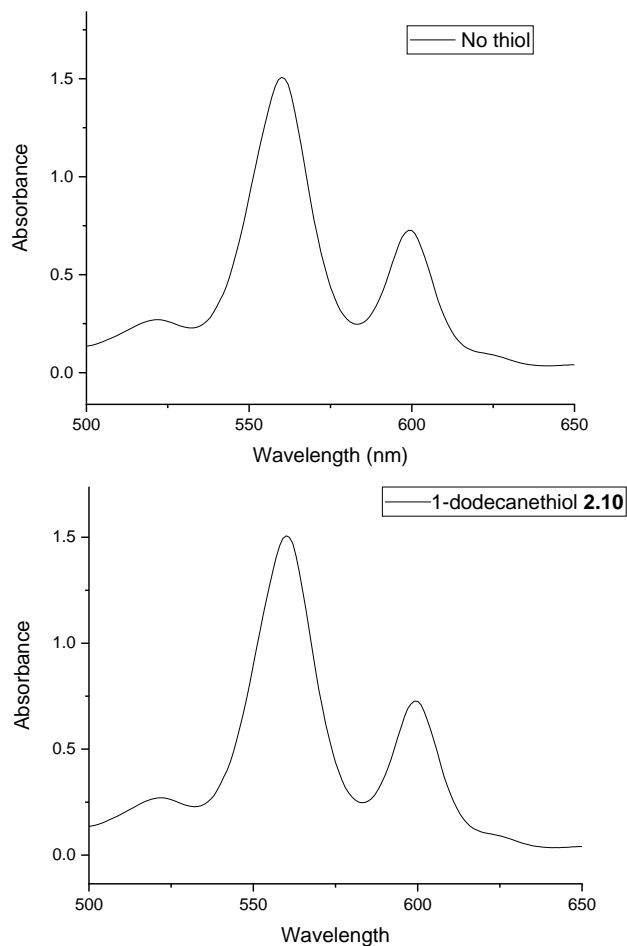


Figure 2.13 – Comparison of the Q region of the UV-vis spectrum of ZnTPP **2.1** without thiol (top) and with 1-dodecanethiol (bottom)

The final process that is possible, is that the excited ZnTPP **2.1** or TPP **2.3** species can act as an oxidizing agent, interacting with 1-dodecanethiol and producing a radical cation which fragments to give the thiyl radical and H^+ . The thiyl radical is then able to initiate the polymerisation. Ruthenium based transition metal catalysts have been shown to act as oxidative photocatalysts of thiol addition to alkenes in air under blue light LED irradiation with oxygen being transformed into peroxide radical *in situ*.²⁷ Similarly, a range of metal TPP and metal free porphyrin derivatives have been shown to generate radical cations from O, S and N containing compounds in a range of simple organic transformations.¹⁴³ In air excited TPP* **2.3**

is able to generate triplet oxygen which can initiate sulfur oxidation and generate peroxides which can in turn generate thiyl radicals.¹⁴⁴

In all of these potential mechanisms, it is important to note that it is the thiol that controls the molecular weight of the polymerisation and not the photocatalyst ZnTPP **2.1** or TPP **2.3**. Therefore, any changes to the photocatalyst should not result in a large change in molecular weight of the polymer produced, however any change in thiol concentration will control molecular weight.

While thiols can mediate the polymerisation of acrylates *via* a radical pathway, multifunctional thiols have also been used to produce cross-linked materials *via* thiol-Michael addition polymerisation of acrylates and methacrylates.¹⁴⁵ This mechanistic process is normally mediated by base (e.g. amine) or nucleophile (e.g. phosphine) catalysis. More recently, photoinitiated Michael processes have been developed using UV and blue light and wavelength-selective switching between a thiol-Michael reaction (400-500 nm) and a radical mediated process (365 nm) has been reported.¹³⁵ Although the exact mechanism of the thiol / ZnTPP **2.1** process described above is unclear it may be possible that both a radical and Michael process is occurring simultaneously in air.

2.3.11 Summary

In this chapter it has been shown that ZnTPP **2.1** and metal free TPP **2.3** are effective photocatalysts for the polymerisation of MA **2.4**, using a range of thiols **2.10** – **2.12** as co-initiators. This was possible in both blue and red LED light, with polymerisations in blue light being more effective due to a better matched absorption profile of catalyst and light. ZnTPP **2.1** can also be used as a photocatalyst in visible light 3D printing of a commercial TEGDMA **2.5** / UDMA **2.6** mix on the Photocentric liquid crystal precision printer using blue light, producing a print of a similar standard to the commercial 3D print using multifunctional thiols. However, the levels of thiol **2.12** and photocatalyst **2.1** necessary was too high to be commercially attractive and the speed of the 3D print is significantly slower to that desired (300,000 ms vs 50 ms per layer). A 600-fold increase in rate with a 5-fold drop in catalyst and thiol loading would be required to make the process commercially attractive.

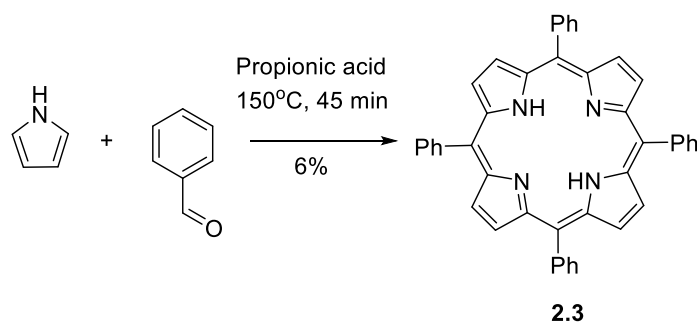
In addition, TPP **2.3** was also shown to be able to polymerise MA **2.4**, albeit not as efficiently as ZnTPP **2.1** due to the UV-Vis absorption properties being blue shifted

away from the ideal range and with lower extinction coefficients in the Q band range. However, TPP **2.3** is still able to be used in 3D printing as a photocatalyst when using blue light and the ability to readily functionalise this porphyrin structure to improve solubility and absorption ranges maybe an advantage in future research.

3 Assessment of tetraphenylporphyrin derivatives in 3D printing

3.1 Introduction

The synthesis of tetraphenylporphyrins was well established by Adler *et al.*¹³⁹ The method involved refluxing pyrrole with benzaldehyde, with the functional groups present on the benzaldehyde giving the desired tetraphenylporphyrin (Scheme 3.1).



Scheme 3.1 – Synthetic route of TPP **2.3**¹³⁹

Consequently, the procedure of functionalising TPP **2.3** at the *meso* position is relatively simple by replacing benzaldehyde for functionalised aromatic aldehyde variants. It is known that visible light polymerisation is initiated by electron transfer from the π -system of the porphyrin,⁸⁷ so adding electron withdrawing and electron donating functional groups should change the rate at which this happens, which may lead to improved photocatalytic ability. Also, functionalising the peripheral substituents of porphyrins has been shown to affect the absorption properties of the porphyrin.¹⁴⁶ This gives the ability to fine tune the wavelengths at which the porphyrins can absorb light to more desirable wavelengths (blue light 420-460 nm and red light 580-640 nm).

3.2 Aims and objectives

The aim of this chapter is to functionalise the peripheral phenyl rings of tetraphenylporphyrin in a variety of ways to tune the absorption properties and reactivity of the photocatalyst. To do this, the following objectives were set:

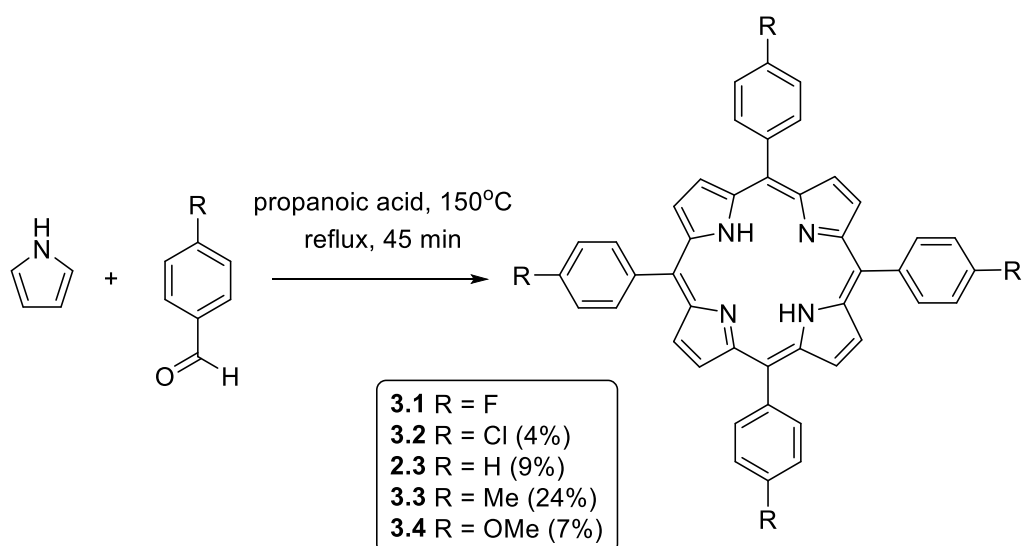
- Synthesise *para* substituted variants of both metalated and metal-free porphyrins containing electron donating and withdrawing groups
- Study the spectroscopic properties and photocatalytic ability of *para* substituted porphyrins in the polymerisation of MA **2.4** and 3D printing.
- Synthesise *ortho* and *meta* variants of porphyrins and study the effect on photocatalytic ability.

- Synthesise multifunctional porphyrin variants and study the effect on photocatalytic ability
- Synthesise a protonated porphyrin variant and study the effect on photocatalytic ability

3.3 Results and discussion

3.3.1 Synthesis of tetraphenylporphyrin derivatives **3.1** – **3.4**

The first modification made to the porphyrins was to add electron donating (Me, OMe) and withdrawing substituents (F, Cl) to the *para* position of the phenyl ring. It was expected that the addition of electron donating groups would increase the electron density of the aromatic system of the porphyrin, leading to increased resonance effects which would shift the visible absorption towards a higher wavelength (more favourable for 3D printing).



Scheme 3.2- Synthesis of *para* modified porphyrins **3.1** – **3.4** ¹³⁹

The synthesis of these porphyrins involved using a modified Adler method (Scheme 3.2)¹³⁹, refluxing pyrrole with the appropriate benzaldehyde in propionic acid for 45 minutes (Scheme 3.2). The reaction mixture was then filtered, and the filtrate washed with hot water and cold methanol. This produced the desired functionalised porphyrins **3.1** – **3.4** in low yields (4-20 %). At this point there was no focus on optimising the synthesis to improve yields as it was unclear at this stage whether the new catalysts would be better than the control **2.3**.

The absorption data for these porphyrins was obtained in DMSO (the solvent for the control polymerisations) and compared to TPP **2.3**. The fluoro substituted porphyrin **3.1** did not dissolve in DMSO or chloroform, which meant that recording a comparative UV-Vis spectrum was not possible, therefore it was not studied any further.

The 3-dimensional structure of TPP **2.3** is such that the meso-phenyl groups at the β -position on the porphyrin are almost perpendicular to the plane of the porphyrin.¹⁴⁶ This would suggest any resonance effect between the porphyrin core and the aryl group would be minimal. However, despite the noncoplanar configuration of the phenyl and porphyrin planes, it has been shown that the resonance-type effects from the substituents at the β -position of the porphyrin are significant enough to influence the electronics of the porphyrin.¹⁴⁶ An analysis of the UV-Vis spectrum allowed us to observe this influence (Figure 3.1).

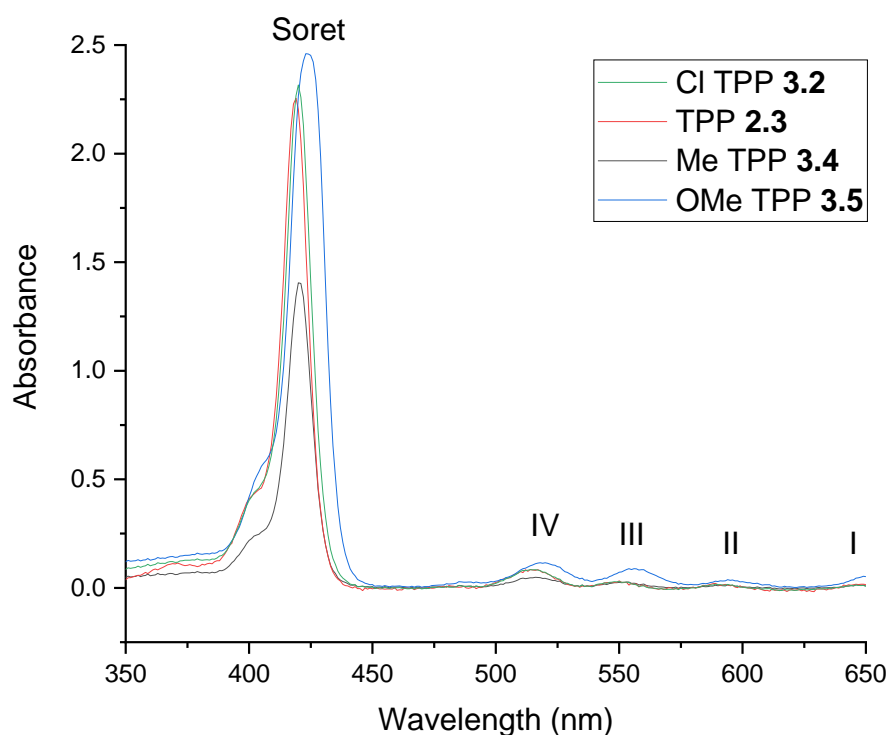


Figure 3.1 - UV-Vis of metal free porphyrins **2.3** and **3.2** – **3.4** in DMSO (0.1475 mM)

Run	Functional group	Soret band (nm)	ϵ ($M^{-1}cm^{-1}$) ¹
1	4-Cl 3.2	418	15700
2	H 2.3	419	15300
3	4-Me 3.3	420	9500
4	4-OMe 3.4	423	16700

¹ Molar extinction coefficient of soret band

Table 3.1 – Soret bands of *para* modified porphyrins **2.3** and **3.2** – **3.4** in DMSO (0.1475 mM)

Firstly, the increase in the electron donating power of the *para* substituents (Cl < H < Me < OMe) led to a small red shift in the absorption of the porphyrins for all bands (Table 3.1, run 1→4). With a 5 nm shift in the soret band from the Cl porphyrin **3.2** (run 1) to the methoxy porphyrin 4-MeO-TPP **3.4** (run 4). This small shift may allow for the methoxy porphyrin 4-MeO-TPP **3.4** to be a more effective photocatalyst as its absorption range is more in the desirable range. The molar extinction coefficients ϵ of the 4-MeO-TPP **3.4** and 4-Cl-TPP **3.2** variants were like the unmodified TPP **2.3** at the soret band, with values between 15000-17000 $M^{-1}cm^{-1}$, although the methoxy derivative **3.4** was the highest. The 4-Me-TPP **3.3** was found to have a weaker ϵ , suggesting it could be a less effective photocatalyst.

Run	Functional group	Q bands (nm)	ϵ ($M^{-1}cm^{-1}$) ¹	Ratio of ϵ ²
1	4-Cl 3.2	590, 549, 514	610, 200, 140	1: 0.33: 0.23
2	H 2.3	591, 551, 515	610, 200, 140	1: 0.33: 0.23
3	4-Me 3.3	591, 551, 515	270, 140, 70	1: 0.52: 0.26
4	4-OMe 3.4	595, 556, 519	820, 610, 270	1: 0.74: 0.32

¹ Q region bands – IV, III, II ²Ratio of Q region bands IV: III: II

Table 3.2 – Q region bands of *para* modified porphyrins **3.2** – **3.4** compared to TPP **2.3**

There is also an effect on the 2nd important region of the visible spectrum, the Q region (Table 3.2). Porphyrins can be grouped depending on the relative intensities of the Q bands, with porphyrins **3.2** – **3.4** being part of the *etioporphyrin* group.⁵⁶ This is due to the relative intensities of the Q bands following the pattern – IV > III > II > I. But by comparing the ratio of intensities of these bands, it can be seen that there has been

a reddening effect towards a *rhodo*-type porphyrin (III > IV > II > I), with the intensity of band III increasing with the electro donating ability of the substituents (runs 1→4).

To determine the effect of changing the functional groups on the photocatalytic ability of each porphyrin, each porphyrin was used as a photocatalyst for the polymerisation of MA **2.4** (Table 3.3). 1-Dodecanethiol **2.10** was chosen as the co-initiator, and the ratio of reactants MA **2.4**: 1-dodecanethiol **2.10**: porphyrin was 200:1:1x10⁻². The reaction mixtures were degassed and irradiated with light for 2 h from 4 cm away. Conversion was determined by 400 MHz ¹H NMR by integrating ratio of peaks at 3.6-4.0 ppm and 5.8-6.5 ppm.

Due to the red shifting of the methoxy porphyrin **3.4** absorption, it was expected that conversion would be greatest when utilising it as a photocatalyst, and this was the case in both blue and red light (approximately a 15% increase in conversion in blue light TPP **2.3** → 4-MeO-TPP **3.4** = 56 → 71% and a 17% increase in conversion in red light TPP **2.3** → 4-MeO-TPP **3.4** = 43 → 60%). The chloro modified porphyrin 4-Cl-TPP **3.2** gave the lowest conversion (with no conversion in red light), suggesting that addition of electron withdrawing substituents has a significant negative effect on photocatalytic reactivity. The measured conversion using the methyl substituted porphyrin 4-Me-TPP **3.4** was similar to that of TPP **2.3**, this is likely due to their similar absorption and electronic profiles.

Run	Porphyrin	Light source ¹	Conversion (%) ²
1	4-Cl 3.2	Blue	5
2	4-Cl 3.2	Red	0
3	H 2.3	Blue	56
4	H 2.3	Red	43
5	4-Me 3.3	Blue	59
6	4-Me 3.3	Red	45
7	4-OMe 3.4	Blue	71
8	4-OMe 3.4	Red	60

Reaction conditions: MA **2.4**: thiol **2.10**: porphyrin – 200: 1: 1x10⁻², degassed and irradiated with light for 2 h from 4 cm away. ¹ Blue light (420-460 nm) and red light (580-640 nm) ²Determined by 400 MHz ¹H NMR by integrating ratio of peaks at 3.6-4.0 ppm and 5.8-6.5 ppm

Table 3.3 -Polymerisation of MA **2.4** using *para* modified porphyrin variants **3.1** – **3.4**

To further study the effect of adding a methoxy functional group to the *para* position of the phenyl ring, a conversion study was undertaken (Table 3.4). The reaction conditions were MA **2.4**: thiol **2.10**: porphyrin **3.4** – 200: 1: 1×10^{-2} , with aliquots taken at 30-minute intervals, and conversion determined using 400 MHz ^1H NMR. From the polymerisation results, it can be seen that the change in photocatalyst has little effect on the molecular weight of the polymer produced. This is to be expected, as discussed in section 2.3.10, it is the thiol that controls molecular weight, not the photoinitiator. These results further support this hypothesis, as a change in photoinitiator has little to no effect on molecular weight, as the change in photocatalyst will make the generation of initial radicals more efficient. The results show that the reaction rate is faster when using the methoxy porphyrin (run 1→run 2), showing that the *para* substituted methoxy porphyrin has improved photocatalytic ability.

Run	Porphyrin ¹	Time (min)	Conversion (%) ²	M_n^3	M_w^3	Đ^3
1	2.3	30	25	32k	44k	1.60
2	3.4	30	40	34k	46k	1.70
3	2.3	60	30	33k	45k	1.61
4	3.4	60	53	34k	47k	1.71
5	2.3	90	42	34k	45k	1.58
6	3.4	90	60	35k	47k	1.63
7	2.3	120	50	34k	45k	1.60
8	3.4	120	71	36k	48k	1.58

Reaction conditions: MA **2.4**: thiol **2.10**: porphyrin – 200: 1: 1×10^{-2} , degassed and irradiated with light for 2 h from 4 cm away. ¹Polymerisation in blue light (420-460 nm) ²Determined by 400 MHz ^1H NMR by integrating ratio of peaks at 3.6-4.0 ppm and 5.8-6.5 ppm. ³ molecular weight and polydispersity index were determined by GPC analysis (CHCl_3 as eluent) calibrated to poly (methyl methacrylate)

Table 3.4 - Conversion study of polymerisation of MA **2.4** using TPP **2.3** and 4-MeO-TPP **3.4**

3.3.2 3D prints with functionalised metal free porphyrins **3.1** -**3.4**

In section 3.3.1 it was shown that that the methoxy modified porphyrin 4-MeO-TPP **3.4** gave the highest conversion in the polymerisation of MA **2.4**, so the next step was to see if this translated to improved 3D printing. The hypothesis is that 4-MeO-TPP **3.4** would give the most defined image, as it was the most effective photocatalyst in

the polymerisations studied. And the greater reactivity may allow for a lower irradiation time between layers.

The 3D print was performed using a 50:50 w: w mixture of TEGDMA **2.5** / UDMA **2.6**, with the exposure per layer being 300,000 ms. The ratio of reactants of monomer: thiol **2.12**: porphyrin was chosen as 200: 25: 0.25, using pentaerythritol thiol **2.12** as the co-initiator and 15g of monomer mixture for each run. All three photocatalysts produced 3D prints, although there was a clear difference in the quality of the prints produced (Figure 3.2). Print **G** (using the chloro modified porphyrin 4-Cl-TPP **3.2**), was very under cured, with much of the image not printed / resolved. The print showed a significant inhomogeneity of colour and exhibited a green tinge possible due to cleavage of the C-Cl bond generating traces of chlorine. This suggests that the polymerisation rate was too slow and / or the catalyst was unstable, such that the chloro photocatalyst **3.2** was not suitable for further study. Both the 4-Me-TPP **3.3** and 4-OMe-TPP **3.4** catalysts produced better images (prints **H** and **I** respectively) than the control **2.3** TPP (print **F**), with all aspects of the test print visible. It is interesting to note that all the prints (prints **F** –**I**) are of a different colour. While each catalyst exhibits a slightly different UV / visible spectrum the differences are small, and this was not expected to affect the final colour of the print. Print **I** generated from 4-OMe-TPP **3.4** looked a better standard of print, due to the text being more visible, as well as more protruding cylinders being visible.

It is interesting to compare print **I** with the original Photocentric test print **A**. It appears there is more definition around the ridges (circled areas **A** and **B**, row 2) and there also appears to be better resolution of the hollow circles (circled **C**, row 2). The resolution is also enhanced in the text between the letters in the two prints (Print **I** vs Print **A**, row 3). While Print **I** was prepared using a 300,000ms curing time per layer and Print **A** utilised a lower 50ms value and so a direct comparison is not possible, although the resolution of the test Print **A** is deemed acceptable by the industrial partner. Interestingly, Print **I** shows a slanting of the text in the top right corner and other loss of resolution caused by ‘movement’ of the print at the edges. This is almost certainly due to insufficient curing at the edges and due to lower viscosity movement at the edges.



Print A



Print G



Print F



Print H



Print I



Print I



Photocentric test Print A



Print I

Print A

Figure 3.2 – Row one: Photocentric test print **A** and 3D print using modified porphyrin. Print **G** = 4-Cl-TPP. Row two: 3D print using modified porphyrins: Print **F** = TPP 2.3, Print **H** = 4-Me-TPP 3.3, Print **I** = 4-OMe-TPP 3.4. Row three: Comparison of key areas in Print **I** = 4-OMe-TPP 3.4 and photocentric test print **A**. Row four: Resolution of the text in Print **I** and Print **A**

The thermal stability of the prints was measured using TGA, with the prints heated at 10 °C per minute over the temperature range 0-600 °C in air, using a Mettler-Toledo TGA instrument (Table 3.5). The overall TGA results suggest that the changing of the photocatalyst only has a minor effect on the thermal properties of the prints (Figure 3.3). This is interesting, as print **G** is undercured yet has very similar thermal properties to the more complete prints. These results show that *para* functionalisation of the porphyrin has little effect on the thermal properties of the resulting print.

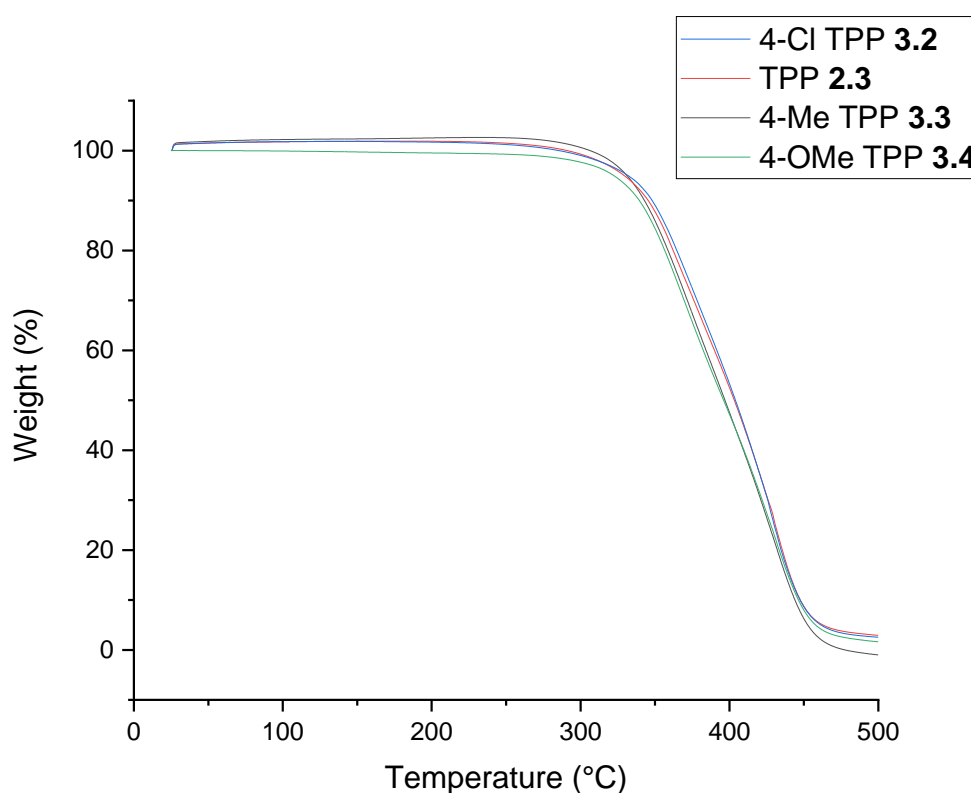


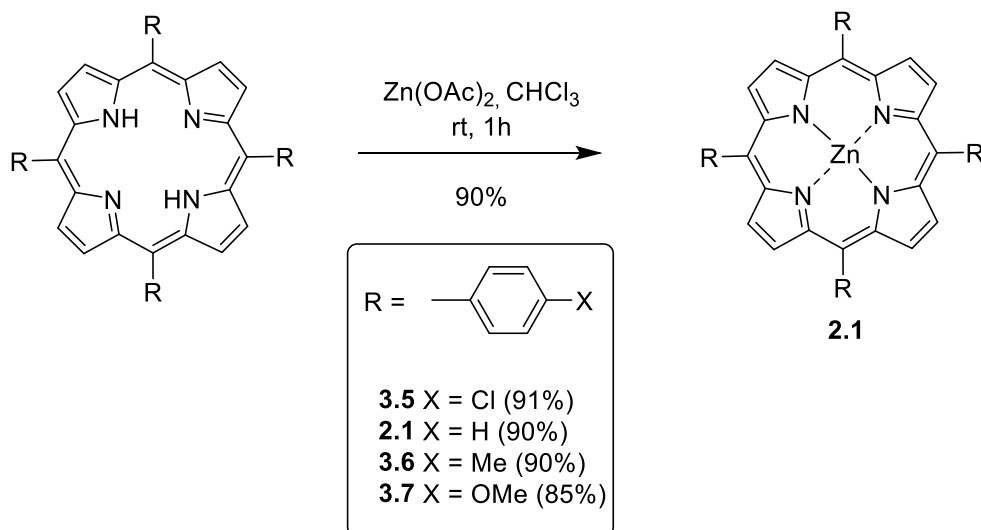
Figure 3.3 - TGA data of 3D prints using modified metal-free porphyrins **3.1** – **3.4** as photocatalysts

Run	Porphyrin	T _{50%} (°C)	T _{5%} (°C)
1	3.2	461	404
2	2.3	463	403
3	3.3	460	403
4	3.4	462	403

Table 3.5 - T_{50%} and T_{5%} for TGA data of metal-free porphyrins **3.1** – **3.4** (Figure 3.3)

3.3.3 Incorporation of zinc into porphyrins **3.1** – **3.4**

Incorporation of zinc into the porphyrin is likely to increase efficiency of the catalyst, as the photocatalytic ability of ZnTPP **2.1** was shown to be more effective than that of TPP **2.3** in chapter 2, and it is a simple process to metalate the metal-free porphyrins (Scheme 3.3).¹⁴⁰



Scheme 3.3 – Synthetic route of zinc porphyrins **3.1** and **3.5** – **3.7** ¹⁴⁰

To synthesise the zinc porphyrins **3.5** – **3.7**, the corresponding metal-free porphyrin was dissolved in chloroform, then Zn(OAc)_2 in MeOH is added and stirred for 1 h at room temperature (Scheme 3.3). The reaction mixture was washed with water and brine, the organic layer was dried, and the solvent removed. This gave **3.5** – **3.7** as purple solids with 85-91 % yield.

The UV-Vis of each metalated porphyrin was measured in DMSO (Figure 3.4 and Table 3.6). As seen in chapter 2, the absorption for all metalated porphyrins was shifted towards a higher wavelength, with the Soret bands shifted between 8-11 nm and the Q region no longer containing four bands, but just the two α and β bands indicating successful complexation of the metal. As previously for the non-metalated derivatives the 4-MeO-ZnTPP **3.7** exhibited the most red shifted Soret and Q region (although the differences were negligible). Interestingly, the addition of the chloro group 4-Cl-ZnTPP **3.5** also led to an increase in the wavelength.

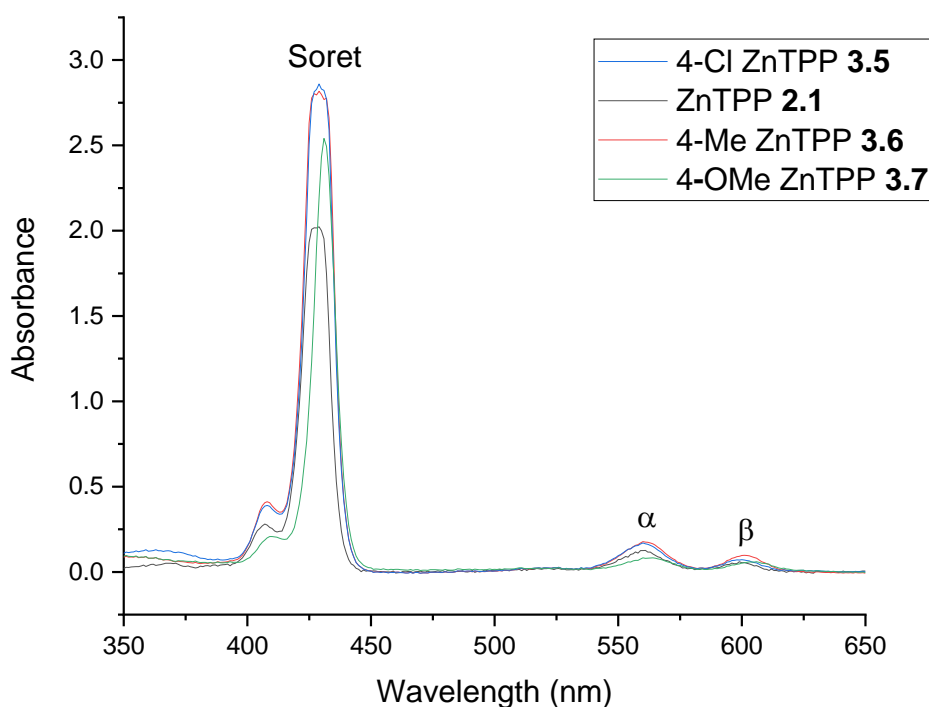


Figure 3.4- UV-Vis of zinc *para* substituted porphyrins **2.1** and **3.5 – 3.7** in DMSO (0.1475 mM)

However, when looking at the relative intensities of the α and β bands, they increase in the order from **3.5** > **2.1** > **3.6** > **3.7** as the electron donating ability increases (run 1→4). This suggests that even with the addition of the zinc metal centre, the addition of a more electron donating functional groups leads to a reddening effect on the absorption properties.

Run	Functional group	Soret band (nm)	ϵ ($M^{-1}cm^{-1}$)	Q region bands ¹ (nm)	ϵ^2 ($M^{-1}cm^{-1}$)	Ratio of ϵ^3
1	Cl 3.5	429	19200	560,600	1800, 480	1:0.27
2	H 2.1	427	13700	560, 599	820, 340	1:0.41
3	Me 3.6	429	19000	560, 600	1200, 680	1:0.56
4	OMe 3.7	431	17000	563, 605	540, 410	1:0.76

¹ Q region bands – α . β ² Molar extinction coefficient of Q region bands. ³Ratio of molecular extinction coefficient of Q bands – α : β

Table 3.6 - UV-vis data of zinc *para* substituted porphyrins **2.1** and **3.5 – 3.7** in DMSO (0.1475 mM)

The photocatalytic ability of the zinc modified porphyrins were then tested by repeating the polymerisation of MA **2.4**, under the same reaction conditions as the

non-metal variants (MA **2.4**: thiol **2.10**: porphyrin **3.5 – 3.7** is 200: 1: 1×10^{-2}) in order for a comparison to be made.

Run	Porphyrin	Light source ¹	Conversion (%) ²
1	4-Cl 3.5	Blue	75 (5)
2	4-Cl 3.5	Red	68 (0)
3	H 2.1	Blue	90 (56)
4	H 2.1	Red	74 (43)
5	4-Me 3.6	Blue	71 (59)
6	4-Me 3.6	Red	42 (45)
7	4-OMe 3.7	Blue	92 (71)
8	4-OMe 3.7	Red	85 (66)

Reaction conditions: MA **2.4**: thiol **2.10**: porphyrin – 200: 1: 1×10^{-2} , degassed and irradiated with light for 2 h from 4 cm away. ¹Blue light (420-460 nm) and red light (580-620 nm) ²Determined by 400 MHz ¹H NMR by integrating ratio of peaks at 3.6-4.0 ppm and 5.8-6.5 ppm. The numbers in parentheses are the conversions when using the non-metalated analogues **3.2 – 3.4** and **2.3**

Table 3.7 – Polymerisations of MA **2.4** using modified zinc porphyrins **2.1** and **3.5 – 3.7** as photocatalysts

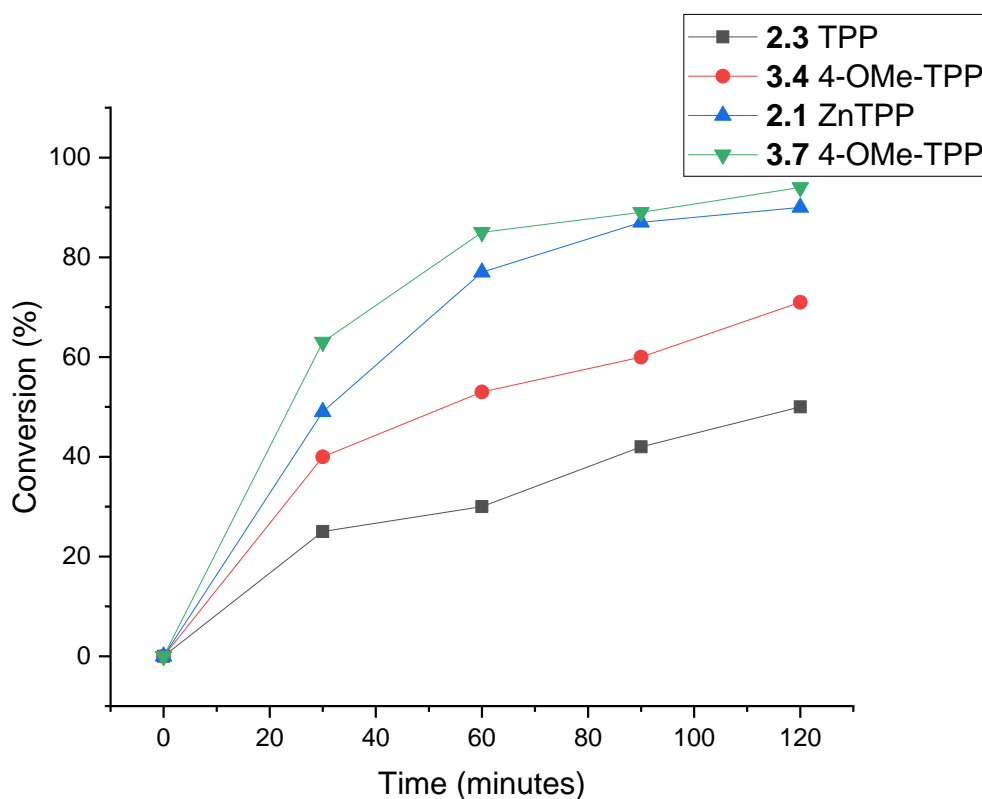
As expected from results in the previous chapter conversion is much greater when using the metalated porphyrins in both blue (420 – 460 nm) and red (580 – 640 nm) light (Table 3.7). The conversions are consistently lower in red light (580 – 640 nm), due to the absorption profiles of the porphyrins being favourable towards blue light (420-460 nm). Unlike the result using 4-Cl-TPP **3.2** (5% conversion in blue light) there was significant conversion for the metalated derivative 4-Cl-ZnTPP **3.5** (75%), suggestive that relative solubility of the catalyst in the reaction medium may be key in explaining the difference here. While conversions were significantly improved in all cases by metalation (18-70% increase) the methoxy derivative 4-OMe-ZnTPP **3.7** still provided the highest conversion over 2 hours.

To confirm this improved photocatalytic ability, the conversion over time of the 4-OMe-ZnTPP **3.7** mediated reaction was compared to ZnTPP **2.1** (Table 3.8, Graph 3.1). The reaction conditions for the kinetic studies were the same as for the previous polymerisations (MA **2.4**: thiol **2.10**: porphyrin – 200: 1: 1×10^{-2}), with aliquots taken at 30-minute intervals, and conversion determined using 400 MHz ¹H NMR.

Run	Time (mins)	Porphyrin	Conversion (%) ¹	M_n^2	M_w	\bar{D}
1	30	3.7	63	37k	62k	1.71
2	30	2.1	49	35k	60k	1.70
3	60	3.7	85	37k	61k	1.68
4	60	2.1	77	35k	59k	1.64
5	90	3.7	89	38k	62k	1.68
6	90	2.1	87	35k	61k	1.70
7	120	3.7	94	38k	62k	1.65
8	120	2.1	90	36k	60k	1.67

Reaction conditions: MA **2.4**: thiol **2.10**: porphyrin – 200: 1: 1×10^{-2} , degassed and irradiated with blue light for 2 h from 4 cm away. ¹Determined by 400 MHz ¹H NMR by integrating ratio of peaks at 3.6-4.0 ppm and 5.8-6.5 ppm. ²molecular weight and polydispersity index were determined by GPC analysis (CHCl₃ as eluent) calibrated to poly (methyl methacrylate)

Table 3.8 – Conversion study of the polymerisation of MA **2.4** using ZnTPP **2.1** and 4-OMe-ZnTPP **3.7** as photocatalysts



Graph 3.1 - Conversion vs time comparison of polymerisation of MA using TPP **2.3**, 4-OMe-TPP **3.4**, ZnTPP **2.1** and 4-OMe-TPP **3.7** as photocatalysts

Conversion is significantly enhanced suggesting that the 4-OMe-ZnTPP **3.7** is a more effective photocatalyst and should be more suitable for 3D printing as the polymerisation rate is faster.

3.3.4 3D prints with zinc functionalised porphyrins **3.5** – **3.7**

All three modified porphyrins **3.5** – **3.7** were tested as photocatalysts in 3D printing, with the methoxy porphyrin expected to produce the clearest image. The 3D print was performed using a 50:50 w: w mixture of TEGDMA **2.5**/ UDMA **2.6**, with the exposure per layer being 300,000 ms. The ratio of reactants monomer: thiol **2.12**: porphyrin **3.5** – **3.7** was 200: 25: 0.25, using pentaerythritol thiol **2.12** as the co-initiator and 15g of monomer mixture for each run (Figure 3.5).

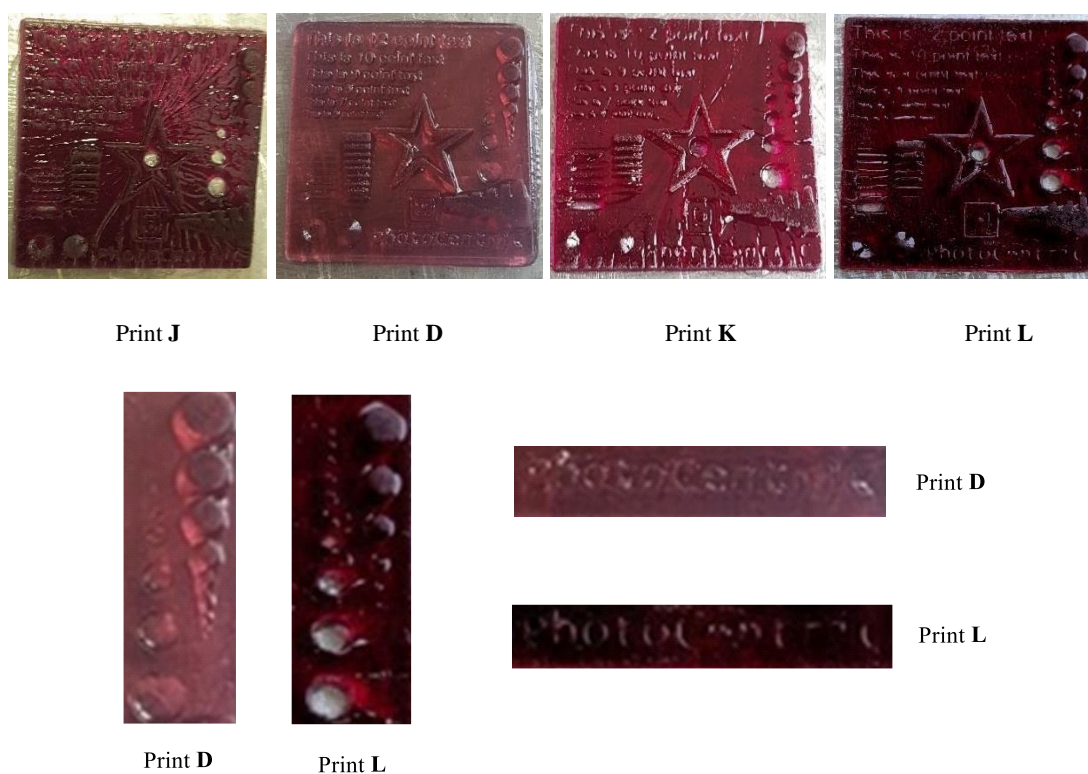


Figure 3.5 - 3D print using modified zinc porphyrin **3.1** and **3.5** – **3.7**. Row one: Print **J** = 4-Cl-ZnTPP **3.5**, print **D** = ZnTPP **2.1**, print **K** = 4-Me-ZnTPP **3.6**, print **L** = 4-OMe-ZnTPP **3.7**. Row two (left): Resolution of cylinders and holes in prints **D** and **L**. Row two (right): Resolution of text in Print **D** and print **L**.

All three modified porphyrins produced an image, however using the 4-Cl-ZnTPP **3.5** produced a print with a range of internal fault (lines highlighted by the circle). There is not too much difference overall between print **D** (ZnTPP **2.1**) and print **L**

(4-MeO-ZnTPP **3.7**), with the test producing better resolved circles (right) and shapes (bottom left) for print **L**.

The thermal stability of the prints was measured using TGA, with the prints heated at 10 °C per minute over the temperature range 0-500 °C in air, using a Mettler-Toledo TGA instrument.

The TGA data shows that the point of degradation is similar when using all four porphyrins (Figure 3.6, Table 3.9). When looking at the TGA data for the 3D prints, the $T_{5\%}$ and $T_{50\%}$ is greater for all modified porphyrins, however this difference can be attributed to the error of the TGA machine, with the general trend of the TGA results being very similar. As explained in the chapter 2, due to the overlapping thermal characteristics of UDMA **2.6** and TEGDMA **2.5**, there is one major decomposition step for all four 3D prints. This data suggests that the changing of photocatalyst has little effect on the thermal properties of the 3D print.

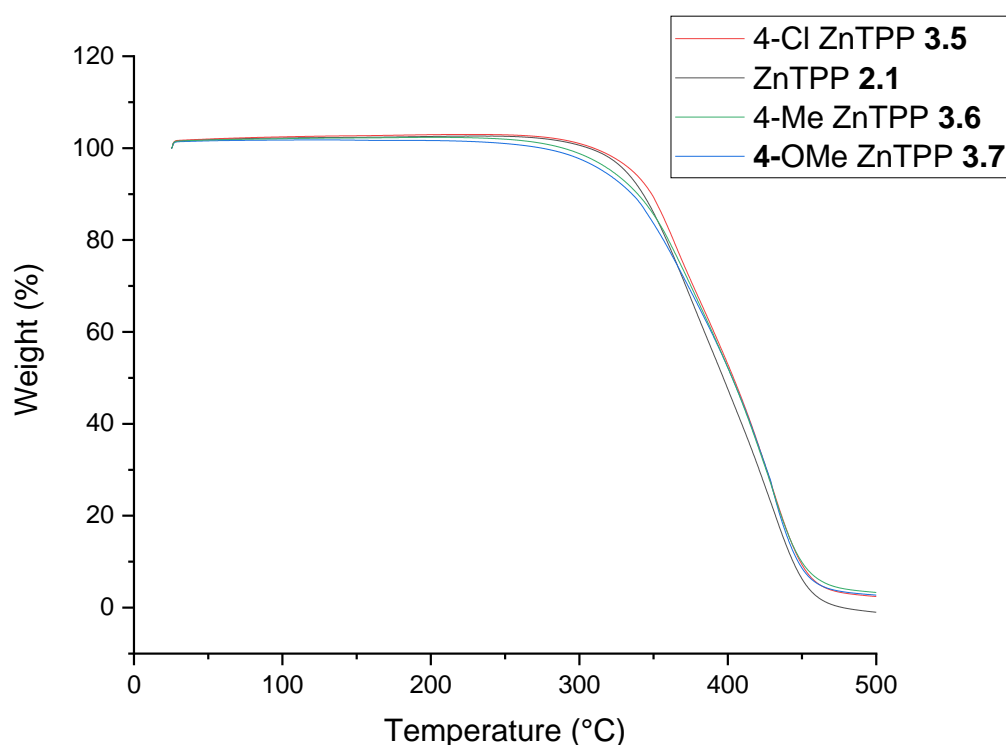


Figure 3.6 - TGA data of ZnTPP **2.1** and *para* modified zinc porphyrins **3.5-3.7** 3D prints

Run	Porphyrin	T _{50%} (°C)	T _{5%} (°C)
1	3.5	461	404
2	2.1	452	396
3	3.6	460	403
4	3.7	462	403

Table 3.9 - T_{50%} and T_{5%} for TGA data for 3D prints using *para* modified zinc porphyrins **2.1** and **3.5** – **3.7**.

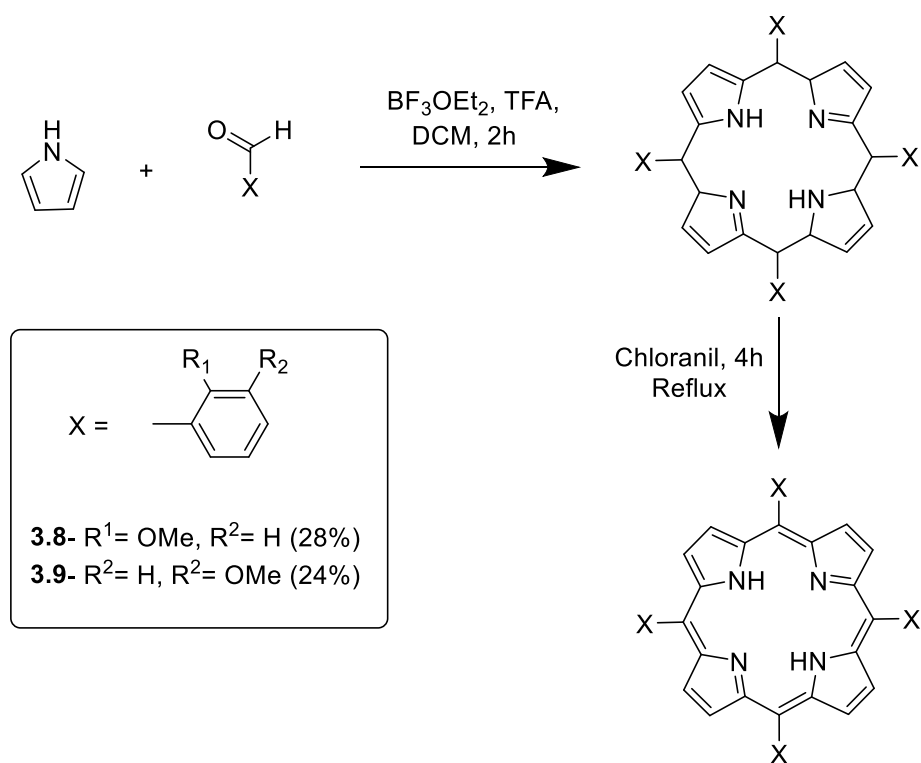
3.3.5 Position of the methoxy substituent on the aromatic ring:

Preparing 2-MeO, 3-MeO derivatives of TPP **2.3**

After looking at the effect of functionalising the porphyrins with electron donating and withdrawing groups, another avenue to explore is the position of the functional groups on the benzene ring of the porphyrins. In the previous section, it was shown that the addition of the methoxy group at the *para* position on the benzene ring of tetraphenylporphyrin increased photocatalytic ability. To study the effect of changing the position of functionalisation, 3 methoxy variants were synthesised.

The synthesis of *para* methoxy porphyrins involved refluxing 4-methoxybenzaldehyde with pyrrole to give the resulting modified porphyrin. This is one of the two widely established methods of synthesising symmetrical modified porphyrins. The other method was developed by Lindsey *et al*, which involved condensation of aromatic aldehydes with pyrrole under mixed-acid catalysis.¹⁴⁷ To synthesise the *ortho* and *meta* variants of methoxy porphyrin, the Lindsey method was used (Scheme 3.4).

To synthesise the *ortho* and *meta* variants of 5,10,15,20-(4-methoxy) tetraphenylporphyrin **3.4**, the appropriate benzaldehyde (0.6 mL) and pyrrole (0.35 mL) were dissolved in DCM (500 mL). Boron trifluoride diethyl etherate (6 µL) and trifluoroacetic acid (0.35 mL) were added and the mixture stirred at rt for 2 h. Chloranil (1.01g) was then added and the reaction mixtures were heated at reflux for 4 h (Scheme 3.4). The solvent was removed, and the mixtures purified via column chromatography (CH₂Cl₂), yielding purple solids **3.8** (28%) and **3.9** (24%).



Scheme 3.4 – Synthetic route of *ortho* and *meta* methoxy modified porphyrins **3.8** and **3.9**

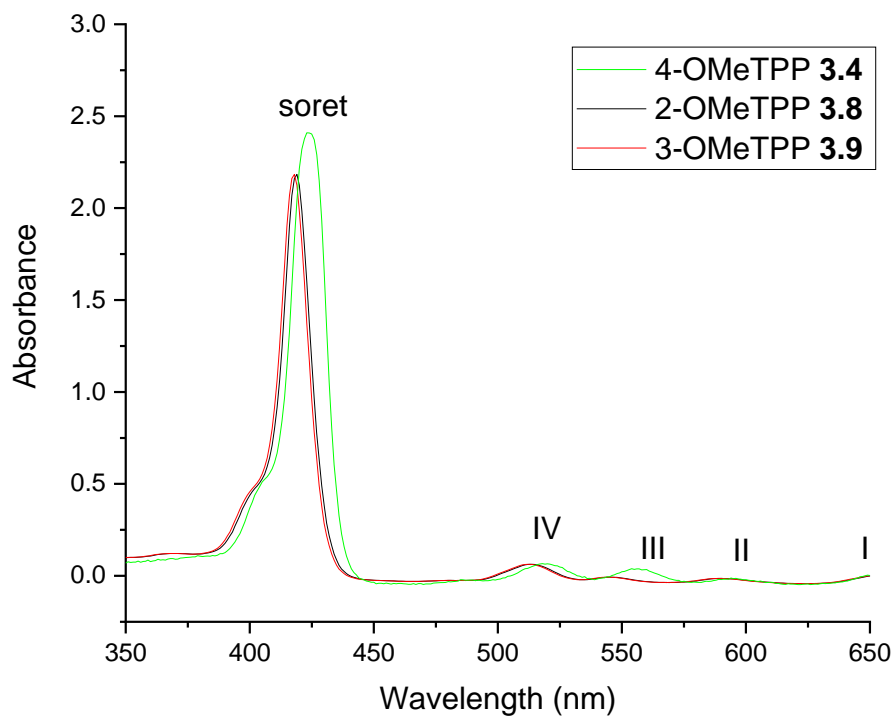


Figure 3.7- UV-Vis spectrum of methoxy substituted porphyrins **3.4**, **3.8** and **3.9** in DMSO (0.1475mM)

Run	Porphyrin	Soret band (nm)	ϵ^1 ($M^{-1}cm^{-1}$)	Q region bands (nm)	ϵ^2 ($M^{-1}cm^{-1}$)	Ratio of ϵ^3
1	3.4	424	16700	519, 556, 595	800, 610, 270	1:0.74: 0.33
2	3.8	419	22700	514, 548, 590	200, 410, 340	1:0.21:0.17
3	3.9	418	15200	514, 545, 591	750, 270, 200	1:0.36: 0.26

¹ Molar extinction coefficient of Soret band ² Molar extinction coefficient of Q region bands ³Ratio of molar extinction coefficients in the Q region, comparing band IV to bands III:II

Table 3.10 – UV-Vis spectrum data of methoxy modified porphyrins **3.4**, **3.8**, and **3.9** in DMSO (0.1475 mM)

The UV-Vis of the 4-OMe-TPP **3.5**, 2-OMeTPP **3.8** and 3-OMeTPP **3.9** porphyrins were measured in DMSO (Figure 3.7, Table 3.10). In general, it has been found that substitution at the *ortho* position of TPP **2.3** derivatives has less of an effect on the absorption properties when compared to substitution at the *meta* and *para* positions.¹⁴⁸ When looking at the absorption of 2-OMe-TPP **3.8**, the wavelength is blue shifted when compared to 4-OMe-TPP **3.4**. This is due to the direct steric interaction between the porphyrin ring and the methoxy group as opposed to the resonance effects that occur when substituted at the *para* position. However, there is a similar effect with 3-OMe-TPP **3.9**, which may also be due to this interaction, although this would be expected to be weaker.

The polymerisation of MA **2.4** was undertaken, with the ratio of reactants being MA **2.4**: thiol **2.10**: porphyrin = 200: 1: 1×10^{-2} , with a reaction time of 2 h at rt (Table 3.11). Conversion is lower after 2h when using both 2-OMe-ZnTPP **3.8** and 3-OMe-TPP **3.9** variants in both blue and red light when compared to using 4-OMe-ZnTPP. This is expected as the absorption properties of both porphyrins are further away from the optimal range of the LED light emission than when compared to 4-OMe-TPP **3.4**.

Run	Porphyrin	Light source ¹	Conversion (%) ²
1	4-OMe 3.4	Blue	71
2	4-OMe 3.4	Red	60
3	2-OMe 3.8	Blue	40
4	2-OMe 3.8	Red	32
5	3-OMe 3.9	Blue	51
6	3-OMe 3.9	Red	42

Reaction conditions: MA **2.4**: thiol **2.10**: porphyrin – 200: 1: 1×10^{-2} , degassed and irradiated with light for 2 h from 4 cm away. ¹Blue light (420-460 nm) and red light (580-640 nm) ²Determined by 400 MHz ¹H NMR by integrating ratio of peaks at 3.6-4.0 ppm and 5.8-6.5 ppm

Table 3.11 - Polymerisation data using methoxy modified porphyrins **3.4** and **3.8** – **3.9** as photocatalysts in the polymerisation of MA **2.4**

3.3.6 3D prints derived from 2-, 3- and 4-MeO-TPP derivatives

All three methoxy modified porphyrins were tested as photocatalysts in 3D printing, with the 4-OMe-TPP expected to produce the clearest image. The 3D print was performed using a 50:50 w: w mixture of TEGDMA **2.5**/ UDMA **2.6**, with the exposure per layer being 300,000 ms in blue light. The ratio of monomer: thiol **2.12**: porphyrin was 200: 25: 0.25, using pentaerythritol tetrakis (3-mercaptopropionate) **2.12** as the co-initiator and 15g of monomer mixture (Figure 3.8).



Figure 3.8 - 3D prints using methoxy substituted porphyrins **2.1**, **3.7** and **3.8** as photocatalysts. 2-OMe-TPP **3.8** (**M**), 3-OMeTPP **3.9** (**N**) and 4-OMeTPP (**L**)

There was a clear effect on photocatalytic ability when looking at the 3D prints using the modified porphyrins (Figure 3.8). Both the 2-OMe-TPP **3.8** and the 3-OMe-TPP **3.9** produced inferior prints (prints **M** and **N**) when compared to 4-OMe-TPP (print **L**). Print **M** (2-OMe-TPP) was very under cured, suggesting the polymerisation rate was too slow. This was likely due to the steric interactions from the *ortho* substituted methoxy group blue shifting the absorption properties of the porphyrin. Print **N** (3-OMe-TPP) is also under cured, with less of the cylinders being printed, as well as the

text being less clear and the shapes at the bottom right of the print being smaller and less defined when compared to the print **L** (4-OMe-TPP). These results show that substitution at the *para* position of the phenyl ring has the most positive effect on photocatalytic ability due to a mixture of resonance and steric effects.

The thermal stability of prints **L**, **M** and **N** was measured using TGA, with the prints heated at 10 °C per minute over the temperature range 0-500 °C in air, using a Mettler-Toledo TGA instrument (Figure 3.9, Table 3.12).

The initial degradation point of prints **L** (4-OMe-TPP) and **N** (3-OMe-TPP) was ~ 300 °C, however for print **M** (2-OMe-TPP) this degradation point was ~ 250 °C. The print was very undercured, which may mean that the degree of crosslinking is smaller, which may explain why degradation starts at a lower temperature. Another difference in the TGA data is that there is a noticeable shoulder on the trace of print **M** (2-OMe-TPP), which suggests increased inhomogeneity in the structure of the polymer, which results in weak links in the polymer network.

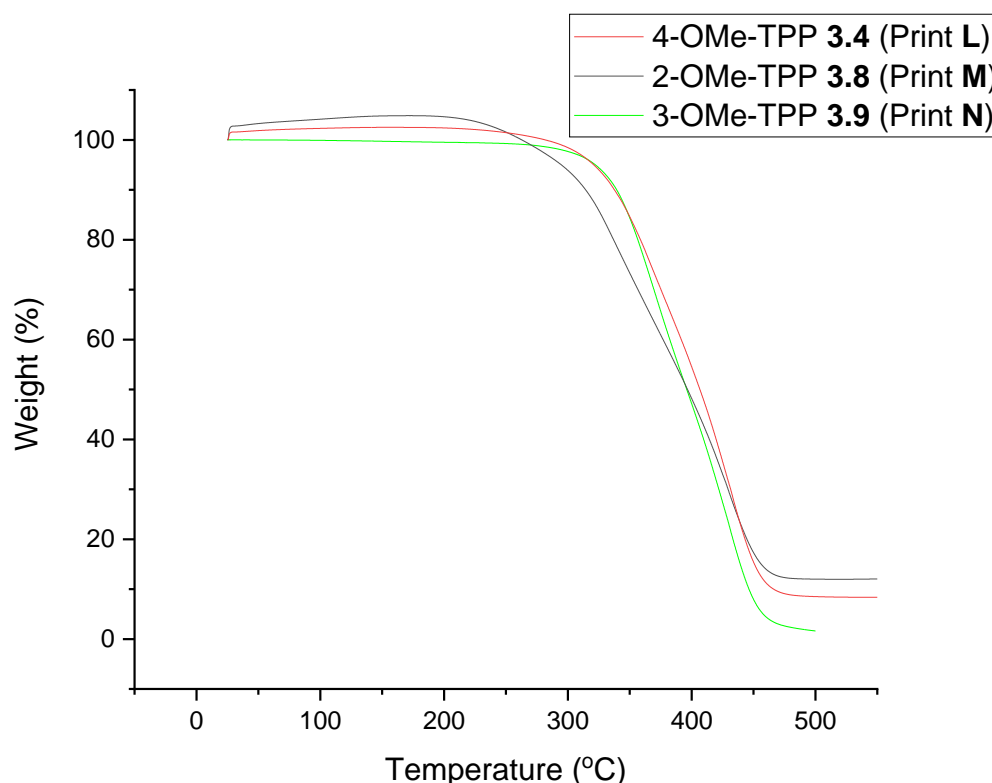


Figure 3.9 - TGA of 3D prints photocatalyzed by methoxy modified porphyrin **3.4**, **3.8**, **3.9** (Figure 3.8)

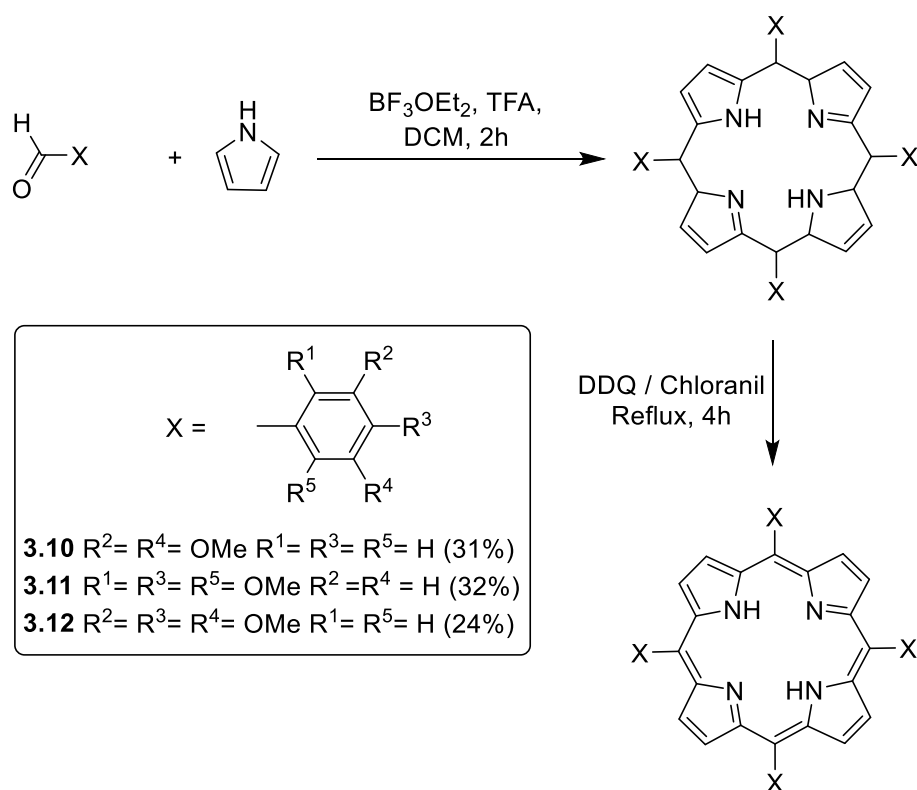
Run	Porphyrin	T _{50%} (°C)
1	3.4	403
2	3.8	396
3	3.9	396

Table 3.12 - TGA data of 3D prints photocatalyzed by methoxy modified porphyrin **3.4**, **3.8**, **3.9** (Figure 3.9)

3.3.7 Studying the effect of increasing the amount of methoxy functional groups on photocatalytic ability

It has been shown that the addition of a methoxy group at the *para* position of the phenyl ring leads to a red shift in the absorption spectrum due to resonance effects. This addition of the methoxy group at the *para* position has led to the improved photocatalytic ability, however the addition at *ortho* and *meta* positions has not had a similar effect mainly due to steric interactions. In order to probe this in more detail, a number of di- and tri-substituted methoxy derivatives **3.10-3.12** were synthesised.

The synthesis of the multi-substituted porphyrins **3.10-3.12** was attempted via the same route as for the preparation of **3.8** and **3.9**, using the method developed by Lindsey *et al*, however reaction conditions varied slightly (Scheme 3.5).¹⁴⁷ For all variants, the appropriate benzaldehyde (5 mmol) was dissolved with pyrrole (0.35 mL) in DCM and degassed, then stirred with boron trifluoride dietherate and trifluoroacetic acid for 2h. This produced the corresponding porphyrinogen macrocycle, which were then oxidized by the addition of either DDQ (**3.11**) or chloranil (**3.10** and **3.12**) (weak oxidizing agents) and heated at reflux for 4 hours, followed by purification by column chromatography to give **3.10** (31%), **3.11** (32%) and **3.12** (24%) as purple solids.



Scheme 3.5 – Synthetic route of di- and tri-substituted methoxy porphyrins **3.10-3.12**

The UV-Vis spectra of these porphyrins were recorded in DMSO (Table 3.13).

Run	Porphyrin	Soret band (nm)	ϵ ($\text{M}^{-1}\text{cm}^{-1}$)	Q region bands (nm)	ϵ ($\text{M}^{-1}\text{cm}^{-1}$) ¹
1	3.10	421	3200	515, 547, 589	140, 70, 70
2	3.11	421	2500	514, 546, 590,	140, 70, 70
3	3.12	423	9400	516, 551, 591	610, 220, 200
4	3.5	424	16700	519, 556, 595	820, 610, 270

¹ Molar extinction coefficient of Q region bands IV, III, II

Table 3.13 - UV-Vis data of di-substituted **3.10** and tri-substituted porphyrins **3.11-3.12** compared to 4-OMe-TPP **3.5** in DMSO (0.1475 mM)

As expected, the results indicate that adding additional functional methoxy groups does not red shift the absorption properties of the porphyrin compared to 4-OMe-TPP **3.5**. In fact, there is a small blue shift, presumably caused by the steric interactions highlighted in the previous section. A comparison of both 3,5-OMe-TPP **3.10** and 3,4,5-OMe-TPP **3.11** soret bands highlights the red shifting nature of the 4-methoxy substituent. When looking at the Q region, all three porphyrins are still part of the

etioporphyrin group, further showing that there has been no reddening effect with the addition of the functional groups.

The photocatalytic ability of porphyrins **3.10-3.12** were tested by repeating the polymerisation of MA **2.4**, under the same reaction conditions as used previously in the chapter (MA **2.4**: thiol **2.10**: porphyrin **3.10-3.12** is 200: 1: 1×10^{-2}) in order for a comparison to be made. The reaction mixture was irradiated with blue and red light for 2 h, with the light source 4 cm away (Table 3.14).

Run	Porphyrin	Light source ¹	Conversion (%) ²
1	3.4	Blue	71
2	3.4	Red	60
3	3.11	Blue	40
4	3.11	Red	29
5	3.12	Blue	42
6	3.12	Red	33
7	3.13	Blue	51
8	3.13	Red	32

Reaction conditions: MA **2.4**: thiol **2.10**: porphyrin – 200: 1: 1×10^{-2} , degassed and irradiated with light for 2 h from 4 cm away. ¹Blue light (420-460 nm) and red light (580-640 nm). ²Determined by 400 MHz ¹H NMR by integrating ratio of peaks at 3.6-4.0 ppm and 5.8-6.5 ppm

Table 3.14 – Polymerisation of MA **2.4** using -di and tri-substituted porphyrins **3.11-3.13** as photocatalysts, compared to TPP **2.3**.

The polymerisation results are in line with what was expected when considering the absorption properties of the multi substituted porphyrins. Conversion is lower when using all three photocatalysts, with the additional methoxy groups not improving the photocatalytic ability. This is likely due to the absorption properties being slightly blue shifted, resulting in a less favourable match of absorption of the porphyrin and wavelength of the light. These results suggest that the addition of additional functional groups to the 2- and 3-positions of the phenyl ring does not improve photocatalytic activity.

3.4 Summary

In this chapter it has been shown that the addition of electron withdrawing and donating groups at the *para* position of the phenyl groups of tetraphenylporphyrin

effects the absorption properties of the porphyrin by resonance effects. The more electron donating the substituent, the redder shifted the absorption. The compound 4-OMe-TPP **3.4** performed the best as a photocatalyst for the polymerisation of MA **2.4**, suggesting that shifting absorption towards a higher wavelength improves photocatalytic activity. This was also true when using 4-OMe-TPP **3.4** as a photocatalyst in the 3D printing of TEGDMA **2.5**/UDMA **2.6** in blue light. A similar observation was found on the corresponding metalated variants of the porphyrin **3.5–3.7**. The polymerisation of MA using 4-OMe-TPP **3.4** as a photocatalyst showed an increase in polymerisation rate, however the molecular weight of the polymer formed was comparable to when TPP **2.3** was used as a photocatalyst. This supports the theory that the molecular weight of the polymerisation is controlled by the thiol as opposed to the photocatalyst.

The effect of changing the position of the functionalisation was also studied, with *ortho* **3.10** and *meta* **3.11** and di- and tr-substituted variants **3.11–3.13** of the methoxy porphyrin synthesised. However, it was shown that substitution at either the *ortho* or *meta* positions (irrespective of the substitution elsewhere) led to a minimal effect on the absorption properties of the porphyrin and did not improve photocatalytic ability due to a mixture of both steric and resonance effects.

4 The absorption properties and photocatalytic activity of alkenyl-substituted porphyrins

4.1 Introduction

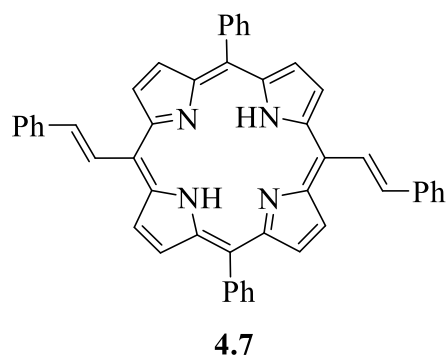
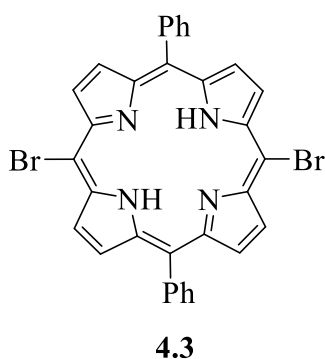
In chapter 3, the absorption properties of TPP **2.3** was red shifted by 4 nm when a methoxy group is substituted at the *para* position of the phenyl ring **3.4**. This modification resulted in an increase in photocatalytic activity, however the wavelength at which 5,10,15,20-tetrakis(4-methoxyphenyl) porphyrin **3.4** most strongly absorbed light was at 424 nm. The blue light in the 3D printer has a wavelength of 420-460 nm, therefore it would be favourable to further red shift the absorption properties of the porphyrin.

It has been shown that an extension in conjugation of the porphyrin macrocycle has two major effects on the properties of porphyrins: broadening of the absorption bands and a red shift of the absorption profile.¹⁴⁹ The broadening of the absorption bands will increase the range in which the porphyrin absorbs light, making it more likely to absorb light in the desired wavelength range (420-460 nm), with the red shifting of the absorption properties also helping to achieve this.

4.2 Aims and objectives

The aim of this chapter is to modify the structure of TPP **2.3** by increasing the conjugation of the porphyrin macrocycle to tune the absorption properties and reactivity of the photocatalyst. To do this, the following objectives were set:

- Synthesise 5,15-diphenyl-10,20-dibromoporphyrin **4.3**.
- Synthesise 5,15-diphenyl-10,20-distyrylporphyrin **4.7** and other conjugated derivatives utilising the Heck coupling reaction with **4.3**.
- Study the absorption properties and photocatalytic activity of 5,15-diphenyl-10,20-distyrylporphyrin **4.7** and its derivatives.

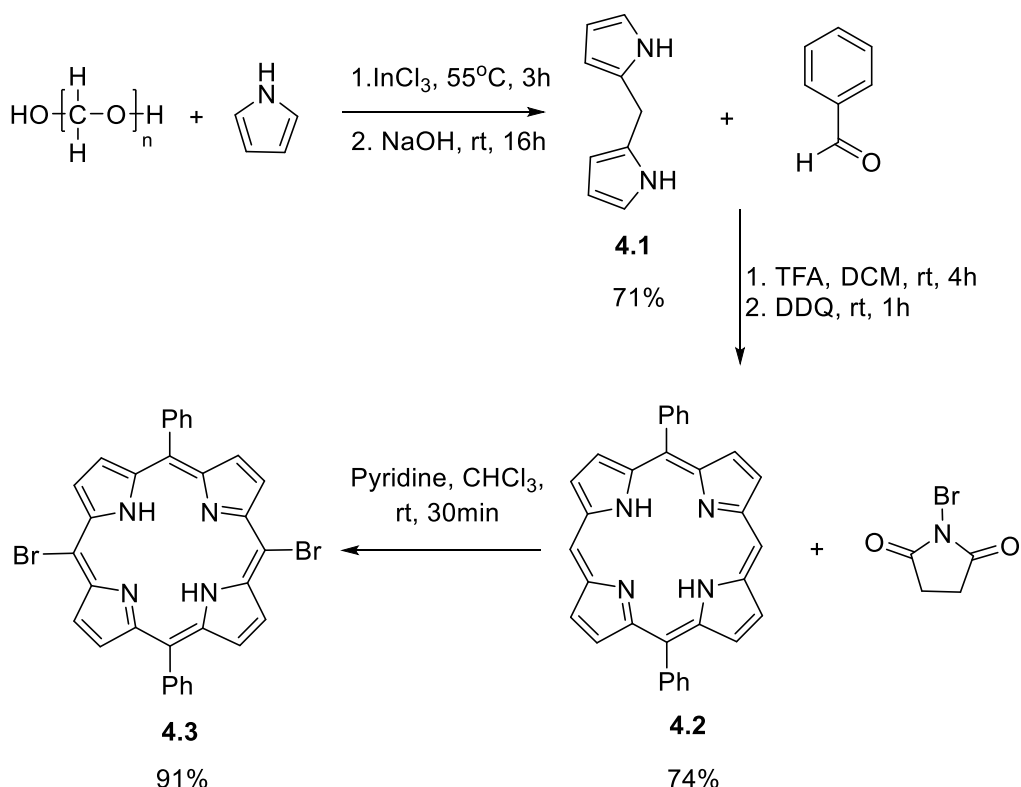


4.3 Results and discussion

4.3.1 Synthesis of 5,15-diphenyl-10,20-distyrylporphyrin **4.7**

To introduce further conjugation in the macrocycle of the porphyrin ring, a styrene was chosen to be introduced at the *meso* positions of diphenylporphyrin **4.2**. While the mono-styryl derivative 5,10,15-triphenyl-20-styrylporphyrin **4.6** is known (Soret band $\lambda_{\text{max}} = 427 \text{ nm}$),¹⁵⁰ in order to increase conjugation further, 5,15-diphenyl-10,20-distyrylporphyrin **4.7** was prepared by slightly modifying the synthetic approach. In addition, the replacement of a phenyl substituent directly appended to the porphyrin (which is twisted lessening resonance effects due to steric hindrance) with a styryl group (where the alkene is directly attached) should provide for better overlap of conjugating orbitals.

To synthesise 5,15-diphenyl-10,20-distyrylporphyrin **4.7**, 5,15-diphenyl-10,20-dibromoporphyrin **4.3** was prepared (Scheme 4.1), which was coupled to styrene *via* the Heck reaction.



Scheme 4.1 – Synthetic route of 5,15-dibromo-10,20-diphenylporphyrin **4.3**

The first step of in the synthesis of 5,15-dibromo-10,20-diphenyl porphyrin **4.3** was to synthesise dipyrromethane **4.1** from paraformaldehyde, pyrrole and InCl_3 at 55°C

for 3h.¹⁵¹ This mixture was left to cool to rt, and then NaOH was added and stirred overnight. The solvent was removed, and the reaction mixture purified *via* column chromatography to give **4.1** in 63% yield. Then 5,15-diphenylporphyrin **4.2** was prepared by dissolving dipyrromethane **4.1** and benzaldehyde in DCM.¹⁵² A large amount of solvent was required due to the poor solubility of dipyrromethane **4.1**, and in fact porphyrin derivatives are notoriously insoluble in a range of organic solvents often making their handling and purification difficult. The solution was degassed, trifluoroacetic acid (TFA) was added and the mixture stirred at rt for 4h. This produced the reduced variant of diphenylporphyrin, which was oxidised *in situ* by the addition of 2,3-dichloro-5,5-dicyano-1,4-benzoquinone (DDQ). After neutralisation by the addition of triethylamine and purification by column chromatography the compound 5,15-diphenylporphyrin **4.2** was isolated in 44% yield. To synthesise 5,15-dibromo-10,20-diphenylporphyrin **4.3**, 5,15-diphenylporphyrin **4.2** was dissolved in CHCl₃ and pyridine and *N*-bromosuccinimide were added and stirred for 30 minutes.¹⁵³ After work-up a mixture of mono- **4.4** and the desired di-substituted **4.3** variants were isolated (Figure 4.1). These were separated by column chromatography (DCM: petroleum ether – 1:1) to give **4.3** in 90% yield.

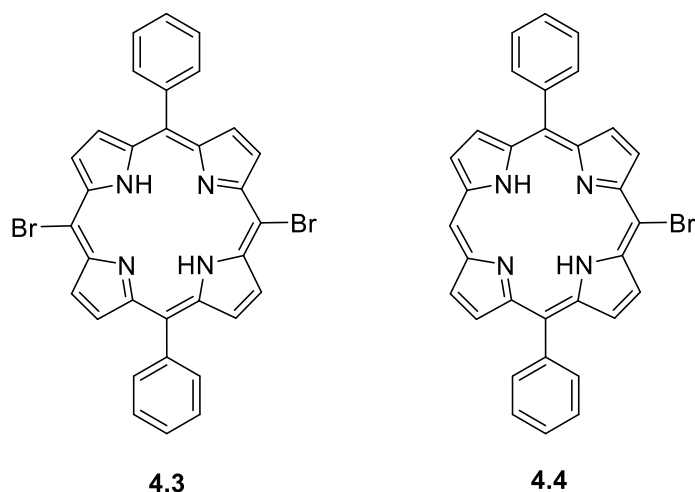


Figure 4.1 - Structures of 5,15-dibromo-10,20-diphenylporphyrin (**4.3**) and 5-bromo-10,20-diphenylporphyrin (**4.4**) porphyrin

The 400 MHz ¹H NMR in CDCl₃ showed the characteristic doublet resonances for the β-pyrrole porphyrin protons at 9.63 (*J* = 4.5 Hz) and 8.84 ppm (*J* = 4.5 Hz) respectively. The 2-substituted phenyl proton signals were identified at 8.16 ppm (d, *J* = 7.1 Hz) and the remaining aromatic signals were between 7.82 – 7.75 ppm. Note

that the resonances for the NH protons are found at -2.73 ppm due to the aromatic ring current, (Figure 4.2).

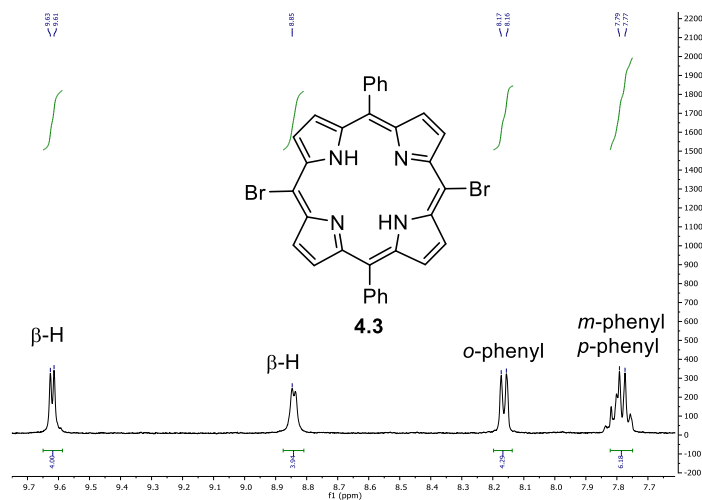
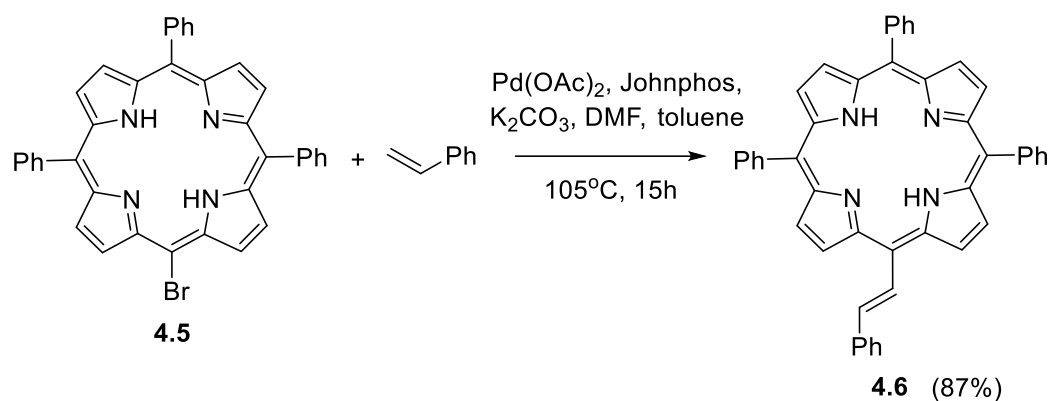


Figure 4.2 - 400 MHz ^1H NMR in CDCl_3 of dibromoporphyrin **4.3**

To synthesise 5,15-diphenyl-10,20-distyrylporphyrin **4.7**, the Heck coupling reaction was chosen. It has been previously shown that it is possible to couple styrene with the related 5-bromo-10,15,20-triphenylporphyrin **4.5**,¹⁵⁰ however coupling styrene with 5,15-dibromo-10,20-distyrylporphyrin **4.3** had not been previously reported, (Scheme 4.2).



Scheme 4.2 - Synthesis route of 5,10,15-triphenylporphyrin-20-styrylporphyrin (**4.6**)¹⁵⁰

Utilising a similar procedure to that previously reported, styrene was added to 5,15-dibromo-10,20-diphenylporphyrin **4.3**, $\text{Pd}(\text{OAc})_2$, di-*tert*-butylbiphenylphosphine (Johnphos) and K_2CO_3 in a mixture of dry DMF and dry toluene. This solution was degassed *via* the freeze-thaw technique and heated overnight at 105°C . The mixture was then cooled to rt and washed with water. Purification by column chromatography was difficult and the major spot isolated gave the desired product **4.7** in addition to a

minor impurity as an inseparable mixture (Figure 4.3). The major peak in the ESI mass spectrum at 667.3, confirmed the presence of 5,15-diphenyl-10,20-distyrylporphyrin **4.7** and aromatic region of the ^1H NMR spectrum also confirmed the incorporation of the styryl groups (with the (*E*)-geometry being the major isomer, $\text{H}^{\text{a}} = 9.62$ ppm, $J = 15.9$ Hz, Scheme 4.3). Although the desired compound **4.7** was not isolated completely pure it was decided to further study this material in photo polymerisation reactions.

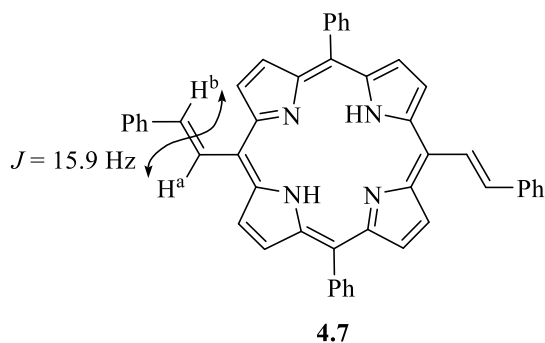
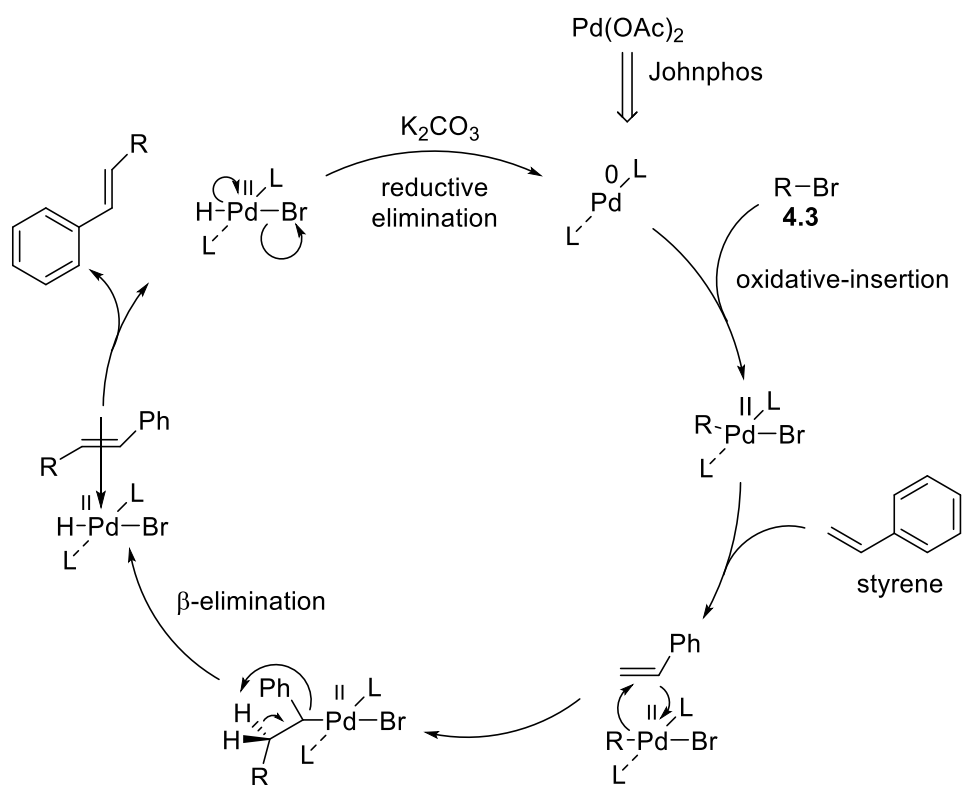


Figure 4.3 - Structure of distyryl porphyrin **4.7**

The mechanism for this reaction proceeds *via* organopalladium intermediates. $\text{Pd}(\text{II})(\text{OAc})_2$, is first reduced by di-*tert*-butylbiphenylphosphine (Johnphos) to produce a $\text{Pd}(0)$ complex, (Scheme 4.4).



Scheme 4.3 - Reaction mechanism of the Heck reaction of **4.3** to **4.7**.

This allows for the oxidative addition in which the reduced palladium compound inserts itself into the C-Br bond of 5,15-dibromo-10,20-diphenylporphyrin **4.3**. This produces an intermediate which can interact with the alkene functional group on styrene, which inserts onto the palladium. This compound then undergoes a β -hydride elimination, which forms an alkene-palladium complex and ultimately **4.7**. The palladium complex is regenerated by potassium carbonate *via* reductive elimination and the catalytic cycle continues.

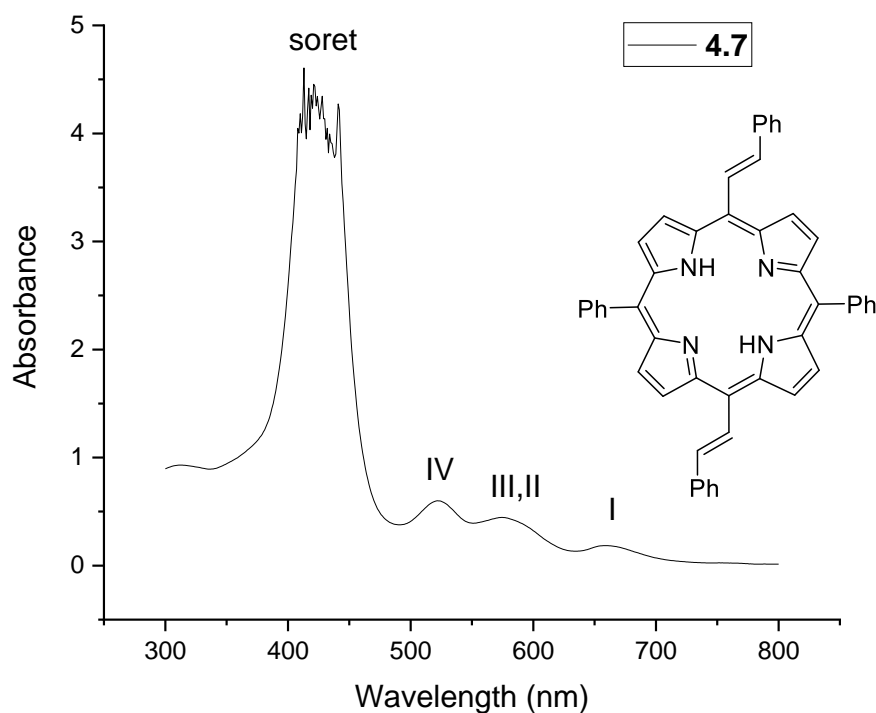


Figure 4.4 - UV-Vis spectrum of 5,15-distyryl-10,20-diphenylporphyrin **4.7** in DMSO (0.1475 mM)

To determine the effect that the extended conjugation of the porphyrin core has on absorption properties, the UV-Vis spectra was measured in DMSO (0.1475mM), (Figure 4.4, Table 4.1). There was a red shift of the absorption properties of the UV-Vis spectrum, with a significant broadening of the Soret band due to the extended conjugation of the porphyrin core through the styryl groups and a significantly increased extinction coefficient. The Q bands are less resolved than in the other porphyrins studied. Due to the presence of trace aromatic impurities, it is unwise to make any firm conclusions around absorbance characteristics and extinction coefficients.

Run	Porphyrin	Soret bands (nm)	ϵ ($M^{-1}cm^{-1}$)	Q region bands (nm) ¹	ϵ ($M^{-1}cm^{-1}$) ²
1	4.7	407-442	27500	523, 577, 660	4000, 3000, 1200
2	2.3	419	15300	515, 551, 589	610, 200, 140

¹ Molar extinction coefficient of soret band ² Absorption of bands IV, (III, II), I. ³ Molar extinction coefficients of Q region bands

Table 4.1 - UV-Vis bands of 5,15-distyryl-10,20-diphenylporphyrin **4.7** compared to TPP **2.3** in DMSO (0.1475mM)

However, on balance it was expected that photocatalytic activity should increase relative to TPP **2.3** itself as the absorption characteristics of the sample better matched the wavelength of the light used for the polymerisation (420 – 460 nm).

4.3.2 Polymerisation of MA using 5,15-distyryl-10,20-diphenylporphyrin **4.7**

To determine the effect that the addition of two styryl functional groups had on the photocatalytic activity of the porphyrin, the functionalised porphyrins were used to polymerise MA **2.4** in blue (420-460 nm) and red light (580 – 640), (Table 4.2). The ratio of MA **2.4**: 1-dodecanethiol **2.10**: 5,15-distyryl-10,20-diphenylporphyrin **4.7** was 200: 1: 1×10^{-2} and the mixture was irradiated with light for 2 h from 4 cm away as in all previous comparative experiments.

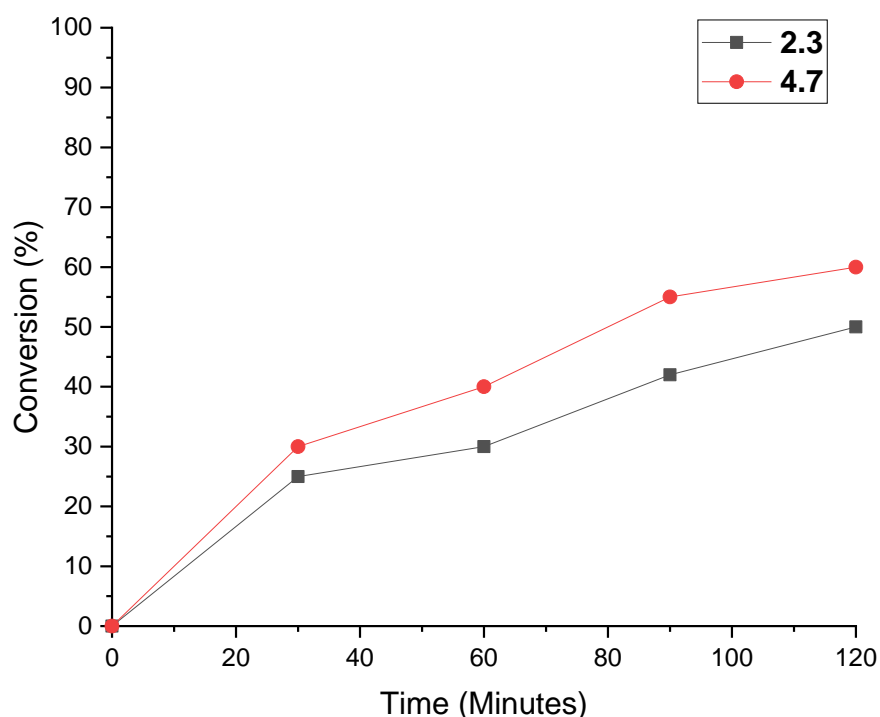
Run	Porphyrin ¹	Light ²	Conversion (%) ³
1	2.3	Red	43
2	3.4	Red	60
3	4.7	Red	50
4	2.3	Blue	56
5	3.4	Blue	70
6	4.7	Blue	60

¹ Experimental conditions: Reaction mixture degassed in DMSO and irradiated with light for 2 hours from 4cm away. MA **2.4**: 1-dodecanethiol **2.10**: porphyrin - 200: 1: 1×10^{-2} Blue light (420-460 nm) and red light (580-640 nm) ³ Determined by 400 MHz ¹H NMR by integrating ratio of peaks at 3.6-4.0 ppm and 5.8-6.5 ppm

Table 4.2 - Polymerisation of MA using TPP **2.3**, 5,10,15,20-tetrakis(4-methoxyphenyl)porphyrin **3.4** and 5,15-distyryl-10,20-diphenylporphyrin **4.7** as photocatalysts

When using 5,15-distyryl-10,20-diphenylporphyrin **4.7** as a photocatalyst for the polymerisation of MA, the conversion is slightly higher in both blue and red light when compared to TPP **2.3**. However, the reaction was not as efficient as the 4-methoxy derivative 4-OMe-TPP **3.4** despite the apparent more beneficial absorption characteristics. As highlighted earlier part of the measured absorption may be due to trace impurities which may not act (or hinder) the photocatalytic behaviour expected.

To study the conversion of the polymerisation, aliquots of the reaction mixture were taken every 30 minutes and using ^1H NMR to determine conversion at each stage (Graph 4.1). As expected, the rate of the polymerisation was faster when 5,15-distyryl-10,20-diphenylporphyrin **4.7** was used as a photocatalyst compared to **2.3**. However, reaction rate was only marginally faster, therefore it would be worthwhile to attempt to synthesise further alkenyl-substituted porphyrins (with increased purity) to try and probe any effects.



Graph 4.1 – Conversion studies of the polymerisation of MA **2.4** using TPP **2.3** and 5,15-distyryl-10,20-diphenylporphyrin **4.7** in blue light

4.3.3 Extending the conjugation in alkenyl-substituted porphyrins

The extended conjugation of the porphyrin core **4.7** compared to TPP **2.3** has resulted in a red shift of the absorption properties. A range of other increasingly conjugated derivatives **4.8-4.10** were identified as candidates to study where styrene was substituted for 1-phenyl-1,3-butadiene, 1-vinyl naphthalene and 9-vinyl anthracene respectively (Figure 4.5).

The first derivative that was attempted to be synthesised was 5,15-diphenyl-10,20-bis(4-phenylbuta-1,3-dien-1-yl)porphyrin **4.8**. As before Heck reaction with

$\text{Pd}(\text{OAc})_2$, di-*tert*-butylbiphenylphosphine (Johnphos) and K_2CO_3 in a mixture of dry DMF and dry toluene at 105°C was attempted.

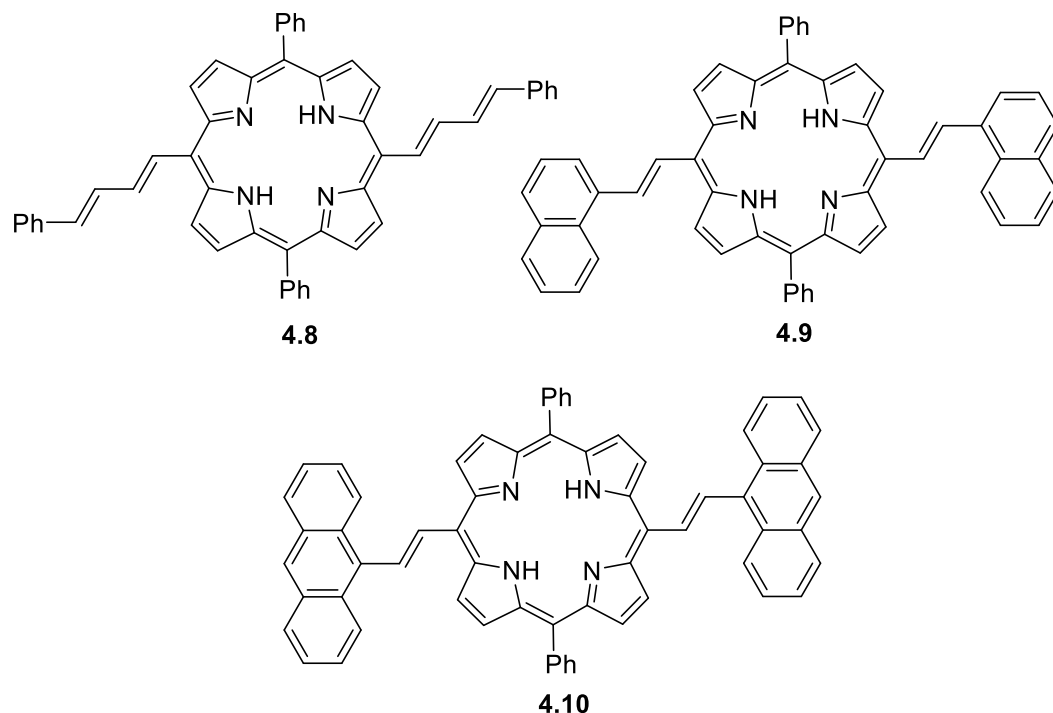
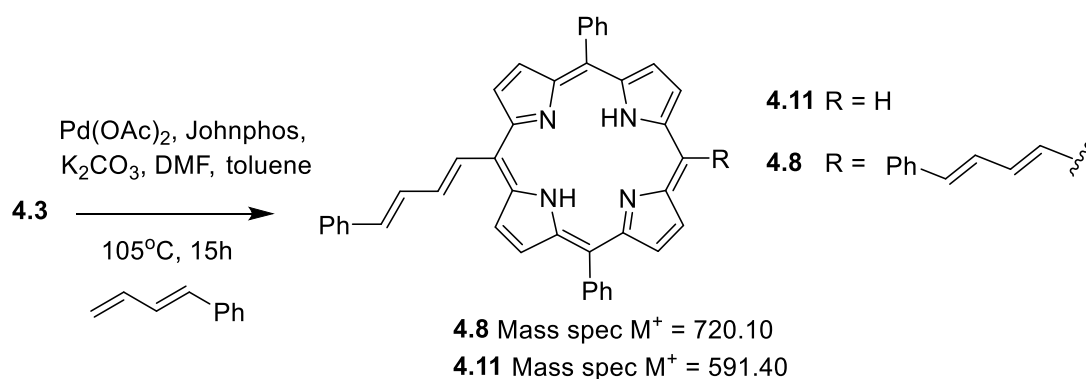


Figure 4.5 – Structure of alkenyl substituted porphyrins **4.8** – **4.10** with extended conjugation of the porphyrin core

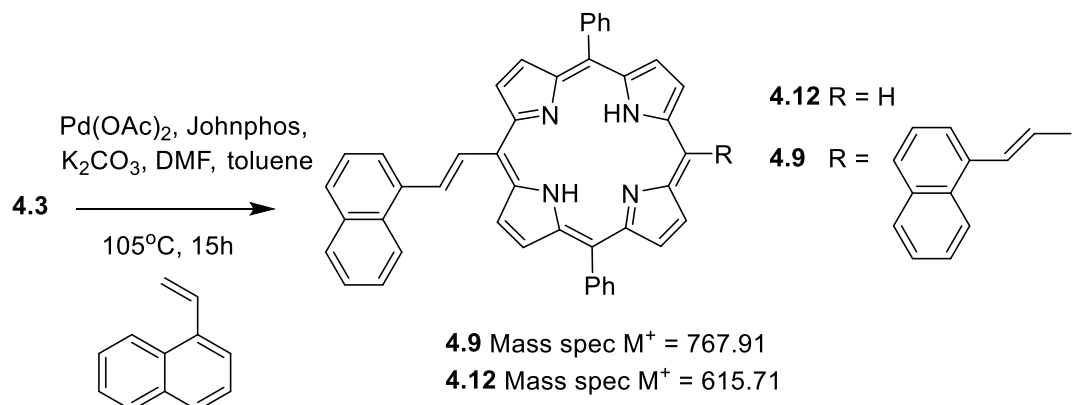
After purification by column chromatography, compound **4.8** ($\text{C}_{52}\text{H}_{38}\text{N}_4$) was isolated as the major component ($\text{MH}^+ = 719.90$) along with the mono functionalised porphyrin **4.11** ($\text{C}_{42}\text{H}_{30}\text{N}_4$) ($\text{MH}^+ = 591.50$) as an 5:1 inseparable mixture (Scheme 4.5).



Scheme 4.4 – Synthesis route of 5,15-diphenyl-10,20-bis(4-phenylbuta-1,3-dien-1-yl)porphyrin **4.8**

It is known that protolytic cleavage of the C-Br bond is often a competing reaction to the desired C/C coupling Heck process under palladium catalysis.¹⁵⁰ The results suggest that the rate of Heck coupling of **4.3** was slower than the protolytic cleavage of bromine leading to significant mono-functionalisation. It proved impossible to

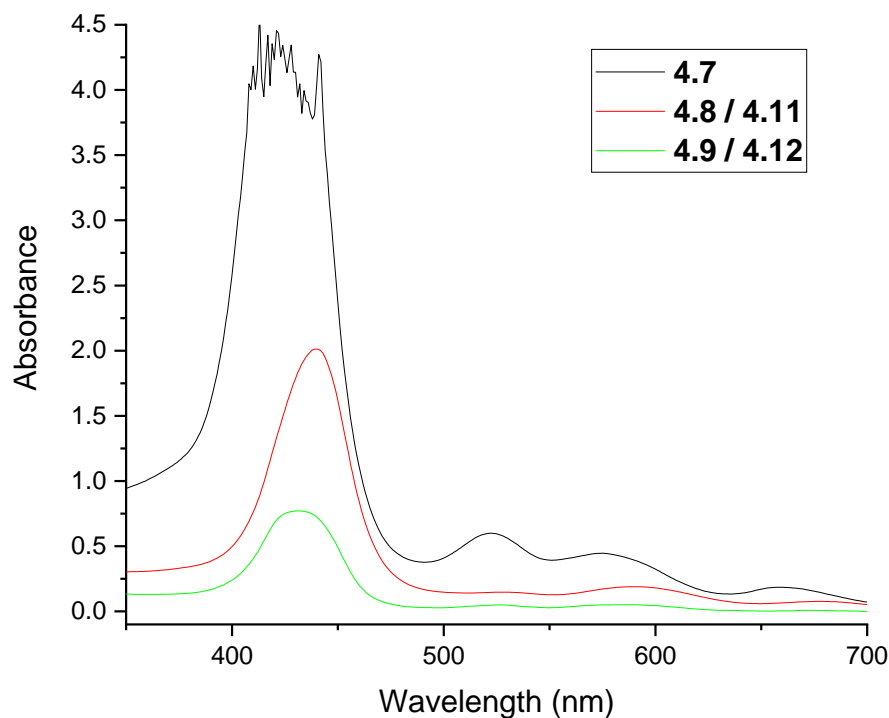
separate **4.8** and **4.11** *via* column chromatography, therefore the mixture of both was used for further study, Scheme 4.6.



Scheme 4.5 - Synthetic route of 5,15-bis(2-(naphthalen-1-yl)vinyl)-10,20-diphenylporphyrin **4.9**

A similar inseparable mixture was obtained when attempting to prepare 5,15-bis(2-(naphthalen-1-yl)vinyl)-10,20-diphenylporphyrin **4.9**, with the mono-substituted **4.12** also produced. Attempts to prepare 5,15-bis(2-(anthracen-9-yl)vinyl)-10,20-diphenylporphyrin **4.10** using the Heck protocol failed and a similar outcome was reported for the related reaction with 5-bromo-10,15,20-triphenylporphyrin.¹⁵⁰

The UV visible spectra of the porphyrin mixtures (**4.8** / **4.11** and **4.9** / **4.12**) were measured in DMSO (0.1475mM) (Graph 4.2, Table 4.3).



Graph 4.2 - UV-Vis of porphyrin mixture **4.8 / 4.11** and **4.9 / 4.12** compared to **4.7**

Runs	Porphyrin	Soret band (nm)	Q region bands ¹ (nm)
1	4.7	407-442	523, 577, 660
2	4.8 / 4.11	430-446	528, 589, 678
3	4.9 / 4.12	419-442	526, 583, 670

¹ Absorption of bands IV, III, II

Table 4.3- UV-Vis bands of porphyrin mixtures **4.8 / 4.11** and **4.9 / 4.12** compared to **4.7**

The major difference in the UV-Vis spectrums of **4.8 / 4.11** and **4.9 / 4.12** compared to **4.7** is the lower intensity of the Soret and Q absorption bands, suggesting that light will be absorbed less strongly, which would be expected to lower the rate of propagation during photocatalysis. Offsetting this is the red shift of the Soret bands further into the desired blue LED wavelength region. Interestingly, the solubility of the porphyrins **4.6-4.10** were relatively poor compared to those reported in chapter 2 and 3.

4.3.4 Polymerisation of MA using mixtures **4.8/ 4.11** and **4.9/ 4.12**

The polymerisation of MA **2.4** was attempted in blue (420-460 nm) and red light (580 – 640), using porphyrin mixtures **4.8 / 4.11** and **4.9 / 4.12** as photocatalysts (Table

4.4). The ratio of MA **2.4**: 1-dodecanethiol **2.10**: porphyrin was 200: 1: 1×10^{-2} , and the mixture was irradiated with light for 2 h from 4 cm away as previously.

Run	Porphyrin ¹	Light ²	Conversion (%) ³
1	4.8 / 4.11	Red	25
2	4.9 / 4.12	Red	8
3	4.7	Red	50
4	4.8 / 4.11	Blue	50
5	4.9 / 4.12	Blue	20
6	4.7	Blue	60

¹ Experimental condition: Reaction mixture degassed in DMSO and irradiated with light for 2 hours from 4cm away. MA **2.4**: 1-dodecanethiol **2.10**: porphyrin - 200:1: 1×10^{-2} Blue light (420-460 nm) and red light (580- 640 nm) ³ Determined by 400 MHz ¹H NMR by integrating ratio of peaks at 3.6-4 ppm and 5.8-6.5 ppm

Table 4.4 - Polymerisation of MA **2.4** using porphyrin mixtures **4.8 / 4.11** and **4.9 / 4.12**

It can be seen from the polymerisation data that conversion when using **4.8 / 4.11** and **4.9 / 4.12** as a photocatalysts, conversion is significantly lower in red light. This is consistent with the lower absorption of the Q bands, resulting in the propagation constant being lower. A similar observation was found for polymerisation in blue light, indicating that although the absorption properties of **4.8 / 4.11** and **4.9 / 4.12** are more red shifted than **4.7**, the effect of the lower intensity of absorption has had a negative effect on photo catalytic activity.

4.3.5 Study of methoxy variants of alkenyl-substituted porphyrins

The extension of the conjugation found in porphyrin core has resulted in the red shift of absorption properties as expected, however lower intensity absorptions for some catalysts in the region of interest has resulted in the photocatalytic activity being lower. Interestingly the styryl derivative **4.7** exhibited significantly higher extinction coefficients in the Soret and Q regions compared to the other catalysts described. In Chapter 3 it was discussed how adding a *para* substituted electron donating methoxy substituent to the *meso* aryl functionality of TPP **2.3** also increased the rate of polymerisation, primarily due to red shifting the absorbance characteristics of the porphyrin. Therefore, the next approach was to combine both approaches around the styryl derivative **4.7** as a template. There are two different *para* positions available for functionalisation, the phenyl ring directly connected at the *meso* position (Figure 4.3 - **A**), and that on the phenyl group on styrene functionality (Figure 4.3 - **B**).

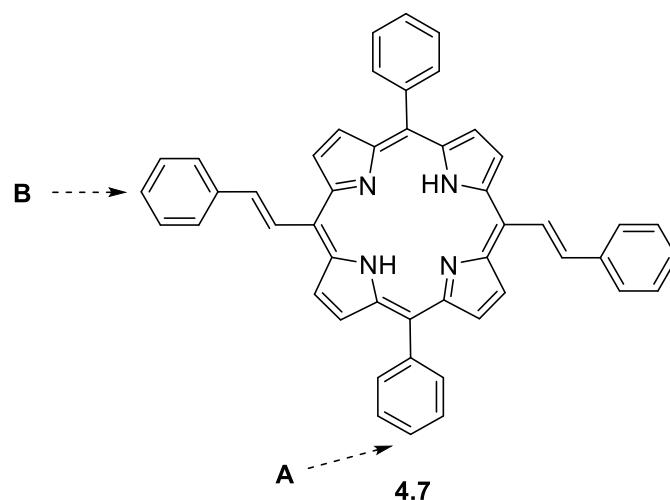
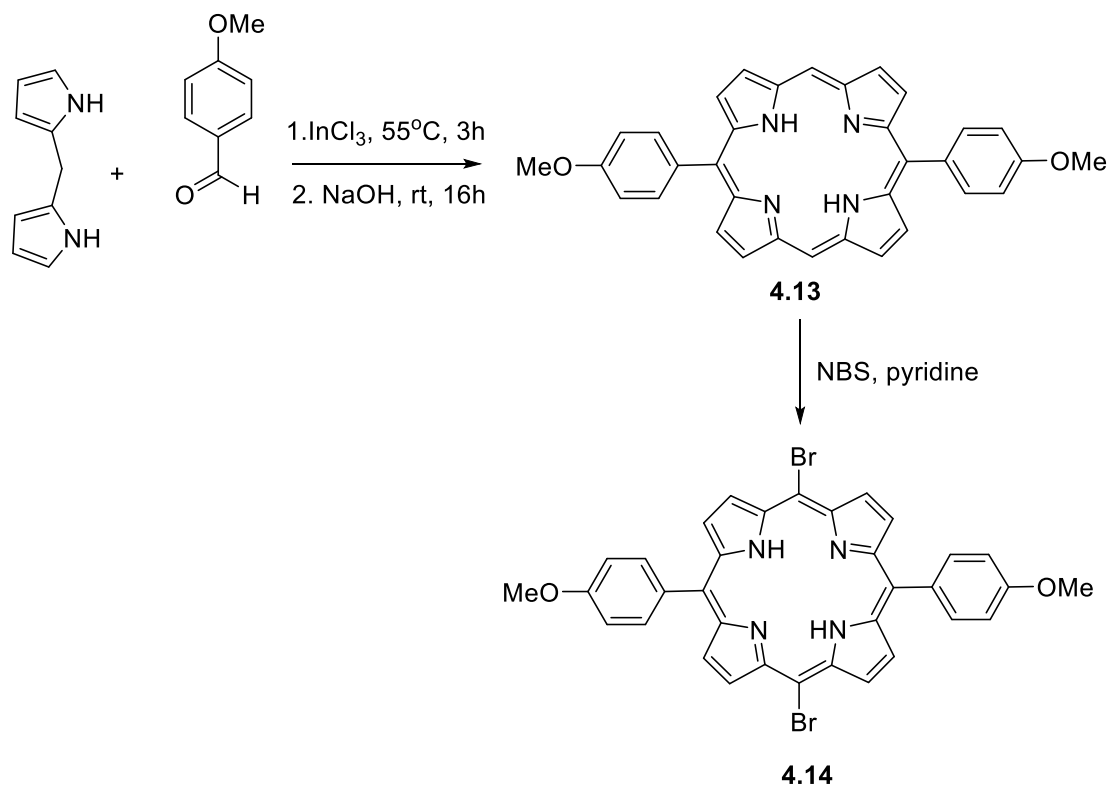


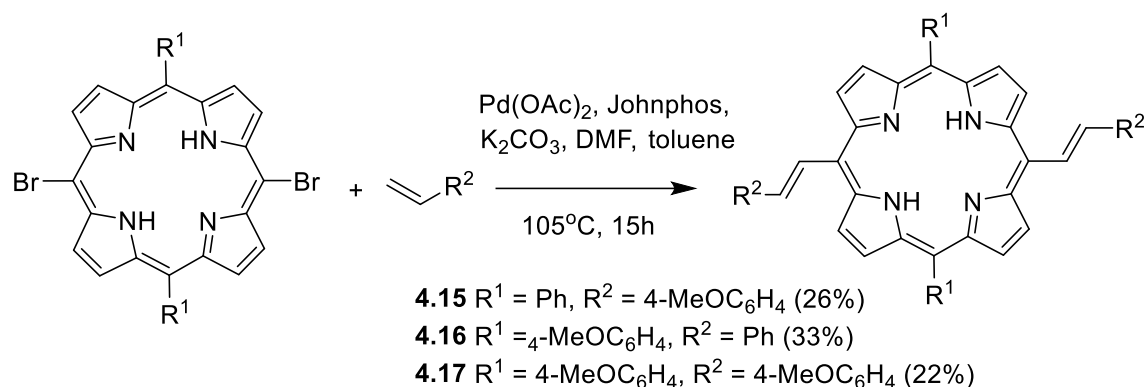
Figure 4.6 - Positions of possible functionalisation on 5,15-diphenyl-10,20-distyrylporphyrin **4.7**

To functionalise position **A** (Figure 4.6), the first compound that needed to be synthesised was 5,15-dibromo-10,20-bis(4-methoxyphenyl)porphyrin **4.13**. To do this the synthesis of diphenylporphyrin **4.2** was modified, substituting benzaldehyde for anisaldehyde to produce 5,15-bis(4-methoxyphenyl)porphyrin **4.13** in 58% yield. This was then treated with NBS and pyridine to yield 5,15-dibromo-10,20-bis(4-methoxyphenyl)porphyrin **4.14** in 87% yield (Scheme 4.7)



Scheme 4.6 – Synthetic route of 5,15-dibromo-10,20-bis(4-methoxyphenyl)porphyrin **4.14**

Three further derivatives **4.15-4.17** were then prepared by reacting either 5,15-dibromo-10,20-bis(4-methoxyphenyl)porphyrin **4.14** or 5,15-dibromo-10,20-bis(phenyl)porphyrin **4.3** with styrene or 4-methoxy styrene using the existing Heck protocol previously described, (Scheme 4.8).



Scheme 4.7 – Synthetic route of methoxy modified alkenyl-substituted porphyrins **4.15 – 4.17**

Reaction of **4.14** with styrene gave the porphyrin **4.15** in 26% yield after purification. Unlike the related molecule **4.7** it was possible to isolate this molecule pure as one isomer. The ¹H 400 MHz of **4.15** in CDCl₃ is shown in Figure 4.7. The (*E*)-geometry of the styryl group was confirmed (H^a 9.61 ppm, d, *J* = 15.9 Hz, H^b 7.38 ppm, d, *J* = 15.9 Hz) and the relatively high chemical shift of H^a is due to porphyrin ring current.

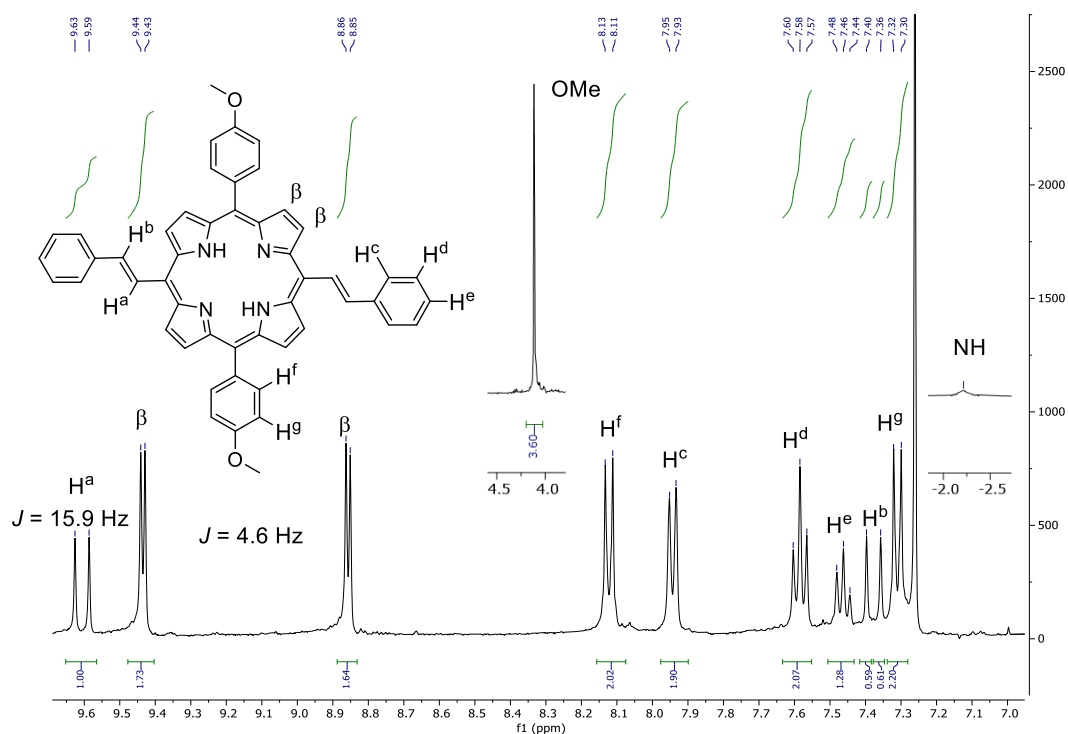


Figure 4.7 - ¹H 400 MHz NMR in CDCl₃ of **4.16**

The two chemical environments of β -pyrrole protons are identified at 9.43 ppm and 8.85 ppm respectively with the characteristic coupling constant of 4.5 Hz, which is characteristic of the porphyrin ring. The protons H^f at 8.12 ppm are also relatively downfield to where they would normally be expected due to ring current. As highlighted earlier before the NH protons are significantly up field (-2.22 ppm) as they sit within the aromatic porphyrin ring

The absorption properties of porphyrins **4.15** – **4.17** were measured in DMSO (0.1475mM) (Figure 4.8) and compared to 5,15-distyryl-10,20-diphenylporphyrin **4.7** (Figure 4.4, Table 4.5).

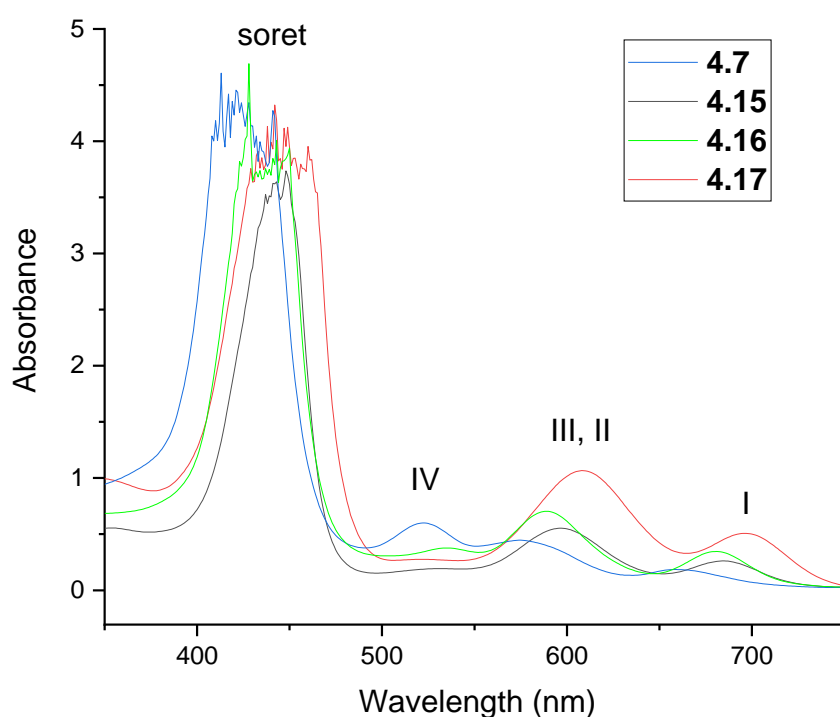


Figure 4.8 - UV-Vis spectra of methoxy modified alkenyl-substituted porphyrins (**4.15** – **4.17**) in DMSO (0.1475mM) compared to of 5,15-distyryl-10,20-diphenylporphyrin **4.7**

Runs	Porphyrin	Soret band (nm)	ϵ ($M^{-1}cm^{-1}$)	Q region bands ¹ (nm)	ϵ ($M^{-1}cm^{-1}$)
1	4.7	407-442	27500	523, 577, 660	4000, 3000, 1200
2	4.15	432-453	24500	527, 596, 684	1300, 3700, 1800
3	4.16	423-448	25300	535, 589, 680	2600, 4700, 2300
4	4.17	427-462	26000	608, 696	7200, 3500

¹ Wavelength of Q region bands IV, III, II. Bands III and II for porphyrin **4.15**

Table 4.5 - UV-Vis bands of methoxy modified alkenyl-substituted porphyrins **4.15-4.17** compared to 5,15-distyryl-10,20-diphenylporphyrin **4.7**

The absorption of all three porphyrins (**4.15** – **4.17**) were red shifted compared to **4.7**. The largest shift in absorption was observed for 5,15-bis(4-methoxyphenyl)-10,20-bis(4-methoxystyryl)porphyrin **4.17**, resulting in a shift of 18 nm from 5,15-diphenyl-10,20-distyrylporphyrin **4.7** for the Soret band (run 1 → run 4). This is likely due to a mixture of factors, with the increased resonance due to the electron donating nature of the methoxy substituents and the extended conjugation of the porphyrin core from the two alkene groups contributing to the red shifting. It is interesting to note that methoxy substitution at the *para* position of the phenyl group of TPP **2.3** resulted in 4 nm red shift in the absorption properties, whereas the same substitution to 5,15-diphenyl-10,20-distyrylporphyrin **4.7** led to a 9 nm shift. The greatest shifts of the Soret band occur for 4-methoxystyryl analogues **4.15** and **4.17** indicating substitution at the styryl groups was more important in red shifting this peak than substitution at the *meso* phenyl substituent. More importantly for **4.17** the Q bands are significantly more intense in the red LED region of the spectrum (580-640 nm) indicating that this catalyst should perform better in red light polymerisation than the others.

4.3.6 Polymerisation of MA **2.4** using methoxy modified alkenyl-substituted porphyrins

To determine the effect of modifying the alkenyl-substituted porphyrins on the photocatalytic ability of each porphyrin, each porphyrin was used as a photocatalyst for the polymerisation of MA **2.4** (Graph 4.3). 1-Dodecanethiol **2.10** was chosen as the co-initiator, and the ratio of reactants MA **2.4**: 1-dodecanethiol **2.10**: porphyrin was 200: 1: 1×10^{-2} . The reaction mixtures were degassed and irradiated with blue and red light for 2 h from 4 cm away. Conversion was determined by 400 MHz ^1H NMR by integrating ratio of bands at 3.6-4.0 ppm and 5.8-6.5 ppm.

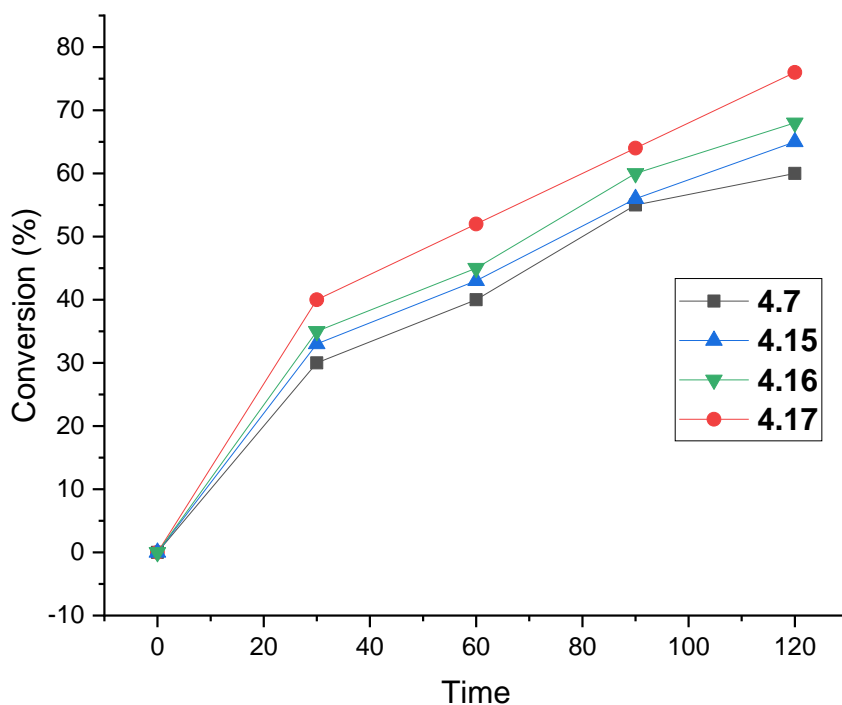
The results of the polymerisation of MA **2.4** (Table 4.6) when utilising porphyrins **4.15** – **4.17** showed that conversion was greatest after two hours when using 5,15-bis(4-methoxyphenyl)-10,20-bis(4-methoxystyryl)porphyrin **4.17** as a photocatalyst in both blue and red light. The conversion difference between reactions in red light verses blue light for each catalyst is much lower for this class of four catalysts compared to those discussed in previous chapters. Conversion increased as expected as the absorption properties of the porphyrin became more red shifted (**4.17** > **4.15** > **4.16** > **4.7**), with the rate of the polymerisation also increasing (Graph 4.3). The

significant red shifting and higher extinction coefficients of the Q band in **4.17** explains the relatively high conversion under red light illumination.

Run	Porphyrin ¹	Light ²	Conversion (%) ³
1	4.4	Red	50
2	4.15	Red	57
3	4.16	Red	55
4	4.17	Red	60
5	4.4	Blue	60
6	4.15	Blue	68
7	4.16	Blue	65
8	4.17	Blue	76

¹ Experimental condition: Reaction mixture degassed in DMSO and irradiated with light for 2 hours from 4cm away. MA **2.4**: 1-dodecanethiol **2.10**: porphyrin - 200:1:1x10⁻² Blue light (420-460 nm) and red light (580- 640 nm) ³ Determined by 400 MHz ¹H NMR by integrating ratio of peaks at 3.6-4 ppm and 5.8-6.5 ppm

Table 4.6 - Polymerisation of MA using porphyrins **4.7** and **4.15** – **4.17** as photocatalysts in blue and red light



Graph 4.3 - Conversion studies of polymerisation of MA **2.4** using methoxy-modified alkenyl-substituted porphyrin **4.15-4.17** compared to 5,15-distyryl-10,20-diphenylporphyrin **4.7**

4.4 Summary

5,15-Diphenyl-10,20-distyrylporphyrin **4.7** was synthesised, which resulted in red shifting of the absorption properties and broadening of the absorption bands due to increased resonance within the porphyrin ring. 5,15-Diphenyl-10,20-distyrylporphyrin **4.7** was then used as a photocatalyst in the polymerisation of MA and was shown to be more effective than TPP **2.3**.

The next modification that was attempted was to increase conjugation in the porphyrin structure further by increasing the alkene chain length by synthesising 5,15-diphenyl-10,20-bis(4-phenylbuta-1,3-dien-1-yl)porphyrin **4.9**, and increasing the amount of phenyl groups connected to the alkenyl group by synthesising 5,15-bis(2-(naphthalen-1-yl)vinyl)-10,20-diphenylporphyrin **4.10**. However, when attempting to synthesise these variants, an inseparable mixture of the mono- and disubstituted derivatives were formed. Despite this, the absorption properties were further red shifted when compared to 5,15-diphenyl-10,20-distyrylporphyrin **4.7**, showing further conjugation has a tangible effect on absorption properties. The absorptions for these porphyrins were much less intense than 5,15-diphenyl-10,20-distyrylporphyrin **4.7**, resulting in lower photocatalytic activity in the polymerisation of MA **2.4**.

Combining the extension of the conjugation of the porphyrin ring at the *meso* positions and further functionalising the aromatic groups with electron donating 4-methoxy substituent has a larger effect on the absorption properties. It broadens the absorption bands, increases the extinction coefficients of absorbance and red shifts the absorption properties. When using the porphyrins (**4.15** – **4.17**) as photocatalysts in the polymerisation of MA, there was a correlation between higher photocatalytic activity and these properties.

Unfortunately, it was not possible to further test these catalysts in 3D printing applications, as in late 2020 the 3D platform malfunctioned. It was not possible to have this repaired or parts replaced due to supply chain issues and changes within the sponsoring company. Purchasing a new machine would also have made it difficult to compare prints with those previously described in this thesis.

5 Chlorophyll as a photocatalyst in visible light 3D printing

5.1 Introduction

Chlorophyll is a green photosynthetic pigment found in plants, algae, and cyanobacteria. It absorbs light strongly in the blue region and to a lesser extent in the red region of the electromagnetic spectrum. The structure of chlorophyll a **5.1a** (Figure 5.1) contains a porphyrin-like heterocycle called a chlorin ring, similar to tetraphenyl porphyrin TPP **2.3**. Boyer *et al* managed to perform a PET-RAFT polymerisation of MA **2.4** with both chlorophyll a **5.1a** and ZnTPP **2.3** using similar reaction conditions.⁹⁷ Chlorophyll a **5.1a** was extracted from spinach with acetone (crude extract), followed by column chromatography.

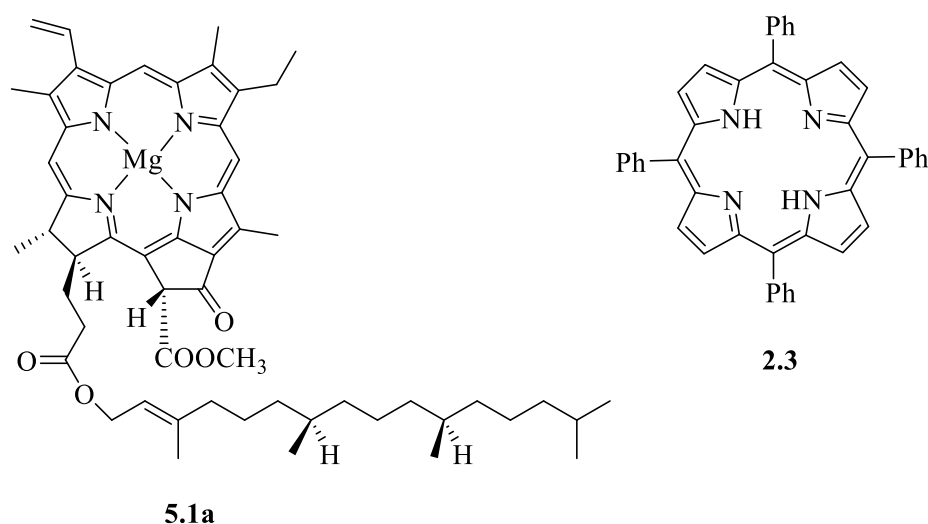


Figure 5.1- Structure of chlorophyll a **5.1a** (left) and tetraphenylporphyrin **2.3** (right)

Run	Photocatalyst	N ₂	Time (min)	Conversion (%)
1	Chlorophyll a 5.1a	YES	120	83
2	Crude extract	YES	180	82
3	Chlorophyll a 5.1a	NO	120	80
4	Crude extract	NO	240	76

Table 5.1 – PET-RAFT polymerisation of MA **2.4** using chlorophyll a **5.1a** and crude spinach extracts a photocatalyst⁹⁷

Polymerisation of a range of acrylate and methacrylate monomers with a variety of xanthate initiators *via* PET-RAFT was possible. While polymerisation of MA **2.4** with pure chlorophyll a **5.1a** was more efficient than the crude extract, Table 5.1, both procedures were successful in the presence of oxygen. Mechanistically, the process

was reported to be similar to that for other PET-RAFT process with porphyrins (see Chapter 1, section 1.9), notably electron transfer from the excited state of chlorophyll a* **5.1a*** to the RAFT agent initially produced a radical anion which fragmented generating an initiating radical and a xanthate anion. Lower conversions occurred using the crude extract and a 1-hour incubation period was found when compared to the pure extract due to the presence of β -carotene and other carotenoids that would otherwise be removed during purification. This led to the assumption that scale up of the reaction was not suitable due to presence of these carotenoids, however this was not investigated further.

5.2 Aims and objectives

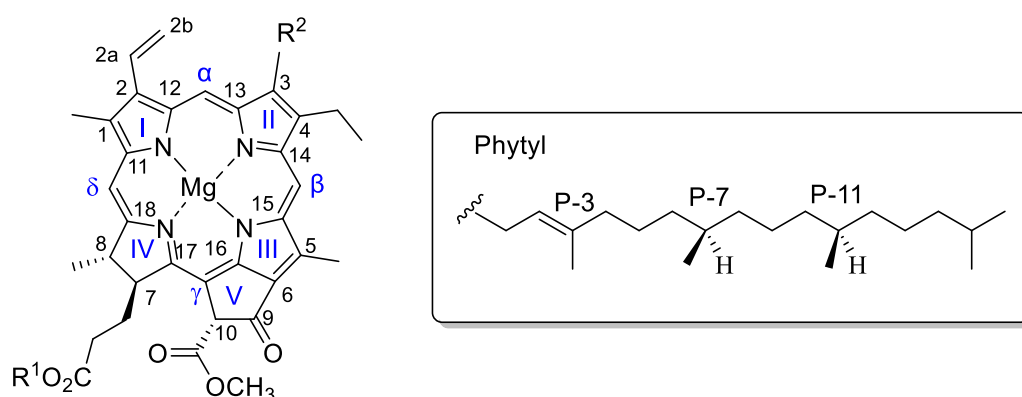
The work of Boyer showed that chlorophyll a **5.1a** extracted from spinach could be a suitable photocatalyst for visible light polymerisation in PET-RAFT, in both pure and crude forms and that polymerisation in the presence of oxygen was possible. While the isolation of pure chlorophyll a **5.1a** would likely be too expensive for an industrial process the use of crude extracts (many of which are commercially available as health supplements) would be attractive for renewable 3D printing applications. We chose to study whether purified chlorophyll a **5.1a** (as well as crude extracts) could be used in 3D printing in air using thiol initiators instead of RAFT initiators. Initial aims included:

- Isolation of purified chlorophyll a **5.1a** from spinach and application in polymerisation of MA **2.4** using decanethiol with both blue and red light.
- Application of purified chlorophyll a **5.1a** as a photocatalyst in 3D printing in air.
- Determination of the ability of crude chlorophyll mixtures (including carotenes) as photocatalysts for the polymerisation of MA **2.4** and 3D printing.
- Determination of the ability of chlorella extract (a health supplement) and purified chlorella extract as an alternative source of chlorophyll a **5.1a** for the polymerisation of MA **2.4** and in 3D printing.

5.3 Results and discussion

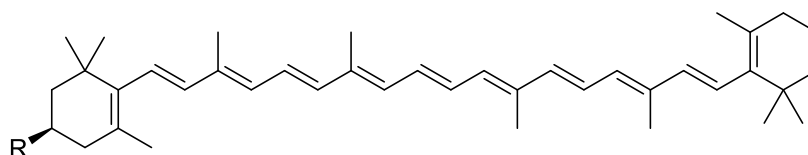
5.3.1 Isolation of chlorophyll a **5.1a** from spinach

Chlorophyll a **5.1a** consists of a porphyrin ring (rings I, II, III and IV, Figure 5.2) where a further ring (ring V) is attached to the *meso* γ -position and C-6. The chlorophyll Fischer nomenclature numbers the *meso* positions α , β , γ , and δ with the carbons of the vinyl group at C-2 being labelled C-2a and C-2b respectively. There are two ester groups, a methyl ester at C-10 and a phytol ester on the chain attached to C-7. Numbering of the phytol chain uses the P-suffix initiated from the ester.



5.1a Chlorophyll a, $R^1 = \text{phytyl}$, $R^2 = \text{Me}$

5.1b Chlorophyll b, $R^1 = \text{phytyl}$, $R^2 = \text{CHO}$



5.2a Beta-carotene, $R = \text{H}$

5.2b Cryptoxanthin (xanthophyll), $R = \text{OH}$

Figure 5.2 - Structures and nomenclature of Chlorophyll a and b **5.1a/b** other components in spinach

To first study the photocatalytic activity of chlorophyll a **5.1a**, it first needed to be isolated from a suitable source. Isolation of chlorophyll a **5.1a**, has been shown to be most efficient from spinach, which is a cheap source of chlorophyll with a very high chlorophyll a **5.1a** content.¹⁵⁴ Isolating chlorophyll a **5.1a** is a two-step process.¹⁵⁵ The most common approach involves extracting the plant pigments from the ground leaves using magnesium sulphate, sand, and acetone, followed by chromatography to isolate the chlorophyll a **5.1a** from the other components such as β -carotene **5.2a**, xanthophyll **5.2b**, chlorophyll b **5.1b** and lipids, (tri-, di- and monoglycerides and fatty acids), Figure 5.2.

However, chlorophyll a **5.1a** is very susceptible to degradation. Consequently, some alternative procedures which use freezing or drying techniques to extract the chlorophyll a **5.1a** can also be used, although in some cases the magnesium ion is lost in these processes.^{156–160} The method most suited to was involved blending the spinach leaves with magnesium sulphate and sand.¹⁶¹ This removes water and minimizes the chance of magnesium loss. Due to spinach being a renewable and affordable source of chlorophyll, a combination of approaches was chosen. Spinach (25 g) was blended with magnesium sulphate (50 g) and sand (50 g) to form a light green powder. This powder was submerged in acetone (~ 200 mL), left to stand for 10 minutes, then the acetone decanted. This was repeated three times, and the extracts combined, and the solvent removed to produce a green solid (crude extract). Chlorophyll a **5.1a** was then isolated *via* column chromatography. The solvent system used for the column chromatography involved using petroleum ether to initially remove the carotenoids and triglycerides, then using petroleum ether 95%/ ethyl acetate 5% to remove chlorophyll b **5.1b**, then finally changing the solvent to petroleum ether 90% / ethyl acetate 10% to elute chlorophyll a **5.1a**. The purification process was not efficient and large volumes of solvents were required giving chlorophyll a **5.1a** (3 mg).

It has been reported that the magnesium atom at the centre of chlorophyll a **5.1a** can be displaced during the process of isolation to produce pheophytin a **5.3a**. To determine if pheophytin a **5.3a** was present in the purified extract both mass spectroscopy and ¹H NMR were used. Mass spectrometry revealed that both chlorophyll a **5.1a** (m/z – 893.5) and pheophytin a **5.3a** (m/z – 871.6) were present, while ¹H 400 MHz NMR confirmed their presence in a ratio of 1.33 : 1 respectively (Figure 5.3).¹⁶² No chlorophyll b **5.1b** was detected (there was no characteristic proton signal for the *meso* a position at 9.87 ppm or aldehyde peak at 10.92 ppm).¹⁶³ The characteristics signals of the *meso* positions were easily differentiated by comparison to published data, mindful of the fact that the exact positions are concentration dependent (due to potential π -stacking of the porphyrins in the solvent, CDCl₃), Figure 5.3.¹⁶⁴

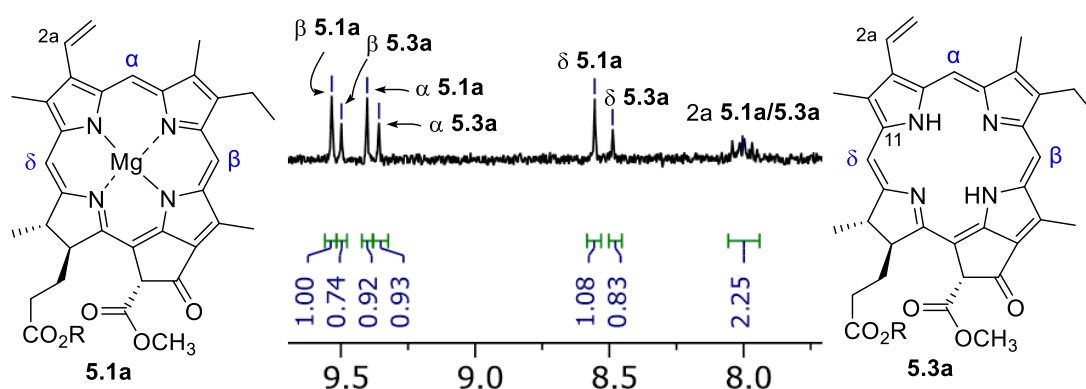


Figure 5.3 – ^1H NMR spectrum of chlorophyll a **5.1a** and pheophytin a **5.2a** mixture.

Further analysis of the ^1H NMR confirmed the presence of the main two compounds **5.1a** and **5.3a**, with a minor impurity detected at 5.40 ppm superimposed upon the signals for the P-2 alkene proton, between 4.50 – 4.10 superimposed on the signals for P-1, C-8 and C-7 protons, and signals at 2.80, 2.35 and 2.10 ppm superimposed upon signals for C-7a and C-7b, Figure 5.4. The impurity is mostly likely a tri-, di- or monoglyceride with high linolenic acid content (the linolenic chain **5.4** is highlighted below with the parts of the molecule identified in the ^1H NMR spectrum are shown).

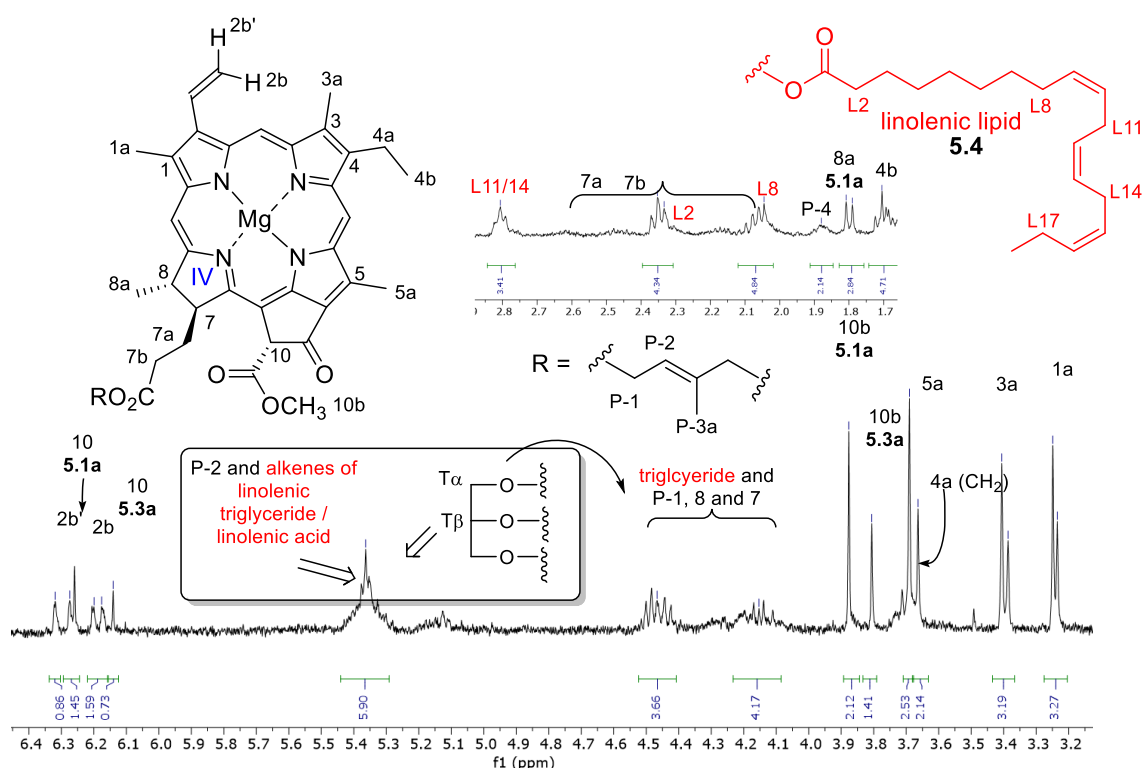


Figure 5.4 - ^1H NMR spectrum of chlorophyll a **5.1a** and pheophytin a **5.2a** mixture.

Analysis of the fatty acids and triglyceride composition found in spinach shows that between 18–30% of the dry weight in chloroplasts are lipids including tri-, di- and mono-glycerides with the main component (68%) being C-18 linolenic acid (18:3) **5.4** derived.¹⁶⁵ The ¹H NMR of the crude spinach extract clearly confirms the presence of these linolenic derived lipids, although there will likely be minor contributions from lipids containing other polyunsaturated fatty acids (16%) as well as galactosyl and digalactosyl diglycerides in this mixture, Figure 5.5.¹⁶⁶ Consequently, purification has not managed to remove all traces of these lipids.

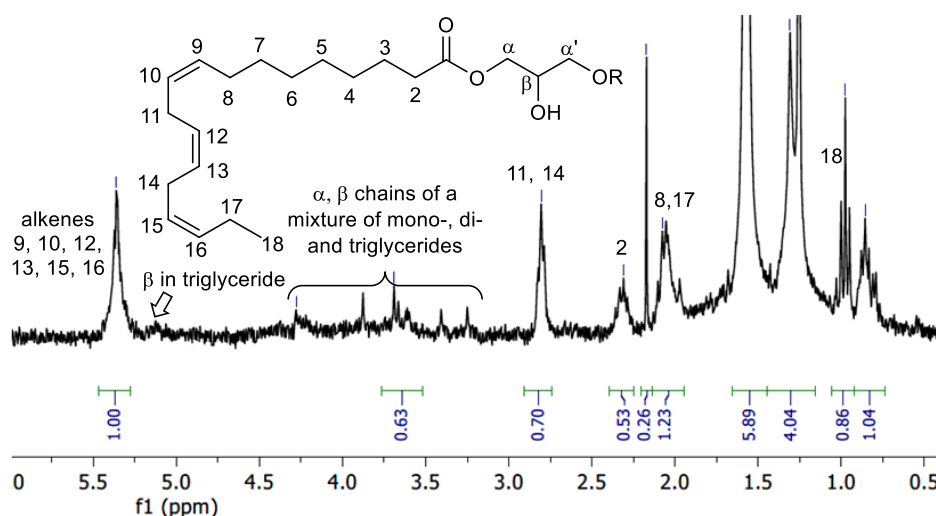


Figure 5.5 - ¹H NMR spectrum of crude spinach extract showing linolenate derived lipids.

For chlorophyll a **5.1a** the signals for the terminal protons on the vinyl group (C-2b) and the enolizable proton at C-10 can be resolved between 6.14–6.32 ppm, while the CH₂ (P-1) in the phytol chain and the protons attached to ring IV (C-8, C-7) resonate between 4.00–4.55 ppm, Figure 5.4. The methyl groups, C-10b, C-5a, C-1a and C-3a respectively (Fischer numbering) can also be easily resolved. There was no evidence of any carotenoids,¹⁶⁷ those being removed in the final purification step.

Due to the similarity of the structures of compounds **5.1a** and **5.3a**, it is difficult to separate these compounds further, and to do so would be very expensive. In addition, while it would theoretically be possible to add the Mg atom back into the non-metalled compound the added expense of further chemical steps was discounted, and further study of the mixture as a photocatalyst was undertaken.

5.3.2 Absorption properties of chlorophyll a **5.1a**

It is known that chlorophyll a **5.1a** absorbs light in the visible spectrum for photosynthesis, the absorption properties of the **5.1a/5.3a** mixture obtained in the procedure described above were recorded in DMSO (0.1475mM) (Figure 5.6, Table 5.2). The significantly increased absorption of the Q I band 667 nm compared to TPP **2.4** and its derivatives is notable.

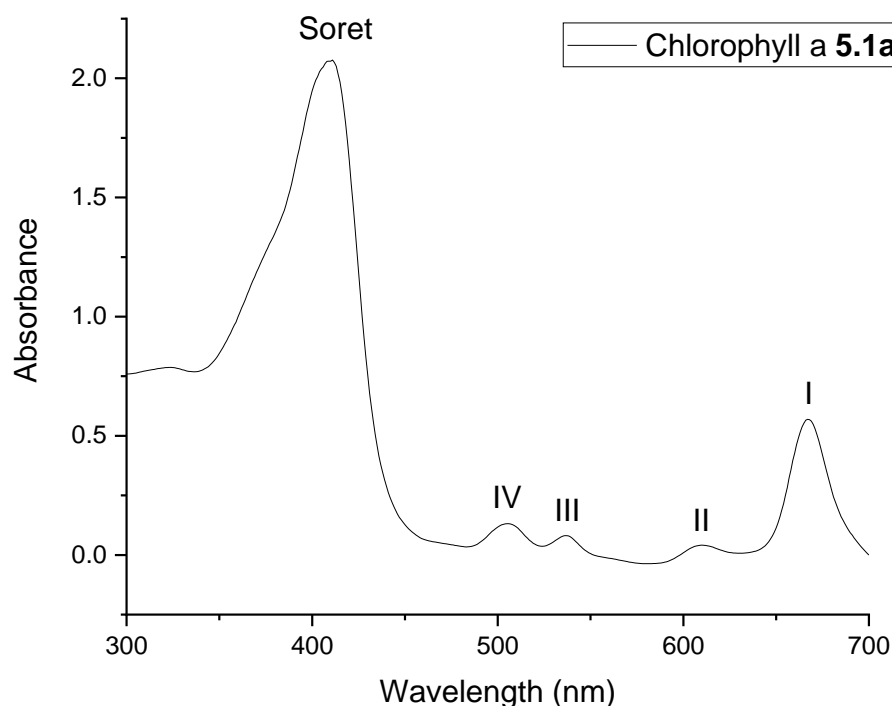


Figure 5.6 – UV-Vis spectra of the **5.1a/5.3a** mixture in DMSO (0.1475mM)

Run	Band	UV-Vis bands (nm)	ϵ ($M^{-1}cm^{-1}$)
1	Soret	410	13700
2	IV	505	830
3	III	537	510
4	II	610	270
5	I	667	3900

Table 5.2 – Data from the UV-Vis spectra of the **5.1a/5.3a** in DMSO (0.1475mM)

5.3.3 Polymerisation with chlorophyll a **5.1a** from spinach

While chlorophyll a **5.1a** has been shown to mediate PET-RAFT polymerisation⁹⁷ the initiation of a radical polymerisation using thiols such as 1-dodecanethiol **2.10** has not been explored, although it has been used in air with fluorescent light to prepare

disulfides *via* PET.¹⁶⁸ Thiols have been reported to add to the C-2 vinyl group of chlorophyll a **5.1a** to give chlorophyll d **5.1d** under radical conditions, Figure 5.7.¹⁶⁹

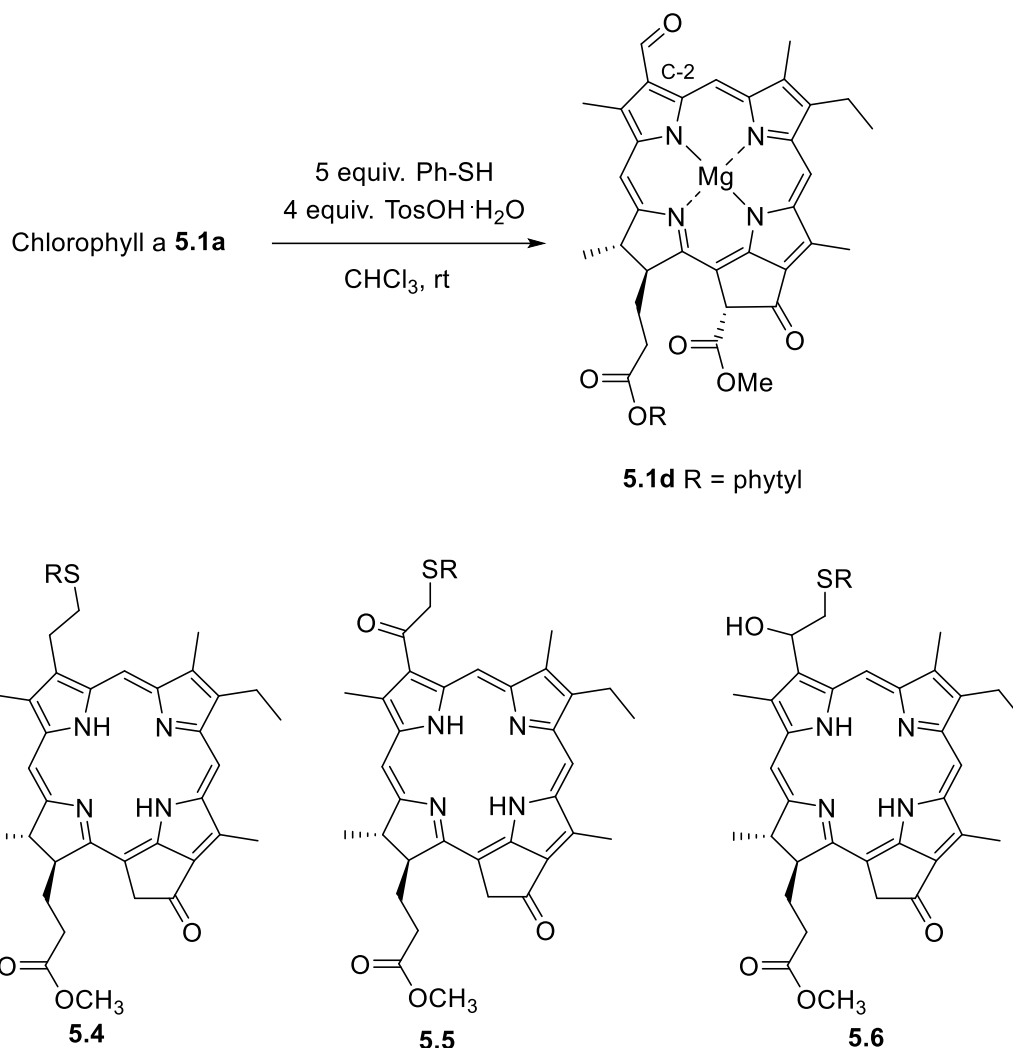


Figure 5.7 – Structures of chlorophyll d **5.1d** and modified derivatives *via* thiol additions¹⁷⁰

The anti-Markovnikov addition of thiols to pheophytin a **5.3a** has also been reported (Figure 5.7). Michael addition of a thiyl radical to the vinyl group of **5.3a** followed by trapping of the resulting radical by either a H-abstraction or by oxygen led to **5.4** – **5.6** respectively. In both reactions the UV /Vis spectrum is not appreciably altered during the process.¹⁷⁰ Consequently, if 1-dodecanethiol **2.10** does undergo reaction at the C-2 vinyl group it should not alter the ability of any modified chlorophylls produced to absorb light in the blue and red region of the spectrum. Most recently, chlorophyll a **5.1a** has been shown to catalyse the generation of radicals from thiols in the presence of oxygen *via* a PET mechanism in DMSO.¹⁶⁸ The process occurs *via* generation of a thiyl radical cation which fragments to generate a thiyl radical and a

proton. In order to determine how effective a chlorophyll a **5.1a** would be in the generation of thiyl radicals and the consequent radical polymerisation of MA **2.4**, the optimised conditions for the polymerisation of MA **2.4** from chapter 2 (MA: thiol **2.10**: photocatalyst– 200: 5: 5×10^{-2}) was used as a comparison (Table 5.3).

After 4 h, polymer conversion was 35% in red light and 42% in blue light. As with the synthetic porphyrins in the previous three chapters, conversion is greater in blue light. This is due to the greater absorption intensity in the blue region of the visible spectrum Soret band; however, conversion is lower when compared to ZnTPP **2.1** (96% in blue light and 81% in red light).

Run	Light ¹	Time	Conversion (%) ²	<i>Mn</i> ³	<i>Mw</i> ³	<i>D</i> ³
1	-	24h	0	-	-	-
2	Red	1h	11	32k	50k	1.48
3	Blue	1h	21	37k	58k	1.56
4	Red	2h	20	33k	49k	1.51
5	Blue	2h	28	37k	58k	1.55
6	Red	3h	27	33k	49k	1.43
7	Blue	3h	33	36k	59k	1.55
8	Red	4h	35	33k	50k	1.41
9	Blue	4h	42	38k	60k	1.58

¹ Experimental condition: Reaction mixture degassed in DMSO and irradiated with light for 4 hours from 4cm away. MA **2.4**: 1-dodecanethiol **2.10**: photocatalyst - 200:1: 1×10^{-2} Blue light (420-460 nm) and red light (580-640 nm) ³ Determined by 400 MHz ¹H NMR by integrating ratio of peaks at 3.6-4 ppm and 5.8-6.5 ppm. ¹ Molecular weight and polydispersity index were determined by GPC analysis (CHCl₃ as eluent) calibrated to poly (methyl methacrylate)

Table 5.3- Polymerisation of MA **2.4** using chlorophyll a **5.1a** as a photocatalyst in both blue and red light

The polymerisation conditions were repeated in darkness, which resulted in no conversion, showing that light was essential for both polymerisations and that **5.1a** must be acting as a photocatalyst. Repeating the reaction without added thiol **2.10**, resulted in negligible conversion (<1%), showing that the interaction between photoexcited chlorophyll a **5.1a** and MA **2.4** is minimal, but as highlighted in chapter 2 this minor background process maybe important in providing an alternative pathway in the initiation of the reaction without thiols.

Although conversion was lower than with ZnTPP **2.1**, the chlorophyll a / pheophytin a mixture is still able to act as a photocatalyst for the polymerisation of MA **2.4** in both blue and red light, albeit at a much slower rate. The PDI's of the polymers are suggestive of a radical process and the lower molecular weights and PDI's for reactions with red light are presumably due to lower conversions. Having shown that the mixture was able to polymerise MA **2.4**, the next step was to attempt a 3D print using the TEGDMA **2.5**/ UDMA **2.6** solution using chlorophyll a **5.1a** as the photocatalyst (monomer: thiol **2.10**: chlorophyll a **5.1a** – 200: 25: 0.25), in blue light (Figure 5.8).

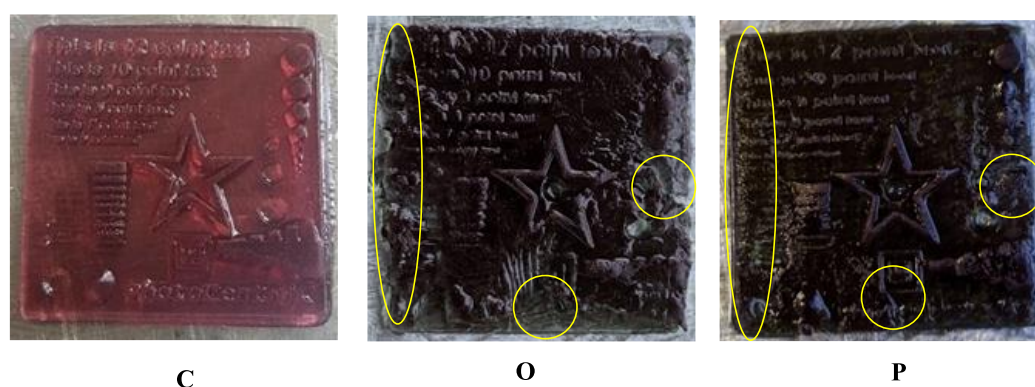


Figure 5.8 - 3D print using chlorophyll a as a photocatalyst. Exposure per layer: 300,000 ms (Print **O**) and 400,000 ms (Print **P**). Monomer: thiol: catalyst 200: 25: 0.25. Compared to print **C** (Exposure time 300,000ms, photocatalyst – ZnTPP **2.1**)

Unlike the process mediated by ZnTPP **2.1** the prints produced (print **O** and **P**) were dark green in colour due to the high concentration of chlorophyll a **5.1a** captured in the matrix. The initial light exposure time per layer was 300,000 ms, as this was what was used in previous prints. However, it was clear that the print produced (Print **O**) was under cured, the circles on the image highlighting the sections in which it was most clear. Therefore, the 3D print was repeated with the exposure time increased to 400,000 ms (Print **P**). This produced a clearer image, with the areas highlighted showing better resolution when compared to print **O**. However, when compared to print **C**, the text at the bottom right of the print was not clear, as well as some of the cylinders at the top right of the print not printing. Consequently, it is possible to 3D print using chlorophyll a **5.1a** as a catalyst in visible light, albeit with a long exposure time which is industrially unpractical. The longer exposure time was necessary due to the reduced reactivity of chlorophyll a **5.1a** compared to ZnTPP **2.1**.

5.3.4 Polymerisation using crude spinach extract

The process of extracting and purifying chlorophyll a **5.1a** from spinach is resource and time intensive, making it difficult to repeat on a larger scale and only generating low yields (0.02%) of the desired catalyst at any one time. Therefore, it would be favourable economically if it was possible to use the initial crude extract of spinach (still containing β -carotenes and other natural products) as the photocatalyst instead. While the other components of the crude extracts are likely to contain antioxidants (e.g. β -carotenes) which would inhibit any radical polymerisation, and although the concentration of chlorophyll a **5.1a** will be lower in the crude spinach extract, Boyer *et al* showed that it was possible to mediate PET-RAFT polymerisation of MA **2.4** with an inhibition/incubation period of 1 hour using the crude spinach extract as a photocatalyst.⁹⁹ It was found this initial inhibition was due to the carotenoids in the crude extract acting as radical inhibitors. In Figure 5.5, it is shown that the crude spinach extract contained linolenate derived lipids. Spinach leaves are known to contain high levels of mono- and digalactosyl diglycerides (containing linolenate chains) which degrade over three days of storage at room temperature to liberate di- and mono-glycerides. These glycerides can undergo oxidation *in vivo via* lipoxygenase to give hydroperoxides which themselves can interact with chlorophyll. It is possible that these hydroperoxides may also act as initiators in radical polymerisation under visible light.

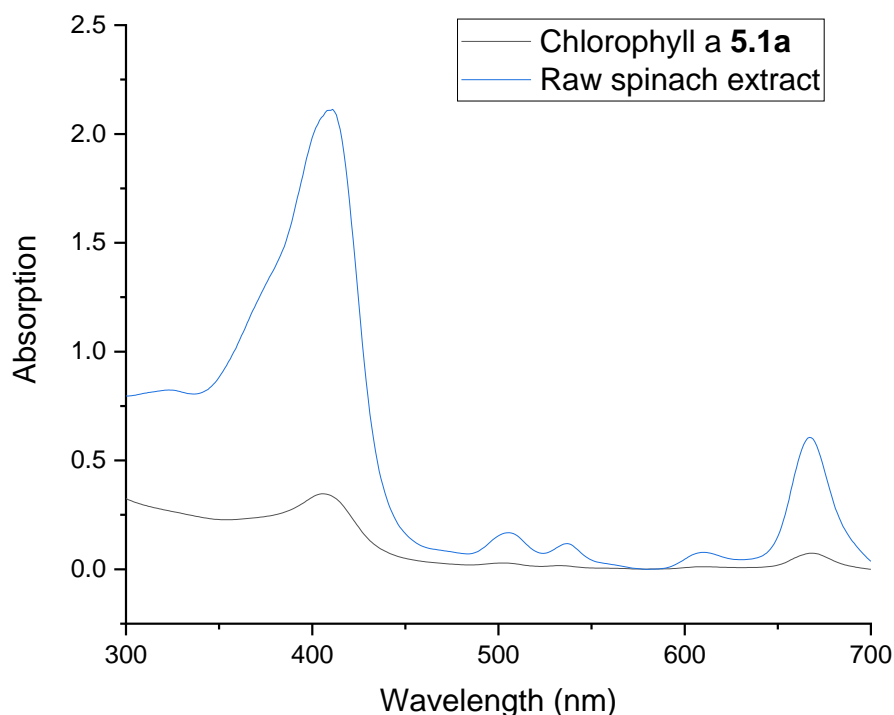


Figure 5.9 - UV-Vis of chlorophyll a **5.1a** vs crude spinach extract in DMSO (0.1475mM)

The UV-Vis spectrum of the crude spinach extract showed that light was absorbed at the same wavelengths as chlorophyll a **5.1a**, however absorption is much weaker, which is expected due to the concentration of chlorophyll a **5.1a** being lower. The concentration of chlorophyll a **5.1a** in the crude spinach extract was calculated by comparing the absorbance of the Soret peaks of pure chlorophyll a **5.1a** and the crude extract of spinach, Figure 5.9. This showed that the concentration of chlorophyll a **5.1a** in the crude extract was 6 times lower than that in the pure sample (1.47×10^{-4} mM vs 2.38×10^{-5} mM). Therefore the expected polymerisation rate would be 6 times slower when using the crude spinach extract as a photocatalyst in the polymerisation of MA **2.4**.

Despite the lower levels of chlorophyll a **5.1a** in the crude extract the polymerisation of MA **2.4** was repeated using the same ratios of ‘catalyst’ (MA **2.4**: thiol **2.12**: photocatalyst– 200: 5: 5×10^{-2}), substituting the crude spinach extract for chlorophyll a **5.1a** (Table 5.4, 5.5).

Run	Photocatalyst ¹	Light ²	Conversion (%) ³
1	Crude spinach	-	0
2	Chlorophyll a 5.1a	Red	35
3	Crude spinach	Red	26
4	Chlorophyll a 5.1a	Blue	42
5	Crude spinach	Blue	31

¹ Experimental condition: Reaction mixture degassed in DMSO and irradiated with light for 4 hours from 4cm away. MA **2.4**: 1-dodecanethiol **2.10**: photocatalyst- 200:1:1x10⁻² Blue light (420-460 nm) and red light (580-640 nm) ³ Determined by 400 MHz ¹H NMR by integrating ratio of peaks at 3.6-4 ppm and 5.8-6.5 ppm

Table 5.4 - Polymerisation of MA **2.4** using chlorophyll a **5.1a** and crude spinach as photocatalysts in blue and red light

The first experiment was performed in darkness, to make sure that the other components of the crude extract did not result in other polymerisation processes, and after 24h, no conversion occurred. As expected, in both blue and red light, conversion was lower when using the crude spinach extract, which can be explained by the lower concentration of the active component chlorophyll a **5.1a** in the crude extract. Conversion was also higher in blue light, which was consistent with the polymerisation of MA **2.4** using chlorophyll a **5.1a** as a photocatalyst. This result has shown that the crude spinach extract is able to polymerise MA **2.4** without further purification, albeit less efficiently than pure chlorophyll a **5.1a**. However, the conversion was not 6 times lower than expected due to the relative concentration ratios of **5.1a** and the presence of the linolenate glycerides and their potential hydroperoxides are likely to also influence the polymerisation. There may well be other minor components within the crude extract which are also helping catalyse the process.

Run	Light ¹	Time	Conversion (%) ²
1	Chlorophyll a 5.1a	1h	21
2	Crude spinach	1h	10
3	Chlorophyll a 5.1a	2h	28
4	Crude spinach	2h	17
5	Chlorophyll a 5.1a	3h	33
6	Crude spinach	3h	25
7	Chlorophyll a 5.1a	4h	42
8	Crude spinach	4h	31

Experimental condition: Reaction mixture degassed in DMSO and irradiated with light for 4 hours from 4cm away. MA **2.4**: 1-dodecanethiol **2.10**: photocatalyst - 200:1:1x10⁻² Blue light (420-460 nm) ² Determined by 400 MHz ¹H NMR by integrating ratio of peaks at 3.6-4 ppm and 5.8-6.5 ppm

Table 5.5 – Conversion study of the polymerisation of MA **2.4** using chlorophyll a **5.1a** and crude spinach extract as photocatalysts in blue light

5.3.5 3D printing using crude spinach extract

Although the conversion of MA **2.4** was lower when using the crude spinach extract as a photocatalyst, it was still worthwhile to see if it was possible to photocatalyse a 3D print of TEGDMA **2.5**/ UDMA **2.6**. The generation of linolenate derived hydroperoxides *in situ* may also be accelerated *via* irradiation in air. The same reaction conditions as previously established were used (monomer: thiol: photocatalyst - 200: 25: 0.25), with an exposure per layer of 400,000 ms in blue light, Figure 5.10.

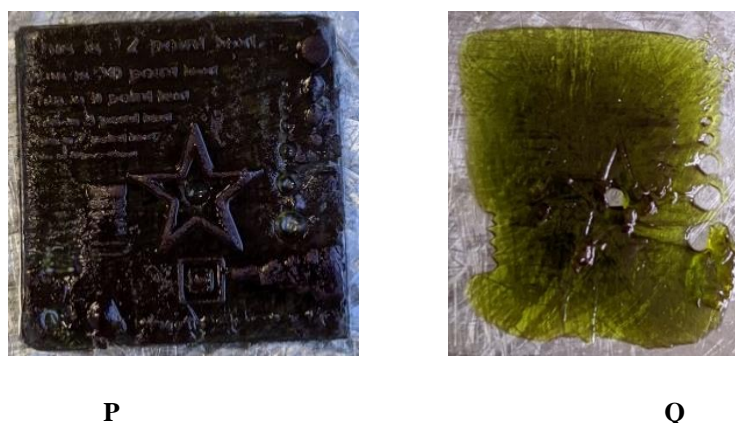


Figure 5.10 – 3D prints using crude spinach extract as a photocatalyst, exposure per layer 400,000 ms. Print **P** (chlorophyll a) and print **R** (crude spinach extract).

It is clear to see that the 3D print produced (print **Q**), when using crude spinach as a photocatalyst, is very undercured when compared to print **P**, with none of the text being printed and the edges of the print not being cured at all. This suggests that

polymerisation rate is too low, and the crude spinach extract is not a suitable candidate to be used in visible light 3D printing. This is likely due to the lower concentration of chlorophyll a **5.1a** in the crude extract, as well as any inhibition period caused by the presence of carotenoids which would slow the polymerisation rate.

5.3.6 Alternate chlorophyll sources to spinach, *Chlorella pyrenoidosa*.

Spinach as a crop has a short shelf life and needs to be stored under refrigeration. It also requires a large amount of space to store, and 5000 g of spinach are required to produce 1 g of catalyst. In addition, the extraction process was expensive and non-sustainable. A range of alternative sources of chlorophyll a **5.1a** were identified. A potential alternative to use was chlorella extract, a commercial product which contains a single-celled green algae (*chlorella pyrenoidosa*). Commercially, it is marketed as a nutrition or medicinal supplement and when dried contains protein (45%), lipids (20%), carbohydrates (20%) and other trace vitamins as well as chlorophyll. It has been proposed as a sustainable food source as it produces more protein per area than any other plant source.¹⁷¹ While commercial extracts contain vitamins B and C (and other antioxidants) they have a greater shelf life than spinach and do not need to be stored under refrigeration.

As chlorella is produced commercially in two solid forms, it was decided that both the (a) powdered (Mysuperfoods organic chlorella powder) and (b) tablet forms (Mysuperfoods organic chlorella tablets) would be studied. To extract crude chlorophyll a **5.1a** the chlorella powder (10 g) was submerged in acetone (100 mL) and left to stand for 10 minutes. The acetone was decanted, and this process repeated twice. The extracts were combined, and the solvent removed under vacuum to produce the crude extract. The same approach was used to extract from the chlorella tablets; however, the tablet was first crushed into a powder in a pestle and mortar. Purified chlorophyll a **5.1a** was then isolated from the crude extract *via* column chromatography, using the solvent system as for the chlorophyll a **5.1a** extraction from the crude spinach extract. As for spinach a mixture of chlorophyll a **5.1a** and pheophytin a **5.3a** was isolated. Significantly more **5.1a** was present in the mixture and there was minimal residual lipid (compare to red boxes), providing purer material, Figure 5.11. The cleaner material allowed for easier assignment of the ¹H NMR spectrum.

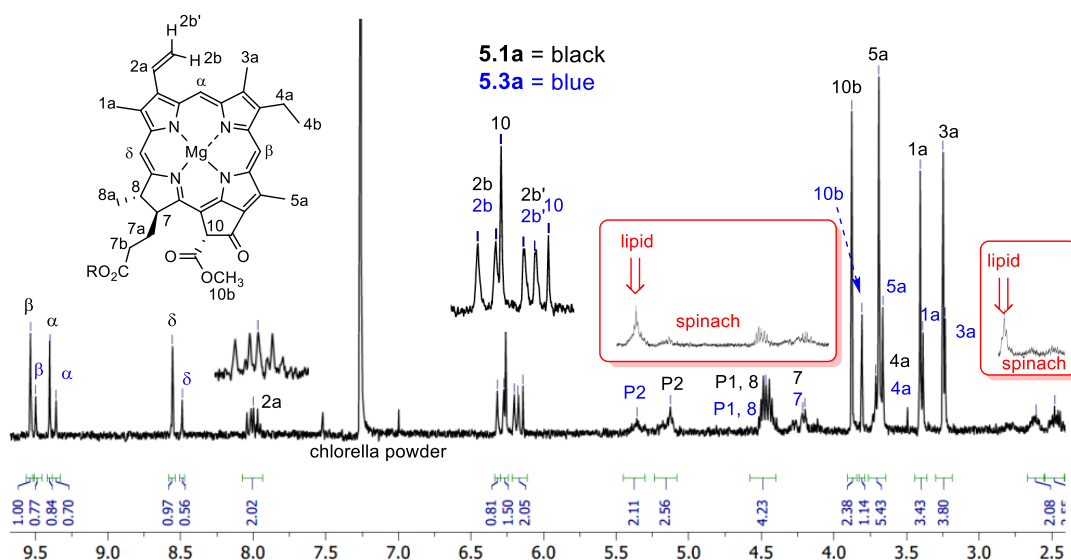


Figure 5.11 - ^1H NMR spectrum of purified chlorella powder (black) and purified spinach (red).

When attempting to isolate chlorophyll a **5.1a** from powdered chlorella, 1 mg of chlorophyll a **5.1a** was extracted for 1 g of chlorella powder, whereas 0.8 mg of chlorophyll a **5.1a** was extracted from the tablet. This is 4-5 times more efficient respectively than the 0.2 mg of chlorophyll a **5.1a** extracted from 1 g of spinach. In addition, the purity of the chlorophyll was significantly improved. This is important because the most resource intensive aspect of the isolation of chlorophyll comes from column chromatography, so the more efficient the isolation, the less resources are required for extraction.

The polymerisation of MA **2.4** was repeated using the chlorophyll extracted from chlorella (MA **2.4**: thiol **2.10**: photocatalyst– 200: 5: 5×10^{-2}), in both blue and red light. Conversion was 33% in red light (spinach chlorophyll a **5.1a** -35%) and 44% in blue light (spinach chlorophyll a **5.1a** – 42%). This showed that the chlorophyll a **5.1a** extracted from chlorella was of a similar reactivity as a photocatalyst to that extracted from spinach.

As with spinach, the use of purified chlorella extracts required the expense of chromatography with significant amounts of solvents. As before with spinach the reactivity of crude chlorella extract was investigated to determine if purification *via* chromatography was necessary. Analysis of the crude initial extract of chlorella (either with the powder or the tablets) indicated most of the extract was made up of lipids (mainly of linoleic, linolenic acid and palmitic acid chains) similar to that of spinach, Figure 5.12. The main difference, however, was that the lipids were triglyceride in

origin as determined by the characteristic splitting of the diastereotopic protons in the CH₂ groups (α chains) of the glycerol esters, Figure 5.12. The extract from the chlorella powder did also contain a further unidentified minor component.

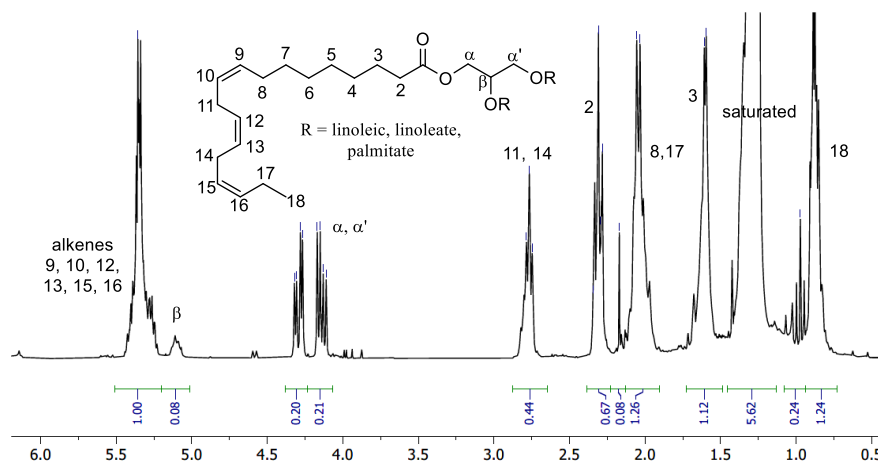


Figure 5.12 - ¹H NMR spectrum of crude extracted chlorella tablet showing triglycerides.

The concentration of the active chlorophyll a **5.1a** in the crude extracts was similar to that determined for spinach, Figure 5.13. The lower concentration in the crude extract from the chlorella tablet should manifest in lower conversions when these extracts are tested in polymerisation reactions.

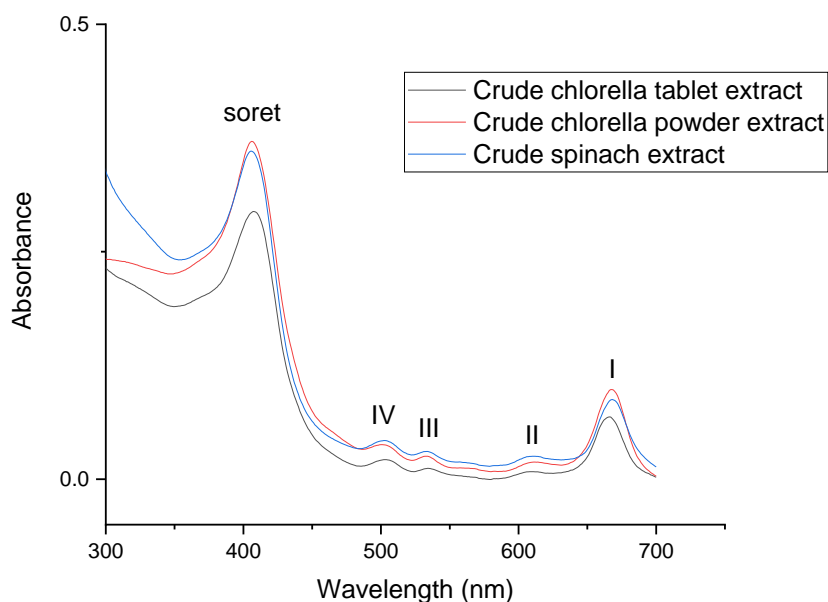


Figure 5.13 - UV Vis of crude chlorella and spinach extracts in DMSO (0.1 mg/mL)

5.3.7 Polymerisation of MA 2.4 using crude chlorella extracts

To determine how effective the crude chlorella extracts are as photocatalysts, they were tested in the polymerisation of MA 2.4 (MA 2.4: thiol 2.10: photocatalyst– 200: 1: 1×10^{-2}) in both blue and red light, using the crude chlorella extract photocatalysts. The solution was degassed and irradiated with light for 4 h from 4 cm away (Table 5.6).

The initial polymerisations were performed in darkness to confirm that it was the light initiating the reaction, and no polymerisation occurred after 24 h.

Run	Photocatalyst ¹	Light ²	Conversion (%) ³
1	Crude chlorella (tablet)	-	0
2	Crude chlorella (powder)	-	0
3	Crude spinach	Red	26
4	Crude chlorella (tablet)	Red	20
5	Crude chlorella (powder)	Red	48
6	Crude spinach	Blue	31
7	Crude chlorella (tablet)	Blue	27
8	Crude chlorella (powder)	Blue	60

Experimental condition: Reaction mixture degassed in DMSO and irradiated with light for 4 hours from 4cm away. MA 2.4:1-dodecanethiol 2.10: photocatalyst - 200:1: 1×10^{-2} Blue light (420-460 nm) and red light (580 - 640 nm) ² Determined by 400 MHz ¹H NMR by integrating ratio of peaks at 3.6-4 ppm and 5.8-6.5 ppm

Table 5.6 - Polymerisation of MA 2.4 using crude spinach and chlorella extracts as photocatalysts

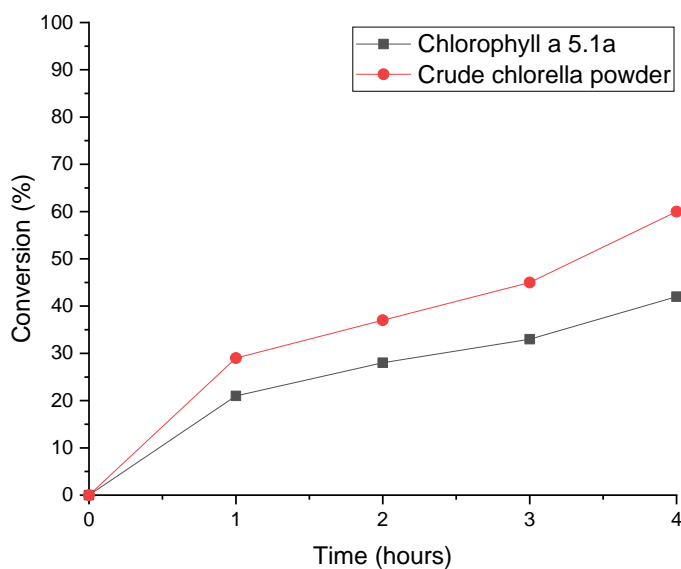
The initial results of the polymerisation show that conversion when using the crude extract from the chlorella tablet is similar to that of crude spinach (runs 3→4 and 6→7) in both blue and red light. This was expected due to the similar absorption spectra of both extracts showing that concentration of chlorophyll a 5.1a is similar. When the crude chlorella, extracted from the powdered version, was used as a photocatalyst, it was interesting to see that conversion was greater in both blue and red light (runs 5 and 8), given the absorption spectrum was similar to that of the crude spinach and crude chlorella tablet extracts (Table 5.7, Graph 5.1). One reason for this may be the presence of the further unidentified compound in the crude powder extract (Mysuperfoods organic chlorella powder) that was not present in the crude tablet form (Mysuperfoods organic chlorella tablets), which increases the speed of polymerisation. However due to the large mixture of minor components in the extracts,

it would be challenging to determine which specific compound is affecting polymerisation.

Run	Photocatalyst ¹	Time	Conversion (%) ²	M_n ³	M_w ³	\bar{D} ³
1	Chlorophyll a 5.1a	1h	21	37k	58	1.56
2	Crude chlorella (powder)	1h	29	32k	56k	1.54
3	Chlorophyll a 5.1a	2h	28	37k	58	1.55
4	Crude chlorella (powder)	2h	37	33k	55k	1.54
5	Chlorophyll a 5.1a	3h	33	36k	59	1.55
6	Crude chlorella (powder)	3h	45	33k	55k	1.58
7	Chlorophyll a 5.1a	4h	42	38k	60	1.58
8	Crude chlorella (powder)	4h	60	33k	55k	1.55

Experimental condition: Reaction mixture degassed in DMSO and irradiated with light for 4 hours from 4cm away. MA **2.4**: pentaerythritol tetrakis (3-mercaptopropionate) **2.12**: porphyrin - 200:1:1x10⁻² Blue light (420-460 nm) ² Determined by 400 MHz ¹H NMR by integrating ratio of peaks at 3.6-4 ppm and 5.8-6.5 ppm. ³ Molecular weight and polydispersity index were determined by GPC analysis (CHCl₃ as eluent) calibrated to poly (methyl methacrylate)

Table 5.7 – Conversion study of polymerisation of MA **2.4** comparing chlorophyll a **5.1a** and crude chlorella powder in blue light



Graph 5.1 - Conversion study of polymerisation of MA **2.4** comparing chlorophyll a **5.1a** and crude chlorella powder in blue light

5.3.8 3D printing using crude chlorella as a photocatalyst

Crude chlorella extracts are able to polymerise MA **2.4** in both blue and red light, with the crude chlorella powder showing higher photocatalytic activity. To determine the ability to of the crude extracts to photocatalyse a 3D print, the crude extracts were used to polymerise TEGDMA / UDMA (monomer: thiol: photocatalyst - 200: 25: 0.25) with an exposure time of 400,000 ms in blue light.

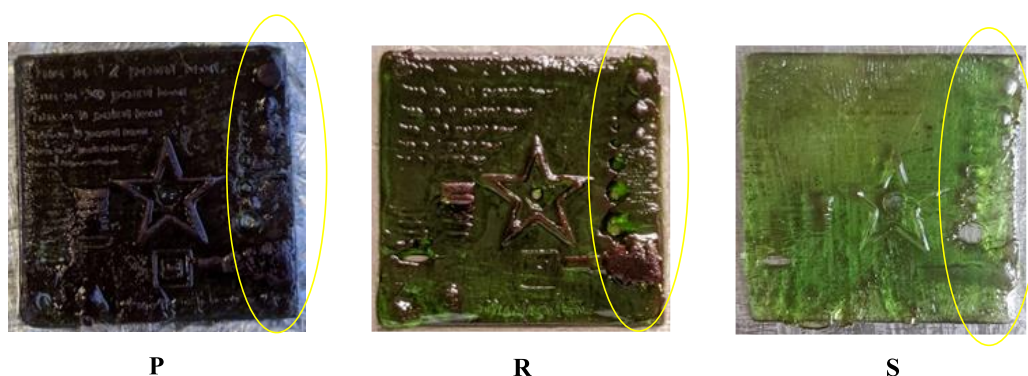


Figure 5.14 - 3D prints using crude chlorella (**R** - powder and **S** - tablet) as photocatalyst compared to print **P** (using chlorophyll a **5.1a** as a photocatalyst)

The attempt to 3D print using the crude chlorella extracts did result in a print being produced (Prints **R** and **S**), however there was a noticeable difference in the resolution (Figure 5.14). The right-hand side of print **S** was under cured, with the cylinders partially printed and none of the text printed. This suggests that the polymerisation rate was too slow, which was expected after the poor conversion of the polymerisation of MA **2.4**. The print produced when using the crude chlorella powder extract was of a better quality, with all of the shapes and text in the top left of the print being printed. This shows that the crude chlorella powder extract is more suitable as a photocatalyst for 3D printing due to the better print quality. When comparing print **R** to print **P**, the first thing to notice is the difference in colour. Print **P** is a much darker green, which is likely due to the higher concentration of chlorophyll a **5.1a**. The quality of both prints is comparable, with the cylindrical shapes and the text being present on both prints in similar resolution.

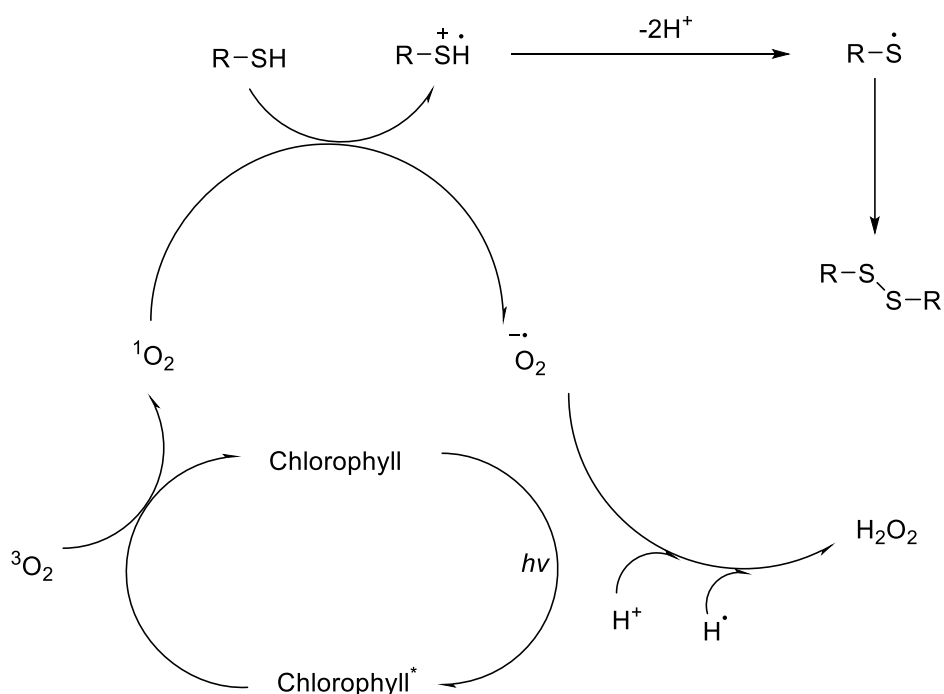
5.4 Summary

We have managed to show that it is possible to polymerise MA **2.4** using chlorophyll a **5.1a** (extracted from spinach), as a photocatalyst in both blue and red light. Furthermore, chlorophyll a **5.1a** can be utilised as a photocatalyst for 3D printing in

blue light, however with a longer exposure time (400,000 ms vs 300,000 ms) compared with synthetic porphyrins. The crude spinach extract was also used to polymerise MA in blue and red light, however, was found to be less effective than chlorophyll a **5.1a**, which resulted in the 3D print attempted using the crude spinach to be undercured.

The results have shown that it is possible to extract chlorophyll a **5.1a** with better efficiency than from chlorella sources, making them a more viable alternative as a source of chlorophyll a **5.1a**. Also, the use of the crude extract from chlorella is able to be utilised as a photocatalyst in 3D printing, producing somewhat better results. The higher conversions are likely due to other impurities within the commercial chlorella extracts. Further work could entail analysing in more detail the components of the commercial chlorella extracts to determine if they are contributing to the catalysis and analysing other commercial sources of chlorophyll from the health industry to improve any applications.

Mechanistically, the chlorophyll mediated polymerisation during 3D printing utilising thiols in air is likely to proceed *via* a radical cation intermediate (Scheme 5.1).



Scheme 5.1 - Potential mechanism of action for polymerisation using chlorophyll a **5.1a** as a photocatalyst.

Hence, excited chlorophyll can generate a thiol radical cation (either directly) or *via* formation of singlet oxygen. Loss of a proton from the thiol radical cation would generate the corresponding thiol radical which would initiate the polymerisation. The excess protons could either be quenched by an advantageous basic entities within the crude extracts or via the superoxide radical anion.¹⁶⁸

6 Concluding remarks

6.1 Conclusion

This thesis has explored the use of both natural and synthetic porphyrin as photocatalysts in visible light polymerisation, further extending to use in visible light 3D printing. In chapter 2, ZnTPP **2.1** was utilised as a photocatalyst for the polymerisation of MA **2.4** in both blue and red light, using a variety of thiols as photocatalysts. It was then shown that ZnTPP **2.1** was able to photocatalyse a 3D print of TEGDMA **2.5** / UDMA **2.6** in blue light, showing it is an effective photocatalyst to be used in 3D printing. The use of the metal-free porphyrin TPP **2.3** as a photocatalyst was also explored. It had been previously shown that TPP **2.3** was unable to be used as a photocatalyst due to the lack of central metal ion.⁸⁷ However TPP **2.3** was used to catalyse the polymerisation of MA **2.4** in both blue and red light, albeit with less efficiency than ZnTPP **2.1**. It was also shown to be a suitable photocatalyst for 3D printing, with resolution of prints similar to that of ZnTPP **2.1**.

In chapter 3, the effect of modifying TPP **2.3** with electron withdrawing and donating substituents was explored. It was expected that the addition of electron donating groups would increase the electron density of the aromatic system of the porphyrin, leading to increased resonance effects which would shift the visible absorption towards a higher wavelength (more favourable for 3D printing). Porphyrins were functionalised with chloro, methyl and methoxy groups. It was found that 5,10, 15, 20-tetrakis(4-methoxyphenyl) porphyrin **3.4** shifted absorption properties by 4 nm towards the red end of the spectrum. Although only a small shift in absorption properties, **3.4** was shown to have improved photocatalytic ability, increasing the polymerisation rate, and producing high quality 3D prints. The position of functionalisation was also studied, with ortho **3.10** and meta **3.11** methoxy-substituted variants being studied. However, there was little effect on absorption properties and photocatalytic activity. The effect of functionalising the phenyl groups at the meso positions of TPP **2.3** with additional methoxy groups was also studied, however it was shown that this did not improve photocatalytic ability due to a mixture of both steric and resonance effects.

The introduction of electron-donating and withdrawing groups to the porphyrin system only shifted the absorption properties to a small degree (4 nm), therefore another avenue of polymer functionalisation was explored. It is known that extending the

conjugation of the porphyrin core results in broadening of the absorption bands of porphyrins, as well as shifting them towards the red end of the spectrum. Therefore 5,15-diphenyl-10,20-distyrylporphyrin **4.7** was synthesised by utilising the heck reaction, resulting in red shifting of the absorption properties. The effect of this was an increase in photocatalytic activity for the polymerisation of MA **2.4** in both blue and red light. Attempts were made to synthesise derivatives with extended conjugation, however a mixture of mono- and di- substituted variants were synthesised. Despite this, absorption properties were shifted favourably, but low absorption of these species meant that photocatalytic activity was not improved. Finally, using the results from chapter 2, methoxy groups were introduced to the alkenyl-substituted porphyrins at the styryl and phenyl positions **4.15-4.17**. This resulted in the largest shift in absorption properties, due to a mixture of extended porphyrin core conjugation, as well as increased electron density from the electron donating methoxy groups. There was a direct correlation between absorption properties of porphyrins **4.15 – 4.17** and photocatalytic ability to polymerise MA in blue and red light. The more the absorption properties were shifted towards the red end of the spectrum, the higher the photocatalytic ability.

Finally, the ability of chlorophyll a **5.1a** to catalyse a visible light 3D print was studied. Chlorophyll a **5.1a** was isolated from spinach and was isolated as an inseparable mixture with pheophytin a **5.3a**. Despite this, the mixture was able to photo catalyse the polymerisation of MA **2.4** in both blue and red light. However, conversion was lower than when using synthetic porphyrins in both blue and red light. Furthermore, the mixture of **5.1a / 5.3a** was able to be used as a photocatalyst in the 3D printing of TEGDMA **2.5** / UDMA **2.6** in blue light, however exposure time had to be increased to 400,000 ms per layer to print an image of acceptable resolution (300,000 ms for synthetic porphyrins). The crude extract from spinach was also used as a photocatalyst for 3D printing, however, was found to be unsuitable for 3D printing as the print produced was of much lower quality. This was likely due to the low concentration of chlorophyll a **5.1a**. Due to the short shelf life of spinach and the requirement to store under refrigeration, alternative sources of chlorophyll were studied. Chlorella was chosen due to its long shelf life and high concentration of chlorophyll a **5.1a**. It was found that 5x the amount of chlorophyll a **5.1a** could be extracted from chlorella powder when compared to spinach, making chlorella a viable source of chlorophyll a

5.1a. The crude extract of chlorella was also used as a photocatalyst in 3D printing, and it was found that the photocatalytic ability was much greater than crude spinach extract, likely due to other compounds in the raw extract effecting polymerisation as chlorophyll concentration was similar. Crude chlorella was also shown to be an effective photocatalyst for 3D printing in blue light and produced a similar quality of print when compared to using pure chlorophyll a **5.1a** as a photocatalyst.

7 Experimental

7.1 General information

Chemicals: The inhibitor was removed from methyl acrylate (MA **2.4**) by percolating over a basic alumina column. All other solvents and starting materials were used as received without purification. Column chromatography was performed using Aldrich chemistry[®] silica gel, technical grade, pore size 60 Å, 40 – 63 μM.

Analysis: ¹H NMR and ¹³C NMR were measured on Bruker Avance 300, 400 and 600 MHz spectrometers. Chemical shifts are given in parts per million (ppm) relative to CHCl₃ - δ: 7.26. Coupling constants are expressed in Hertz (Hz).

ES-MS was achieved using an Agilent 6310B single Quad. UV-Vis measurements were recorded using a Agilent Cary 60 UV-Vis Spectrometer, using a quartz cuvette with a path length of 1 cm. Wavelengths are given in nm, with molar extinction coefficients given in M⁻¹ cm⁻¹.

GPC analysis of compounds with CHCl₃ as eluent were obtained using an Agilent Infinity II MDS instrument equipped with differential refractive index (DRI), viscometry (VS), dual angle light scatter (LS) and multiple wavelength UV detectors. The system was equipped with 2 x PLgel Mixed C columns (300 x 7.5 mm) and a PLgel 5 μm guard column. The eluent was CHCl₃ with 2 % TEA (triethylamine) additive. Samples were run at 1mL/min at 30°C. Poly(methyl methacrylate) standard (Agilent EasyVials) were used for calibration. Ethanol was added as a flow rate marker. Analyte samples were filtered through a GVHP membrane with 0.22 μm pore size before injection.

TGA was obtained using a Mettler-Toledo TGA with autosampler. TGA samples, in air, were heated from 25 °C to 600 °C at 10 °C / min in 40 μl aluminium pans.

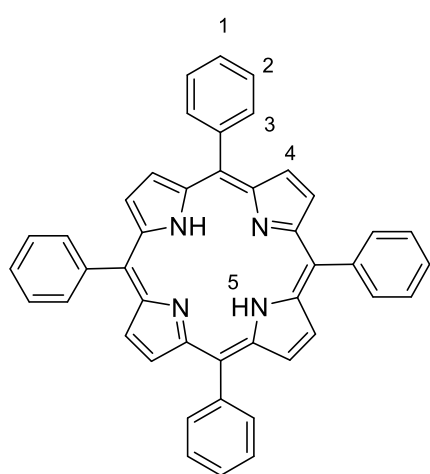
Photo polymerisations were carried out in a glass vial fitted with a rubber septum and irradiated by RS PRO ES/E27 LED Cluster Lamp (5 W). The distance between the sample and the light source was 4 cm. The two colours of light studied were blue ($\lambda_{\text{max}} = 420 - 460$ nm) and red ($\lambda_{\text{max}} = 580 - 640$ nm).

The 3D printer used for all 3D prints was the photocentric liquid crystal precision printer. All 3D prints were performed using blue light in atmospheric conditions, with an exposure time of 300,000 ms unless stated otherwise. TEGDMA and UDMA was provided by Photocentric for 3D prints.

7.2 Chapter 2

7.2.1 Synthesis of tetraphenylporphyrin **2.3**.¹³⁹

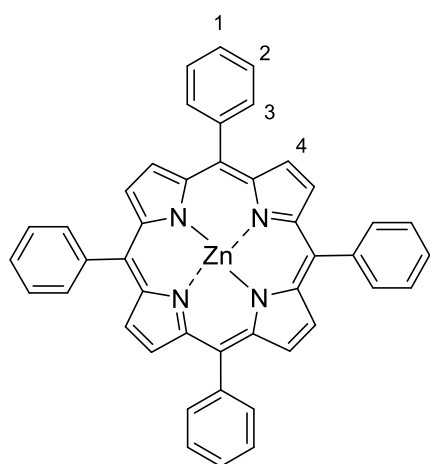
A solution of pyrrole (1.0 mL, 14 mmol) and benzaldehyde (1.4 mL, 14 mmol, 1 equivalent) was added to propanoic acid (50 mL). This solution was heated at reflux for 45 minutes at 150 °C, then cooled to room temperature. The solid formed was filtered, then washed with cold methanol (20 mL). The solid was washed with hot water (20 mL) and dried, yielding purple crystals of tetraphenylporphyrin **2.3** (0.19 g, 9% yield). Spectroscopic data matched that reported.¹⁷²



¹H NMR (CDCl₃, 400MHz): δ 8.84 (s, 8H, H⁴), 8.20 (d, *J* = 9.0 Hz, 8H, H¹), 7.77 (m, 16H, H^{2,3}), -2.77 (s, 2H, H⁵); ¹³C NMR (CDCl₃, 125MHz): δ 142.2, 134.6, 132.6, 130.5, 127.7, 126.9, 120.1; MS (ESI): *m/z* (C₄₄H₃₀N₄) found: 615.4 (MH⁺). UV-Vis (DMSO): 419 (15300), 515 (610), 551 (200), 589 (0.14). Melting point: > 300 °C

7.2.2 Synthesis of ZnTPP **2.1**.¹⁴⁰

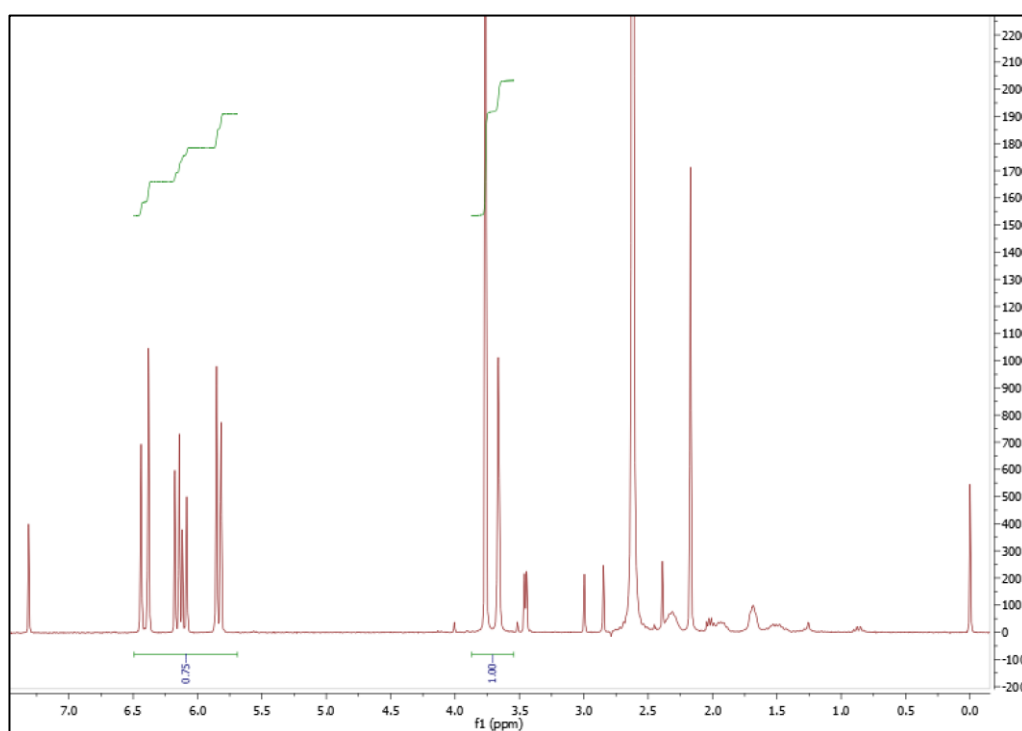
Tetraphenylporphyrin **2.3** (0.10g, 0.16 mmol) was dissolved in chloroform (20 mL). A saturated solution of Zn(OAc)₂ (0.05 g, 0.23 mmol, 1.4 equivalent) in MeOH (5 mL) was added. The solution was stirred for 1 h after which the reaction mixture was washed with water (2 x 20 mL) and brine (2 x 20 mL). The organic layer was then dried with MgSO₄, the mixture was filtered, and solvent removed in *vacuo*, yielding a purple solid (0.11 g, 90%). Spectroscopic data matched that reported¹⁷³



^1H NMR (CDCl_3 , 400MHz): δ 8.95 (s, 8H, H^4), 8.23 (m, 8H, H^1), 7.76 (m, 12H, $\text{H}^{2,3}$). ^{13}C NMR (CDCl_3 , 125MHz): δ 150.2, 142.8, 134.4, 131.9, 127.5, 126.6, 121.1 MS (ESI): m/z ($\text{C}_{44}\text{H}_{28}\text{N}_4\text{Zn}^{64}$) found: 677.5 (MH^+). UV-Vis(DMSO): 427 (13700), 560 (820), 599 (340). Melting point: > 300 $^\circ\text{C}$.

7.2.3 RAFT polymerisation of MA **2.4** using BPTA **2.2**⁸⁷

To a glass vial was added MA **2.4** (0.38 mL, 4.2 mmol) DMSO (277 μL), BPTA (5 mg, 20.97 μmol) and ZnTPP **2.1** (142 μL of 1.475 mM solution in DMSO, 0.21 μmol). The vial was wrapped in aluminium foil and degassed with N_2 for 10 minutes. This mixture was then irradiated in red light (5W, LED, 580-640 nm) or blue light (5W, LED, 420-460 nm) from 4 cm away at rt for 2 h. Conversion was determined by ^1H 400 MHz NMR by comparing the integration of the resonances of the alkene protons on the monomer (5.5-6.5 ppm) and the repeating O- CH_3 peak of the polymer (3.5-4.0 ppm). In the example below, the conversion is 25%.



7.2.4 General procedure for polymerisation of MA **2.4** using ATRP initiators

To a vial, MA **2.4** (0.38 mL, 4.2 mmol), DMSO (277 μ L), alkyl halide initiator (20.97 μ mol) and ZnTPP **2.1** (142 μ L of 1.475 mM solution in DMSO, 0.21 μ mol) was added, and the mixture was degassed with N₂ for 10 minutes. The reaction mixture was irradiated in red light (5W, LED, 580-640 nm) or blue light (5W, LED, 420-460 nm) from 4 cm away at rt for 2 h. Conversion was determined by ¹H 400 MHz NMR by comparing the integration of the resonances of the alkene protons on the monomer (5.5-6.5 ppm) and the repeating O-CH₃ peak of the polymer (3.5-4.0 ppm).

Polymerisation of MA using alkyl halide co-initiators, ratio of MA **2.4: co-initiator: ZnTPP **2.1** was 200: 1: 1x10⁻⁵, reaction time 2h**

General procedure for polymerisation of MA **2.4** using ATRP initiators. Alkyl halide initiators used were benzyl bromide (2 μ L, 20.97 μ mol), ethyl 2-bromopropionate (3 μ L, 20.97 μ mol) and ethyl α -bromoisobutyrate (3 μ L, 20.97 μ mol).

Co-initiator	Light source¹	Conversion (%)²
2.6	Blue	10
2.6	Red	5
2.7	Blue	4
2.7	Red	4
2.8	Blue	9
2.8	Red	10

¹ Blue light (420-460 nm) and red light (580-640 nm) at 4 cm. ² Determined by 400 MHz ¹H NMR by integrating ratio of peaks at 3.6-4.0 ppm and 5.8-6.5 ppm.

7.2.5 General procedure for the polymerisation of MA **2.4**, changing the concentration of thiol **2.10**

To a vial, MA **2.4** (0.38 mL, 4.2 mmol), DMSO (277 μ L), 1-dodecanethiol and ZnTPP **2.1** (142 μ L of 1.475 mM solution in DMSO, 0.21 μ mol) was added, and the mixture was degassed with N₂ for 10 minutes. The reaction mixture was irradiated in blue light (5W, LED, 420-460 nm) from 4 cm away at rt for 2 h. Conversion was determined by ¹H 400 MHz NMR by comparing the integration of the resonances of the alkene

protons on the monomer (5.5-6.5 ppm) and the repeating O-CH₃ peak of the polymer (3.5-4.0 ppm).

The effect of changing thiol **2.10** concentration on the polymerisation of MA **2.4**

General procedure for the polymerisation of MA **2.4**, changing the concentration of thiol **2.10**. The amount of thiol used for the polymerisations was (5 μ L, 0.02 mmol), (10 μ L, 0.04 mmol), (25 μ L, 0.1 mmol) and (50 μ L, 0.2 mmol). Reaction mixture was irradiated with blue light (420-460 nm).

Run	2.4: 2.10: 2.1 ¹	Conversion (%) ²	<i>Mn</i> ³	<i>Mw</i> ³	\bar{D} ³
1	200: 0: 1x10 ⁻²	5	16k	21k	1.35
2	200: 1: 1x10 ⁻²	90	53k	96k	1.79
3	200: 2: 1x10 ⁻²	91	43k	61k	1.43
4	200: 5: 1x10 ⁻²	90	6.3k	13k	1.95
5	200: 10: 1x10 ⁻²	94	2.6k	3.8k	1.44

¹ Experimental procedure: Run 3 – 0.38 mL MA **2.4**, 0.28 mL DMSO, 0.14 mL ZnTPP **2.1** (1.475mM in DMSO), 5 μ L 1-dodecanethiol **2.10** degassed in vial for 10 minutes. Irradiated with blue light for 2h at rt. ² Determined by 400 MHz ¹H NMR by integrating ratio of peaks at 3.6-4 ppm and 5.8-6.5 ppm. ³ Molecular weight and polydispersity index were determined by GPC analysis (CHCl₃ as eluent) calibrated to poly (methyl methacrylate).

Conversion study on the effect of changing the concentration of thiol **2.10** on the polymerisation of MA **2.4** using ZnTPP **2.1** as a photocatalyst

General procedure for the polymerisation of MA **2.4** changing the concentration of thiol **2.10**. The amount of 1-dodecanethiol used was (5 μ L, 20.97 μ mol) and (25 μ L, 104.9 μ mol). The reaction mixture was irradiated with blue light (420 – 460 nm). The conversion of the polymerisation was determined every 30 minutes, with aliquots taken from the reaction and conversion was determined by ¹H 400 MHz NMR.

Run	Time (mins)	2.4: 2.10: 2.1	Conversion (%) ¹	<i>M_n</i> ²	<i>M_w</i>	Đ
1	30	200: 5: 1x10 ⁻²	88	5.9k	11k	1.95
2	30	200: 1: 1x10 ⁻²	49	35k	60k	1.70
3	60	200: 5: 1x10 ⁻²	94	6.3k	12k	2.12
4	60	200: 1: 1x10 ⁻²	77	35k	59k	1.64
5	90	200: 5: 1x10 ⁻²	95	6.7k	13k	2.08
6	90	200: 1: 1x10 ⁻²	87	35k	61k	1.70
7	120	200: 5: 1x10 ⁻²	97	6.3k	13k	1.95
8	120	200: 1: 1x10 ⁻²	96	36k	60k	1.67

¹ Determined by 400 MHz ¹H NMR by integrating ratio of peaks at 3.6-4 ppm and 5.8-6.5 ppm.² Molecular weight and polydispersity index were determined by GPC analysis (CHCl₃ as eluent) calibrated to poly (methyl methacrylate)

7.2.6 General procedure for the polymerisation of MA **2.4**, changing the concentration of ZnTPP **2.1**

To a vial, MA **2.4** (0.38 mL, 4.2 mmol), DMSO (277 μL), 1-dodecanethiol (5 μL, 0.02 mmol) and ZnTPP **2.1** was added, and the mixture was degassed with N₂ for 10 minutes. The reaction mixture was irradiated in blue light (5W, LED, 420-460 nm) from 4 cm away at rt for 2 h. Conversion was determined by ¹H 400 MHz NMR by comparing the integration of the resonances of the alkene protons on the monomer (5.5-6.5 ppm) and the repeating O-CH₃ peak of the polymer (3.5-4.0 ppm).

The effect of changing ZnTPP **2.1** concentration on the polymerisation of MA **2.4**.

General procedure for the polymerisation of MA **2.4**, changing the concentration of ZnTPP **2.1**. 0.14 mL ZnTPP solutions were studied (0.015 mM solution in DMSO, 0.0021 μmol), (0.148 mM solution in DMSO, 0.021 μmol), (1.475 mM solution in DMSO, 0.21 μmol), (2.950 mM solution in DMSO, 0.42 μmol), (7.375 mM solution in DMSO, 1.05 μmol), (14.75 mM, 2.10 μmol).

Run	24: 2.10: 2.1 ¹	Conversion (%) ²
1	200: 1: 0	0
2	200: 1: 1x10 ⁻⁴	25
3	200: 1: 1x10 ⁻³	37
4	200: 1: 1x10 ⁻²	90
5	200: 1: 2x10 ⁻²	95
6	200: 1: 5x10 ⁻²	96
7	200: 1: 0.1	95

¹Irradiated with blue light for 2 hours. ²Determined by 400 MHz ¹H NMR by integrating ratio of peaks at 3.6-4.0 ppm and 5.8-6.5 ppm

Conversion study on the effect of changing the concentration of ZnTPP 2.1 on the polymerisation of MA 2.4

General procedure for the polymerisation of MA 2.4, changing the concentration of ZnTPP 2.1. 0.14 mL ZnTPP solutions were studied (1.475 mM solution in DMSO, 0.21 μmol and 7.375 mM solution in DMSO, 1.05 μmol). The conversion of the polymerisation was determined every 30 minutes, with aliquots taken from the reaction and conversion was determined by ¹H 400 MHz NMR.

Run	Time (mins)	MA 2.4: thiol 2.10: ZnTPP 2.1	Conversion (%) ¹	Mn ²	Mw	Đ
1	30	200:1:5x10 ⁻²	65	33k	48k	1.65
2	30	200:1:1x10 ⁻²	49	35k	60k	1.70
3	60	200:1:5x10 ⁻²	86	33k	48k	1.62
4	60	200:1:1x10 ⁻²	77	35k	59k	1.64
5	90	200:1:5x10 ⁻²	93	34k	48k	1.67
6	90	200:1:1x10 ⁻²	87	35k	61k	1.70
7	120	200:1:5x10 ⁻²	98	34k	49k	1.67
8	120	200:1:1x10 ⁻²	90	36k	60k	1.67

¹Determined by 400 MHz ¹H NMR by integrating ratio of peaks at 3.6-4 ppm and 5.8-6.5 ppm. ²molecular weight and polydispersity index were determined by GPC analysis (CHCl₃ as eluent) calibrated to poly (methyl methacrylate)

7.2.7 General procedure for the polymerisation of MA **2.4**, studying the effect of changing the thiol

To a vial, MA **2.4** (0.38 mL, 4.2 mmol), DMSO (277 μ L), thiol (20.97 μ mol) and ZnTPP **2.1** (142 μ L of 7.375 mM solution in DMSO, 1.05 μ mol) was added, and the mixture was degassed with N₂ for 10 minutes. The reaction mixture was irradiated in red (5W, LED, 540-680 nm) or blue light (5W, LED, 420-460 nm) from 4 cm away at rt for 2 h. Conversion was determined by ¹H 400 MHz NMR by comparing the integration of the resonances of the alkene protons on the monomer (5.5-6.5 ppm) and the repeating O-CH₃ peak of the polymer (3.5-4.0 ppm).

Polymerisation of MA **2.4** with multifunctional thiols (**2.11** and **2.12**) vs 1-dodecanethiol **2.10** in blue and red light

General procedure for the polymerisation of MA **2.4**, studying the effect of changing the thiol. The thiols that were studied were 1-dodecaethiol (5 μ L, 20.97 μ mol), trimethylolpropane tris(3-mercaptopropionate) (8 μ L, 20.97 μ mol) and pentaerythritol tetrakis(3-mercaptopropionate) (10 μ L, 20.97 μ mol).

Run	Light source ¹	Thiol	Time (h)	Conversion (%) ²	<i>Mn</i> ³	<i>Mw</i> ³	<i>Đ</i> ³
1	Blue	-	16	0	-	-	-
2	Red	-	16	0	-	-	-
3	Blue	2.10	2	94	33k	45k	1.36
4	Red	2.10	2	80	33k	47k	1.41
5	Blue	2.11	2	96	24k	37k	1.52
6	Red	2.11	2	74	20k	33k	1.63
7	Blue	2.12	2	90	11k	17k	1.46
8	Red	2.12	2	86	12k	17k	1.46

Reaction conditions – MA **2.4**: thiol: ZnTPP **2.1** 200: 1: 5x10⁻², irradiated with light for 2 hours in DMSO ¹ Blue light (420-460 nm) and red light (580-640 nm) ² Determined by 400 MHz ¹H NMR by integrating ratio of peaks at 3.6-4 ppm and 5.8-6.5 ppm. ³ Molecular weight and polydispersity index were determined by GPC analysis (CHCl₃ as eluent) calibrated to poly (methyl methacrylate)

7.2.8 Polymerisation of MA **2.4**, using TPP **2.3** as a photocatalyst

To a vial, MA **2.4** (0.38 mL, 4.2 mmol), DMSO (277 μ L), 1-dodecanethiol (5 μ L, 20.97 μ mol) and TPP **2.3** (142 μ L of 1.475 mM solution in DMSO, 0.21 μ mol) was added, and the mixture was degassed with N₂ for 10 minutes. The reaction mixture was irradiated in red (5W, LED, 540-680 nm) or blue light (5W, LED, 420-460 nm) from 4 cm away at rt for 2 h. Conversion was determined by ¹H 400 MHz NMR by comparing the integration of the resonances of the alkene protons on the monomer (5.5-6.5 ppm) and the repeating O-CH₃ peak of the polymer (3.5-4.0 ppm).

Run	Photocatalyst	Light source ¹	Conversion (%) ¹
1	TPP 2.3	Blue	56
2	TPP 2.3	Red	43

Reaction conditions – MA **2.5**: thiol **2.10**: ZnTPP **2.1** or TPP **2.3** = 200: 1: 1x10⁻², irradiated with light for 2 hours in DMSO at 4 cm. ¹ Blue light (420-460 nm) and red light (580-640 nm) ²Determined by 400 MHz ¹H NMR by integrating ratio of peaks at 3.6-4.0 ppm and 5.8-6.5 ppm.

7.2.9 General procedure for 3D printing

A mixture of 15g of a 50:50 w: w UDMA **2.5**/ TEGDMA **2.6** mixture was used for 3D printing. To this solution, thiol and porphyrin was added, and the solution stirred in darkness for 10 minutes. The 3D prints were performed at room temperature using the photocentric liquid crystal precision printer. The light exposure time per layer was 300,000 ms.

Print B – General procedure for 3D printing, using trimethylolpropane tris(3-mercaptopropionate) (0.42 g, 1.1 mmol) and ZnTPP **2.1** (7 mg, 0.01 mmol).

Print C - General procedure for 3D printing, using pentaerythritol tetrakis(3-mercaptopropionate) (0.51 g, 1.1 mmol) and ZnTPP **2.1** (7 mg, 0.01 mmol).

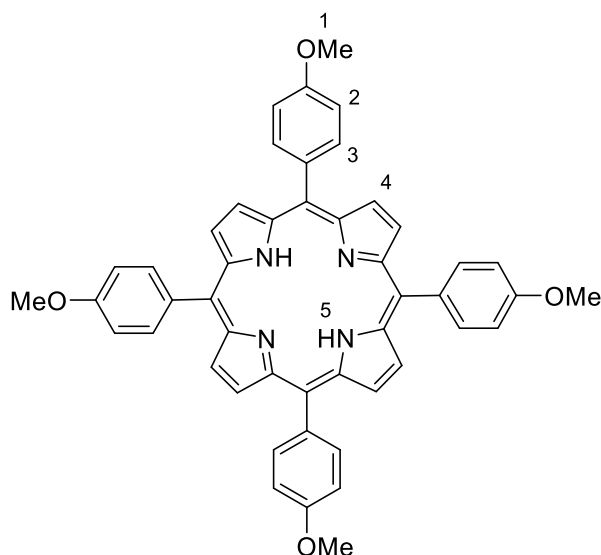
Print D - General procedure for 3D printing, using pentaerythritol tetrakis(3-mercaptopropionate) (1.02 g, 2.2 mmol) and ZnTPP **2.1** (35 mg, 0.05 mmol).

Print E - General procedure for 3D printing, using pentaerythritol tetrakis(3-mercaptopropionate) (1.02 g, 2.2 mmol) and ZnTPP **2.1** (35 mg, 0.05 mmol), 200,000 ms exposure time per layer.

Print F - General procedure for 3D printing, using pentaerythritol tetrakis(3-mercaptopropionate) (1.02 g, 2.2 mmol) and TPP **2.3** (31 mg, 0.05 mmol).

7.3 Chapter 3

7.3.1 Synthesis of 5,10,15,20-(4-methoxy)tetraphenylporphyrin **3.4**¹³⁹

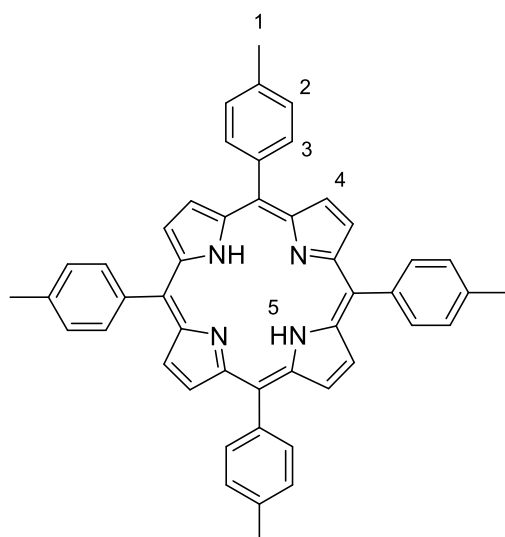


A solution of pyrrole (1.0 mL, 14 mmol) and p-anisaldehyde (2.02 mL, 14 mmol, 1 equivalent) was added to propanoic acid (50 mL). This solution was heated at reflux for 45 minutes at 150 °C, then cooled to room temperature. The solid formed was filtered, then washed with cold methanol (20 mL). The solid was washed with hot water (20 mL) and dried, yielding purple crystals of

5,10,15,20-(4-methoxy)tetraphenylporphyrin **3.4** (0.16 g, 6.4%). Spectroscopic data matched that reported¹⁷⁴; ¹H NMR (CDCl₃, 400MHz) δ: 8.86 (s, 8H, H⁴), 8.13 (d, J=8.0Hz, 8H, H³), 7.28 (m, 8H, H²), 4.10 (s, 12H, H¹), -2.75 (s, 2H, H⁵); ¹³C NMR (CDCl₃, 125 MHz) δ: 159.3, 136.6, 134.6, 131.2, 119.7, 112.2, 55.5; MS (ESI): m/z (C₄₈H₃₈N₄O₄) found: 735.8 (MH⁺). UV-Vis(DMSO): 423 (16600), 595 (820), 556 (610), 519 (270).

7.3.2 5,10,15,20-(4-Methyl)tetraphenylporphyrin **3.3**¹³⁹

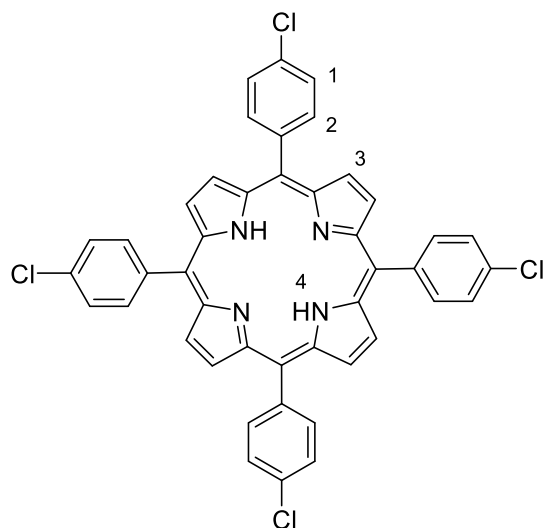
A solution of pyrrole (1.0 mL, 14 mmol) and p-tolualdehyde (1.73 mL, 14 mmol, 1 equivalent) was added to propanoic acid (50 mL). This solution was heated at reflux for 45 minutes at 150 °C, then cooled to room temperature. The solid formed was filtered, then washed with cold methanol (20 mL). The solid was washed with hot water (20 mL) and dried, yielding purple crystals of 5,10,15,20-(4-



515 (70).

methyl)tetraphenylporphyrin **3.3** (0.55 g, 23%). Spectroscopic data matched that reported¹⁷⁵; ¹H NMR (CDCl₃, 400MHz): δ 8.85 (s, 8H, H⁴), 8.09 (d, J = 7.5Hz, 8H, H³), 7.55 (d, J = 7.5Hz, 8H, H²), 2.65 (s, 12H, H¹), -2.77 (s, 2H, H⁵); ¹³C NMR (CDCl₃, 125MHz): δ 139.5, 137.4, 134.7, 131.4, 127.5, 120.2, 21.7; MS (ESI): m/z (C₄₈H₃₈N₄) found: 671.5 (MH⁺). UV-Vis(DMSO): 420 (9500), 591 (270), 551 (140),

7.3.3 5,10,15,20-(4-Chloro)tetraphenylporphyrin **3.2**¹³⁹



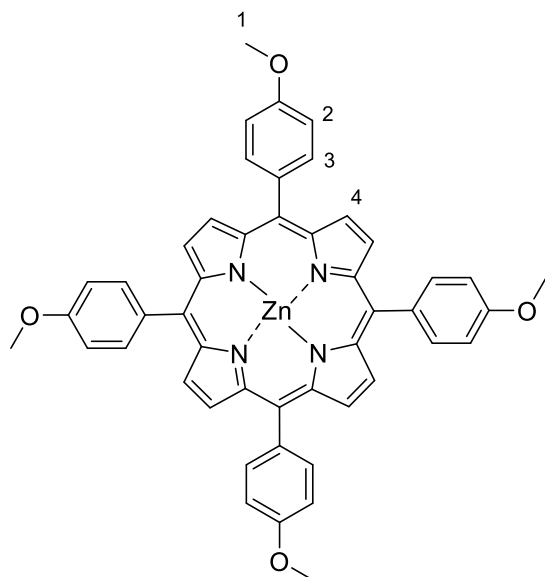
5,10,15,20-(4-chloro)tetraphenylporphyrin **3.2** (0.11 g, 4%). Spectroscopic data matched that reported¹⁷⁶; ¹H NMR (CDCl₃, 400MHz): δ 8.84 (s, 8H, H³), 8.13 (d, J = 7.5Hz, 8H, H²), 7.75 (d, J = 8.0 Hz, 8H, H¹), -2.86 (s, 2H, H⁴); ¹³C NMR (CDCl₃, 125MHz): δ 140.3, 135.5, 134.4, 131.5, 127.0, 119.1; MS (ESI): m/z (C₄₄H₂₆Cl₄N₄) found: 753.6 (MH⁺). UV-Vis(DMSO): 418 (15700), 590 (610), 549 (200), 514 (140).

7.3.4 General procedure for metalation of porphyrins with zinc¹⁷³

Porphyrin (0.16 mmol) was dissolved in chloroform (20 mL). A saturated solution of Zn(OAc)₂ (0.05 g, 0.23 mmol, 1.4 equivalent) in MeOH (5 mL) was added. The solution was stirred for 1 h after which the reaction mixture was washed with water (2 x 20 mL) and brine (2 x 20 mL). The organic layer was then dried with MgSO₄, the

mixture was filtered, and solvent removed in *vacuo*, yielding a purple solid (0.11 g, 90%).¹⁷³

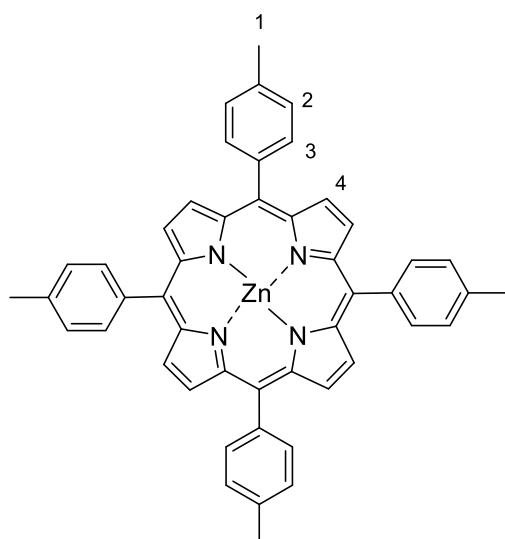
7.3.5 5,10,15,20-(4-Methoxy) zinc tetraphenylporphyrin **3.7**



General procedure for the metalation of porphyrins with zinc, using **3.4** (0.10g, 0.16mmol) yielding a purple solid (0.13 g, 85%). Spectroscopic data matched that reported¹⁷⁷; ¹H NMR (CDCl₃, 400MHz) δ 8.97 (s, 8H, H⁴), 8.13 (d, J = 8.5 Hz, 8H, H³), 7.29 (d, J = 8.5 Hz, 8H, H²), 4.11 (s, 12H, H¹); ¹³C NMR (CDCl₃, 125MHz): δ 153.7, 136.8, 134.1, 131.2, 119.7, 113.1, 56.3 MS (ESI): m/z (C₄₈H₃₆N₄O₄Zn⁶⁴) found: 797.5 (MH⁺).

UV-Vis(DMSO): 431 (17000), 563 (540), 605 (410).

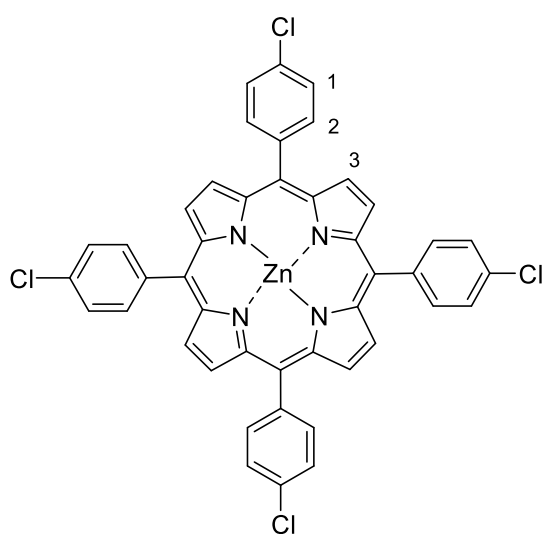
7.3.6 5,10,15,20-(4-Methyl) zinc tetraphenylporphyrin **3.6**



General procedure for the metalation of porphyrins with zinc, using **3.3** (0.10g, 0.16mmol) yielding a purple solid (0.12 g, 90%). Spectroscopic data matched that reported¹⁷⁷; ¹H NMR (CDCl₃, 400MHz) δ 8.96 (s, 8H, H⁴), 8.11 (d, J = 8.0 Hz, 8H, H³), 7.56 (d, J = 8.0 Hz, 8H, H²), 2.71 (s, 12H, H¹); ¹³C NMR (CDCl₃, 125MHz): δ 139.9, 137.8, 134.3, 131.1, 126.7, 120.8, 22.4 (ESI): m/z (C₄₈H₃₆N₄Zn⁶⁴) found: 733.4

(MH⁺). UV-Vis(DMSO): 429 (19000), 560 (1200), 600 (680).

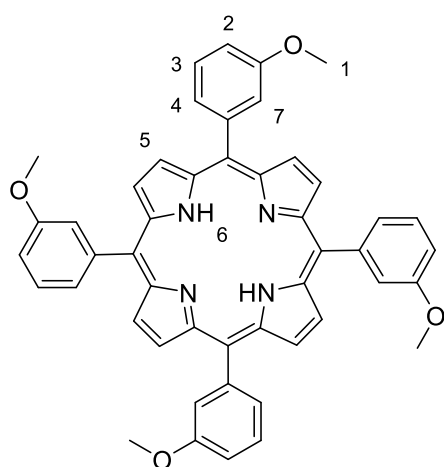
7.3.7 5,10,15,20-(4-Chloro) zinc tetraphenylporphyrin **3.5**



General procedure for the metalation of porphyrins with zinc, using **3.2** (0.10g, 0.16mmol) yielding a purple solid (0.12 g, 91%). Spectroscopic data matched that reported¹⁷⁸; ¹H NMR (CDCl₃, 400MHz) δ 8.95 (s, 8H, H³), 8.14 (d, J = 8.0Hz, 8H, H²), 7.74 (d, J = 8.0Hz, 8H, H¹); ¹³C NMR (CDCl₃, 125MHz): δ 141.3, 136.3, 133.6, 132.2, 126.3, 118.3 (ESI): m/z (C₄₄H₂₄Cl₄N₄Zn⁶⁴) 813.4 (MH⁺). UV-

Vis(DMSO): 429 (19200), 560 (1770), 600 (480).

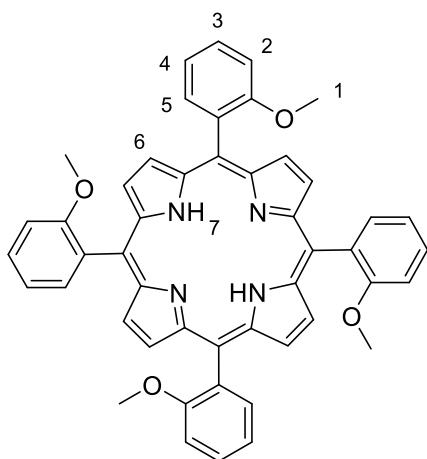
7.3.8 Synthesis of 5,10,15,20-tetrakis(3-methoxyphenyl)porphyrin **3.9**¹⁷⁹



Pyrrole (0.35 mL, 0.34 g, 5.0 mmol) and 3-methoxy benzaldehyde (0.61 mL, 5.0 mmol, 1 equivalent) were dissolved in DCM (500 mL). Boron trifluoride diethyl etherate (6 μL, 0.05 mmol) and trifluoroacetic acid (0.35 mL, 4.6 mmol) were added to the mixture and stirred at rt for 2h. Chloranil (1.01 g, 41, mmol) was added to the reaction mixture and heated at reflux for 4 h. The solvent was removed in *vacuo*, and the

mixture purified via column chromatography (CH₂Cl₂), yielding a purple solid (24%, 0.22 g). Spectroscopic data matched that reported¹⁷⁹; ¹H NMR (CDCl₃, 400MHz) δ 8.91(s, 8H, H⁵), 7.85 – 7.35 (m, 16H, H^{2,3,4,7}), 4.01 (s, 12H, H¹), -2.77 (s, 2H, H⁶). ¹³C NMR (CDCl₃, 125 MHz) δ: 158.3, 135.5, 131.1, 129.6, 129.1, 121.7, 116.7, 111.5, 53.9. MS (ESI): m/z (C₄₈H₃₈N₄O₄) found: 797 (MH⁺). UV-Vis(DMSO): 418 (15100), 514 (750), 545 (270), 591 (200).

7.3.9 Synthesis of 5,10,15,20-tetrakis(2-methoxyphenyl)porphyrin



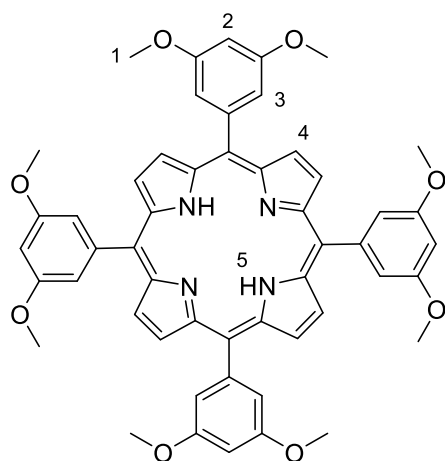
3.8¹⁸⁰

Pyrrole (0.35 mL, 0.34 g, 5.0 mmol) and 2-methoxy benzaldehyde (0.61 mL, 5.0 mmol, 1 equivalent) were dissolved in DCM (500 mL). Boron trifluoride diethyl etherate (6 μ L, 0.05 mmol) and trifluoroacetic acid (0.35 mL, 4.6 mmol) were added to the mixture and stirred at rt for 2h. Chloranil (1.01 g, 4.1 mmol) was added to the reaction mixture and heated at reflux for 4 h. The

solvent was removed in *vacuo*, and the mixture purified via column chromatography (CH_2Cl_2), yielding a purple solid (28%, 0.26 g). Spectroscopic data matched that reported¹⁸⁰; $^1\text{H NMR}$ (400MHz, CDCl_3) δ : 8.74 (s, 8H, H^6), 7.73—7.78 (m, 8H, $\text{H}^{2,3,4,5}$), 7.32—7.36 (m, 8H, $\text{H}^{2,3,4,5}$), 3.55—3.61 (m, 12H, H^1), -2.61 (s, 2H, H^7). $^{13}\text{C NMR}$ (CDCl_3 , 125 MHz) δ : 159.7, 135.9, 131.5, 130.3, 129.6, 119.8, 115.5, 110.9, 55.7 MS (ESI): m/z ($\text{C}_{48}\text{H}_{38}\text{N}_4\text{O}_4$) found: 797 (MH^+). UV-Vis(DMSO): 419 (22700), 514 (1900), 548 (4100), 590 (340).

7.3.10 Synthesis of 5,10,15,20-tetrakis(3,5-dimethoxyphenyl)porphyrin

3.10¹⁸¹



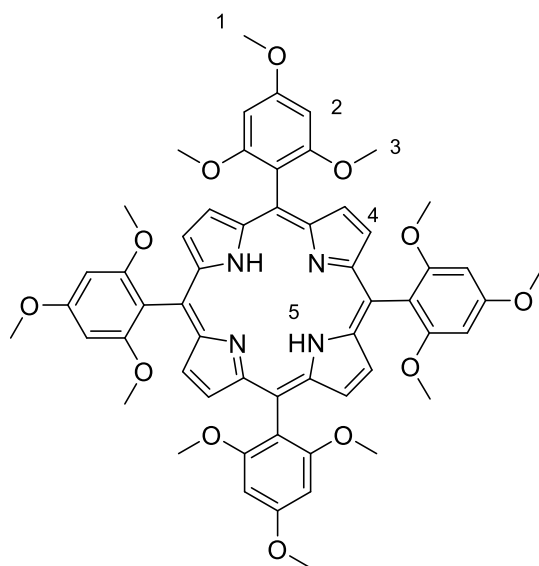
Pyrrole (0.35 mL, 0.34 g, 5.0 mmol) and 3,5 dimethoxy benzaldehyde (0.82 g, 5.0 mmol, 1 equivalent) in DCM (500 mL) and degassed, then stirred with boron trifluoride dietherate (6 μ L, 0.05 mmol) and trifluoroacetic acid (0.35 mL, 4.6 mmol) for 2h. Then chloranil (1.01 g, 4.1 mmol) was added and heated at reflux for 4 hours, which is purified by column chromatography to afford purple crystals (0.33 g,

31%). Spectroscopic data matched that reported¹⁸¹; $^1\text{H NMR}$ (CDCl_3 , 400 MHz): δ 8.93 (s, 8H, H^4), 7.40 (s, 8H, H^3), 6.90 (s, 4H, H^2), 3.96 (s, 24H, H^1), -2.83 (s, 2H, H^5). $^{13}\text{C NMR}$ (CDCl_3 , 125 MHz): δ 159.2, 144.3, 119.8, 130.1, 114.1, 55.9. MS (ESI):

m/z (C₅₂H₄₆N₄O₈) found: [MH⁺] 855. UV-Vis(DMSO): 421 (3200), 515 (140), 547 (70), 589 (70).

7.3.11 Synthesis of 5,10,15,20-tetrakis(2,4,6-trimethoxyphenyl)

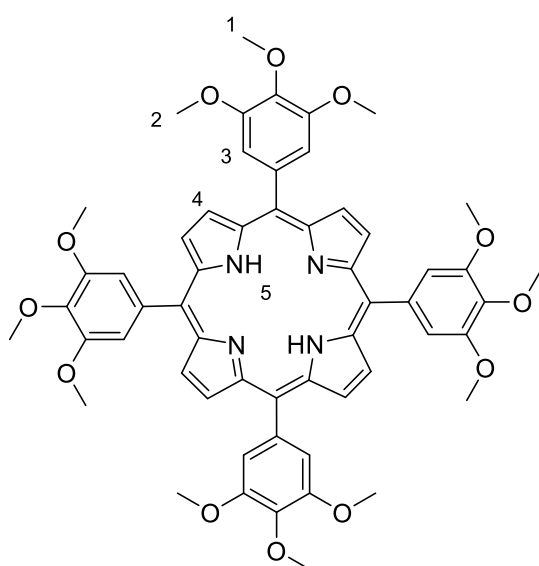
porphyrin **3.11**¹⁸²



Pyrrole (0.35 mL, 0.34 g, 5.0 mmol) and 2,4,6 dimethoxy benzaldehyde (0.96 g, 5.0 mmol, 1 equivalent) in DCM (500 mL) and degassed, then stirred with boron trifluoride dietherate (6 μ L, 0.05 mmol) and trifluoroacetic acid (0.35 mL, 4.6 mmol) for 2h. Then DDQ (0.93 g, 4.1 mmol) was added and heated at reflux for 4 hours, which is purified by column chromatography to afford purple crystals (0.39 g, 32%). Spectroscopic data

matched that reported¹⁸²; ¹HNMR (400MHz, CDCl₃): δ 8.72 (s, 8H, H⁴), 6.56 (s, 8H, H²), 4.12 (s, 12H, H¹), 3.47 (s, 24H, H³), -2.50 (s, 2H, H⁵). MS (ESI): m/z (C₅₆H₅₄N₄O₁₂) found: 976 (MH⁺). UV-Vis(DMSO): 421 (2450), 514 (140), 546 (70), 590 (70).

7.3.12 Synthesis of 5,10,15,20-tetrakis(3,4,5-trimethoxyphenyl)porphyrin **3.12**¹⁸³



Pyrrole (0.35 mL, 0.34 g, 5.0 mmol) and 3,4,5 dimethoxy benzaldehyde (0.96 g, 5.0 mmol, 1 equivalent) in DCM (500 mL) and degassed, then stirred with boron trifluoride dietherate (6 μ L, 0.05 mmol) and trifluoroacetic acid (0.35 mL, 4.6 mmol) for 2h. Then chloranil (1.01 g, 4.1 mmol) was added and heated at reflux for 4 hours, which is purified by column chromatography to afford purple crystals (0.29 g, 24%). Spectroscopic data matched

that reported¹⁸³; ¹H NMR (CDCl₃, 400 MHz): δ 8.95 (s, 8H, H⁴), 7.47 (s, 8H, H³), 4.18 (s, 12H, H¹), 3.98 (s, 24H, H²), -2.75 (s, 2H, H⁵). ¹³C NMR (125 MHz, CDCl₃): δ = 151.5, 138.0, 137.6, 120.1, 112.7, 61.5, 56.6. MS (ESI): m/z (C₅₆H₅₄N₄O₁₂) found: 974 (M - H⁺). UV-Vis(DMSO): 423 (9400), 516 (610), 551 (220), 591 (200)

7.3.13 General procedure for polymerisation of MA **2.4** using modified porphyrin variants

To a vial, MA **2.4** (0.38 mL, 4.2 mmol), DMSO (277 μ L), 1-dodecaethiol (5 μ L, 0.02 mmol) and porphyrin (142 μ L of 1.475 mM solution in DMSO, 2.0 x 10⁻⁴ mol) was added to a vial, and the mixture was degassed with N₂ for 10 minutes. The reaction mixture was irradiated in red light (5W, LED, 580-640 nm) or blue light (5W, LED, 420-460 nm) from 4 cm away at rt for 2 h. Conversion was determined by ¹H 400 MHz NMR by comparing the integration of the resonances of the alkene protons on the monomer (5.5-6.5 ppm) and the repeating O-CH₃ peak of the polymer (3.5-4.0 ppm).

Polymerisation of MA **2.4 using para modified porphyrin variants **3.2** – **3.4****

General procedure for polymerisation of MA **2.4** using modified porphyrin variants, using porphyrins **3.2**, **3.3** and **3.4**.

Run	Porphyrin	Light source ¹	Conversion (%) ²
1	4-Cl 3.2	Blue	5
2	4-Cl 3.2	Red	0
3	H 2.3	Blue	56
4	H 2.3	Red	43
5	4-Me 3.3	Blue	59
6	4-Me 3.3	Red	45
7	4-OMe 3.4	Blue	71
8	4-OMe 3.4	Red	60

Reaction conditions: MA **2.4**: thiol **2.10**: porphyrin – 200: 1: 1x10⁻², degassed and irradiated with light for 2 h from 4 cm away. ¹ Blue light (420-460 nm) and red light (580-640 nm) ²Determined by 400 MHz ¹H NMR by integrating ratio of peaks at 3.6-4.0 ppm and 5.8-6.5 ppm

Conversion study of polymerisation of MA **2.4** using TPP **2.3** and 4-MeO-TPP **3.4**

General procedure for polymerisation of MA **2.4** using modified porphyrin variants. Polymerisations were performed in blue light (420 – 460 nm) and aliquots were taken from the reaction vessel every 30 minutes and conversion was determined by ¹H 400 MHz NMR.

Run	Porphyrin ¹	Time (min)	Conversion (%) ²	<i>Mn</i> ³	<i>Mw</i> ³	<i>Đ</i> ³
1	2.3	30	25	32k	44k	1.60
2	3.4	30	40	34k	46k	1.70
3	2.3	60	30	33k	45k	1.61
4	3.4	60	53	34k	47k	1.71
5	2.3	90	42	34k	45k	1.58
6	3.4	90	60	35k	47k	1.63
7	2.3	120	50	34k	45k	1.60
8	3.4	120	71	36k	48k	1.58

Reaction conditions: MA **2.4**: thiol **2.10**: porphyrin – 200: 1: 1x10⁻², degassed and irradiated with light for 2 h from 4 cm away. ¹Polymerisation in blue light (420-460 nm) ²Determined by 400 MHz ¹H NMR by integrating ratio of peaks at 3.6-4.0 ppm and 5.8-6.5 ppm. ³ molecular weight and polydispersity index were determined by GPC analysis (CHCl₃ as eluent) calibrated to poly (methyl methacrylate)

Polymerisations of MA 2.4 using modified zinc porphyrins 2.1 and 3.5 – 3.7 as photocatalysts

General procedure for polymerisation of MA 2.4 using modified porphyrin variants, using porphyrins 3.5, 3.6 and 3.7.

Run	Porphyrin	Light source ¹	Conversion (%) ²
1	4-Cl 3.5	Blue	75 (5)
2	4-Cl 3.5	Red	68 (0)
3	H 2.1	Blue	90 (56)
4	H 2.1	Red	74 (43)
5	4-Me 3.6	Blue	71 (59)
6	4-Me 3.6	Red	42 (45)
7	4-OMe 3.7	Blue	92 (71)
8	4-OMe 3.7	Red	85 (66)

Reaction conditions: MA 2.4: thiol 2.10: porphyrin – 200: 1: 1×10^{-2} , degassed and irradiated with light for 2 h from 4 cm away. ¹Blue light (420-460 nm) and red light (580-620 nm) ²Determined by 400 MHz ¹H NMR by integrating ratio of peaks at 3.6-4.0 ppm and 5.8-6.5 ppm. The numbers in parentheses are the conversions when using the non-metalated analogues 3.2 – 3.4 and 2.3

Conversion study of the polymerisation of MA 2.4 using ZnTPP 2.1 and 4-OMe-ZnTPP 3.7 as photocatalysts.

General procedure for polymerisation of MA 2.4 using modified porphyrin variants. Polymerisations were performed in blue light (420 – 460 nm) using porphyrins 2.1 and 3.7, and aliquots were taken from the reaction vessel every 30 minutes and conversion was determined by ¹H 400 MHz NMR,

Run	Time (mins)	Porphyrin	Conversion (%) ¹	<i>Mn</i> ²	<i>Mw</i>	Đ
1	30	3.7	63	37k	62k	1.71
2	30	2.1	49	35k	60k	1.70
3	60	3.7	85	37k	61k	1.68
4	60	2.1	77	35k	59k	1.64
5	90	3.7	89	38k	62k	1.68
6	90	2.1	87	35k	61k	1.70
7	120	3.7	94	38k	62k	1.65
8	120	2.1	90	36k	60k	1.67

Reaction conditions: MA **2.4**: thiol **2.10**: porphyrin – 200: 1: 1×10^{-2} , degassed and irradiated with blue light for 2 h from 4 cm away. ¹Determined by 400 MHz ¹H NMR by integrating ratio of peaks at 3.6-4.0 ppm and 5.8-6.5 ppm. ² molecular weight and polydispersity index were determined by GPC analysis (CHCl₃ as eluent) calibrated to poly (methyl methacrylate)

Polymerisation data using methoxy modified porphyrins **3.4** and **3.8** – **3.9** as photocatalysts in the polymerisation of MA **2.4**.

General procedure for polymerisation of MA **2.4** using modified porphyrin variants, using porphyrin **3.4**, **3.8** and **3.9**.

Run	Porphyrin	Light source ¹	Conversion (%) ²
1	4-OMe 3.4	Blue	71
2	4-OMe 3.4	Red	60
3	2-OMe 3.8	Blue	40
4	2-OMe 3.8	Red	32
5	3-OMe 3.9	Blue	51
6	3-OMe 3.9	Red	42

Reaction conditions: MA **2.4**: thiol **2.10**: porphyrin – 200: 1: 1×10^{-2} , degassed and irradiated with light for 2 h from 4 cm away. ¹Blue light (420-460 nm) and red light (580-640 nm) ²Determined by 400 MHz ¹H NMR by integrating ratio of peaks at 3.6-4.0 ppm and 5.8-6.5 ppm

Polymerisation of MA 2.4 using -di and tri-substituted porphyrins 3.11-3.13 as photocatalysts, compared to TPP 2.3.

General procedure for polymerisation of MA 2.4 using modified porphyrin variants.

Run	Porphyrin	Light source ¹	Conversion (%) ²
1	3.4	Blue	71
2	3.4	Red	60
3	3.11	Blue	40
4	3.11	Red	29
5	3.12	Blue	42
6	3.12	Red	33
7	3.13	Blue	51
8	3.13	Red	32

Reaction conditions: MA 2.4: thiol 2.10: porphyrin – 200: 1: 1×10^{-2} , degassed and irradiated with light for 2 h from 4 cm away. ¹Blue light (420-460 nm) and red light (580-640 nm). ²Determined by 400 MHz ¹H NMR by integrating ratio of peaks at 3.6-4.0 ppm and 5.8-6.5 ppm

7.3.14 General procedure for 3D printing in chapter 3

A mixture of 15g of a 50:50 w: w UDMA 2.5/ TEGDMA 2.6 mixture was used for 3D printing. To this solution, pentaerythritol tetrakis(3-mercaptopropionate) 2.12 (1.02 g, 2.2 mmol) and porphyrin (0.05 mmol) was added, and the solution stirred in darkness for 10 minutes. The 3D prints were performed at room temperature using the photocentric liquid crystal precision printer. The light exposure time per layer was 300,000 ms.

Print G – General procedure for 3D printing in chapter, using 4-Cl-TPP 3.2 (38 mg, 0.05 mmol),

Print H - General procedure for 3D printing in chapter, using 4-Me-TPP 3.3 (34 mg, 0.05 mmol),

Print I - General procedure for 3D printing in chapter, using 4-OMe-TPP 3.4 (37 mg, 0.05 mmol),

Print J - General procedure for 3D printing in chapter, using 4-Cl-ZnTPP 3.5 (41 mg, 0.05 mmol),

Print K – General procedure for 3D printing in chapter, using 4-Me-ZnTPP (37 mg, 0.05 mmol),

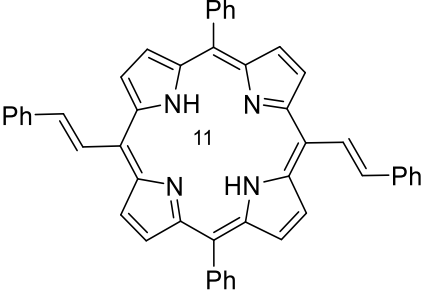
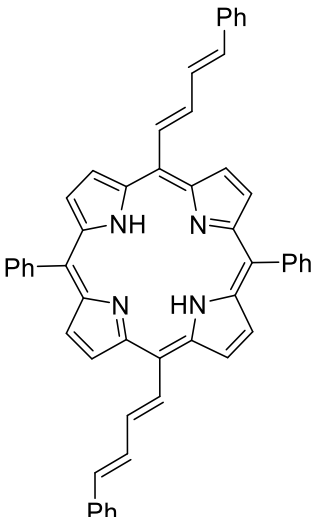
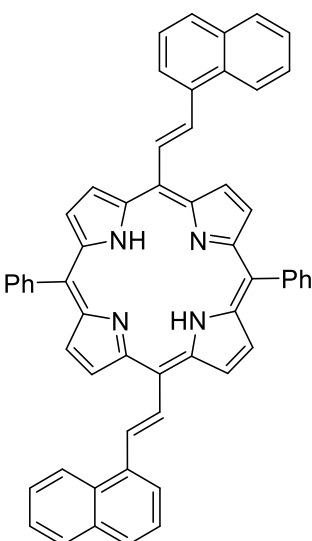
Print L - General procedure for 3D printing in chapter, using 4-OMe-ZnTPP (40 mg, 0.05 mmol),

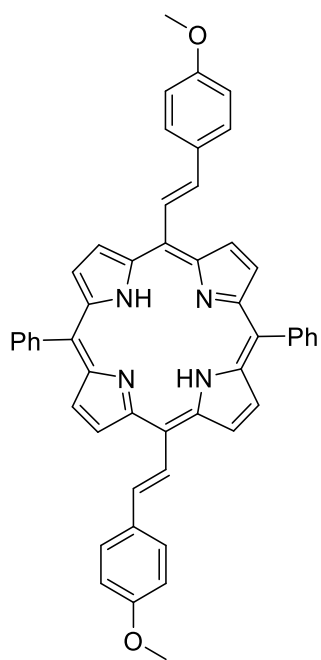
Print M - General procedure for 3D printing in chapter, using 2-OMe-TPP **3.8** (37 mg, 0.05 mmol),

Print N - General procedure for 3D printing in chapter, using 3-OMe-TPP **3.9** (37 mg, 0.05 mmol).

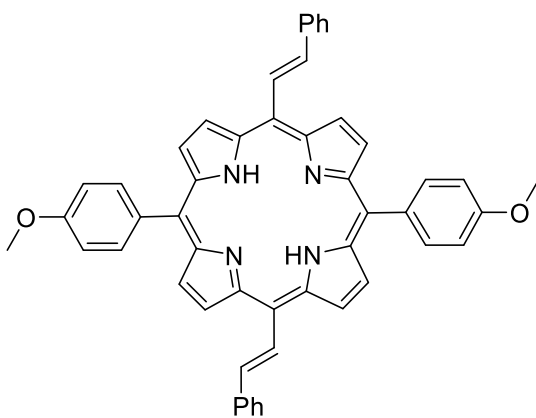
7.4 Chapter 4

Data for alkenyl substituted porphyrins:

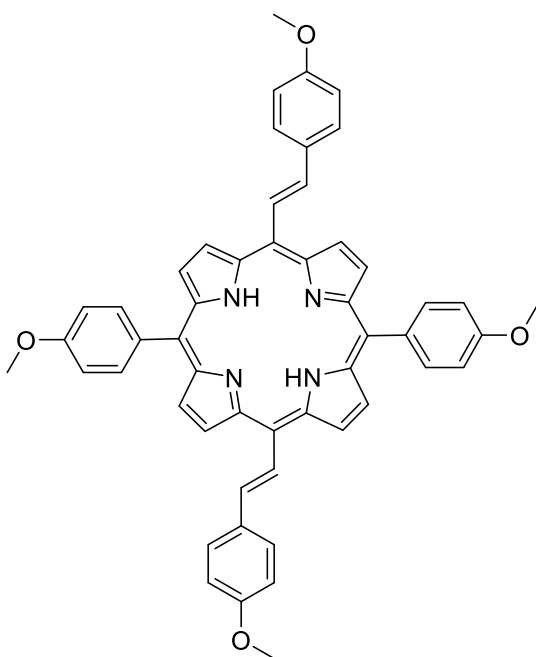
Porphyrin	UV-Vis (DMSO)	Yield	MS (ESI)
	425 (27500), 523 (4000), 577 (3000), 660 (1220)	8 mg, 33%	m/z (C ₄₈ H ₃₄ N ₄) found: 667.3 (M + H ⁺)
	439 (13700), 528 (1100), 589 (1300), 678 (610)	6 mg, 24%	m/z (C ₅₂ H ₃₈ N ₄) found: 719.3 (M + H ⁺), 591.3
	431 (590), 526 (100), 583 (100), 670 (90)	9 mg, 35%	m/z (C ₅₆ H ₃₈ N ₄) found: 767.5 (M + H ⁺), 615.3



443 (23900), 7 mg, m/z
 527 (3800), 26% (C₅₀H₃₈N₄O₂)
 596 (1800), found: 727.3
 684 (1300) (M - H⁺)

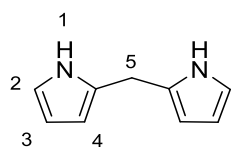


435 (25000), 9 mg, m/z
 535 (2500), 33% (C₅₀H₃₈N₄O₂)
 589 (4800), found: 727.3
 680 (2400) (M - H⁺)



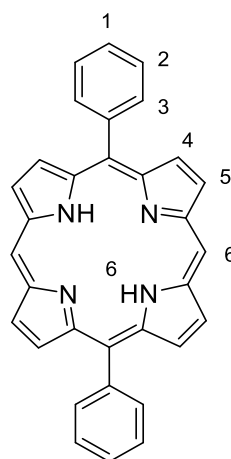
444 (26000), 6 mg, m/z
 608 (7300), 22% (C₅₂H₄₂N₄O₄)
 696 (3400) found: 787.5 (M - H⁺).

7.4.1 Synthesis of dipyrromethane **4.1**¹⁸⁴



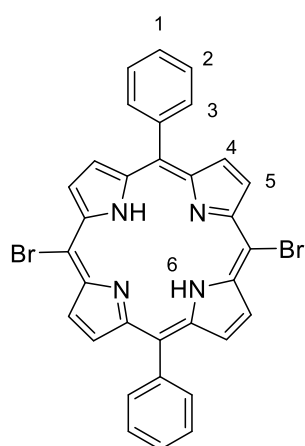
Paraformaldehyde (1 g, 30 mmol) was dissolved in pyrrole (48g, 0.72 mol). This solution was degassed for 10 minutes, after which InCl_3 (0.72 g, 3.3 mmol) was added, and the reaction was stirred at 55 °C for 3h. This mixture was left to cool to rt, and then NaOH (1.3g, 33mmol) was added and stirred overnight. The solvent was removed, and the reaction mixture purified *via* column chromatography (petroleum ether/ethyl acetate, 9:1). A colourless solid was produced (1.70 g, 70%). Spectroscopic data matched that reported¹⁸⁴; ^1H NMR (CDCl_3 , 400 MHz): δ 7.90 (s, 2H, H^1), 6.69 (td, $J = 2.9, 1.6$ Hz, 2H, H^2), 6.16 (q, $J = 2.9$ Hz, 2H, H^3), 6.06-6.00 (m, 2H, H^4), 4.00 (s, 2H, H^5). ^{13}C NMR (125 MHz, CDCl_3): $\delta = 129.2, 117.5, 108.4, 106.6, 26.4$. MS (ESI): m/z ($\text{C}_9\text{H}_{10}\text{N}_2$) found: 147.2 (MH^+),

7.4.2 Synthesis of 5,15-diphenylporphyrin **4.2**¹⁸⁵



Dipyrromethane **4.1** (392 mg, 2.70 mmol) and benzaldehyde (0.28mL, 0.29 g, 2.7 mmol, 1 equivalent) were dissolved in DCM (500 mL). The solution was degassed, trifluoroacetic acid (TFA) (0.12 mL, 1.6 mmol) was added and stirred at rt for 4h. 2,3-dichloro-5,5-dicyano-1,4-benzoquinone (DDQ) (0.74 g, 3.2 mmol) was added at rt and stirred for 1h. Triethylamine (4 mL, 28.7 mmol) was added, solvent removed and purified by column chromatography (DCM) to give 5,15-diphenylporphyrin **4.2** as a white solid (0.62 g, 74%). Spectroscopic data matched that reported¹⁸⁵; ^1H NMR (CDCl_3 , 400 MHz): δ 10.32 (s, 2H, H^6), 9.40 (d, $J = 4.5$ Hz, 4H, H^4), 9.10 (d, $J = 4.5$ Hz, 4H, H^5), 8.33 – 8.26 (m, 4H, H^3), 7.85-7.80 (m, 6H, $\text{H}^{1,2}$), -3.10 (s, 2H, H^6). ^{13}C NMR (125 MHz, CDCl_3): δ 147.3, 145.4, 141.5, 135.0, 131.8, 131.2, 127.9, 127.1, 119.3, 105.4. MS (ESI): m/z ($\text{C}_{32}\text{H}_{22}\text{N}_4$) found: 463.3 (MH^+),

7.4.3 5,15-Dibromo-10,20-diphenylporphyrin **4.3**¹⁸⁶

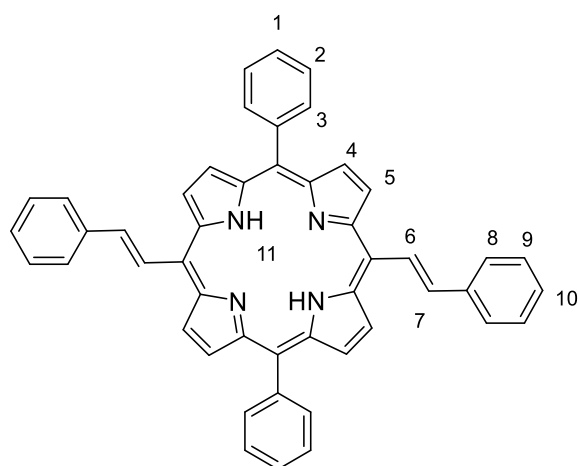


5,15-diphenylporphyrin **4.2** (80 mg, 0.17 mmol) was dissolved in 50 mL CHCl_3 . To this solution, pyridine (0.5 mL, 6.2 mmol) and *N*-bromosuccinimide (NBS) (77 mg, 0.43 mmol) were added and stirred for 30 minutes. Acetone (5 mL) was added to quench the reaction and the solvent removed. Mixture separated by column chromatography (DCM/petroleum ether, 1:1) to give purple solid (0.11 g, 91%). Spectroscopic data matched that reported²⁶; ^1H NMR (400 MHz, CDCl_3): 9.63 (d, $J = 4.3$ Hz, 4H, H^4), 8.84 (d, $J = 4.3$ Hz, 4H, H^5), 8.17-8.15 (m, 4H, H^3), 7.82 – 7.75 (m, 6H, $\text{H}^{1,2}$), -2.73 (s, 2H, H^6). ^{13}C NMR (125 MHz, CDCl_3): δ 141.4, 134.5, 129.5, 128.1, 127.9, 126.8, 110.0. MS (ESI): m/z ($\text{C}_{32}\text{H}_{20}\text{Br}_2^{79}\text{N}_4$) found: 619 (MH^+),

7.4.4 General procedure for synthesis of alkenyl-substituted porphyrins

Dibromoporphyrin **4.3** (24 mg, 36 μmol), $\text{Pd}(\text{OAc})_2$ (3 mg, 0.01 mmol), JohnPhos (8.6 mg, 0.03 mmol) and K_2CO_3 (13 mg, 0.09 mmol) were dried under vacuum in a Schlenk tube. Then dry DMF (5 mL), dry toluene (10 mL) and vinyl reagent (2.4 mmol) were added. This solution was degassed *via* freeze-thaw and heated overnight at 105°C. The mixture was then cooled to rt and washed with water. The reaction mixture was dried with MgSO_4 , filtered, the solvent removed and purified via column chromatography.

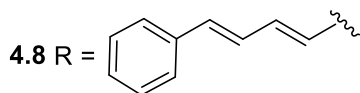
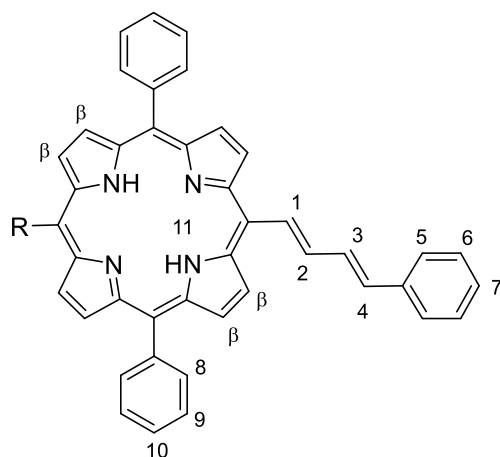
7.4.5 5,15-Diphenyl-10,20-di((*E*)-styryl)porphyrin **4.7**



General procedure for synthesis of alkenyl-substituted porphyrins, using styrene (0.28 mL, 2.4 mmol) and purified *via* column chromatography (DCM/petroleum ether, 8:2) producing a purple solid (8 mg, 33%). ^1H NMR (CDCl_3 , 400 MHz): δ 9.54 (d, $J = 15.9$ Hz, 2H, H^6), 9.28 (d, $J = 4.8$ Hz, 4H, $\text{H}^{4,5}$), 8.76 (d, $J = 4.8$ Hz,

4H, H^{4,5}), 8.13 (m, 4H, H³), 7.87 (d, $J = 7.3$ Hz, 4H, H⁸), 7.70 (m, 6H, H^{1,2}), 7.50-7.20 (m, 7H, H^{7,9,10}). MS (ESI): m/z (C₄₈H₃₄N₄) found: 667.3 (MH⁺). UV-Vis(DMSO): 425 (27500), 523 (4000), 577 (3000), 660 (1220).

7.4.6 5,15-Diphenyl-10,20-bis((1E,3E)-4-phenylbuta-1,3-dien-1-yl)porphyrin **4.8** and 5,15-Diphenyl-10-((1E,3E)-4-phenylbuta-1,3-dien-1-yl)porphyrin **4.11**

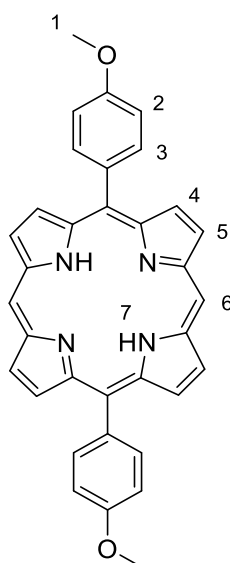


4.11 R = H

General procedure for synthesis of alkenyl-substituted porphyrins, using 1-phenyl-1,3-butadiene (0.42 mL, 2.4 mmol) and purified *via* column chromatography (DCM/petroleum ether, 1:1) producing purple crystals (6 mg, 24%) as a 5:1 inseparable mixture of **4.8** and **4.11**. Discernible data for **4.8**: ¹H NMR (CDCl₃, 400 MHz): δ 9.39 (d, $J = 4.8$ Hz, 4H, H ^{β}), 9.16 (d, $J = 15.9$ Hz, 2H, H¹), 8.80 (d, $J = 4.8$ Hz, 4H, H ^{β}), 8.20 (d, $J = 7.0$ Hz, 4H, H⁸), 7.87 (d, $J = 7.3$ Hz, 4H, H⁸), 7.85-7.75 (m,

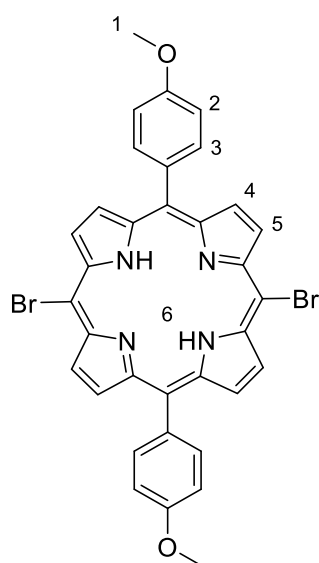
6H, H^{9,10}), 7.65-7.52 (m, 6H, H^{5,2}), 7.45-7.21 (m, 8H, H^{6,7,3}), 6.96 (d, $J = 15.9$ Hz, 2H, H⁴), -2.04 (brs, 2H, H¹¹). Discernible data for **4.11**: ¹H NMR (CDCl₃, 400 MHz): δ 9.52 (d, $J = 4.8$ Hz, 2H, H ^{β}), 9.26 (d, $J = 4.8$ Hz, 2H, H ^{β}), 9.16 (d, $J = 15.9$ Hz, 1H, H¹), 8.95 (d, $J = 4.8$ Hz, 2H, H ^{β}), 8.93 (d, $J = 4.8$ Hz, 2H, H ^{β}), 8.24 (d, $J = 7.0$ Hz, 4H, H⁸), 7.85-7.75 (m, 6H, H^{9,10}), 7.65-7.52 (m, 3H, H^{5,2}), 7.45-7.21 (m, 4H, H^{6,7,3}), 6.98 (m, 1H, H⁴), -2.73 (brs, 2H, H¹¹). Data for the mixture of **4.8** and **4.11** MS (ESI): m/z **4.8** (C₅₂H₃₈N₄) found: 719.90 (MH⁺), MS (ESI): m/z **4.11** (C₄₂H₃₀N₄) found: 591.40 (MH⁺). UV-Vis(DMSO): 439 (13700), 528 (1100), 589 (1300), 678 (610).

7.4.7 5,15-Bis(4-methoxyphenyl)porphyrin **4.13**¹⁷⁴



Dipyrromethane **4.1** (392 mg, 2.70 μ mmol) and 4-methoxybenzaldehyde (0.35 mL, 2.7 mmol, 1 equivalent) were dissolved in DCM (500 mL). The solution was degassed, TFA (0.12 mL, 1.6 mmol) was added and stirred at rt for 4h. DDQ (0.74 g, 3.2 mmol) was added at rt and stirred for 1h. Triethylamine (4 mL, 28.7 mmol) was added, solvent removed and purified by column chromatography (DCM) to give 5,15-bis(4-methoxyphenyl)porphyrin **4.2** as a white solid (410 mg, 58%). Spectroscopic data matched that reported¹⁷⁴; ¹H NMR (CDCl₃, 400MHz): δ 10.30 (s, 2H, H⁶), 9.40 (d, J = 4.9 Hz, 4H, H^{4,5}), 9.11 (d, J = 4.9 Hz, 4H, H^{4,5}), 8.19 (d, J = 8.2 Hz, 4H, H^{2,3}) 7.35 (d, J = 8.2 Hz, 4H, H^{2,3}), 4.10 (s, 6H, H¹), -3.07 (s, 2H, H⁷) MS (ESI): m/z (C₃₄H₂₆N₄O₂) found: 523.80 (MH⁺).

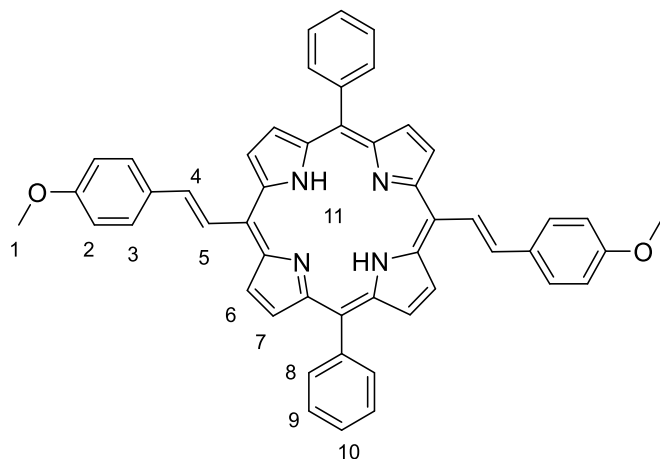
7.4.8 5,15-Dibromo-10,20-bis(4-methoxyphenyl)porphyrin **4.14**¹⁸⁷



5,15-Bis(4-methoxyphenyl)porphyrin **4.2** (80 mg, 0.17 mmol) was dissolved in 50 mL CHCl₃. To this solution, pyridine (0.5 mL) and N-Bromosuccinimide (NBS) (77 mg) were added and stirred for 30 minutes. Acetone (5 mL) was added to quench the reaction and the solvent removed. Purified by column chromatography (DCM:petroleum ether, 1:1) (100 mg, 87%) ¹H NMR (CDCl₃, 400MHz): 9.61 (d, J = 4.8 Hz, 4H, H^{4,5}), 8.81 (d, J = 4.8 Hz, 4H, H^{4,5}), (d, J = 8.1 Hz, 4H, H^{2,3}), 7.31 (d, J = 8.1 Hz, 4H, H^{2,3}), 4.12 (s, 6H, H¹), -2.71 (s, 2H, H⁶). MS (ESI): m/z (C₃₄H₂₄Br₂⁷⁹N₄O₂) found: 679.4 (MH⁺).

7.4.9 5,15-Bis((E)-4-methoxystyryl)-10,20-diphenylporphyrin **4.15**

General procedure for synthesis of alkenyl-substituted porphyrins, using 4-methoxystyrene (0.35 mL, 2.4 mmol), purified by column chromatography (DCM /



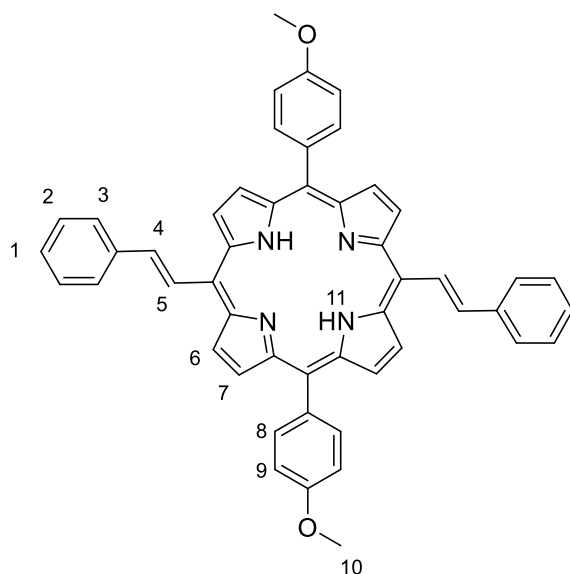
petroleum ether, 8:2) producing purple solid (7 mg, 26%). ^1H NMR (CDCl_3 , 400 MHz): δ 9.62 (d, $J = 15.9$ Hz, 2H, H^5), 9.43 (d, $J = 4.8$ Hz, 4H, $\text{H}^{6,7}$), 8.86 (d, $J = 4.8$ Hz, 4H, $\text{H}^{6,7}$), 8.12 (d, $J = 8.1$ Hz, 4H, H^3), 7.94 (d, $J = 7.3$ Hz, 4H, H^8), 7.58 (t, $J = 7.3$ Hz, 4H, H^9), 7.48

(t, $J = 7.3$ Hz, 2H, H^{10}), 7.38 (d, $J = 15.9$ Hz, 2H, H^4), 7.31 (d, $J = 8.1$ Hz, 4H, H^2), 3.95 (s, 6H, H^1), -2.18 (brs, 2H, H^{11}). MS (ESI): m/z ($\text{C}_{50}\text{H}_{38}\text{N}_4\text{O}_2$) found: 727.3 (MH^+). UV-Vis(DMSO): 443 (23900), 527 (3800), 596 (1800), 684 (1300).

7.4.10 Synthesis of 5,15-bis(4-methoxyphenyl)-10,20-distyrylporphyrin

4.16

5,15-Dibromo-10,20-bis(4-methoxyphenyl)porphyrin **4.14** (26 mg, 36 μmol), $\text{Pd}(\text{OAc})_2$ (3 mg, 10 μmol), JohnPhos (8.6 mg, 29 μmol) and K_2CO_3 (13 mg, 94 μmol) were dried under vacuum in a Schlenk tube. Then dry DMF (5 mL), dry toluene (10

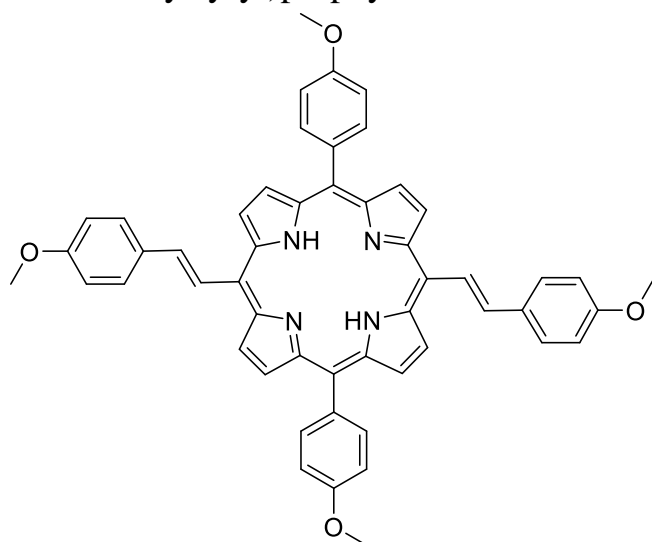


mL) and styrene (0.28 mL, 2.4 mmol) were added. This solution was degassed *via* freeze-thaw and heated overnight at 105°C. The mixture was then cooled to rt and washed with water. The reaction mixture was dried with MgSO_4 , filtered, the solvent removed and purified via column chromatography (DCM) giving a purple solid (9 mg, 33%). ^1H NMR (CDCl_3 , 400 MHz): δ 9.48 (d, $J = 15.9$

Hz, 2H, H^5), 9.43 (d, $J = 4.8$ Hz, 4H, $\text{H}^{6,7}$), 8.80 (d, $J = 4.8$ Hz, 4H, $\text{H}^{6,7}$), 8.21 (d, $J = 7.3$ Hz, 4H, H^3), 7.88 (d, $J = 8.1$ Hz, 4H, H^8), 7.82 – 7.75 (m, 12H, $\text{H}^{2,3}$), 7.31 (d, $J = 15.9$ Hz, 2H, H^4), 7.10 (d, $J = 8.1$ Hz, 4H, H^9), 4.10 (s, 6H, H^{10}), -2.25 (brs, 2H, H^{11}).

MS (ESI): m/z ($C_{50}H_{38}N_4O_2$) found: 727.3 (MH^+). UV-Vis($DMSO$): 435 (25000), 535 (2500), 589 (4800), 680 (2400).

7.4.11 5,15-bis(4-methoxyphenyl)-10,20-bis((E)-4-methoxystyryl)porphyrin **4.17**



5,15-Dibromo-10,20-bis(4-methoxyphenyl)porphyrin **4.14** (26 mg, 36 μ mol), Pd(OAc)₂ (3 mg, 10 μ mol), JohnPhos (8.6 mg, 29 μ mol) and K₂CO₃ (13 mg, 94 μ mol) were dried under vacuum in a Schlenk tube. Then dry DMF (5 mL), dry toluene (10 mL) and 4-methoxystyrene (0.35 mL, 2.4

mmol) were added. This solution was degassed *via* freeze-thaw and heated overnight at 105°C. The mixture was then cooled to rt and washed with water. The reaction mixture was dried with MgSO₄, filtered, the solvent removed and purified via column chromatography (DCM / petroleum ether - 8:2) giving a purple solid (6 mg, 22%). MS (ESI): m/z ($C_{52}H_{44}N_4O_2$) found: 787.5 (MH^+). UV-Vis($DMSO$): 444 (26000), 608 (7300), 696 (3400).

7.4.12 General procedure for the polymerisation of MA **2.4** using alkenyl substituted porphyrins

To a vial, MA **2.4** (0.38 mL, 4.2 mmol), DMSO (277 μ L), 1-dodecaethiol (5 μ L, 20.97 μ mol) and porphyrin (142 μ L of 1.475 mM solution in DMSO, 0.21 μ mol) was added, and the mixture was degassed with N₂ for 10 minutes. The reaction mixture was irradiated in red light (5W, LED, 580-640 nm) or blue light (5W, LED, 420-460 nm) from 4 cm away at rt for 2 h. Conversion was determined by ¹H 400 MHz NMR by comparing the integration of the resonances of the alkene protons on the monomer (5.5-6.5 ppm) and the repeating O-CH₃ peak of the polymer (3.5-4.0 ppm).

Polymerisation of MA 2.4 using TPP 2.3, 5,10,15,20-tetrakis(4-methoxyphenyl)porphyrin 3.4 and 5,15-distyryl-10,20-diphenylporphyrin 4.7 as photocatalysts

General procedure for the polymerisation of MA 2.4 using alkenyl substituted porphyrins, using porphyrin, using porphyrin 2.3, 3.4 and 4.7.

Run	Porphyrin ¹	Light ²	Conversion (%) ³
1	2.3	Red	43
2	3.4	Red	60
3	4.7	Red	50
4	2.3	Blue	56
5	3.4	Blue	70
6	4.7	Blue	60

¹ Experimental conditions: Reaction mixture degassed in DMSO and irradiated with light for 2 hours from 4cm away. MA 2.4: 1-dodecanethiol 2.10: porphyrin - 200: 1: 1×10^{-2} Blue light (420-460 nm) and red light (580- 640 nm) ³ Determined by 400 MHz ¹H NMR by integrating ratio of peaks at 3.6-4.0 ppm and 5.8-6.5 ppm

Polymerisation of MA 2.4 using porphyrin mixtures 4.8 / 4.11 and 4.9 / 4.12

General procedure for the polymerisation of MA 2.4 using alkenyl substituted porphyrins, using porphyrin mixtures 4.8 / 4.11 and 4.9 / 4.12.

Run	Porphyrin ¹	Light ²	Conversion (%) ³
1	4.8 / 4.11	Red	25
2	4.9 / 4.12	Red	8
3	4.7	Red	50
4	4.8 / 4.11	Blue	50
5	4.9 / 4.12	Blue	20
6	4.7	Blue	60

¹ Experimental condition: Reaction mixture degassed in DMSO and irradiated with light for 2 hours from 4cm away. MA 2.4: 1-dodecanethiol 2.10: porphyrin - 200:1: 1×10^{-2} Blue light (420-460 nm) and red light (580- 640 nm) ³ Determined by 400 MHz ¹H NMR by integrating ratio of peaks at 3.6-4 ppm and 5.8-6.5 ppm

Polymerisation of MA using porphyrins 4.7 and 4.15 – 4.17 as photocatalysts in blue and red light

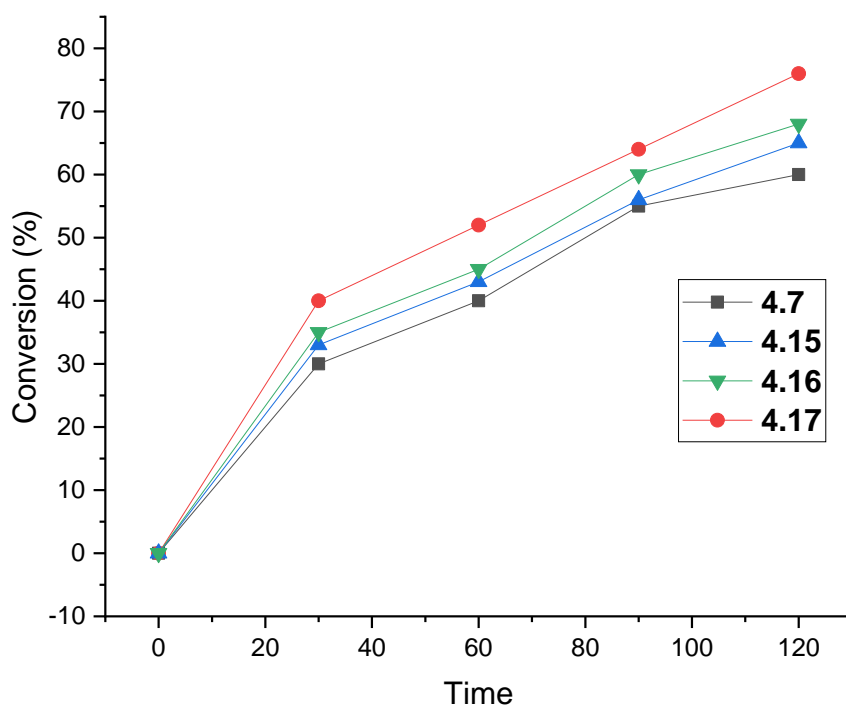
General procedure for the polymerisation of MA 2.4 using alkenyl substituted porphyrins, using porphyrins 4.15, 4.16 and 4.17.

Run	Porphyrin ¹	Light ²	Conversion (%) ³
1	4.4	Red	50
2	4.15	Red	57
3	4.16	Red	55
4	4.17	Red	60
5	4.4	Blue	60
6	4.15	Blue	68
7	4.16	Blue	65
8	4.17	Blue	76

¹ Experimental condition: Reaction mixture degassed in DMSO and irradiated with light for 2 hours from 4cm away. MA **2.4**: 1-dodecanethiol **2.10**: porphyrin - 200:1:1x10⁻² Blue light (420-460 nm) and red light (580- 640 nm) ³ Determined by 400 MHz ¹H NMR by integrating ratio of peaks at 3.6-4 ppm and 5.8-6.5 ppm

Conversion studies of polymerisation of MA 2.4 using methoxy-modified alkenyl-substituted porphyrin 4.15-4.17 compared to 5,15-distyryl-10,20-diphenylporphyrin 4.7

General procedure for the polymerisation of MA 2.4 using alkenyl substituted porphyrins, using porphyrins **4.7**, **4.15**, **4.16** and **4.17**. Polymerisations were performed in blue light (420 – 460 nm) and aliquots were taken from the reaction vessel every 30 minutes and conversion was determined by ¹H 400 MHz NMR

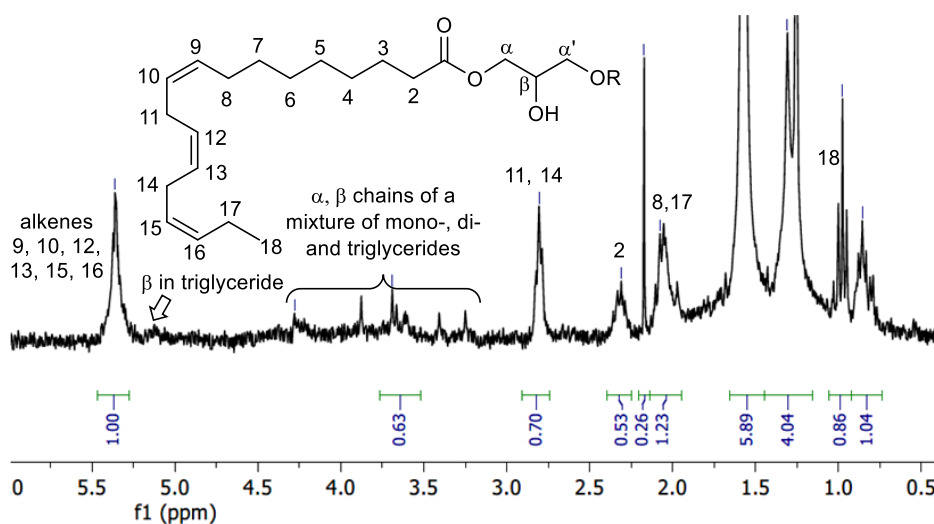


7.5 Chapter 5

7.5.1 Procedure to produce crude spinach extract

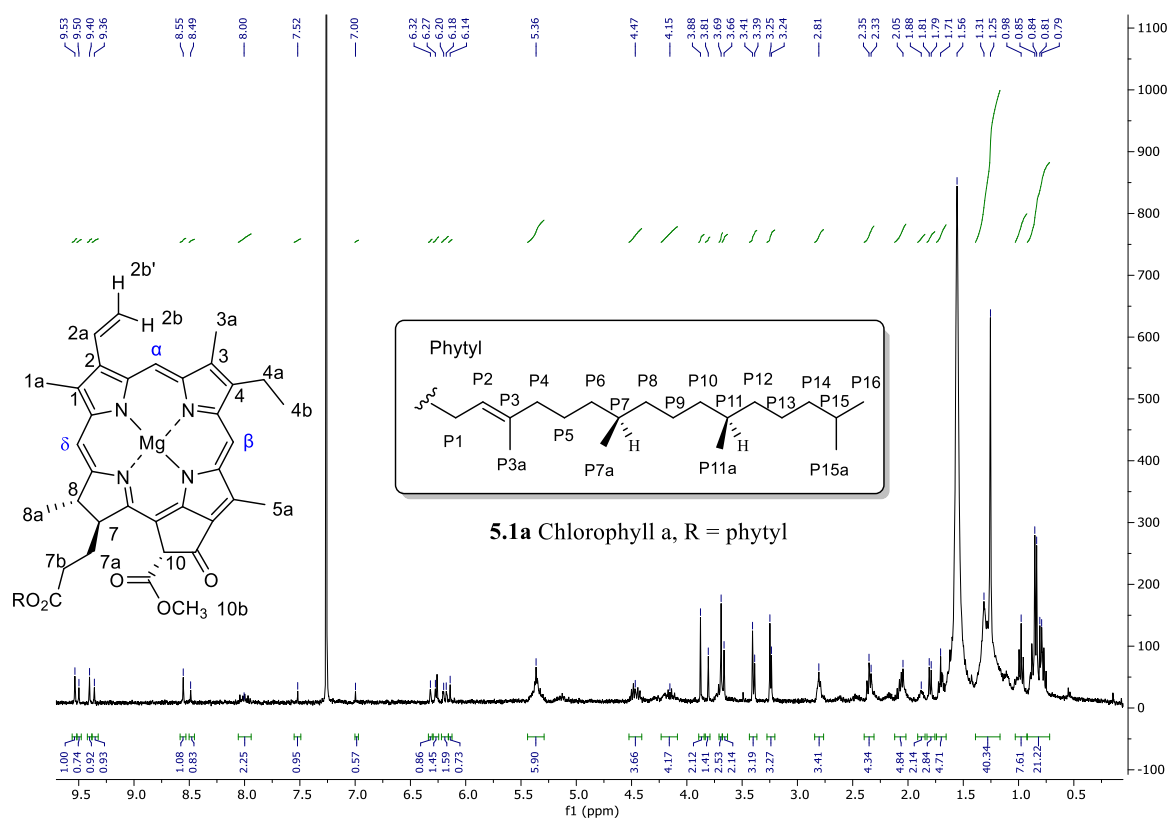
Spinach (25 g) was added to sand (50 g) and magnesium sulphate (50 g). This mixture was blended to give a light green powder. The powder was then submerged in acetone (200 mL) for 10 minutes, after which the acetone was decanted. This was repeated three times, and the extracts were then combined, and the solvent was removed to give a green solid consisting of a mixture of chlorophyll, carotenoids but mainly tri-, di- and monoglycerides of polyunsaturated fatty acids (mainly linolenic acid).

^1H NMR 400 MHz spectrum of crude spinach extract:



7.5.2 Extraction of chlorophyll a from spinach¹⁵⁷

Chlorophyll a **5.1a** was then isolated from the crude extract *via* column chromatography. The solvent system used for the column chromatography involved initially using petroleum ether to remove carotenes, then using petroleum ether 95% / ethyl acetate 5% to remove xanthophyll, then finally changing the solvent to petroleum ether 90% / ethyl acetate 10% to elute chlorophyll a **5.1a**. This produced a green solid which contained chlorophyll a **5.1a** and pheophytin a **5.3a** and traces amounts of lipids.



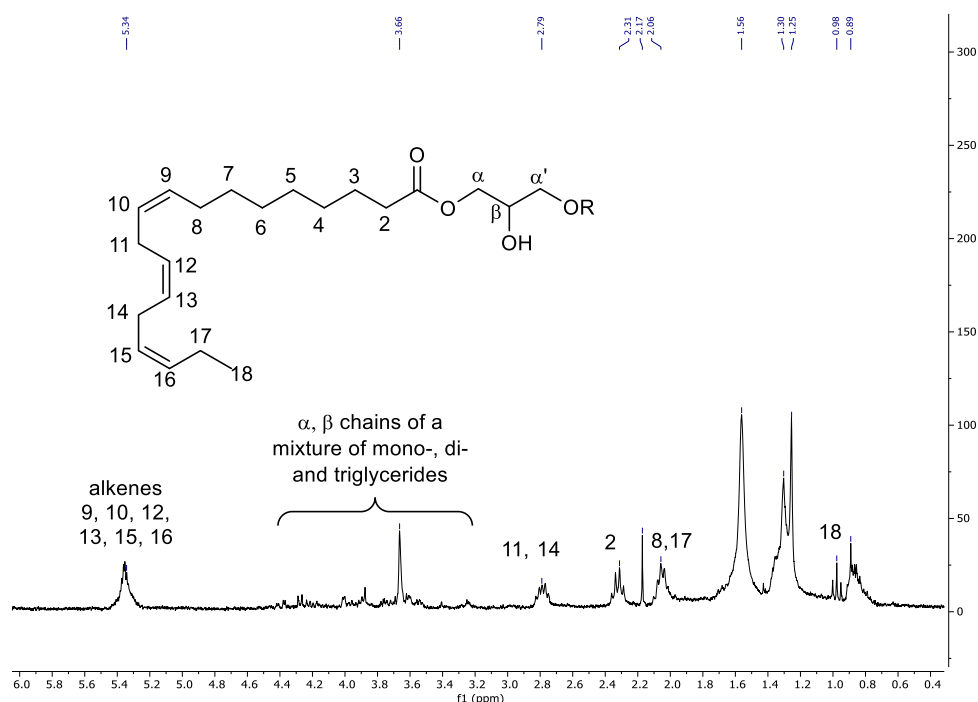
Discernible data for chlorophyll a **5.1a**: ¹H NMR (CDCl₃, 400MHz): δ 9.53 (s, 1H, H-β), 9.40 (s, 1H, H-α), 8.55 (s, 1H, H-δ), 8.05-7.95 (m, 1H, H^{2a}), 6.32-6.28 (m, 1H, H^{2b}), 6.20-6.18 (m, 1H, H^{2c}), 6.14 (s, 1H, H¹⁰), 5.13 (m, 1H, H^{P2}), 4.50-4.40 (m, 1H, H⁸), 4.26-4.08 (m, 3H, H^{P1}, H⁷), 3.88 (s, 3H, H^{10b}), 3.69 (s, 3H, H^{5a}), 3.41 (s, 3H, H^{1a}), 3.25 (s, 3H, H^{3a}), 2.53-2.08 (m, 4H, H^{7a}, H^{7b}), 1.83 (m, 2H, H^{P4}), 1.80 (d, *J* = 8.0 Hz, 3H, H^{8a}), 1.71 (t, *J* = 7.0 Hz, H^{4b}), 1.70-1.40 (m, 25H, H^{P5}, H^{P6}, H^{P7}, H^{P7a}, H^{P8}, H^{P9}, H^{P10}, H^{P11}, H^{P12}, H^{P13}, H^{P14}, H^{P15}, H^{P8}), 0.90-0.75 (m, 9H, H^{P11a}, H^{P15a}, H^{P16}). MS (ESI): *m/z* (C₅₅H₇₂MgN₄O₅) found: 893.5 (MH⁺).

Discernible data for pheophytin a **5.3a**: ¹H NMR (CDCl₃, 400MHz): δ 9.50 (s, 1H, H-β), 9.36 (s, 1H, H-α), 8.49 (s, 1H, H-δ), 8.05-7.95 (m, 1H, H^{2a}), 6.32-6.28 (m, 1H, H^{2b}), 6.20 (s, 1H, H¹⁰), 6.20-6.18 (m, 1H, H^{2c}), 5.36 (m, 1H, H^{P2}), 4.50-4.40 (m, 3H, HP1, H⁸), 4.26-4.08 (m, 1H, H⁷), 3.81 (s, 3H, H^{10b}), 3.66 (s, 3H, H^{5a}), 3.39 (s, 3H, H^{1a}), 3.24 (s, 3H, H^{3a}), 2.63-2.19 (m, 4H, H^{7a}, H^{7b}), 1.90 (m, 2H, H^{P4}), 1.80 (d, *J* = 8.0 Hz, 3H, H^{8a}), 1.71 (t, *J* = 7.0 Hz, H^{4b}), 1.70-1.40 (m, 25H, H^{P5}, H^{P6}, H^{P7}, H^{P7a}, H^{P8}, H^{P9}, H^{P10}, H^{P11}, H^{P12}, H^{P13}, H^{P14}, H^{P15}, H^{P8}), 0.90-0.75 (m, 9H, H^{P11a}, H^{P15a}, H^{P16}). MS (ESI): *m/z* (C₅₅H₇₄N₄O₅) found: 871.6 (MH⁺).

UV-Vis(DMSO): 410 (13700), 505 (830), 537 (510), 610 (270), 667 (3900).

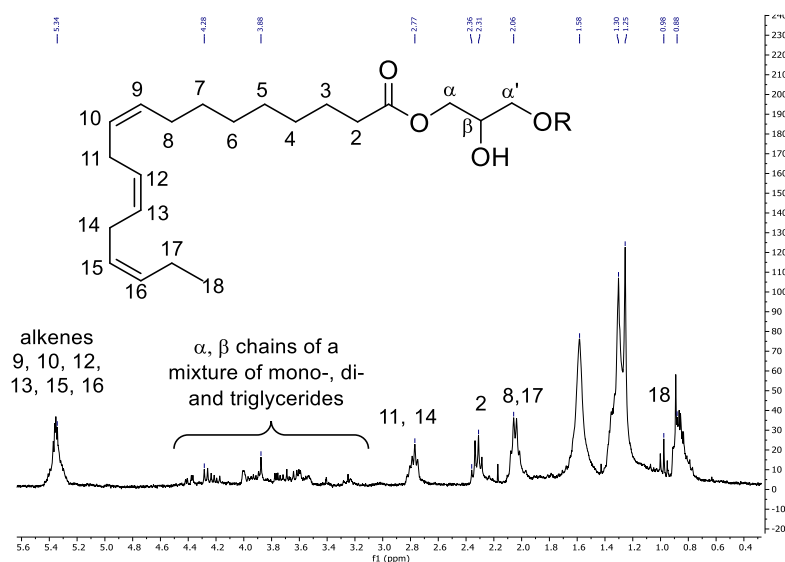
7.5.3 Procedure to extract crude chlorella extract from chlorella powder
 Chlorella powder (5 g) was added to acetone (50 mL) and stirred for 10 minutes. The acetone was then decanted. This was repeated twice, and the extracts were combined, and the solvent removed under vacuum to give the crude chlorella extract as a green solid.

^1H NMR (CDCl_3 , 400 MHz) spectrum of crude chlorella powder extract mainly shows tri-, di- and monoglycerides of polyunsaturated fatty acids:



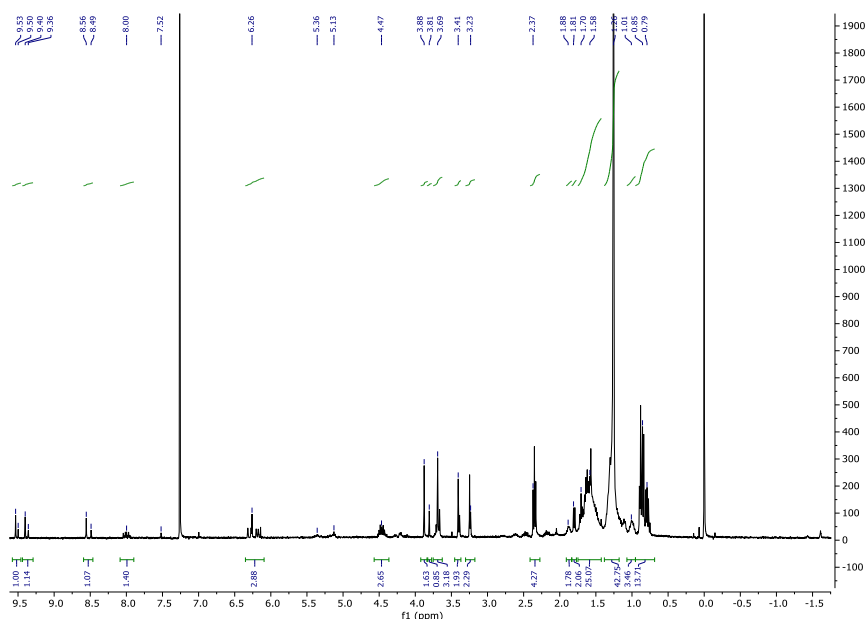
7.5.4 Procedure to extract crude chlorella extract from chlorella tablet
 Chlorella tablet (5 g) was crushed into a powder, was added to acetone (50 mL) and stirred for 10 minutes. The acetone was then decanted. This was repeated twice, and the extracts were combined, and the solvent removed under vacuum to give the crude chlorella extract as a green solid.

^1H NMR (CDCl_3 , 400 MHz) spectrum of crude chlorella tablet extract mainly shows tri-, di- and monoglycerides of polyunsaturated fatty acids, however unlike the crude extracts from spinach and the powder there is significantly more triglycerides present:

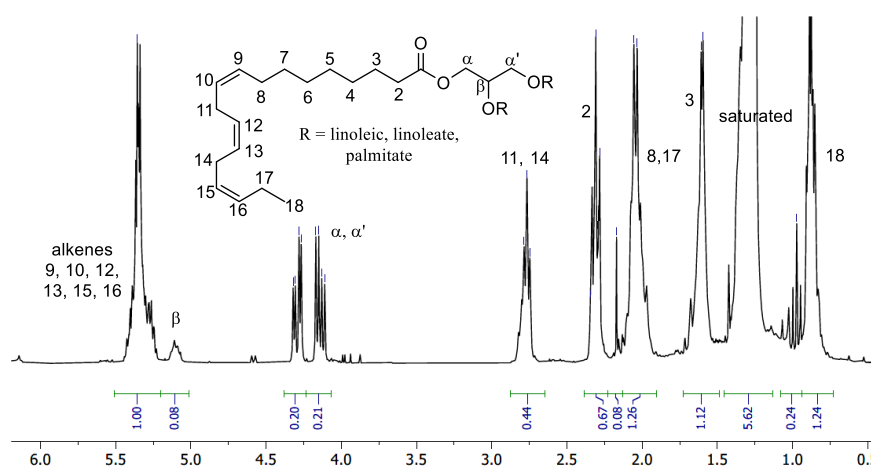


7.5.5 Procedure for extracting chlorophyll a **5.1a from chlorella powder**

Chlorophyll a **5.1a** was then isolated *via* column chromatography. The solvent system used for the column chromatography involved using petroleum ether to remove carotenes, then using petroleum ether 95% / ethyl acetate 5% to remove xanthophyll, then finally changing the solvent to petroleum ether 90% / ethyl acetate 10% to elute chlorophyll a **5.1a**. This produced a green solid made up of chlorophyll a **5.1a** and pheophytin **5.3a**. This was purer than the extracts isolated from spinach. ¹H NMR (CDCl₃, 400 MHz) spectrum of chlorophyll a **5.1a** isolated from crude chlorella powder:



Note the petroleum ether layer consisted mainly of triglycerides



7.5.6 General procedure for the polymerisation of MA **2.4** using spinach and chlorella extracts as photocatalysts

To a vial, MA **2.4** (0.38 mL, 4.2 mmol), DMSO (277 mL), 1-dodecaethiol (5 μ L, 20.97 μ mol) and photocatalyst (142 μ L of 7.375 mM solution in DMSO, 1.05 μ mol) was added, and the mixture was degassed with N₂ for 10 minutes. The reaction mixture was irradiated in red light (5W, LED, 580-640 nm) or blue light (5W, LED, 420-460 nm) from 4 cm away at rt for 2 h. Conversion was determined by ¹H 400 MHz NMR by comparing the integration of the resonances of the alkene protons on the monomer (5.5-6.5 ppm) and the repeating O-CH₃ peak of the polymer (3.5-4.0 ppm).

Polymerisation of MA **2.4 using chlorophyll a **5.1a** as a photocatalyst in both blue and red light**

General procedure for the polymerisation of MA **2.4** using spinach and chlorella extracts as photocatalysts, using chlorophyll a **5.1a** isolated from spinach. Aliquots were taken from the reaction vessel every hour and conversion was determined by ¹H 400 MHz NMR.

Run	Light ¹	Time	Conversion (%) ²	<i>Mn</i> ³	<i>Mw</i> ³	<i>Đ</i> ³
1	-	24h	0	-	-	-
2	Red	1h	11	32k	50k	1.48
3	Blue	1h	21	37k	58k	1.56
4	Red	2h	20	33k	49k	1.51
5	Blue	2h	28	37k	58k	1.55
6	Red	3h	27	33k	49k	1.43
7	Blue	3h	33	36k	59k	1.55
8	Red	4h	35	33k	50k	1.41
9	Blue	4h	42	38k	60k	1.58

¹ Experimental condition: Reaction mixture degassed in DMSO and irradiated with light for 4 hours from 4cm away. MA **2.4**: 1-dodecanethiol **2.10**: porphyrin - 200:1:1x10⁻² ² Blue light (420-460 nm) and red light (580- 640 nm) ³ Determined by 400 MHz ¹H NMR by integrating ratio of peaks at 3.6-4 ppm and 5.8-6.5 ppm. ¹ Molecular weight and polydispersity index were determined by GPC analysis (CHCl₃ as eluent) calibrated to poly (methyl methacrylate)

Polymerisation of MA **2.4** using chlorophyll a **5.1a** and crude spinach as photocatalysts in blue and red light

General procedure for the polymerisation of MA **2.4** using spinach and chlorella extracts as photocatalysts, using chlorophyll a **5.1a** and crude spinach extract as photocatalysts.

Run	Photocatalyst ¹	Light ²	Conversion (%) ³
1	Crude spinach	-	0
2	Chlorophyll a 5.1a	Red	35
3	Crude spinach	Red	26
4	Chlorophyll a 5.1a	Blue	42
5	Crude spinach	Blue	31

¹ Experimental condition: Reaction mixture degassed in DMSO and irradiated with light for 4 hours from 4cm away. MA **2.4**: 1-dodecanethiol **2.10**: photocatalyst - 200:1:1x10⁻² ² Blue light (420-460 nm) and red light (580- 640 nm) ³ Determined by 400 MHz ¹H NMR by integrating ratio of peaks at 3.6-4 ppm and 5.8-6.5 ppm

Conversion study of the polymerisation of MA 2.4 using chlorophyll a 5.1a and crude spinach extract as photocatalysts in blue light

General procedure for the polymerisation of MA 2.4 using spinach and chlorella extracts as photocatalysts, using chlorophyll a 5.1a and crude spinach as photocatalysts. Polymerisations were irradiated with blue light (420 – 460 nm) and aliquots were taken from the reaction vessel every hour and conversion was determined by ¹H 400 MHz NMR.

Run	Light¹	Time	Conversion (%)²
1	Chlorophyll a 5.1a	1h	21
2	Crude spinach	1h	10
3	Chlorophyll a 5.1a	2h	28
4	Crude spinach	2h	17
5	Chlorophyll a 5.1a	3h	33
6	Crude spinach	3h	25
7	Chlorophyll a 5.1a	4h	42
8	Crude spinach	4h	31

Experimental condition: Reaction mixture degassed in DMSO and irradiated with light for 4 hours from 4cm away. MA 2.4: 1-dodecanethiol 2.10: photocatalyst - 200:1:1x10⁻² ¹ Blue light (420-460 nm) ² Determined by 400 MHz ¹H NMR by integrating ratio of peaks at 3.6-4 ppm and 5.8-6.5 ppm

Polymerisation of MA 2.4 using crude spinach and chlorella extracts as photocatalysts

General procedure for the polymerisation of MA 2.4 using spinach and chlorella extracts as photocatalysts, using crude chlorella powder, crude chlorella tablet and crude spinach extract as photocatalysts.

Run	Photocatalyst ¹	Light ²	Conversion (%) ³
1	Crude chlorella (tablet)	-	0
2	Crude chlorella (powder)	-	0
3	Crude spinach	Red	26
4	Crude chlorella (tablet)	Red	20
5	Crude chlorella (powder)	Red	48
6	Crude spinach	Blue	31
7	Crude chlorella (tablet)	Blue	27
8	Crude chlorella (powder)	Blue	60

Experimental condition: Reaction mixture degassed in DMSO and irradiated with light for 4 hours from 4cm away. MA **2.4**:1-dodecanethiol **2.10**: photocatalyst - 200:1:1x10⁻² Blue light (420-460 nm) and red light (580 - 640 nm)
² Determined by 400 MHz ¹H NMR by integrating ratio of peaks at 3.6-4 ppm and 5.8-6.5 ppm

Conversion study of polymerisation of MA **2.4** comparing chlorophyll a **5.1a** and crude chlorella powder in blue light

General procedure for the polymerisation of MA **2.4** using spinach and chlorella extracts as photocatalysts, using chlorophyll a **5.1a** and crude chlorella (powder) as photocatalysts. Polymerisations were irradiated with blue light (420 – 460 nm) and aliquots were taken from the reaction vessel every hour and conversion was determined by ¹H 400 MHz NMR.

Run	Photocatalyst ¹	Time	Conversion (%) ²	Mn ³	Mw ³	Đ ³
1	Chlorophyll a 5.1a	1h	21	37k	58	1.56
2	Crude chlorella (powder)	1h	29	32k	56k	1.54
3	Chlorophyll a 5.1a	2h	28	37k	58	1.55
4	Crude chlorella (powder)	2h	37	33k	55k	1.54
5	Chlorophyll a 5.1a	3h	33	36k	59	1.55
6	Crude chlorella (powder)	3h	45	33k	55k	1.58
7	Chlorophyll a 5.1a	4h	42	38k	60	1.58
8	Crude chlorella (powder)	4h	60	33k	55k	1.55

Experimental condition: Reaction mixture degassed in DMSO and irradiated with light for 4 hours from 4cm away. MA **2.4**: pentaerythritol tetrakis (3-mercaptopropionate) **2.12**: photocatalyst - 200:1:1x10⁻² Blue light (420-460 nm) ² Determined by 400 MHz ¹H NMR by integrating ratio of peaks at 3.6-4 ppm and 5.8-6.5 ppm. ³ Molecular weight and polydispersity index were determined by GPC analysis (CHCl₃ as eluent) calibrated to poly (methyl methacrylate)

7.5.7 General procedure for 3D printing

A mixture of 15g of a 50:50 w: w UDMA **2.5**/ TEGDMA **2.6** mixture was used for 3D printing. To this solution, pentaerythritol tetrakis(3-mercaptopropionate) **2.12** (1.02 g, 2.2 mmol) and photocatalyst (0.05 mmol) was added, and the solution stirred in darkness for 10 minutes. The 3D prints were performed at room temperature using the photocentric liquid crystal precision printer.

Print O - General procedure for 3D printing, using chlorophyll a **5.1a** (45 mg, 0.05 mmol), exposure time per layer 300,000 ms.

Print P - General procedure for 3D printing, using chlorophyll a **5.1a** (45 mg, 0.05 mmol), exposure time per layer 400,000 ms.

Print Q - General procedure for 3D printing, using crude spinach extract (45 mg, 0.05 mmol), exposure time per layer 400,000 ms.

Print R - General procedure for 3D printing, using crude chlorella powder extract (45 mg, 0.05 mmol), exposure time per layer 400,000 ms.

Print S - General procedure for 3D printing, using crude chlorella tablet extract (45 mg, 0.05 mmol), exposure time per layer 400,000 ms.

8 References

- 1 A. Albini, *Photochemistry*, 2015.
- 2 E. Baumann, *Justus Liebigs Ann. Chem.*, 1872, **163**, 308–322.
- 3 C. Giacomo, *Science*, 1912, **36**, 385–394.
- 4 J. M. R. Narayanam and C. R. J. Stephenson, *Chem. Soc. Rev.*, 2011, **40**, 102–113.
- 5 C. K. Prier, D. A. Rankic and D. W. C. MacMillan, *Chem. Rev.*, 2013, **113**, 5322–5363.
- 6 S. W. Cao, J. X. Low, J. G. Yu and M. Jaroniec, *Adv. Mater.*, 2015, **27**, 2150–2176.
- 7 J. Xuan and W. J. Xiao, *Angew. Chemie-International Ed.*, 2012, **51**, 6828–6838.
- 8 X. Li, J. G. Yu and M. Jaroniec, *Chem. Soc. Rev.*, 2016, **45**, 2603–2636.
- 9 N. A. Romero and D. A. Nicewicz, *Chem. Rev.*, 2016, **116**, 10075–10166.
- 10 F. Strieth-Kalthoff, M. J. James, M. Teders, L. Pitzer and F. Glorius, *Chem. Soc. Rev.*, 2018, **47**, 7190–7202.
- 11 N. Corrigan, S. Shanmugam, J. Xu and C. Boyer, *Chem. Soc. Rev.*, 2016, **45**, 6165–6212.
- 12 T. Zhang and W. B. Lin, *Chem. Soc. Rev.*, 2014, **43**, 5982–5993.
- 13 L. Shi and W. J. Xia, *Chem. Soc. Rev.*, 2012, **41**, 7687–7697.
- 14 D. Ravelli, S. Protti and M. Fagnoni, *Chem. Rev.*, 2016, **116**, 9850–9913.
- 15 S. Fukuzumi, S. Mochizuki and T. Tanaka, *J. Phys. Chem.*, 1990, **94**, 722–726.
- 16 H. Cano-Yelo and A. Deronzier, *Tetrahedron Lett.*, 1984, **25**, 5517–5520.
- 17 C. Pac, M. Ihama, M. Yasuda, Y. Miyauchi and H. Sakurai, *J. Am. Chem. Soc.*, 1981, **103**, 6495–6497.

- 18 H. Cano-Yelo and A. Deronzier, *J. Chem. Soc. Perkin Trans. 2*, 1984, 1093–1098.
- 19 J.-M. Zen, S.-L. Liou, A. S. Kumar and M.-S. Hsia, *Angew. Chemie Int. Ed.*, 2003, **42**, 577–579.
- 20 J. M. R. Narayanam, J. W. Tucker and C. R. J. Stephenson, *J. Am. Chem. Soc.*, 2009, **131**, 8756–8757.
- 21 M. A. Ischay, M. E. Anzovino, J. Du and T. P. Yoon, *J. Am. Chem. Soc.*, 2008, **130**, 12886–12887.
- 22 D. A. Nicewicz and D. W. C. MacMillan, *Science*, 2008, 322, 77-80
- 23 J. D. Nguyen, E. M. D’Amato, J. M. R. Narayanam and C. R. J. Stephenson, *Nat. Chem.*, 2012, **4**, 854–859.
- 24 H. Kim and C. Lee, *Angew. Chemie Int. Ed.*, 2012, **51**, 12303–12306.
- 25 C.-J. Wallentin, J. D. Nguyen, P. Finkbeiner and C. R. J. Stephenson, *J. Am. Chem. Soc.*, 2012, **134**, 8875–8884.
- 26 M. Pirtsch, S. Paria, T. Matsuno, H. Isobe and O. Reiser, *Chem. – A Eur. J.*, 2012, **18**, 7336–7340.
- 27 E. L. Tyson, M. S. Ament and T. P. Yoon, *J. Org. Chem.*, 2013, **78**, 2046–2050.
- 28 M. H. Keylor, J. E. Park, C.-J. Wallentin and C. R. J. Stephenson, *Tetrahedron*, 2014, **70**, 4264–4269.
- 29 O. O. Fadeyi, J. J. Mousseau, Y. Feng, C. Allais, P. Nuhant, M. Z. Chen, B. Pierce and R. Robinson, *Org. Lett.*, 2015, **17**, 5756–5759.
- 30 D. P. Hari and B. König, *Chem. Commun.*, 2014, **50**, 6688–6699.
- 31 A. K. Yadav, V. P. Srivastava and L. D. S. Yadav, *New J. Chem.*, 2013, **37**, 4119–4124.
- 32 H. Togo and M. Katohgi, *Synlett*, 2001, **2001**, 565–581.
- 33 S. Furuyama and H. Togo, *Synlett*, 2010, **2010**, 2325–2329.

- 34 T. Otsu, M. Yoshida and T. Tazaki, *Die Makromol. Chemie, Rapid Commun.*, 1982, **3**, 133–140.
- 35 M. Chen, M. Zhong and J. A. Johnson, *Chem. Rev.*, 2016, **116**, 10167–10211.
- 36 Y. Kwak and K. Matyjaszewski, *Macromolecules*, 2010, **43**, 5180–5183.
- 37 M. A. Tasdelen, M. Uygun and Y. Yagci, *Macromol. Rapid Commun.*, 2010, **32**, 58–62.
- 38 J. Mosnáček and M. Ilčíková, *Macromolecules*, 2012, **45**, 5859–5865.
- 39 X. Pan, M. Lamson, J. Yan, K. Matyjaszewski and A. C. S. M. Lett, *Konkolewicz, K. Schröder, J. Buback, S. Bernhard, K. Matyjaszewski, ACS Macro Lett*, 2012, **1**, 1219–1223.
- 40 A. Anastasaki, V. Nikolaou, Q. Zhang, J. Burns, S. R. Samanta, C. Waldron, A. J. Haddleton, R. McHale, D. Fox, V. Percec, P. Wilson and D. M. Haddleton, *J. Am. Chem. Soc.*, 2014, **136**, 1141–1149.
- 41 B. P. Fors and C. J. Hawker, *Angew. Chemie Int. Ed.*, 2012, **51**, 8850–8853.
- 42 W. Ma, H. Chen, Y. Ma, C. Zhao and W. Yang, *Macromol. Chem. Phys.*, 2014, **215**, 1012–1021.
- 43 J. Lalevée, N. Blanchard, M.-A. Tehfe, M. Peter, F. Morlet-Savary and J. P. Fouassier, *Polym. Bull.*, 2012, **68**, 341–347.
- 44 K. Iwai, M. Uesugi and F. Takemura, *Polym. J.*, 1985, **17**, 1005–1011.
- 45 X. Pan, N. Malhotra, J. Zhang and K. Matyjaszewski, *Macromolecules*, 2015, **48**, 6948–6954.
- 46 Z. Xue, N. T. B. Linh, S. K. Noh and W. S. Lyoo, *Angew. Chemie Int. Ed.*, 2008, **47**, 6426–6429.
- 47 X. Pan, N. Malhotra, S. Dadashi-Silab and K. Matyjaszewski, *Macromol. Rapid Commun.*, 2017, **38**, 1600651.
- 48 Y. Cao, Y. Xu, J. Zhang, D. Yang and J. Liu, *Polymer (Guildf.)*, 2015, **61**, 198–203.
- 49 Y. Liu, D. Chen, X. Li, Z. Yu, Q. Xia, D. Liang and H. Xing, *Green Chem.*,

- 2016, **18**, 1475–1481.
- 50 J. Xu, K. Jung, A. Atme, S. Shanmugam and C. Boyer, *J. Am. Chem. Soc.*, 2014, **136**, 5508–5519.
- 51 J. Xu, K. Jung and C. Boyer, *Macromolecules*, 2014, **47**, 4217–4229.
- 52 G. M. Miyake and J. C. Theriot, *Macromolecules*, 2014, **47**, 8255–8261.
- 53 J. C. Theriot, C.-H. Lim, H. Yang, M. D. Ryan, C. B. Musgrave and G. M. Miyake, *Science*, 2016, **352**, 1082 – 1086.
- 54 N. J. Treat, H. Sprafke, J. W. Kramer, P. G. Clark, B. E. Barton, J. Read de Alaniz, B. P. Fors and C. J. Hawker, *J. Am. Chem. Soc.*, 2014, **136**, 16096–16101.
- 55 J. Xu, S. Shanmugam, H. T. Duong and C. Boyer, *Polym. Chem.*, 2015, **6**, 5615–5624.
- 56 S. Patients, P. C. in Solid Cancer, B. A. R. Hassan, Z. B. M. Yusoff, M. A. H. Othman, S. Bin, *Intech*, 2012, 13.
- 57 C. M. Che and J. S. Huang, *Chem. Commun.*, 2009, 3996–4015.
- 58 R. W. Wagner, T. E. Johnson and J. S. Lindsey, *J. Am. Chem. Soc.*, 1996, **118**, 11166–11180.
- 59 C. M. Che, V. K. Y. Lo, C. Y. Zhou and J. S. Huang, *Chem. Soc. Rev.*, 2011, **40**, 1950–1975.
- 60 T. F. Schulze and T. W. Schmidt, *ENERGY Environ. Sci.*, 2015, **8**, 103–125.
- 61 B. E. Hardin, H. J. Snaith and M. D. McGehee, *Nat. Photonics*, 2012, **6**, 162–169.
- 62 L. L. Li and E. W. G. Diau, *Chem. Soc. Rev.*, 2013, **42**, 291–304.
- 63 R. BONNETT, *Chem. Soc. Rev.*, 1995, **24**, 19–33.
- 64 E. D. Sternberg, D. Dolphin and C. Bruckner, *Tetrahedron*, 1998, **54**, 4151–4202.
- 65 H. Abrahamse and M. R. Hamblin, *Biochem. J.*, 2016, **473**, 347–364.

- 66 D. N. Hendrickson, M. G. Kinnaird and K. S. Suslick, *J. Am. Chem. Soc.*, 1987, **109**, 1243–1244.
- 67 K. S. Suslick, F. V Acholla and B. R. Cook, *J. Am. Chem. Soc.*, 1987, **109**, 2818–2819.
- 68 H. Inoue, K. Chandrasekaran and D. G. Whitten, *J. Photochem.*, 1985, **30**, 269–284.
- 69 S. Takagi, T. Okamoto, T. Shiragami and H. Inoue, *J. Org. Chem.*, 1994, **59**, 7373–7378.
- 70 T. Shiragami, J. Matsumoto, H. Inoue and M. Yasuda, *J. Photochem. Photobiol. C Photochem. Rev.*, 2005, **6**, 227–248.
- 71 T. Shiragami, K. Kubomura, D. Ishibashi and H. Inoue, *J. Am. Chem. Soc.*, 1996, **118**, 6311–6312.
- 72 H. Inoue, T. Okamoto, Y. Kameo, M. Sumitani, A. Fujiwara, D. Ishibashi and M. Hida, *J. Chem. Soc. Perkin Trans. 1*, 1994, 105–111.
- 73 H. Inoue, S. Funyu, Y. Shimada and S. Takagi, *Pure Appl. Chem.*, 2005, **77**, 1019–1033.
- 74 S. Funyu, T. Isobe, S. Takagi, D. A. Tryk and H. Inoue, *J. Am. Chem. Soc.*, 2003, **125**, 5734–5740.
- 75 K. Rybicka-Jasińska, W. Shan, K. Zawada, K. M. Kadish and D. Gryko, *J. Am. Chem. Soc.*, 2016, **138**, 15451–15458.
- 76 K. Rybicka-Jasińska, B. König and D. Gryko, *European J. Org. Chem.*, 2017, **2017**, 2104–2107.
- 77 X. Liu, L. Liu, Z. Wang and X. Fu, *Chem. Commun.*, 2015, **51**, 11896–11898.
- 78 X. Liu, Z. Wang and X. Fu, *Dalt. Trans.*, 2016, **45**, 13308–13310.
- 79 T. Mandal, S. Das and S. De Sarkar, *Adv. Synth. Catal.*, 2019, **361**, 3200–3209.
- 80 B. B. WAYLAND, G. POSZMIK and M. FRYD, *Organometallics*, 1992, **11**, 3534–3542.

- 81 S. Inoue, T. Aida, Y. Watanabe and K. Kawaguchi, *Makromol. Chemie-Macromolecular Symp*, 1991, **42–3**, 365–371.
- 82 H. Uno, K. Takata and Y. Mizutani, *React. Polym.*, 1991, **15**, 121–129.
- 83 H. Sugimoto, M. Kuroki, T. Watanabe, C. Kawamura, T. Aida and S. Inoue, *Macromolecules*, 1993, **26**, 3403–3410.
- 84 A. Simakova, M. Mackenzie, S. E. Averick, S. Park and K. Matyjaszewski, *Angew. Chemie Int. Ed.*, 2013, **52**, 12148–12151.
- 85 T. Aida and S. Inoue, *Acc. Chem. Res.*, 1996, **29**, 39–48.
- 86 Y. Zhao, M. Yu, S. Zhang, Y. Liu and X. Fu, *Macromolecules*, 2014, **47**, 6238–6245.
- 87 S. Shanmugam, J. Xu and C. Boyer, *J. Am. Chem. Soc.*, 2015, **137**, 9174–9185.
- 88 M. Kuroki, T. Aida and S. Inoue, *J. Am. Chem. Soc.*, 1987, **109**, 4737–4738.
- 89 R. K. Sherwood, C. L. Kent, B. O. Patrick and W. S. McNeil, *Chem. Commun.*, 2010, **46**, 2456–2458.
- 90 X. Pan, M. A. Tasdelen, J. Laun, T. Junkers, Y. Yagci and K. Matyjaszewski, *Prog. Polym. Sci.*, 2016, **62**, 73–125.
- 91 S. Dadashi-Silab, S. Doran and Y. Yagci, *Chem. Rev.*, 2016, **116**, 10212–10275.
- 92 J. Xu, S. Shanmugam and C. Boyer, *ACS Macro Lett.*, 2015, **4**, 926–932.
- 93 G. Noirbent, Y. Xu, A.-H. Bonardi, D. Gigmes, J. Lalevée and F. Dumur, *Eur. Polym. J.*, 2020, **139**, 110019.
- 94 N. R. Baker, *Annu. Rev. Plant Biol.*, 2008, **59**, 89–113.
- 95 M. O. Senge, A. A. Ryan, K. A. Letchford, S. A. MacGowan and T. Mielke, *Symmetry-Basel*, 2014, **6**, 781–843.
- 96 G. H. Krause and E. Weis, *Annu. Rev. Plant Physiol. Plant Mol. Biol.*, 1991, **42**, 313–349.

- 97 S. Shanmugam, J. Xu and C. Boyer, *Chem. Sci.*, 2015, **6**, 1341–1349.
- 98 D. Dolphin and R. H. Felton, *Acc. Chem. Res.*, 1974, **7**, 26–32.
- 99 C. Wu, S. Shanmugam, J. Xu, J. Zhu and C. Boyer, *Chem. Commun.*, 2017, **53**, 12560–12563.
- 100 T. Jungst, W. Smolan, K. Schacht, T. Scheibel and J. Groll, *Chem. Rev.*, 2016, **116**, **3**, 1496–1539.
- 101 B. Wendel, D. Rietzel, F. Kühnlein, R. Feulner, G. Hülder and E. Schmachtenberg, *Macromol. Mater. Eng.*, 2008, **293**, 799–809.
- 102 C. W. Hull, *US Pat*, 4575330A 1984.
- 103 A. C. de Leon, Q. Chen, N. B. Palaganas, J. O. Palaganas, J. Manapat and R. C. Advincula, *React. Funct. Polym.*, 2016, **103**, 141–155.
- 104 W. Zhu, X. Qu, J. Zhu, X. Ma, S. Patel, J. Liu, P. Wang, C. S. E. Lai, M. Gou, Y. Xu, K. Zhang and S. Chen, *Biomaterials*, 2017, **124**, 106–115.
- 105 P. Soman, P. H. Chung, A. P. Zhang and S. Chen, *Biotechnol. Bioeng.*, 2013, **110**, 3038–3047.
- 106 T. J. R., S. David, E. Nikita, J. Rima, J. A. R., K. David, C. Kai, P. Robert, R. J. P., E. Alexander, S. E. T. and D. J. M., *Science*, 2015, **347**, 1349–1352.
- 107 R. Januszewicz, J. R. Tumbleston, A. L. Quintanilla, S. J. Mecham and J. M. DeSimone, *Proc. Natl. Acad. Sci. U. S. A.*, 2016, **113**, 11703–11708.
- 108 R. Liska, *ChemPhysChem*, 2011, **12**, 1389.
- 109 D. Bird, J. Laquidara, E. Caravaca, K. Luhmann and N. Ravindra, *Formulation of UV Curable Resins Utilized in Vat Photo Polymerization for the Additive Manufacturing of Gun Propulsion Charge in 3D Printers*, 2020, 1945–1953.
- 110 D. D. M. Wayner, K. B. Clark, A. Rauk, D. Yu and D. A. Armstrong, *J. Am. Chem. Soc.*, 1997, **119**, 8925–8932.
- 111 H. K. Park, M. Shin, B. Kim, J. W. Park and H. Lee, *NPG Asia Mater.*, 2018, **10**, 82–89.

- 112 A. Al Mousawi, A. Kermagoret, D.-L. Versace, J. Toufaily, T. Hamieh, B. Graff, F. Dumur, D. Gigmes, J. P. Fouassier and J. Lalevée, *Polym. Chem.*, 2017, **8**, 568–580.
- 113 A. Al Mousawi, F. Dumur, P. Garra, J. Toufaily, T. Hamieh, B. Graff, D. Gigmes, J. P. Fouassier and J. Lalevée, *Macromolecules*, 2017, **50**, 2747–2758.
- 114 J. Zhang, F. Dumur, P. Xiao, B. Graff, D. Bardelang, D. Gigmes, J. P. Fouassier and J. Lalevée, *Macromolecules*, 2015, **48**, 2054–2063.
- 115 E. M. Chandler, C. M. Berglund, J. S. Lee, W. J. Polacheck, J. P. Gleghorn, B. J. Kirby and C. Fischbach, *Biotechnol. Bioeng.*, 2011, **108**, 1683–1692.
- 116 J. Warner, P. Soman, W. Zhu, M. Tom and S. Chen, *ACS Biomater. Sci. Eng.*, 2016, **2**, 1763–1770.
- 117 Z. Huang, Y. Gu, X. Liu, L. Zhang, Z. Cheng and X. Zhu, *Macromol. Rapid Commun.*, 2017, **38**, 1600461
- 118 A. Bagheri and J. Jin, *ACS Appl. Polym. Mater.*, 2019, **1**, 593–611.
- 119 J. Niu, D. J. Lunn, A. Pusuluri, J. I. Yoo, M. A. O'Malley, S. Mitragotri, H. T. Soh and C. J. Hawker, *Nat. Chem.*, 2017, **9**, 537–545.
- 120 K. A. Davis and K. Matyjaszewski, *Macromolecules*, 2000, **33**, 4039–4047.
- 121 D. M. Haddleton, M. C. Crossman, B. H. Dana, D. J. Duncalf, A. M. Heming, D. Kukulj and A. J. Shooter, *Macromolecules*, 1999, **32**, 2110–2119.
- 122 K. L. Beers, S. Boo, S. G. Gaynor and K. Matyjaszewski, *Macromolecules*, 1999, **32**, 5772–5776.
- 123 X. Pan, M. Lamson, J. Yan and K. Matyjaszewski, *ACS Macro Lett.*, 2015, **4**, 192–196.
- 124 D. M. Haddleton, C. B. Jasieczek, M. J. Hannon and A. J. Shooter, *Macromolecules*, 1997, **30**, 2190–2193.
- 125 G. L. Xiao, X. L. Hong, H. B. Zhang and X. H. Zhou, *Polym. Bull.*, 2009, **62**, 777–789.

- 126 G. X. Wang, M. Lu, Z. H. Hou, C. A. Yang, E. X. Liang, L. C. Liu, H. Wu, X. L. Li and Y. X. Xu, *J. Polym. Res.*, 2015, **22**, 60.
- 127 B. Otazaghine, B. Boutevin and P. Lacroix-Desmazes, *Macromolecules*, 2002, **35**, 7634–7641.
- 128 B.H. He, J. He, G.X. Wang, L.C. Liu, H. Wu and M. Zhong, *J. Appl. Polym. Sci*, 2016, **23**, 101
- 129 R. Venkatesh, F. Vergouwen and B. Klumperman, *J. Polym. Sci. Part A Polym. Chem.*, 2004, **42**, 3271–3284.
- 130 K. Matyjaszewski, N. V Tsarevsky, W. A. Braunecker, H. Dong, J. Huang, W. Jakubowski, Y. Kwak, R. Nicolay, W. Tang and J. A. Yoon, *Macromolecules*, 2007, **40**, 7795–7806.
- 131 L. C. Lu, N. F. Yang and Y. L. Cai, *Chem. Commun.*, 2005, 5287–5288.
- 132 B. B. Wayland, L. Basicckes, S. Mukerjee, M. L. Wei and M. Fryd, *Macromolecules*, 1997, **30**, 8109–8112.
- 133 P. Shukla and A. K. Srivastava, *Polym. Int.*, 1991, **25**, 159–162.
- 134 V. E. Tumanov and E.T. Denisov , *Pet. Chem.*, 2003, **43**, 368–374.
- 135 X. Zhang, W. Xi, S. Huang, K. Long and C. N. Bowman, *Macromolecules*, 2017, **50**, 5652–5660.
- 136 A. K. Higham, L. A. Garber, D. C. Latshaw, C. K. Hall, J. A. Pojman and S. A. Khan, *Macromolecules*, 2014, **47**, 821–829.
- 137 D. S. Achilias, M. M. Karabela and I. D. Sideridou, *J. Therm. Anal. Calorim.*, 2010, **99**, 917–923.
- 138 D. S. Achilias, M. M. Karabela and I. D. Sideridou, *Thermochim. Acta*, 2008, **472**, 74–83.
- 139 A. D. Adler, F. R. Longo and W. Shergalis, *J. Am. Chem. Soc.*, 1964, **86**, 3145–3149.
- 140 C. He, Q. He, C. Deng, L. Shi, D. Zhu, Y. Fu, H. Cao and J. Cheng, *Chem. Commun.*, 2010, **46**, 7536–7538.

- 141 C. E. Hoyle, T. Y. Lee and T. Roper, *J. Polym. Sci. Part A Polym. Chem.*, 2004, **42**, 5301–5338.
- 142 J. R. Lamb, K. P. Qin and J. A. Johnson, *Polym. Chem.*, 2019, **10**, 1585–1590.
- 143 R. Costa e Silva, L. Oliveira da Silva, A. de Andrade Bartolomeu, T. J. Brocksom and K. T. de Oliveira, *Beilstein J. Org. Chem.*, 2020, **16**, 917–955.
- 144 E. L. Clennan and A. Pace, *Tetrahedron*, 2005, **61**, 6665–6691.
- 145 S. Huang, J. Sinha, M. Podgórski, X. Zhang, M. Claudino and C. N. Bowman, *Macromolecules*, 2018, **51**, 5979–5988.
- 146 M. Meot-Ner and A. D. Adler, *J. Am. Chem. Soc.*, 1975, **97**, 5107–5111.
- 147 F. Chevalier, G. R. Geier and J. S. Lindsey, *J. Porphyr. Phthalocyanines*, 2002, **6**, 186–197.
- 148 A. Ghosh, *J. Mol. Struct. Theochem*, 1996, **388**, 359–363.
- 149 O. S. Finikova, A. V Cheprakov, P. J. Carroll, S. Dalosto and S. A. Vinogradov, *Inorg. Chem.*, 2002, **41**, 6944–6946.
- 150 O. B. Locos and D. P. Arnold, *Org. Biomol. Chem.*, 2006, **4**, 902–916.
- 151 X. Liu, D. Wang, H. Gao, Z. Yang, Y. Xing, H. Cao, W. He, H. Wang, J. Gu and H. Hu, *Dye. Pigment.*, 2016, **134**, 155–163.
- 152 X. Jiang, F. Gou and H. Jing, *J. Catal.*, 2014, **313**, 159–167.
- 153 B. Vaz, R. Alvarez, M. Nieto, A. I. Paniello and A. R. de Lera, *Tetrahedron Lett.*, 2001, **42**, 7409–7412.
- 154 T. Bohn, T. Walczyk, S. Leisibach and R. F. Hurrell, *J. Food Sci.*, 2004, **69**, S347–S350.
- 155 A. Johnston, J. Scaggs, C. Mallory, A. Haskett, D. Warner, E. Brown, K. Hammond, M. M. McCormick and O. M. McDougal, *J. Chem. Educ.*, 2013, **90**, 796–798.
- 156 H. H. Strain, J. Sherma and M. Grandolfo, *Anal. Chem.*, 1967, **39**, 926–932.
- 157 K. Iriyama, M. Yoshiura, M. Shiraki, S. Yano and S. Saito, *Anal. Biochem.*,

- 1980, **106**, 322–326.
- 158 N. Suzuki, K. Saitoh and K. Adachi, *J. Chromatog*, 1987, **408**, 181–190.
- 159 I. Csorba, Z. Buzas, B. Polyak and L. J. Boross, *J. Chromatog*, 1972, **172**, 287–293.
- 160 M.-H. Daurade-Le Vagueresse and M. Bounias, *Chromatographia*, 1991, **31**, 5–10.
- 161 H. T. Quach, R. L. Steeper and G. W. Griffin, *J. Chem. Educ.*, 2004, **81**, 385.
- 162 K. M. Smith, D. A. Goff and R. J. Abraham, *Org. Magn. Reson.*, 1984, **22**, 779–783.
- 163 J. J. Katz and C. E. Brown, *Bull. Magn. Reson.*, 1983, **5**, 3-49
- 164 R. J. Abraham and A. E. Rowan, *J. Chem. Soc., Perkin Trans*, 1991, 2, 515-521
- 165 F. T. Wolf, J. G. Coniglio and J. T. Davis, *Plant Physiol.*, 1962, **37**, 83–85.
- 166 N. Yamauchi, S. Iida, T. Minamide and T. Iwata, *J. Japanese Soc. Hortic. Sci.*, 1986, **55**, 355–362.
- 167 A. M. LaFountain, C. Pacheco, R. O. Prum and H. A. Frank, *Arch. Biochem. Biophys.*, 2013, **539**, 133–141.
- 168 P. Roat, B. K. Malviya, S. Hada, B. Chechani, M. Kumar, D. K. Yadav and N. Kumari, *ChemistrySelect*, 2020, **5**, 9714–9719.
- 169 T. Oba, Y. Uda, K. Matsuda, T. Fukusumi, S. Ito, K. Hiratani and H. Tamiaki, *FEBS.Letters*, 2012, **586**, 2338-2431.
- 170 T. Oba, Y. Tateno, M. Ihara, T. Fukusumi, N. Takei and S. Ito, *Tetrahedron Lett.*, 2014, **55**, 725–727.
- 171 W. Belasco, *Technol. Cult.*, 1997, **38**, 608–634.
- 172 B. Purushothaman, J. Choi, S. Park, J. Lee, A. A. S. Samson, S. Hong and J. M. Song, *J. Mater. Chem. B*, 2019, **7**, 65–79.
- 173 J. C. Manton, C. Long, J. G. Vos and M. T. Pryce, *Dalton Trans.*, 2014, **43**,

- 3576–3583.
- 174 M. Handayani, S. Gohda, D. Tanaka and T. Ogawa, *Chem. – A Eur. J.*, 2014, **20**, 7655–7664.
- 175 A. G. Mojarrad and S. Zakavi, *Eur. J. Inorg. Chem.*, 2017, **2017**, 2854–2862.
- 176 S. M. S. Ló, D. R. B. Ducatti, M. E. R. Duarte, S. M. W. Barreira, M. D. Nosedá and A. G. Gonçalves, *Tetrahedron Lett.*, 2011, **52**, 1441–1443.
- 177 L. Ye, Y. Fang, Z. Ou, L. Wang, S. Xue, J. Sun and K. M. Kadish, *J. Porphyr. Phthalocyanines*, 2018, **22**, 1129–1142.
- 178 G. Hariprasad, S. Dahal and B. G. Maiya, *J. Chem. Soc. Dalt. Trans.*, 1996, 3429–3436.
- 179 C. Zhuo, Y. Qin, X. Wang and F. Wang, *Chinese J. Chem.*, 2018, **36**, 299–305.
- 180 F. Liu, L. Duan, Y.-L. Wang, Q. Zhang and J.-Y. Wang, *Synth. Commun.*, 2009, **39**, 3990–3998.
- 181 J. Cabrera-González, E. Xochitiotzi-Flores, C. Viñas, F. Teixidor, H. García-Ortega, N. Farfán, R. Santillan, T. Parella and R. Núñez, *Inorg. Chem.*, 2015, **54**, 5021–5031.
- 182 M. Elisa Milanesio, F. S. Morán, E. Ines Yslas, M. Gabriela Alvarez, V. Rivarola and E. N. Durantini, *Bioorg. Med. Chem.*, 2001, **9**, 1943–1949.
- 183 S. Banfi, E. Caruso, S. Caprioli, L. Mazzagatti, G. Canti, R. Ravizza, M. Gariboldi and E. Monti, *Bioorg. Med. Chem.*, 2004, **12**, 4853–4860.
- 184 Y. Zhang, J. Liang and Z. Shang, *Chinese J. Chem.*, 2010, **28**, 259–262.
- 185 Z. Abada, L. Ferrié, B. Akagah, A. T. Lormier and B. Figadère, *Tetrahedron Lett.*, 2011, **52**, 3175–3178.
- 186 G. Kuang, Q. Zhang, D. Y. Li, X. S. Shang, T. Lin, P. N. Liu and N. Lin, *Chem. – A Eur. J.*, 2015, **21**, 8028–8032.
- 187 H. Ozawa, M. Kawao, H. Tanaka and T. Ogawa, *Langmuir*, 2007, **23**, 6365–6371.

